

**Structural evolution of the Penninic units
in the Monte Rosa region
(Swiss and Italian Alps)**

Inauguraldissertation

zur

Erlangung der Würde eines Doktors der Philosophie
vorgelegt der
Philosophisch-Naturwissenschaftlichen Fakultät
der Universität Basel

von

Julia Kramer
aus Ulm (Deutschland)

Basel, 2002

Genehmigt von der Philosophisch-Naturwissenschaftlichen Fakultät
auf Antrag von

Prof. Dr. Stefan M. Schmid

Prof. Dr. Rainer Abart

Prof. Dr. Neil Mancktelow

Basel, den 17.09.2002

Prof. Dr. M. Tanner
Dekan der Philosophisch-
Naturwissenschaftlichen Fakultät

Abstract

Structural evolution of the Penninic units in the Monte Rosa region (Swiss and Italian Alps)

The nappe pile in the Monte Rosa region represents the Eo- to Oligocene high-grade accretionary wedge of the Western Alpine arc. It comprises both pre-Permian continental crystalline upper crust and Permo-Mesozoic strata (Siviez-Mischabel and Monte Rosa nappe, Portjengrat and Stockhorn unit) as well as late Jurassic oceanic crust (Zermatt-Saas and Antrona unit). This thesis presents new detailed structural and geochemical data that aid in deciphering the tectonic evolution of the Monte Rosa region from Permo-Mesozoic continental breakup to successive Cenozoic subduction, nappe stacking and exhumation. The investigations aimed at the palinspastic reconstruction of the Monte Rosa region prior to nappe stacking.

The study is based on the detailed structural geologic and petrographic re-mapping of large parts of the Monte Rosa region in a scale of 1:2'500 to 1:25'000. Field- and laboratory work allowed to establish the relative timing and kinematics of four superposed transpressive phases of folding and shear zone activity (D1-D4). Whole rock geochemical analyses of fragmented meta-basaltic intrusives from shear zones and adjacent continental units, and of meta-basalts from the ophiolitic units shed light on the extensional evolution of the Monte Rosa region during Permo-Mesozoic continental breakup and late Jurassic rifting, and on the relative position of the individual tectonic units at that time.

The palinspastic reconstruction was realized by a step-by-step in-plane restoration of the offset of major folds and thrusts, starting at the present-day geometry of the nappe pile. The restoration of the D4 and late-D3 structures leads to the combination of the continental Stockhorn and Portjengrat units to form a continuous unit. The restoration of the remaining D3 thrusts and folds results in a triangle structure, in which the pile of continental nappes is wedged between the ophiolitic units. The ophiolitic Zermatt-Saas unit represents the top and the ophiolitic Antrona unit the base of this triangle structure. Within this structure, the continental Monte Rosa nappe forms the southern- and structurally uppermost, and the Siviez-Mischabel nappe the northern- and structurally lowermost continental unit. The ductile and major lower detachment horizon is located at the boundary of the continental nappes and the ophiolitic Antrona unit. Branch thrusts of this lower detachment separate the continental units. One of those branch thrusts is the Furgg zone, that separates the Monte Rosa nappe from the Stockhorn-Portjengrat unit. A reconstruction of the displacement of the Furgg zone places the Monte Rosa nappe adjacent to the Stockhorn-Portjengrat unit. Since the Monte Rosa nappe and the Stockhorn-Portjengrat unit share a similar high-grade metamorphic evolution, and since the Portjengrat unit and the Furgg zone were intruded by basalts derived from the same magma source, the Monte Rosa nappe and the Stockhorn-Portjengrat unit were considered as a previously continuous tectonic unit.

In accordance to the structural significance of the Furgg zone as a branch thrust of the major lower detachment of the triangle structure, several trails of highly strained Permo-Mesozoic sediments farther in the north (Zwischbergental and Laggintal) were also interpreted as such branch thrusts. The reconstruction of these branch thrusts and the lower detachment places all continental units into the same structural level north of the ophiolitic Zermatt-Saas unit. As the Zermatt-Saas unit represents Southern Penninic oceanic crust, the continental units north of it supposedly formed part of the Briançonnais microcontinent. The low-grade metamorphic Siviez-Mischabel nappe was either situated directly adjacent to the Monte Rosa-Stockhorn-Portjengrat unit or in a distance farther north.

The former position of the Antrona unit relative to the Zermatt-Saas unit could not be unraveled in this study. As there is no connection between the two ophiolitic tectonic units in the investigated area, the Antrona unit was considered as an individual tectonic unit positioned north of the continental tectonic units to represent former Valais oceanic crust. However, it is also conceivable that the Antrona unit formerly was the northernmost part of the Piemont-Ligurian ocean and evolved from the imbrication of this single oceanic nappe by N-directed ramp thrusting. The overthrusting of the newly formed Antrona slice by the Zermatt-Saas unit would then have been the first stage in the evolution of the Penninic nappe pile and have been succeeded by the formation of the triangle structure as described above.

Acknowledgements

In memory of Professor Dr. Martin Frey

A warm thanks to all those who joined freezing, sweating and trembling in the mountains and lowlands as supervisors, discussion and climbing partners, who helped overcoming closed roads, glacier crevasses, fragile walls and imminent dates and contributed with their company, friendship and hospitality to the present work and a good time in Switzerland and Italy.

Namely I thank the Professors Drs. Stefan M. Schmid, Nikolaus Froitzheim, Martin Frey, Rainer Abart, Willem- B. Stern, Neil Mancktelow, Othmar Münthener, Dieter Gebauer, and Hans-Rudolf Pfeifer (Universities of Basel, Bonn and Neuchâtel, ETH Zurich and Lausanne) for their scientific and personal commitment and willingness to discuss at any time.

I thank the diploma and PhD students Kathi Dubach, Christiane Rössler, Lukas Keller, Andreas Weber, Corinne Bacher, Ronan Le Bayon, Sabine Pawlig (Lange), John Reinecker, and Andreas Meier (Universities of Basel, Mainz, Tübingen and ETH Zurich) for the shared time in the field and at conferences, for discussion, team and research spirit.

A thanks goes to the multi-lingual population of the Bernoullianum for the friendly atmosphere at work.

I warmly thank my climbing, mountaineering and ski touring partners for the splendid time shared in the Alps and the Jura mountains: Stephan, Jacopo, Regula, John, Robert, René, Uli, Franziska, Irène, Jon, Andrès, Thomas, Deni, Almar, Cordula, Chantal, Michael, Matthias, Rolf, Christian, Alessandro, Richard & Pauli; the entire Academic Alpine Club (AACB) and Swiss Alpine Club (SAC) Basel.

And, above all, I thank my family, my boyfriend and all of my friends not mentioned yet for their steadfast mental support at any time, day and night: Karin, Harry & Angelika, Katja, Stephan, Sabine, Tine, Meinrad and Arnd.

For financial support during the finalisation of the PhD, I thank the Werenfels Fonds (Freiwillige Akademische Gesellschaft) Basel, and my family.

Danksagung

In Gedenken an Professor Dr. Martin Frey

Ich danke allen ganz herzlich, die als Betreuer, Diskussions- und SeilpartnerInnen in den Bergen und im Flachland mitgefroren, mitgeschwitzt und mitgezittert haben, gesperrte Strassen, Gletscherspalten, brüchige Wände und drohende Termine überwinden halfen und durch ihre Gesellschaft, Freundschaft und Gastfreundschaft zu dieser Arbeit und einer schönen Zeit in der Schweiz und in Italien beigetragen haben.

Namentlich danke ich den Professoren Drs. Stefan M. Schmid, Nikolaus Froitzheim, Martin Frey, Rainer Abart, Willem- B. Stern, Neil Mancktelow, Othmar Münthener, Dieter Gebauer und Hans-Rudolf Pfeifer (Universitäten Basel, Bonn und Neuchâtel, ETH Zürich und Lausanne) für ihr wissenschaftliches und persönliches Engagement und ihre jederzeitige Diskussionsbereitschaft.

Den DiplomandInnen und DoktorandInnen Kathi Dubach, Christiane Rössler, Lukas Keller, Andreas Weber, Corinne Bacher, Ronan Le Bayon, Sabine Pawlig (Lange), John Reinecker und Andreas Meier (Universitäten Basel, Mainz, Tübingen und ETH Zürich) danke ich für die gemeinsame Zeit im Gelände und auf Konferenzen, für Diskussion, Team- und Forschergeist.

Der multi-lingualen Bevölkerung des Bernoullianums sei für die freundschaftliche Atmosphäre am Institut gedankt.

Meinen Kletter-, Hoch- und SkitourenpartnerInnen danke ich für die gemeinsame Zeit in den Alpen und im Basler Jura: Stephan, Jacopo, Regula, John, Robert, René, Uli, Franziska, Irène, Jon, Andrès, Thomas, Deni, Almar, Cordula, Chantal, Michael, Matthias, Rolf, Christian, Alessandro, Richard & Pauli; dem gesamten Akademischen Alpenclub (AACB) und dem Schweizer Alpenclub (SAC) Basel.

Und ganz besonders danke ich meiner Familie, meinem Freund und allen noch nicht erwähnten FreundInnen für die unentwegte geistige Unterstützung zu jeder Tages- und Nachtzeit: Karin, Harry & Angelika, Katja, Stephan, Sabine, Tine, Meinrad und Arnd.

Für die finanzielle Unterstützung in der Endphase der Dissertation danke ich dem Werenfels-Fonds (Freiwillige Akademische Gesellschaft) Basel, und meiner Familie.

Contents

Abstract	I
Acknowledgements	III
1 Introduction	1
1.1 Regional setting.....	1
1.2 Geological setting.....	1
1.3 Motivation and methods applied.....	3
2 Tectonic units and lithostratigraphy	7
2.1 Sedimentary cover - age and stratigraphy.....	7
2.1.1 Pre-rift deposits: Permian - Triassic.....	7
Garnet micaschists & Meta-arkoses	
Quartzites	
Rauhwackes	
Dolomite and Calcite marbles	
2.1.2 Post-rift deposits: Late Jurassic - Cretaceous.....	9
Calcareous micaschists ("Bündnerschiefer", "Schistes lustrés")	
2.1.3 Basaltic sills and dykes.....	10
2.2 Ophiolitic tectonic units.....	11
2.2.1 Zermatt- Saas unit.....	11
2.2.2 Antrona unit.....	11
2.3 Continental tectonic units.....	11
2.3.1 Siviez- Mischabel nappe.....	11
2.3.2 Stockhorn and Portjengrat units.....	12
2.3.3 Monte Rosa nappe.....	12
2.3.4 Furgg zone and intensely strained Monte Rosa cover and basement.....	13
3 Geochemistry of metabasalts	15
3.1 Processes of magmatic element fractionation.....	15
Partial melting	
Fractional crystallisation	
3.1.1 Fractionation of major elements.....	15
Magnesium- iron ratio	
Alkali-silica and alkali-aluminium ratios	
Metasomatism	
3.1.2 Trace element fractionation.....	19
Rare earth elements (REE)	
3.2 Geochemistry of meta-basalts from ophiolitic and adjacent distal continental margin units: evidence from the Monte Rosa region (Swiss and Italian Alps).....	23
Abstract.....	23
1 Introduction.....	23
2 Geological setting.....	25
3 Sample descriptions.....	28
4 Mineralogical composition of meta-basalts.....	30
5 Whole rock chemistry.....	30
6 Discussion and conclusions.....	33
7 References.....	39

4 Structural geology	49
4.1 Characterization of deformation phases and associated metamorphism.....	49
4.1.1 Pre-D1 structures.....	49
4.1.2 D1 and D2 deformation phases (Ragno-Randa phase).....	51
4.1.3 D3 deformation phase (Mischabel phase).....	55
4.1.4 D4 deformation phase (Vanzone phase).....	55
4.2 Meso- and large- scale structures.....	57
4.2.1 Upper Valle d'AYas and Valle di Gressoney.....	61
(cross-sections 625, 627, 630, 633)	
4.2.2 Gornergrat, Mattertal.....	69
(cross-sections 628 & 628 E-W)	
4.2.3 Saastal.....	76
(cross-sections 636 & 638)	
4.2.4 Almagellertal, Zwischbergen pass, and Zwischbergental.....	82
(cross-sections 642 & 646 A)	
4.2.5 Furggtal and western Valle di Loranco.....	90
(cross-sections 643 & 646 B)	
4.2.6 Eastern Valle di Loranco, Passo della Preja, and Valle di Bognanco.....	95
(cross-sections 650 & 653)	
4.3 Major shear zones.....	100
4.3.1 D1/D2 Furgg zone and intensely strained Monte Rosa cover and basement.....	100
4.3.2 D3 Gornergrat-Furggtal shear zone.....	104
4.3.3 D3 Saas shear zone.....	105
4.3.4 D3 Trifhorn thrust.....	106
4.3.5 D3 Portjengrat shear zone.....	108
4.3.6 D3 Mischabel thrust.....	108
4.4 Composite cross-section.....	109
4.5 Kinematic indicators in micro- and outcrop-scale.....	113
5 Kinematic model and reconstruction	125
5.1 Reconstruction of Vanzone phase structures (D4).....	125
5.2 Reconstruction of Mischabel phase structures (D3).....	128
5.2.1 Late-D3 structures.....	128
5.2.2 Early-D3 structures.....	130
5.3 Reconstruction of D1/ D2 structures.....	130
6 Summary	135
7 References	139
Index of figures and tables	145
Curriculum vitae	147

Enclosures

- 1 Monte Rosa South - Geologic-tectonic map 1: 25'000
- 2 Monte Rosa North - Geologic-tectonic map 1: 25'000
- 3 Cross-sections Monte Rosa South and Gornergrat 1: 25'000
- 4 Cross-sections Monte Rosa North 1: 25'000

1 Introduction

1.1 Regional setting

The investigated area is situated between the Rhône valley (Valais, Switzerland) in the north and the Aosta valley (Piemont, Italy) in the south (Fig. 1.1.1). It comprises the Monte Rosa massif at the border crest between Italy and Switzerland, and encloses the highest summits of the two countries: from Pollux (4092 m) in the west across Castor (4228 m), Liskamm (4527 m), Dufourspitze (4633 m), Cima di Jazzi (3803 m), Monte Moro (2846 m), Sonnhorn (3487 m) and Pizzo d'Andolla (3654 m) to Pizzo Straciugo (2713 m) in the east. In the north, the upper parts of the Swiss valleys Mattertal, Saastal, Almagellertal, Furggtal, and Zwischbergental have been investigated. In the east and south, the upper Italian valleys Valle d' Antrona, Valle di Loranco, Valle di Bognanco, Valle d' Anzasca, Valle di Gressoney and Valle d' Ayas are part of the working area. Out of a total of 800 km², some 500 km² have been remapped. Roughly a seventh of this area is glaciated.

The valleys situated at lower elevations (Valle d' Antrona, Valle di Bognanco, and lower Valle di Loranco) are characterised by a relatively gentle topography and good accessibility, although moraine debris and plant growth impair the exposure of rocks. The valleys at higher elevations are generally characterised by a steep topography and, from 3500 m elevation on, by extensive glaciation. The retreat of glaciers leaves thick moraine debris and fragile walls, that often offer spectacular outcrops but are difficult to access. Due to the westward plunge of the major fold axes the structures are usually best exposed at the western slopes of the valleys. Therefore, the cross-sections (enclosures 3 & 4) are all drawn looking towards the west. The best overview of the structures may be gained from the following summits:

Pollux, Liskamm, Dufourspitze: View towards the north onto the W-/ NW-dipping nappe contacts, and view of the Gornergrat E-W cross-section. For cross-sections see enclosures 3 & 4 and Table 4.4.1.

Dom: View towards the west onto the D3 „Mischabel backfold“.

Pizzo d'Andolla/ Portjengrat: View towards the west, ideal view of cross-sections 643 (partly), 638, and 628 (partly).

Monte della Preja: View towards the west, good view of cross-sections 646 A & B.

1.2 Geological setting

In the Monte Rosa region, the Penninic nappe stack consists of slices of both pre-Permian continental crystalline upper crust and its Permo-Mesozoic cover as well as of slices of Late Jurassic oceanic crust (Fig. 1.2.1; Laubscher 1991; Stampfli & Marchant, 1997; Escher, 1988; Escher et al., 1997; Dal Piaz, 1999; Schmid and Kissling, 2000). It comprises the continental Siviez-Mischabel and Monte Rosa nappes as well as the Stockhorn and Portjengrat continental units, that are structurally situated between two ophiolitic units: the Zermatt-Saas unit on top and the Antrona unit at the base (Escher et al, 1988, 1993).

The Penninic nappes of the Monte Rosa region are situated in the hangingwall of the dextral, transtensive Rhône-Simplon line that forms their northern and eastern delimitation (e.g. Mancktelow, 1990, 1992; Mancktelow & Pavlis, 1994). From the south and west, they were overthrust by the Lower Austroalpine Sesia- and Dent Blanche nappes (Coward & Dietrich, 1989; Pennacchioni & Guermani, 1993; Hellwig & Vogler, 2001). Towards the southwest, the units are bent into a steeply south and eventually north dipping orientation (“Southern Steep Belt”), and they are backthrust towards the southwest across the dextral, transpressive Canavese line, a segment of the Periadriatic line (e.g. Schmid et al., 1987, 1989; Zingg & Hunziker, 1990). The palaeogeographic realm of the continental units investigated is situated in the Briançonnais, i.e. at the continental margin north of the Piemont-Ligurian ocean.

Until the Late Triassic, the clastic and carbonatic sedimentary strata of the Briançonnais were deposited in slowly subsiding basins on a stable continental shelf (see Tab. 1.2.1; Mosar et al., 1986). The destabilisation of the Triassic carbonate platforms was caused by transtensional movements (Stampfli & Marchant, 1997) that started in the Carnian and were accompanied by the deposition of

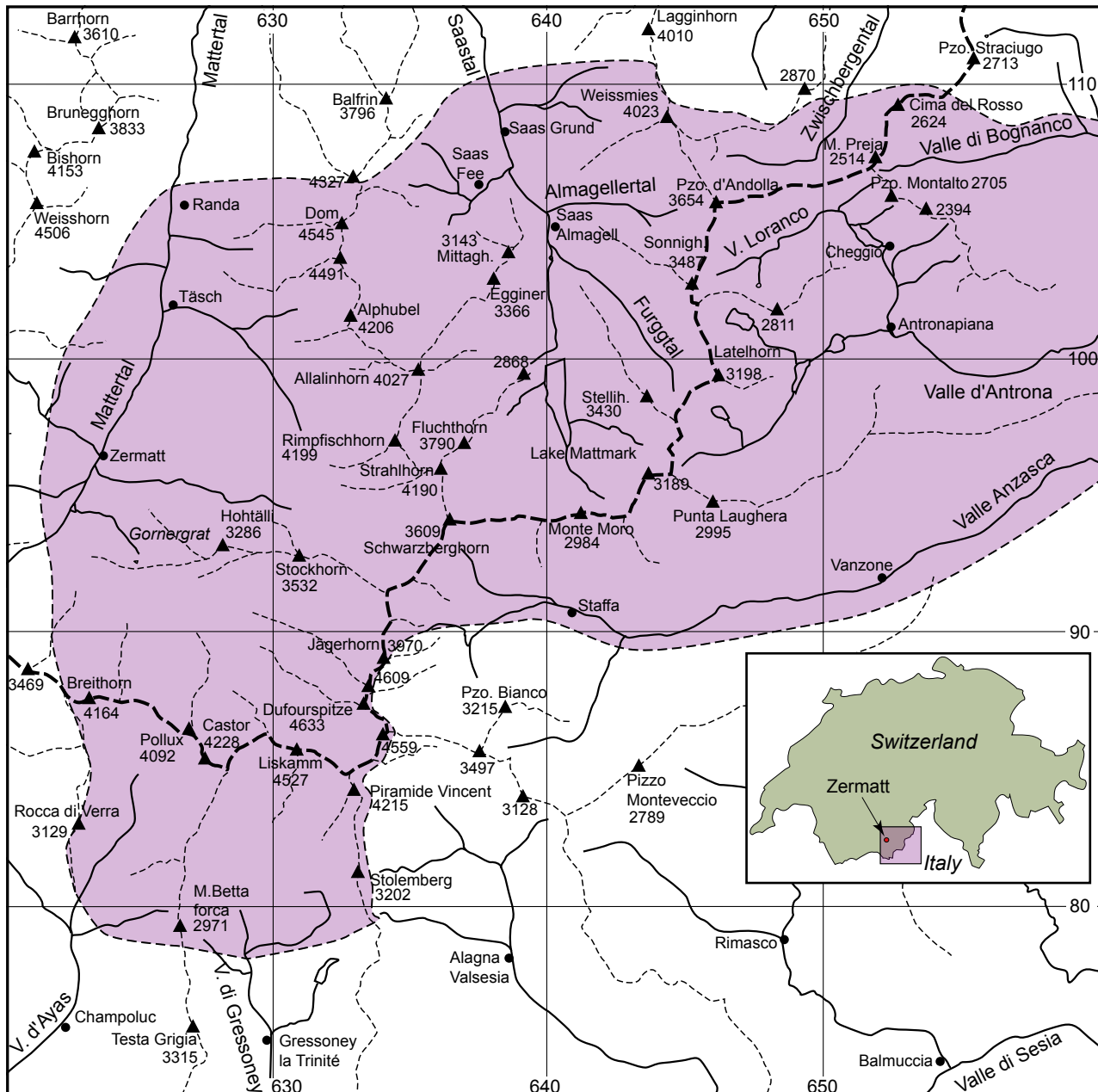


Fig. 1.1.1: Regional overview of the investigated area (indicated in purple).

syn-sedimentary breccias (Baud & Septfontaine, 1980; Mosar et al., 1986). Differential subsidence (Baud & Septfontaine, 1980; Lemoine & Trümpy, 1987) proceeded until the Toarcian, when a phase of thermal uplift resulted in the raise of the rift shoulders and an erosional hiatus in the sedimentary record which is so typical for the Briançonnais realm (Stampfli & Marchant, 1997). The continental break-up culminated in the Mid-Jurassic and led to Late Jurassic sea-floor spreading in the S-Penninic Piemont-Ligurian ocean (180-140 Ma according to Stampfli & Marchant, 1997). Callovo-Oxfordian radiolarian shales deposited in the oceanic basins and on some of the syn-rift sequences mark the drowning and rapid subsidence of the rift shoulders. Contemporaneously with the onset of subduction of the Piemont-Ligurian ocean in the Latest Jurassic to Early Cretaceous (135-110 Ma; Stampfli & Marchant, 1997), the N-Penninic Valais ocean opened, separating the Briançonnais microcontinent from the Eurasian plate. Ongoing contraction resulted in Mid- to Late Eocene NW-directed detachment and stacking of Piemont-Ligurian crust (HP metamorphic peak at 44 Ma?; Gebauer, 1999), Early Oligocene final collision of Briançonnais upper crust (HP metamorphic peak at 35-40 Ma?; Gebauer, 1999) and accretion of the Valais accretionary wedge (HP metamorphic peak at 33-35 Ma?; Gebauer, 1999). Late Eocene to early Oligocene blocking of the accretionary wedge (Escher et al., 1997) initiated S- to SE- directed dextral oblique folding and thrusting in all

the units (Klein, 1978; Milnes et al., 1981; Müller, 1983; Markley et al., 1994; Barnicoat et al., 1995). Ongoing contraction finally led to an updoming of the Monte Rosa nappe by SE- directed folding and dextral oblique thrusting related to shearing along the Canavese line (Steck, 1990; Steck & Hunziker, 1994; Schmid et al., 1987, 1989). The latest pegmatitic and aplitic intrusions into the Southern steep belt occurred at 25 Ma (Gebauer, 1999; Dal Piaz, 1999). They post-date backthrusting and Late Oligocene deformation and thereby place an upper time mark to this deformation.

1.3 Motivation and methods applied

Within the palaeogeographic framework discussed above, the affiliation of the various units in the Monte Rosa region is still a subject of debate. A major aim of this study was therefore to assign the controversially discussed tectonic units in the Monte Rosa region to a palaeogeographic unit and to propose a consistent palaeogeographic reconstruction.

The affiliation of the Zermatt-Saas unit to the Piedmont-Ligurian ocean, and that of the Siviez-Mischabel nappe - the central part of the Grand St. Bernard supernappe - to the northern Briançonnais microcontinent, respectively, is widely accepted (Escher et al., 1997 and references therein; Gebauer, 1999). In contrast, the origin of the other units remains controversial. Several models have been proposed: The Antrona unit is either affiliated to the Piedmont-Ligurian ocean (one of two possible scenarios proposed by Pfeifer et al., 1989) or to the Valais ocean (second possible scenario proposed by Pfeifer et al., 1989; Froitzheim, 2001; Keller & Schmid, 2001). The Monte Rosa nappe has been located (1) in the southern part of the Briançonnais microcontinent by Bearth (1945b, 1954b), Escher et al. (1997), Laubscher (1991), Dal Piaz (1999), Schmid and Kissling (2000); (2) at the southern distal margin of Europe by Froitzheim (2001) and Liati et al. (2001); and (3) at the northern portion of the Austro-Alpine terrane by Stampfli & Marchant (1997). Regarding the Stockhorn and Portjengrat units, a separate terrane was proposed by Robyr et al. (2000).

In order to clarify the affiliation of the discussed tectonic units and propose a consistent palaeogeographic scenario, two approaches were chosen: a petrographic-geochemical and a structural geologic approach.

In a first step, the high-grade metamorphic Permo-Mesozoic sedimentary strata were identified and mapped in the field, analysed in thin section and were assigned to the respective tectonic basement units. Thereby, the sedimentary strata could be used as a tectonic marker horizon for the tectonic reconstruction in a later step. In a second step and in order to support the petrographic correlation, the major and trace element distribution of basaltic intrusions occurring in the sedimentary strata and associated continental basement were compared. In a third step, the results were compared with the major and trace element distribution of basalts of the ophiolitic units. This geochemical comparison led to some rough constraints on the possible palaeogeographic position of the analysed tectonic units.

The structural geologic approach is based on a detailed structural geologic re-mapping of large parts of the Monte Rosa region. The most important geometric details of the present-day nappe pile were illustrated in a composite cross-section. Starting from the present-day geometry, the kinematic evolution of the region was then reconstructed in a third step. For this purpose, kinematic indicators and associated metamorphic grade were also considered. The kinematic indicators were investigated in the field, in thin section and by U-stage analysis. In a final step and by integrating the geochemical results, a careful in-plane restoration of major thrust displacements and folds led to a qualitative palaeogeographic reconstruction of the Monte Rosa region.

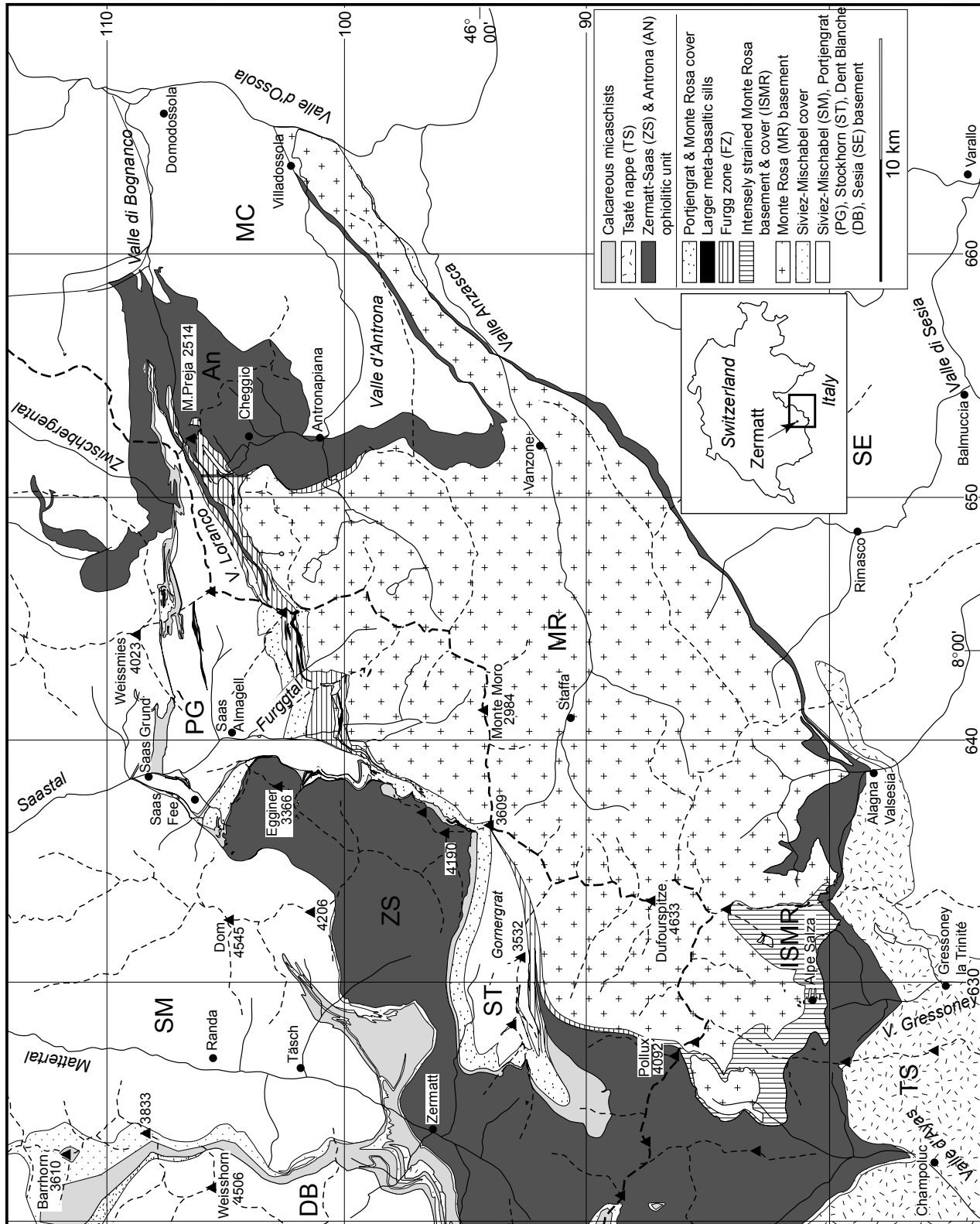
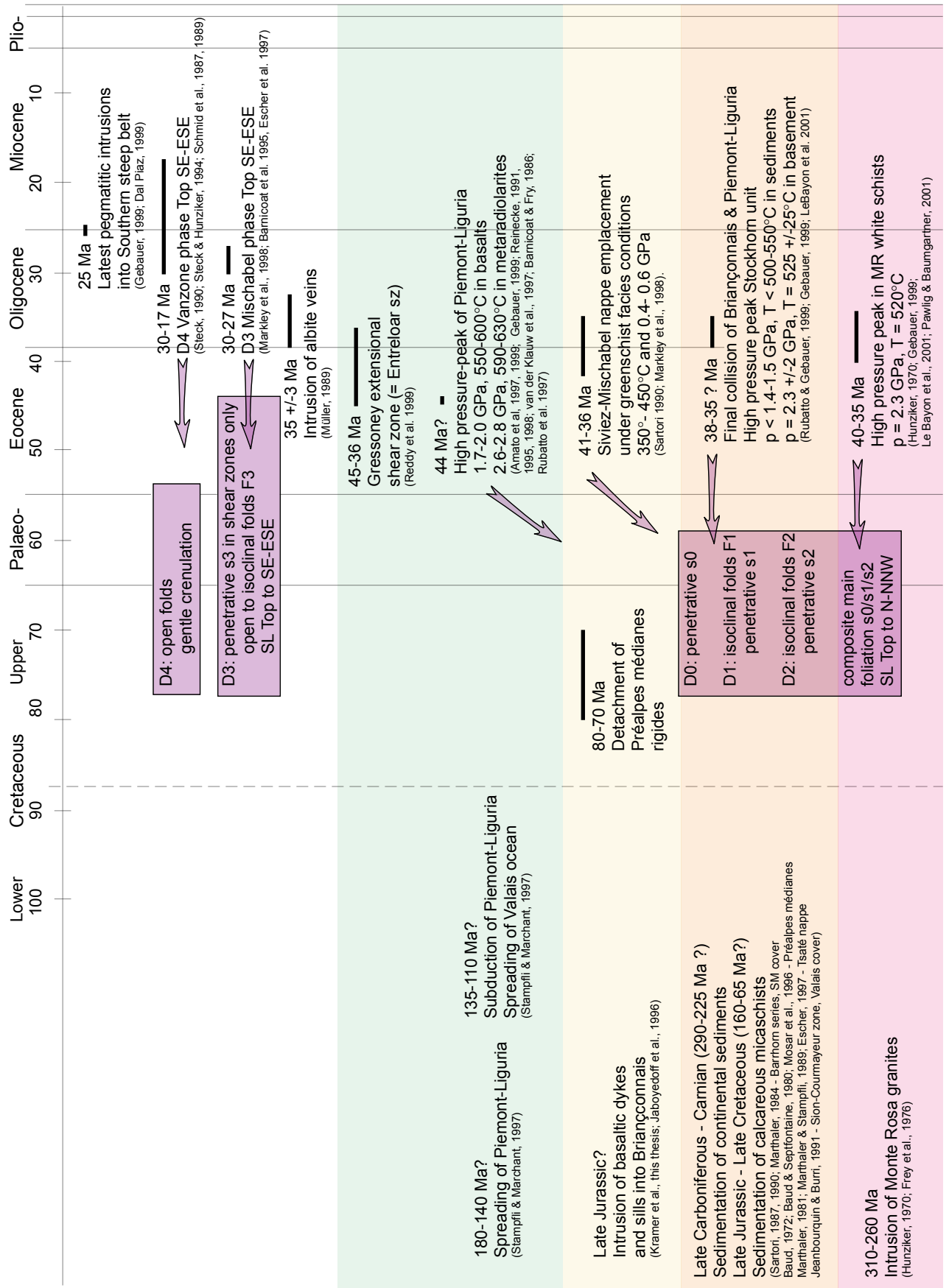


Fig. 1.2.1: Simplified geological sketch map of the Monte Rosa region. Compiled from Dubach (1998), Keller (2000), Rössler (2000), Weber, 2001; Bacher (2002), Bearth (1953a, 1954a+b), Steck et al. (1999), and mapping by Kramer (this thesis).



Tab. 1.2.1: Timing of selected major events affecting the Monte Rosa region. Modified after Escher et al. (1997); supplemented are data from the quoted publications. The structures that formed during the respective time span in the investigated area are depicted in violet boxes.

2 Tectonic units and lithostratigraphy

The tectonic units consist of slices of either oceanic or continental crust, both associated with their sedimentary cover. As the affiliation of the sedimentary cover series, the stratigraphic succession, and the age of sedimentation are the subject of ongoing discussion, the sedimentary cover will be treated independently from its tectonic position in section 2.1. This chapter presents the synthetic stratigraphic profiles and the supposed sedimentation ages. The proposed tectonic and palaeogeographic affiliation of the sedimentary cover will be discussed in chapter 4, as an understanding of the structural geology (ch. 4) is necessary for such a discussion.

2.1 Sedimentary cover - age and stratigraphy

Sedimentation ages

Prograde metamorphism up to eclogite facies conditions (Rubatto & Gebauer, 1999) and retrograde blue and/ or greenschist facies (Wüst & Baehni, 1986) metamorphic overprint of the sediments resulted in the nearly complete destruction of the fossil record. The supposed ages are therefore based on lithostratigraphic correlations with the (partly) dated sedimentary series of the following units: the Barrhorn series - sedimentary cover of the Siviez-Mischabel nappe (Sartori, 1987, 1990; Marthaler, 1984); the Préalpes médianes - detached sedimentary cover of the Gd. St. Bernard supernappe (Baud, 1972; Baud & Septfontaine, 1980; Mosar et al., 1996 and references therein); the Tsaté nappe - supposedly the accretionary wedge of the Piemont-Liguian ocean (Marthaler, 1981; Marthaler & Stampfli, 1989; Escher, 1997); and the Sion-Courmayeur zone - sedimentary cover of the Valais ocean (Jeanbourquin & Burri, 1991).

Stratigraphy & affiliation

Thrusting and two phases of synkinematic isoclinal folding resulted in the multiple repetition of lithologies. This has two effects.

First, it is difficult to establish a detailed unfolded stratigraphic succession, and there is no control of either original sedimentary thicknesses or sedimentary facies changes throughout the investigated area. Every contact has to be considered as a potential tectonic contact, and all the sediments may potentially be found in tectonic contact with the adjacent basement. A quantification of the total amount of displacement of thrusts and shear zones for the whole region is therefore hardly possible.

Second, the lack of younging or facing directions often prohibits an unequivocal decision as to whether the stratigraphy rests in an overturned or upright position with respect to a certain basement nappe. Where a facing or younging can be recognised, however, this can usually be used as an argument for the affiliation of the cover to one or the other of the basement nappes. At a larger scale, however, an overall younging direction can usually be recognized - e.g. from intercalated older meta-arkoses and quartzites towards younger intercalated quartzites and marbles. In such cases, the overall younging direction can be inferred, and the basement originally beneath the intercalated meta-arkoses and quartzites is considered as the affiliated basement. More details concerning the lithostratigraphy will be discussed below. A summary is found in Fig. 2.1.

2.1.1 Pre-rift deposits

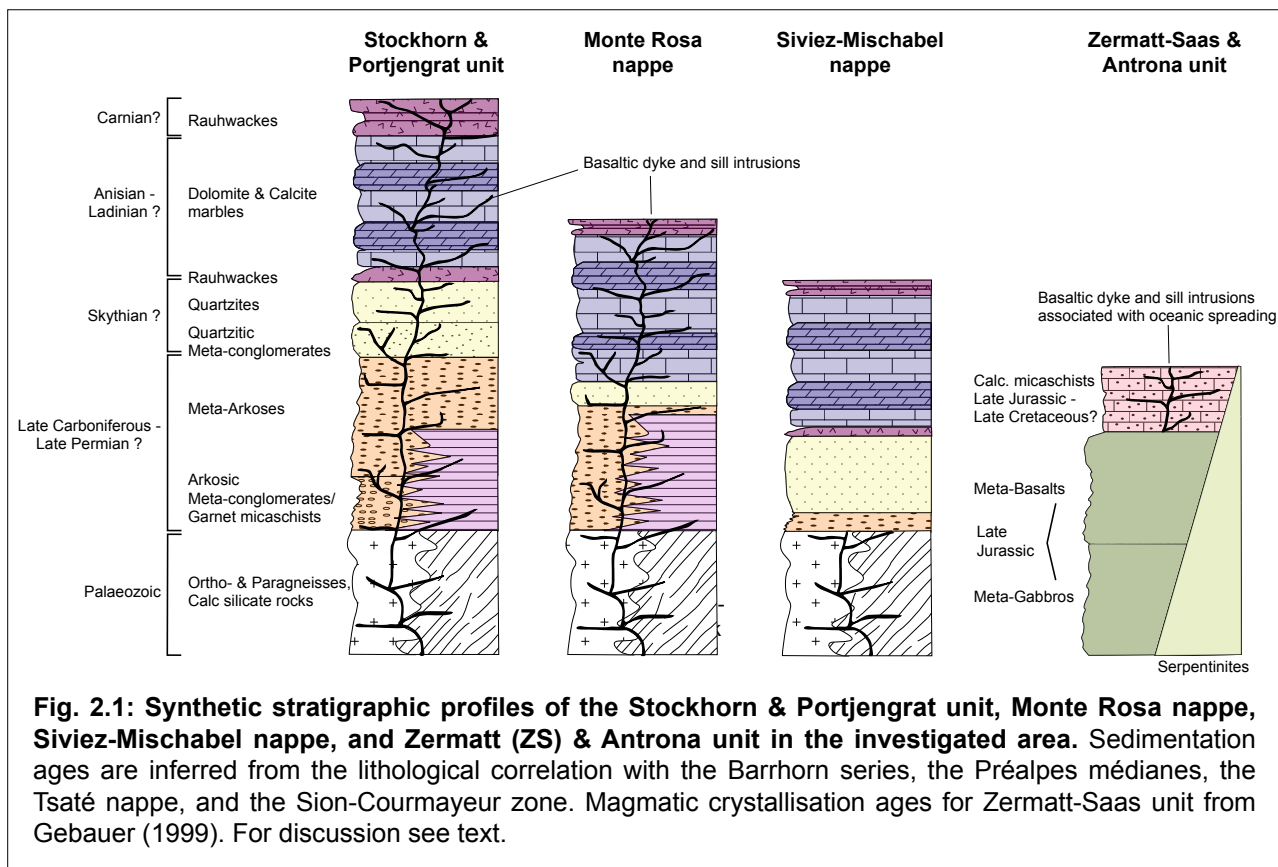
Garnet micaschists & meta-arkoses

The garnet micaschists and meta-arkoses (interpreted as representing Late Carboniferous to Permian) were probably unconformably deposited on older continental basement. The deposition of the meta-arkoses seems to have lasted longer, as they can also be found on top of garnet micaschists.

The **garnet micaschists** predominantly occur at places where the basement consists of paragneisses (Valle d'AYas, Valle di Gressoney, Gornergrat, Furggtal, Valle di Loranco, Monte della Preja). Since they do not contain any pre-alpine minerals, they are considered as sedimentary cover

with Alpine metamorphic overprint only, and not as part of the polymetamorphic Variscan basement. In contrast, Dal Piaz (1966) interprets the absence of pre-Alpine minerals to be due to complete recrystallisation of the polymetamorphic Variscan basement during pervasive Alpine deformation. However, metamorphic mineral zonations that would indicate polyphase growth - e.g. in garnet - are totally absent (M. Frey and R. Le Bayon, pers. comm.). The garnet micaschists consist of silvery-greenish schists or fine-grained gneisses with quartz, garnet, white mica, and chlorite as major components. Accessory minerals are black tourmaline, biotite, opaques, rutile, titanite, albitic plagioclase, apatite, zircon, calcite.

The **meta-arkoses** predominantly overlie meta-granitic basement and are considered as their erosional product. However, they may also be found on top of the garnet micaschists. The meta-arkoses consist of homogenous white gneisses with phengitic white mica, quartz, and eye-shaped albitic plagioclase as major components. Accessory minerals are microcline, considered as a remnant of the granitic educt, chlorite, clinozoisite, black tourmaline, calcite, biotite, apatite and zircon. The meta-arkoses contain conglomeratic horizons with elongated quartz pebbles in a matrix of feldspar and quartz. In places, however, the supposed „quartz pebbles“ unequivocally represent the hinges of intrafolial folded quartz layers (e.g. at Gornergrat in Mattertal or below the Mittaghorn in Saastal).



Quartzites

The quartzites (Skythian?) follow on top of either the garnet micaschists or the meta-arkoses. They are white, greenish or greyish in colour and consist of quartz and phengitic white mica as major components. Chlorite, clinozoisite, and garnet are accessory minerals. In places, the quartzites contain pelitic mica- or garnet-rich horizons, as well as conglomeratic horizons with quartz pebbles in a matrix of fine-grained quartzite. As for the arkosic conglomerates, the supposed „quartz pebbles“ can in places be recognised to be derived from the hinges of intrafolial folded quartz layers (e.g. at Gornergrat in Mattertal and along the Schwarzberg glacier in Saastal).

Rauhwackes

The evaporitic rauhwackes (Fig. 4.2.31) may occur in two stratigraphic levels: either between quartzites and marbles, i.e. at the border between Skythian and Anisian (cf. Mosar 1996 & Baud 1972, for Préalpes médianes; and Sartori, 1987, for Barrhorn series), or on top of the marbles, i.e. in the Carnian (cf. Mosar, 1996 and Baud, 1972 for Préalpes médianes; and Sartori, 1987, 1990, for Barrhorn series). They consist of orange, seldom yellowish or whiteish, pitted sedimentary breccia, with fragments of gypsum, green and gray chlorite-phyllites, green actinolite-albite gneisses, white marbles and yellowish dolomites in a matrix of fine-grained, recrystallized quartz, dolomite, and calcite. Quarternary tillites (e.g. at the Schwarzberg glacier) may look similar, but can be distinguished by the deformation of their components: they contain previously folded quartzites, marbles, serpentinites and amphibolites.

The two levels of rauhwackes serve as major detachment horizons in the sedimentary pile of the region. The Skythian/Anisian level of rauhwackes is either not developed at all, or relatively thin.

Dolomite and Calcite marbles

The dolomite and calcite marbles (Anisian - Ladinian?) follow on top of the lower level of rauhwackes or, sometimes, directly on top of the quartzites. Usually the rigid yellowish dolomite marbles occur as boudinaged horizons within the more incompetent white calcite marbles, indicating an original intercalation of the two lithologies. The major components are dolomite and/ or calcite. Accessory minerals are epidote, clinozoisite, zoisite, tremolite-actinolite retrogressed to talc or chlorite, ankerite, feldspar, quartz, rutile and titanite.

2.1.2 Post-rift deposits

Calcareous micaschists („Bündnerschiefer“, „schistes lustrés“)

The calcareous micaschists (age discussion see below) are found above a major tectonic contact situated on top of one of the two stratigraphic levels of rauhwackes. They are light gray and usually have a reddish weathering color. They consist of a fine intercalation of calc-arenitic and pelitic horizons, considered to be characteristic for turbiditic deposition. From the Gornergrat in Mattertal to Saastal, they are interlayered with thin boudinaged quartzitic layers (millimeters to centimeters in thickness). The boudins are usually elongated and define a stretching lineation. Those quartzitic layers were interpreted as metaradiolaritic intercalations typical for the Piedmont-Ligurian sediments (i.e. Zermatt-Saas unit) by Bearth (1976) and Bearth & Schwander (1981), and they are associated with manganese mineralisations. Such supposedly metaradiolaritic layers are less frequent, but still present in the calcareous micaschists at the Zwischbergen pass in Almagellertal - Zwischbergental, where the calcareous micaschists can be seen resting on top of the Antrona unit. However, they were also mapped by Bearth (1957b) in calcareous micaschists of the Antrona unit west of the Gmeinalp in Zwischbergental.

The major constituents of the calcareous micaschists are calcite, quartz, white mica, biotite, chlorite, +/- chloritoid, +/- garnet. Garnet predominantly grows in the pelitic horizons and is often developed as „snowball garnet“, however without a consistent sense of rotation (e.g. at Felskinn, west of Saas Fee in Saastal). Accessory minerals are plagioclase, pyrite, hematite, and other opaques.

The calcareous micaschists serve as another major detachment horizon in the investigated area. Along the contacts between mafics of the ophiolitic units and the calcareous micaschists, the latter frequently contain mafic boudins of supposedly tectonic origin (e.g. at the western Gornergrat and at Alpe Bettolina in Valle di Gressoney).

Affiliation

The allochthonous position of the calcareous micaschists in respect to the underlying Triassic sedimentary succession does not allow their unequivocal assignment to either oceanic or continental nappes. Lithological or structural criteria cannot be applied, since calcareous micaschists are known from both environments (see age discussion). In the investigated area, they are basically found in three structural positions: in an internal position within ophiolitic nappes (e.g. at Eggnerjoch, Allalinhorn and Feekopf, and at Strahlhorn - Zermatt-Saas unit; and at Alpe Pontimia in Zwischbergental - Antrona unit), at nappe contacts between ophiolitic and continental units (Gornergrat in Mattertal; Saastal; Zwischbergental), and - together with a reduced sedimentary pile - in contact with the continental crystalline basement (two bands above and below Saas Fee which can be followed to the Grundberg and Trifhorn and which represent the contact of Siviez-Mischabel nappe and Portjengrat unit, cf. Fig. 4.2.29). As an understanding of the structural geology (cf. ch. 4) is necessary for the discussion of their affiliation, the various alternatives will be discussed in chapter 5.

Some stratigraphic-tectonic arguments of Sartori (1987), who has worked at the western side of the Mattertal and in the Val Tourtemagne, however, need to be discussed now. This author distinguishes two series of calcareous micaschists. The reddish-weathering, calc-arenitic „série rousse“ is interpreted as transgressively overlying continental sedimentary series (as described in sections 2.2.1 & 2.2.2), and is - according to this author - affiliated to the continental Mont Fort nappe (uppermost unit of the Grand St. Bernhard supernappe). In contrary, the grayish-weathering, pelitic „série grise“ is interpreted as the sedimentary cover of the Piemont-Ligurian ocean, that has been accreted in order to form an ophiolitic mélange known as Tsaté nappe. In respect to the region investigated by this work, however, this separation appears to be rather artificial for two reasons. First, both series are in direct contact with each other at the western side of the Mattertal, and a major tectonic contact separating a continental from an oceanic unit cannot be justified by lithostratigraphic arguments alone. Second, in the area investigated here, the calcareous micaschists are predominantly of the „série rousse“ type. Hence, according to the lithostratigraphic arguments of Sartori (1987), they should be affiliated to the continental units. However, the structural position of „série rousse type“ calcareous micaschists in an internal position within the ophiolitic units, rather argues for their possible affiliation with ophiolitic units. This finding does not necessarily imply that the two series do not delineate a major tectonic contact in the region investigated by Sartori (1987). However, the lithostratigraphic differences cannot be regarded as characteristic for different nappes of the region. Instead, there might be a facies change from rather pelitic to rather calc-arenitic series.

Age

Age determinations based on planctonic foraminifera exist for calcareous micaschists of several units. Late Cretaceous to Early Eocene ages were determined for the Barrhorn series, the cover of the Siviez-Mischabel nappe (Briançonnais microcontinent; Marthaler, 1981, 1984; Sartori, 1987). Cenomanian to Turonian ages were determined for the „Série rousse“ (Marthaler, 1981, 1984) which is interpreted to belong to the Mont Fort nappe (Briançonnais microcontinent) according to Sartori (1987), but supposed to belong to the Zermatt-Saas or Antrona unit in this study. Cenomanian ages were found for the „Série grise“ which is supposed to belong to the Tsaté nappe (accretionary wedge of the Piemont-Ligurian ocean) by Marthaler (1981, 1984) and Sartori (1987). Late Cretaceous to Eocene ages were determined for the Sion-Courmayeur zone (Valais ocean; Bagnoud et al., 1998; Deville et al., 1992).

2.1.3 Basaltic sills & dykes

The sedimentary cover series described above (ch. 2.1.1 and 2.1.2) frequently contain metabasaltic sills and dykes of probably Jurassic age, that often occur as boudinaged horizons oriented parallel to the foliation. Their petrography and geochemistry is subject of chapter 3. Their deformation within the Furgg zone will be treated in chapter 4.3, and the kinematic implications of their presence will be discussed in chapters 3.2 and 5.

Such sills and dykes within the sedimentary cover are less abundant in Saastal along the

Schwarzberg glacier, and at the Zwischbergen pass (between Almagellertal and Zwischbergental). They are absent at the following localities: in Saastal below the Hangende Gletscher glacier; at the western Gornergrat in Mättertal (Ritzengrat, Hohtälligrat, Üsseri Gornerli); west of Saas Fee (at Trift and Berter); and in Furgtal (in Steintälli and south of Börterrück).

2.2 Ophiolitic tectonic units

2.2.1 Zermatt-Saas unit

The Zermatt-Saas unit (Mid- to Late Jurassic, Stampfli & Marchant, 1997; Gebauer, 1999) is exposed in the western part of the investigated area and is structurally situated below the Tsaté nappe and the Siviez-Mischabel nappe, and on top of the Portjengrat and Stockhorn units and the Monte Rosa nappe. It forms a large SE-facing and W-plunging synform (Mittaghorn synform).

The Zermatt-Saas unit consists of metamorphic ultramafics, gabbros and pillow basalts (cf. Meyer, 1983; Colombi, 1989; Pfeifer et al. 1989). A detailed petrographic description of the metabasalts is given in chapter 3.2. The associated sediments are opicalcites, calcareous micaschists, manganese-rich quartzites (meta-radiolarites), and marbles (cf. section 2.1.3; Bearth, 1976; Bearth & Schwander, 1981). High-pressure peak metamorphic conditions of Middle Eocene age (44 Ma; Amato et al., 1997 & 1999; Gebauer, 1999) range from 2.6 to 2.8 GPa and 590 to 630°C in metaradiolarites (Reinecke, 1991, 1995, 1998; van der Klauw et al., 1997), and from 1.75 to 2.0 GPa and 550 to 600°C in the ophiolites (Barnicoat & Fry, 1986). Retrograde greenschist facies overprint occurred during the early Oligocene (Gebauer, 1999) and was accompanied by locally extensive albitisation along fracture zones adjacent to the sediments (Müller, 1989). The Zermatt-Saas unit is derived from the S-Penninic Piemont-Ligurian ocean.

2.2.2 Antrona unit

The Antrona unit (no radiometric data so far; Mid- to Late Jurassic, if part of the Piemont-Ligurian ocean, Early Cretaceous, 135-110 Ma, if part of the Valais ocean; Stampfli & Marchant, 1997) is exposed in the eastern portion of the investigated area and is structurally situated below the Monte Rosa nappe and the Portjengrat unit and on top of the continental Moncucco-Camughera unit. In the east, it is cut off by the Simplon line.

The Antrona unit consists of metamorphic ultramafics, gabbros and basalts (Colombi, 1989; Pfeifer et al., 1989). A detailed petrographic description of the metabasalts is given in chapter 3.2. The associated sediments are marbles and calcareous micaschists (cf. section 2.1.3; Carrupt & Schlup, 1998; Keller, 2000). Recently discovered eclogites (L. Keller, pers. comm.) are probably the remnants of an early high-pressure metamorphic event. Retrograde greenschist facies and prograde amphibolite facies metamorphism of Oligocene age has been described by Colombi (1989) and Pfeifer et al. (1989). The affiliation of the Antrona unit to either the S-Penninic Piemont-Ligurian or N-Penninic Valais ocean is still a matter of debate (cf. ch. 5; e.g. Pfeifer et al., 1989; Froitzheim, 2001; Dal Piaz, 2001).

2.3 Continental tectonic units

2.3.1 Siviez-Mischabel nappe

The Siviez-Mischabel nappe is the central part of the Grand St. Bernard supernappe. The lowermost parts are the Pontis-, Staldener-, and Berisal nappes, and the uppermost part is formed by the Mont Fort nappe. The Siviez-Mischabel nappe is exposed in the northern part of the investigated area (in Mättertal and Saastal). It forms a large SE-facing and W-plunging antiform („Mischabel backfold“), situated on top of the Zermatt-Saas and Portjengrat units.

The Siviez-Mischabel nappe consists of polymetamorphic Palaeozoic para- and orthogneisses (Bearth, 1945a; Escher et al., 1997) that frequently contain boudinaged mafic layers (cf. ch. 3.2) of

supposed Palaeozoic age (Thélin, 1990; Eisele et al. 1997). The associated metasedimentary cover (cf. ch. 2.1) is represented by the Late Carboniferous to Eocene Barrhorn series. However, most of the Middle Triassic and younger strata was detached at the Skythian/ Anisian evaporitic horizon and thrust towards the NW in Eocene to Early Oligocene times, where it nowadays forms the Préalpes médianes. Nappe emplacement occurred under greenschist facies conditions estimated as 350°-450°C and 0.4- 0.6 Gpa by Sartori (1990) in Late Eocene times (41-36 Ma; Markley et al., 1998). The Siviez-Mischabel nappe is derived from the Briançonnais microcontinent.

2.3.2 Stockhorn and Portjengrat units

The **Stockhorn unit** is exposed at the Gornergrat in Mättertal, where it forms a large SE-facing and W-plunging antiform (Stockhorn antiform). It is structurally situated below the Zermatt-Saas unit and on top of the Monte Rosa nappe.

The **Portjengrat unit** is exposed in the Saastal, Almagellertal, Zwischbergental, Valle di Loranco and Valle di Bognanco. Structurally, it is in contact to the Siviez-Mischabel nappe along steep-dipping shear zones in the north and to the Monte Rosa nappe in the south. It rests below the Zermatt-Saas unit and on top of the Antrona unit. For structural (cf. ch. 4 & 5), lithological, and metamorphic reasons, the Stockhorn and Portjengrat units are considered as a single unit.

The Stockhorn and Portjengrat units comprise an association of Palaeozoic basement including **calc silicates and paragneisses** that frequently contain boudinaged mafic layers (cf. ch. 2.1.4 & 3.2), and orthogneisses (Huang, 1935 a+b; Bearth, 1945 a+b, 1953 a+b; Escher et al., 1997).

The **orthogneisses** are deformed meta-granites (augenmylonites) that can usually be distinguished from the Monte Rosa orthogneisses by their higher biotite abundance and by a brownish weathering colour. Their major constituents are alkali-feldspar (partly microcline), plagioclase, quartz, biotite, and white mica. Accessory minerals are chlorite, epidote/ clinozoisite, zircon, apatite, and black tourmaline.

For structural reasons discussed in chapters 4.2 and 5, most of the **Permo-Mesozoic sedimentary strata** (cf. section 2.1) in the investigated area are considered as affiliated to the Stockhorn and Portjengrat units. At Gornergrat in Mättertal, a prograde eclogite facies mineral assemblage of early Oligocene age is preserved in Mesozoic quartzites for which conditions of $P < 1.4-1.5$ GPa, $T < 500-550^\circ\text{C}$ were estimated by Rubatto & Gebauer (1999). Also at Gornergrat, conditions of 2.3 ± 0.2 GPa and $525 \pm 25^\circ\text{C}$ were estimated for garnet micaschists by LeBayon et al. (2001).

Various possibilities of the affiliation of the Stockhorn and Portjengrat units have been suggested and they will be discussed in chapter 3.2 and 5.

2.3.3 Monte Rosa nappe

The basement of the Monte Rosa nappe consists of pre-Carboniferous **paragneisses and calc silicate rocks** that frequently contain boudinaged mafic layers (cf. ch. 3.2; Bearth, 1942, 1945 a+b, 1948, 1949; Dal Piaz, 1966, 1967, 1971; Escher et al., 1997). This Palaeozoic basement was intruded by late Carboniferous to Permian granites (310-260 Ma; Hunziker, 1969; Frey et al., 1976).

During alpine deformation, the **granites** were frequently mylonitised to various degrees (cf. ch. 4.1). They consist of light-coloured, sometimes practically undeformed granites and more intensely deformed gneisses with a penetrative foliation. Major constituents are alkali-feldspar (often microcline), plagioclase, and quartz. Frequent accessory minerals are phengitic white mica, black tourmaline (especially abundant in late pegmatitic veins), opaques, hematite, zircon, and apatite. Rare accessory minerals are biotite, clinozoisite, epidote, pyrite, and titanite. Garnet and calcite grow adjacent to shear zones between ortho- and paragneisses.

White schists are exposed at several localities (e.g. Lake Mattmark and above P.2730 at the Piccolo ghiacciaio di Verra glacier in Valle d'Ayas). Their mineral paragenesis consisting of talc, chloritoid, quartz, phengite, paragonite, and kyanite was subject to detailed studies by Chopin

(1981), Chopin & Monie (1984), Le Bayon et al. (2001) and Pawlig & Baumgartner (2001), who estimated peak metamorphic conditions of 2.3 GPa and 520°C. Those conditions were reached between 35-40 Ma (Hunziker, 1969; Gebauer, 1999).

Permo-Mesozoic sedimentary strata is exposed in the upper Valle d' Ayas, Valle di Gressoney and Valle di Loranco (cf. ch. 2.1).

The palaeogeographic affiliation of the Monte Rosa nappe is controversially discussed. It was located at the southern portion of the Briançonnais microcontinent by Argand (1911), Bearth (1945 a+b, 1954b), Coward & Dietrich (1989), Laubscher (1991), Escher et al. (1997), Dal Piaz (1999, 2001), Schmid & Kissling (2000); at the southern portion of Europe by Froitzheim (2001) and Liati et al. (2001), and at the northern portion of the Austro-Alpine terrane by Stampfli & Marchant (1997). The various possibilities will be discussed in chapter 3.2 and 5.

2.3.4 Furgg zone and intensely strained Monte Rosa cover and basement

The Furgg zone (FZ) and the intensely strained Monte Rosa cover and basement (ISMR) represent up to one km thick mylonitic shear zones found north and south of the Monte Rosa main crest, respectively (cf. ch. 4.3). The Furgg zone extends from the Gornergrat in Mattertal in the SW to the Valle di Bognanco in the NE (Bearth, 1953 a+b, 1954 a+b, 1956, 1957b; Wetzel, 1972; Klein, 1978; Jaboyedoff et al., 1996; Froitzheim, 2001; Rössler, 2000; Keller, 2000; Keller & Schmid, 2001; Dal Piaz, 2001; Liati et al. 2001; Weber, 2001). The intensely strained Monte Rosa cover and basement is exposed on the southern side of the Monte Rosa massif in the Valle d' Ayas and Valle di Gressoney (also referred to as „Furgg zone“ in Dal Piaz, 1964, 2001; and in Wetzel, 1972) and on the northern side of the Monte Rosa massif at Lago d' Antrona in Valle d' Antrona.

The Furgg zone and the intensely strained Monte Rosa cover and basement overprinted basement-cover contacts of the continental tectonic units, as well as nappe contacts between ophiolitic and continental tectonic units during WNW-directed nappe stacking (deformation phases D1 and D2). Mylonitic shearing resulted in the superposition of two phases of isoclinal and/or sheath folding affecting the nappe contacts between Zermatt-Saas unit and Monte Rosa nappe in case of the ISMR, and between Portjengrat and Stockhorn unit, Monte Rosa nappe and Antrona unit in case of the FZ, respectively (see Fig. 3.2.2). Isoclinal folding and the subsequent imbrication of folds during progressive shearing led to the intercalation of lithologies in such a small scale (see Fig. 4.3.2), that individual lithologies cannot be presented in a map-scale of 1:25'000. The Furgg zone and the intensely strained Monte Rosa cover and basement were therefore distinguished as individual lithostratigraphic units in the sense of shear zones which record intense D1 and D2 shearing.

The FZ and the ISMR comprise continental Palaeozoic basement rocks and Permo-Mesozoic sedimentary cover, both with abundant meta-basaltic intrusions. Apart from intense straining, the FZ and the ISMR usually distinguish from the adjacent tectonic units by their high amount of meta-basaltic intrusives, that typically take the form of disrupted layers which were boudinaged during D1 and D2 (see ch. 4.3). In places, these boudins may represent more than 50 % of the rock volume on an outcrop scale (cf. Fig. 4.3.2 a). As, however, meta-basaltic boudins can also be found in the more internal parts of the continental tectonic units throughout the region (cf. Fig. 4.3.1 D), the trace element chemistry of the meta-basaltic boudins served as a further argument for delimiting the Furgg zone (transitional-type MORBs; cf. ch. 3.2) and the intensely strained Monte Rosa cover and basement (plume-type MORBs; cf. ch. 3.2). This study will therefore not follow the definition of Wetzel (1972), who expanded the term „Furgg zone“ onto all boudin-containing zones found in the region. Several larger coherent imbricates of ultramafic and mafic rocks in the Furgg zone represent mappable units and were therefore not regarded as part of the Furgg zone, but assigned to the Zermatt-Saas (at Gornergrat) and the Antrona units (at Monte della Preja and in Furggtal), respectively (see Encl. 1 & 2 and ch. 4.2.2 & 4.2.6).

In the course of ongoing contraction during D3 and D4, parts of the Furgg zone were overprinted by the Gornergrat-Furggtal shear zone (see ch. 4.3.2 and 5). In order to clearly separate

these late tectonic movements (D3) only affecting certain parts of the Furgg zone, from the early D1 and D2 straining that defines the Furgg zone as such, D3 structures in the Furgg zone were assigned to the D3 Gornergrat-Furggtal shear zone.

The intensely strained Monte Rosa basement and cover on the southern side of the Monte Rosa massif was not overprinted by D3 and D4 shearing. There, D1 and D2 shearing mainly resulted in a complex superposition of two mylonitic folding phases on basement and cover of the Monte Rosa nappe. Because of the abundant occurrence of mafic boudins in a highly strained matrix, the ISMR strongly resembles the Furgg zone in the field. However, the two shear zones differ in respect to their tectonic significance and geochemistry that will be discussed in chapters 3.2 and 5.

Contraction during D3 and D4 accounted for large-scale SE-directed folds, in the limbs of which both the Furgg zone and the intensely strained Monte Rosa and cover were tilted into their present-day position.

3 Geochemistry of metabasalts

In the investigated region, the bulk rock composition of metabasalts from the ophiolitic and continental tectonic units was analyzed to allow for a geochemical discrimination of the different geotectonic environments and the ascription of certain tectonic units to a palaeogeographic region. The ascription of the investigated metabasalts to a certain geotectonic setting is based on the comparison with published geochemical trends of recent basalts that stem from a variety of geotectonic environments.

The reason for the development of such characteristic geochemical trends are several mechanisms of element fractionation, that influence the melt composition in various tectonic settings to various degrees. Those mechanisms will be briefly introduced in chapter 3.1. For a comprehensive overview of the processes operating in multi-phase magmatic and metamorphic systems, the reader is advised to refer to the books written by Rollinson (1993), Philpotts (1990), Wilson (1989) and Spear (1993). The results of this investigation are comprehensively described and interpreted in chapter 3.2 and presented in form of a publication (accepted by the Swiss Bulletin of Mineralogy and Petrology in June, 2003).

3.1 Processes of magmatic element fractionation

Magmas from different geotectonic environments show distinct geochemical trends that may originate from several processes (Philpotts, 1990; Wilson, 1989; Rollinson, 1993; Saunders, 1984). Crucial factors that determine the chemical composition of a magma are the chemistry of the source rock, the degree of partial melting, the mechanism of melting, the confining pressure during melting and crystallization, the degree of fractionated crystallisation and the contamination by fluids or by assimilation of crust. After crystallisation, the chemical composition may be affected by secondary element mobility during metamorphism and fluid infiltration.

Partial melting

Melting of natural rocks is usually incongruent. The melts generated by partial melting have a composition different from that of their source rocks. The partitioning of a chemical component between coexisting phases - i.e. between solid (e.g. source rock) and liquid (e.g. magma) - is described by the partition coefficient $K_{D\ S-L} = c_S/c_L$, where c_S is the concentration of the component in phase S (i.e. solid) and c_L is the concentration of the component in phase L (i.e. liquid). Elements with $K_{D\ S-L} < 1$ are called incompatible elements, those with $K_{D\ S-L} > 1$ are called compatible in respect to the particular system (the solid in the example). Incompatible elements will therefore preferentially concentrate in the first-formed liquid. If this batch of liquid is immediately removed from the system by its rise to the surface, it cannot equilibrate with the residuum ("Rayleigh melting"). Hence, this melt will be highly enriched in incompatible elements relative to the original composition of the source rock and leave a residuum depleted in these elements.

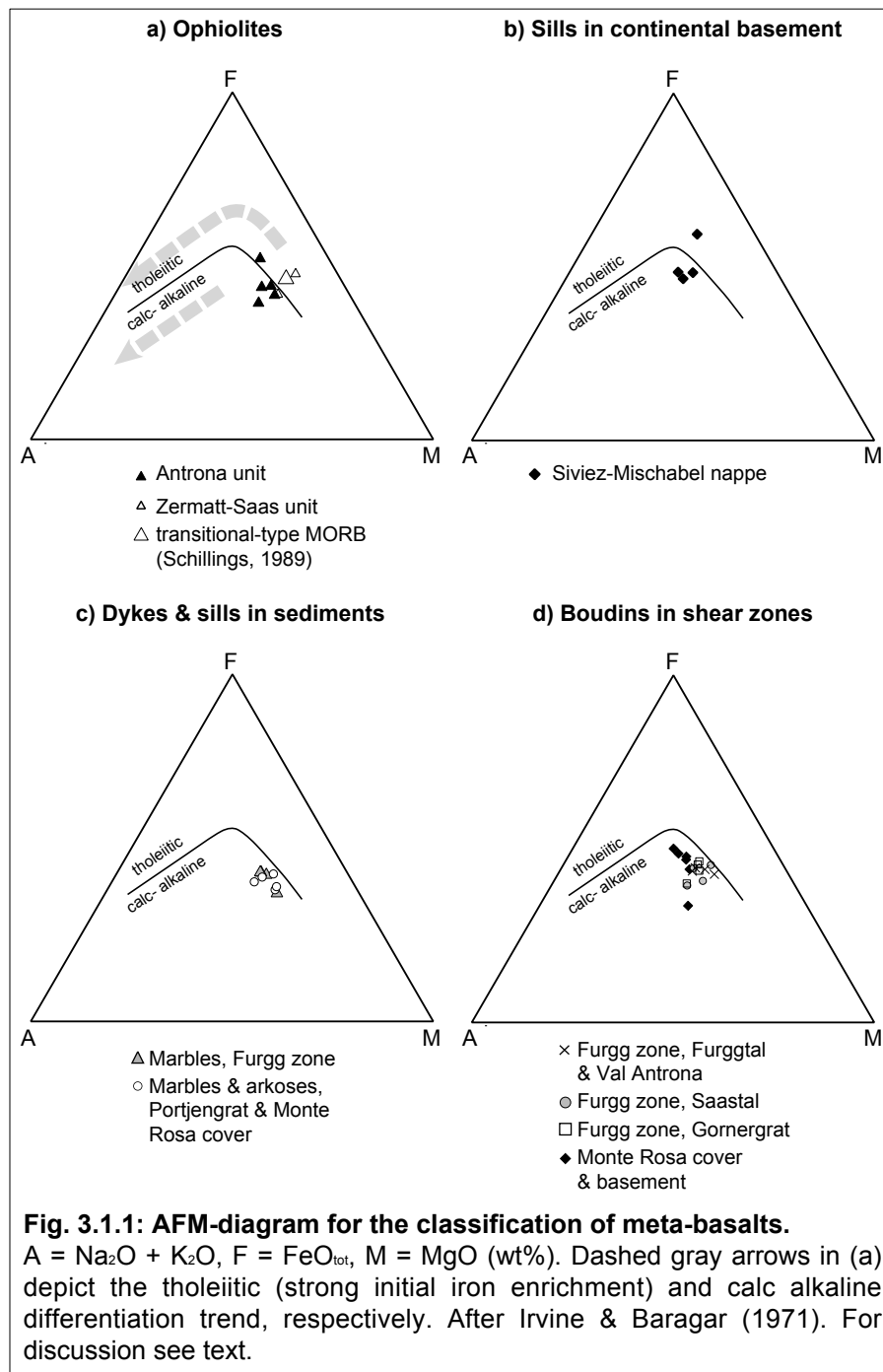
If the partial melt equilibrates with the residuum before being removed, and if the degree of partial melting is higher ("batch melting"), the first-formed melt will be diluted by the additional melt and will have a composition that is closer to the original composition of the source rock.

Fractional crystallisation

Similar processes operate during crystallisation from a magma: early-crystallizing minerals change the composition of the remaining melt. If these early-crystallizing phases are removed from the magma (i.e. by gravitational settling), they will leave a melt which is enriched in incompatible elements.

3.1.1 Fractionation of major elements

The first minerals crystallizing from a melt with tholeiitic basaltic composition are olivine, Mg-Cr-spinel and Ca-rich plagioclase, usually followed by augite and Fe-Ti-oxide (i.e. titanomagnetite). This gives rise to the typical tholeiitic differentiation trend represented by the curved line in the magmatic AFM diagram (Fig. 3.1.1). This trend is characterized by an initial iron-enrichment. With the



onset of the crystallisation of magnetite, the melt evolves towards alkali-rich and iron-/ magnesium-poor compositions. In contrast, generally higher H₂O activity and O₂ fugacity in environments producing calc-alkaline magmas account for a suppression of the iron enrichment and a straight differentiation trend towards alkali-rich, iron-/ magnesium-poor compositions.

In Fig. 3.1.1 c, d, and also - but less marked - in a, the samples (discussed in detail in ch. 3.2) exhibit an iron enrichment as it is typical for tholeiitic volcanic suites, although they lie in the field of calc-alkaline volcanics. Other discriminators, as for example the rare earth elements (REE, see Fig. 6 in ch. 3.2) or certain element ratios (e.g. Ti/Zr, Ce/Ni, Nb/Ni, see Figs. 4, 5, 8, 9 in ch. 3.2), however, unequivocally identify the samples as transitional-type tholeiitic basalts. A secondary metasomatic enrichment in alkalis is therefore considered to be responsible for the shift of samples towards the calc-alkaline field in the AFM diagram (see chapter

"metasomatism" below and section 5.2 in ch. 3.2). The AFM diagram, as well as other diagrams based on major elements (Fig. 3.1.2), will therefore be exhibited to explain possible trends in magmatic fractionation, but they have not been used to discriminate between the sampled meta-basaltic rocks.

Magnesium- iron ratio

The magnesium-iron ratio is another index of crystal fractionation in basaltic magmas (Oskarsson et al., 1982; Rollinson, 1993; Wilkinson, 1982). The iron-magnesium ratio can be expressed in several ways: as M-value ($M = 100Mg/(Mg+Fe^{2+})$) in atomic units if Fe²⁺ and Fe³⁺ are known; or as Mg number ($Mg\# = 100Mg/(Mg+\Sigma Fe)$), when Fe³⁺ is unknown or relatively small.

The latter value was chosen in this study, as the sample preparation for XRD analysis required the oxidation of all iron to Fe₂O₃. Total iron (ΣFe) was then recalculated as FeO using a ratio of FeO (wt%) = 0.8998 Fe₂O₃ (wt%). The factor 0.8998 is the molecular weight of Fe₂O₃ divided by

two times the molecular weight of FeO:

$$0.8998 = \frac{159.69 \text{ g/mol}}{2 \times 71.85 \text{ g/mol}}$$

Mg and Fe are expressed as cation equivalent calculated from the analytical value x of MgO or FeO, respectively, divided by the molecular weight of the oxide:

$$\text{cation equivalent Mg} = \frac{x(\text{wt}\%)}{40.31 \text{ g/mol}} \quad \text{and cation equivalent Fe} = \frac{x(\text{wt}\%)}{71.85 \text{ g/mol}}$$

Mg numbers for mantle peridotite are around 88. For basaltic melts in equilibrium with residual upper mantle source peridotites they are around 70 (Wilkinson, 1982).

Alkali-silica and alkali-aluminium ratios

Based on the alkali (Na_2O , K_2O) versus SiO_2 abundances (Fig. 3.1.2 A & B), volcanic rocks may be divided into two groups: the subalkalic and the alkalic group (Middlemost, 1975). Due to repeated processes of partial melting of the mantle source (see ch. 3.1.2, REE-patterns), tholeiitic MORB are highly depleted in large incompatible cations such as K^+ . Therefore they plot on the subalkalic or low-K subalkalic (tholeiitic) field of the diagrams. Magmas from oceanic islands and continental rift zones are generated by smaller degrees of partial melting from less depleted mantle sources. Therefore they are less depleted in large cations and plot on the alkalic field of the diagrams. Basalts that plot on the subalkalic or low-K subalkalic field in the K_2O versus SiO_2 diagram (Fig. 3.1.2 A), and on the alkalic field in the Na_2O versus SiO_2 diagram (Fig. 3.1.2 B) are referred to as transitional basalts (Middlemost, 1975).

The alkalic group is further subdivided into the high-potassic (high-K), potassic (K-) and the sodic (Na-) series in terms of K_2O versus Na_2O (Fig. 3.1.2 C). The subalkalic group is further subdivided into the tholeiitic and calc-alkalic series based on the Alkali Index $\text{A.I.} = \frac{\text{Na}_2\text{O} + \text{K}_2\text{O}}{0.17(\text{SiO}_2 - 43)}$ (in weight %) versus Al_2O_3 abundances (Fig. 3.1.2 D).

Sometimes low-K sub-alkalic basalts (tholeiites) from mid ocean ridges may plot in the calc-alkalic field on this diagram. This is usually explained by accumulation of plagioclase crystals (Wilson, 1989, p.9).

In summary, high K_2O abundances can be explained by enriched magma sources or small degrees of partial melting (Wilson, 1989, p. 302). Increasing K_2O along with increasing SiO_2 abundances can be explained by fractional crystallisation or crustal contamination.

As for the AFM diagram, all the diagrams in Fig. 3.1.2 are based on alkalis, which are considered to be prone to metasomatic reactions. Again they are shown for the explanation of the fractionation processes, but they have not been used for the discrimination of the sampled metabasalts.

Metasomatism

As major elements are essential for the stability of the rock forming minerals, they are involved in all major metamorphic reactions. This study deals with samples that may have been affected by ocean-floor metamorphism as well as by a later eclogite to greenschist facies metamorphic overprint. Whereas Al, Ti and P are generally regarded as immobile under ocean floor hydrothermal to amphibolite facies conditions, Ca and Na appear to be more mobile (Mottl, 1983; MacGeehan & MacLean, 1980; Pearce, 1976; Gelinis et al. 1982; Rollinson, 1983). At higher metamorphic conditions element mobility is generally not well constrained (Saunders, 1984; Pearce, 1982; Rollinson, 1993; Grauch, 1989 and references therein; Dostal & Capedri, 1979). The infiltration of meta-basalts with Na-rich fluids to form albite veins and Na-rich reaction seams in the Zermatt-Saas unit has been documented by Müller (1989) and can be observed throughout the investigated area. An enrichment in Na and the mobilisation of other incompatible major elements is therefore probable. As, however, the amount of in- or decrease of a specific major element could not be quantified, major elements were not used for a further discrimination in this study.

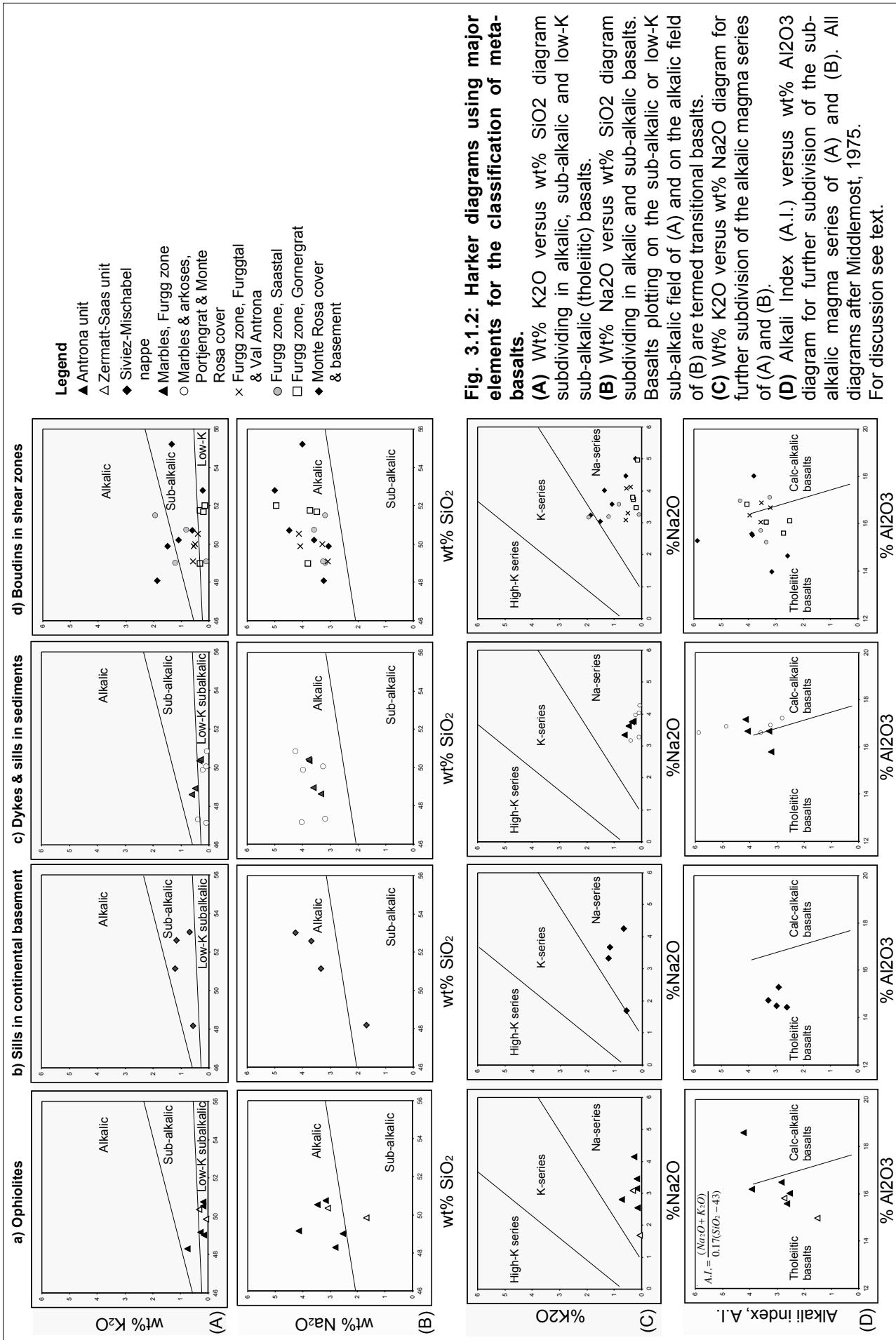


Fig. 3.1.2: Harker diagrams using major elements for the classification of metabasalts.

(A) Wt% K₂O versus wt% SiO₂ diagram subdividing in alkalic, sub-alkalic and low-K sub-alkalic (tholeiitic) basalts.

(B) Wt% Na₂O versus wt% SiO₂ diagram subdividing in alkalic and sub-alkalic basalts. Basalts plotting on the sub-alkalic or low-K sub-alkalic field of (A) and on the alkalic field of (B) are termed transitional basalts.

(C) Wt% K₂O versus wt% Na₂O diagram for further subdivision of the alkalic magma series of (A) and (B).

(D) Alkali Index (A.I.) versus wt% Al₂O₃ diagram for further subdivision of the sub-alkalic magma series of (A) and (B). All diagrams after Middlemost, 1975. For discussion see text.

3.1.2 Trace element fractionation

Unlike major elements, trace elements are not essential for the stability of the rock forming minerals, and thus they usually play a passive role during partial melting and fractional crystallisation. Nonetheless, their concentrations are systematically affected by the processes involved in magma generation. As the rare earth elements are usually immobile even during high grade metamorphic conditions (Humphris, 1984; Grauch, 1989; Pearce, 1983), they are particularly useful for the discrimination of the specific original magmatic processes and the geotectonic environment.

Rare earth elements (REE)

Because of their identical charge (trivalent, except for Eu, which can be divalent) and relatively similar ionic radii, chemical processes do not discriminate strongly between the various REE, and when there is discrimination, it varies systematically through the series. Europium is the only exception because of its ambivalent valence states. The combination of high charge and relatively large ionic radius make the REE incompatible in most early-crystallizing minerals. However, their K_D values vary slightly: the larger the ionic radius, the more incompatible is the element.

The stability of the atomic nuclei is dependent on their atomic number. Even-numbered REE are more stable and therefore more abundant than the adjacent odd-numbered ones. As this pattern of abundances is also found in chondritic meteorites, a normalization relative to chondritic meteorites has two effects: first, it eliminates the abundance variation between odd and even atomic number elements and second, it shows the overall enrichment of elements relative to the presumably primordial composition represented by the chondrite.

The enrichment of a specified REE relative to its abundance in a chondrite is mainly dependent on the degree of fractionated crystallisation and the nature of the early-crystallizing mineral. Early crystallizing clinopyroxene, garnet and amphibole, which are removed from the magma, produce a steep negative slope to the REE pattern of the remaining liquid in the chondrite-normalized plot, as the light rare earth elements (LREE) are highly incompatible with these minerals (Figs. 3.1.3 & 3.1.4). Orthopyroxene produces a similar pattern, but with a less steep negative slope. Early-crystallizing plagioclase under sufficiently reducing conditions removes Eu^{2+} from the liquid,

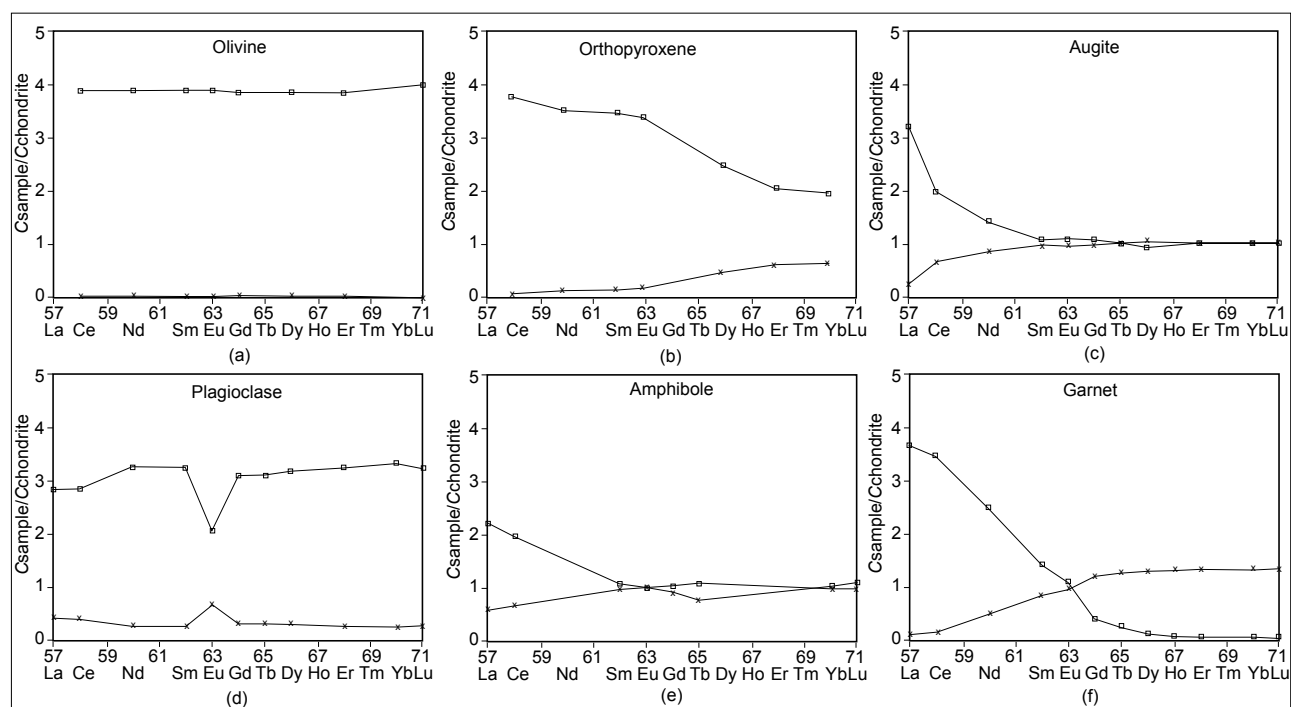
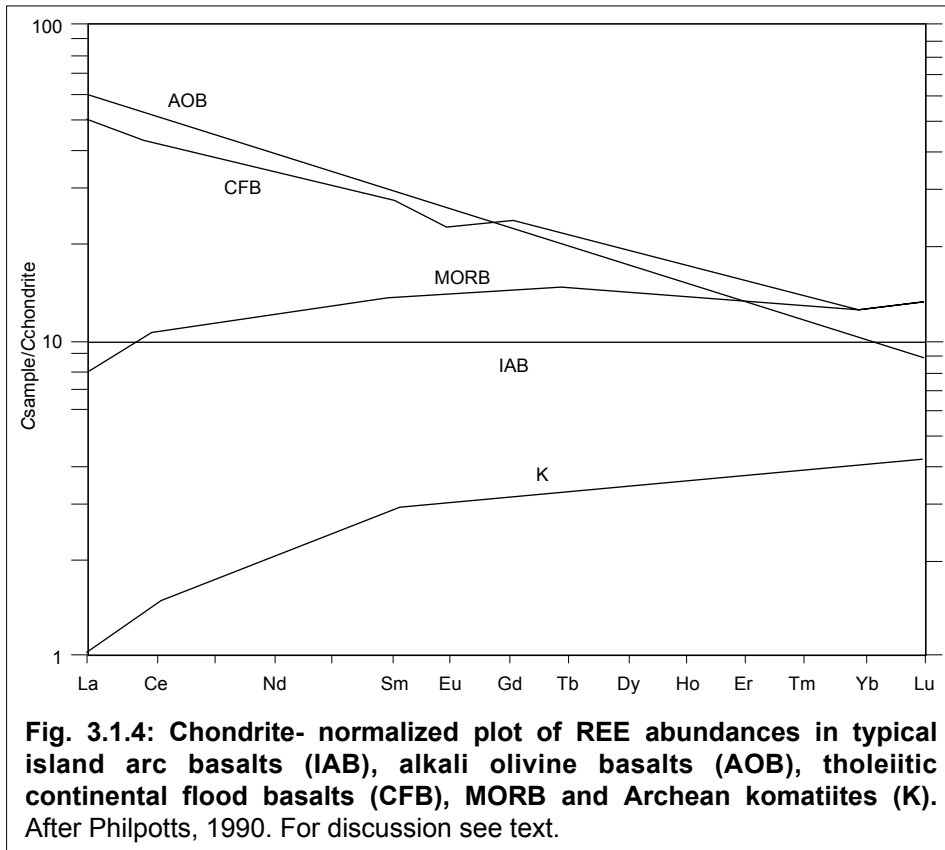


Fig. 3.1.3: Chondrite-normalized abundances of the rare earth elements partitioned between common mineral (crosses) and basaltic melt (squares) following 75% equilibrium crystallisation. The melt initially had a chondritic abundance of REE; that is, $c_{\text{sample}}/c_{\text{chondrite}} = 1$. After Philpotts, 1990. For discussion see text.



giving rise to a negative Eu anomaly of the remaining liquid (Drake & Weill, 1975). Accordingly, a positive Eu anomaly is considered to be derived from cumulus plagioclase. Early-crystallizing olivine produces a strong enrichment of REE in the liquid without differentiation between individual REE.

Mid ocean ridge basalts (MORB): normal, transitional and plume-type

The terms "normal", "transitional" and "plume"-type MORB in general refer to two key parameters in the generation of basaltic magmas: the degree of partial melting and the degree of depletion of the mantle source, from which the basaltic magma is derived. Normal MORB are the most common and most evolved magmas. They are generated by relatively high degrees of partial melting (20-30%) of a highly depleted mantle source. Plume-type MORB are the least evolved magmas and are generated by small degrees of partial melting of a primitive mantle source. Transitional MORB range inbetween those two and they are considered to be influenced by some enriched mantle source. The enrichment in REE relative to chondrite found in this study reaches 10-30 times for transitional MORB and up to 65 times for plume-type MORB (see Fig. 6, ch. 3.2).

Normal to transitional-type MORB REE-patterns

Normal- to transitional-type MORB are less enriched in LREE than in HREE. None of the common early-crystallizing minerals causes such an enrichment (Figs. 3.1.3 & 3.1.4). Fractional crystallization can, therefore, not be responsible for this pattern. However, partial melting of a source with a primordial composition containing augite gives rise to a magma enriched in LREE and leaves residual augite depleted in LREE. Subsequent melts derived from this depleted source will themselves be depleted in LREE. Normal MORB are therefore interpreted to stem from a mantle source that has been depleted in incompatible elements by earlier periods of melting. As the REE-pattern requires a garnet-free source, melts must derive from spinel or plagioclase lherzolite, hence melting occurs at shallow depths of less than 65 km. As the degree of partial melting due to steepened geothermal gradients, resulting from upward-convecting mantle, is moderately high (20-30%), incompatible elements that enter the first-formed liquid are diluted by the additional melt.

In contrast, transitional-type MORB exhibit a stronger overall enrichment in REE compared to normal-type MORB. This suggests a similar depleted mantle source, but with some influence of a

more enriched magma. Present-day transitional-type MORB are known from back-arc basins, young oceans developed from continental rifts or from hot spots (Pfeifer et al., 1989).

Plume-type MORB (p-MORB) REE-patterns

Plume-type MORB show a strong enrichment in LREE and a negative slope of the REE-pattern. This could result from high degrees of fractional crystallization, but commonly high magnesium numbers and consistent REE-patterns argue against such an origin. Instead, the high enrichment is interpreted to result from very small degrees of partial melting in a source region where garnet is likely to be a stable phase. This is the case in the stability field of garnet lherzolite at depths greater than 65 km. Plume-type MORB REE-patterns are expected where the convecting mantle rises beneath a continent prior to its rifting to form ocean floor, or above rising hot spots, where geothermal gradients are not as steep as those found beneath mid ocean ridges. Melting occurs at greater depth and involves a smaller degree of partial melting. This gives rise to alkaline magmas with a higher concentration of incompatible elements.

3.2 Geochemistry of metabasalts from ophiolitic and adjacent distal continental margin units: Evidence from the Monte Rosa region (Swiss and Italian Alps)

Julia Kramer^{*1}, Rainer Abart¹, Othmar Müntener², Stefan M. Schmid¹, Willem-B. Stern¹.

¹Department of Earth Sciences, University of Basel, Bernoullistr. 32, CH-4056 Basel

²Department of Earth Sciences, University of Neuchâtel, Rue Emile Argand 11, CH-2007 Neuchâtel

* corresponding author: Julia.Kramer@unibas.ch, Tel.: 061-267 36 07, Fax: 061-267 36 13

Abstract

In this paper we present new whole rock analyses of amphibolites from the ophiolitic and adjacent continental tectonic units in the Monte Rosa region. Mg numbers and Ni contents indicate that these amphibolites were derived from fractionated magmas with compositions ranging from E- to N-MORB. Based on their Ni, Ti, REE and Nb systematics, the metabasalts from the ophiolitic Zermatt-Saas and Antrona units and from the continental units of the Furgg zone and the Portjengrat are ascribed to a common origin. They represent a coherent suite ranging from T- to N-MORB. In contrast, amphibolites from the continental Siviez-Mischabel and Monte Rosa nappes were derived from enriched MORB and/or gabbroic precursors, which are not related to the metabasalts from the ophiolites, the Furgg zone or the Portjengrat unit.

The geochemical differences between the basalts of the ophiolitic Zermatt-Saas and Antrona units and the adjacent continental Furgg zone and the Portjengrat unit are very subtle. Most mafic rocks were derived from low to moderate degrees of melting of an N-MORB type mantle source. Some compositional parameters such as $(\text{Ce}/\text{Sm})_n$, Zr^* and $(\text{Nb}/\text{Zr})_n$ indicate a transition from T-MORB compositions in the continental units towards less enriched compositions in the ophiolitic units. Y, Ti, V and Zr concentrations are highly correlated in the metabasalts from the Furgg zone, whereas such inter-element correlations are less well defined in the metabasalts from the ophiolitic units. This renders the previously proposed interpretation of the Furgg zone amphibolites as tectonically incorporated ophiolitic fragments unlikely. Our data rather suggest that the distal continental units (Portjengrat unit and Furgg zone) and the nearby ophiolitic units were intruded by similar magmas. Portjengrat unit and Furgg zone are interpreted as a formerly continuous tectonic unit which, based on structural grounds, represents the ocean-continent transition zone of the Briançonnais to the immediately adjacent oceanic Antrona unit. However, the ambiguity in the paleogeographic provenance of the Antrona unit (Valais vs. Piemont-Liguria ocean) cannot be resolved with the existing geochemical data.

Key words: Metabasalt, geochemistry, continental crust, Furgg zone, Monte Rosa, Central-Western Alps

1 Introduction

The Western Alpine Arc is characterized by the occurrence of remnants of different Mesozoic oceanic basins (e.g. Stampfli and Marchant 1997 and references therein, Schmid and Kissling 2000). In the Penninic nappe edifice of the Monte Rosa region, the Zermatt-Saas and the Antrona ophiolitic units represent the remnants of oceanic crust. They are sandwiched between several slivers of continental crust, which pertain to the Monte Rosa and Siviez-Mischabel nappes, and to the Portjengrat and Stockhorn units (Escher et al. 1997). The situation is illustrated in a schematic geological sketch map of the Monte Rosa region (Fig. 1) and in a simplified N-S cross-section (Fig. 2).

The paleogeographic relations were obscured in the course of polyphase Tertiary deformation. NW-directed nappe stacking started in Eocene times under eclogite facies conditions (deformation phases D1 and D2). This was immediately followed by exhumation during ongoing crustal shortening. Post-collisional SE-directed folding and oblique thrusting of the entire nappe pile (deformation phases D3 and D4) finally resulted in the complex present-day geometry (Figs. 1 and 2).

The paleotectonic reconstruction of the Monte Rosa region is still under discussion (Escher et al. 1997, Froitzheim 2001, Keller and Schmid 2001, Kramer 2002). Controversies partially arise from the interpretation of mafic dykes and boudins, which occur within continental units and which possibly represent derivatives from former oceanic domains. In the Monte Rosa region, mafic dykes and boudins are abundant in both the continental and ophiolitic tectonic units, and they occur in Paleozoic continental crystalline crust, as well as in Mesozoic cover sequences. Mafic boudins are particularly abundant in two mylonitic shear zones that overprint the nappe contacts between continental and ophiolitic tectonic units: (1) in the so-called "Furgg zone" and (2) in the "intensely strained Monte Rosa basement and cover" (Figs. 1 and 2; Kramer 2002). Due to the abundant mafic boudins, Froitzheim et al. (2001) interpreted the Furgg zone as a tectonic mélange with ophiolitic fragments. Other authors, however, considered the mafic boudins as dyke intrusions into continental

lithosphere (e.g. Jaboyedoff et al. 1996), and the Furgg zone as an intracontinental shear zone (Escher et al. 1997, Keller and Schmid 2001, Kramer 2002).

In this paper we present new whole rock major and trace element data on mafic rocks collected in (1) the Furgg zone, (2) the adjacent continental Portjengrat unit and in the Monte Rosa and Siviez-Mischabel nappes as well as (3) in the ophiolitic Zermatt-Saas and Antrona units. Our own and

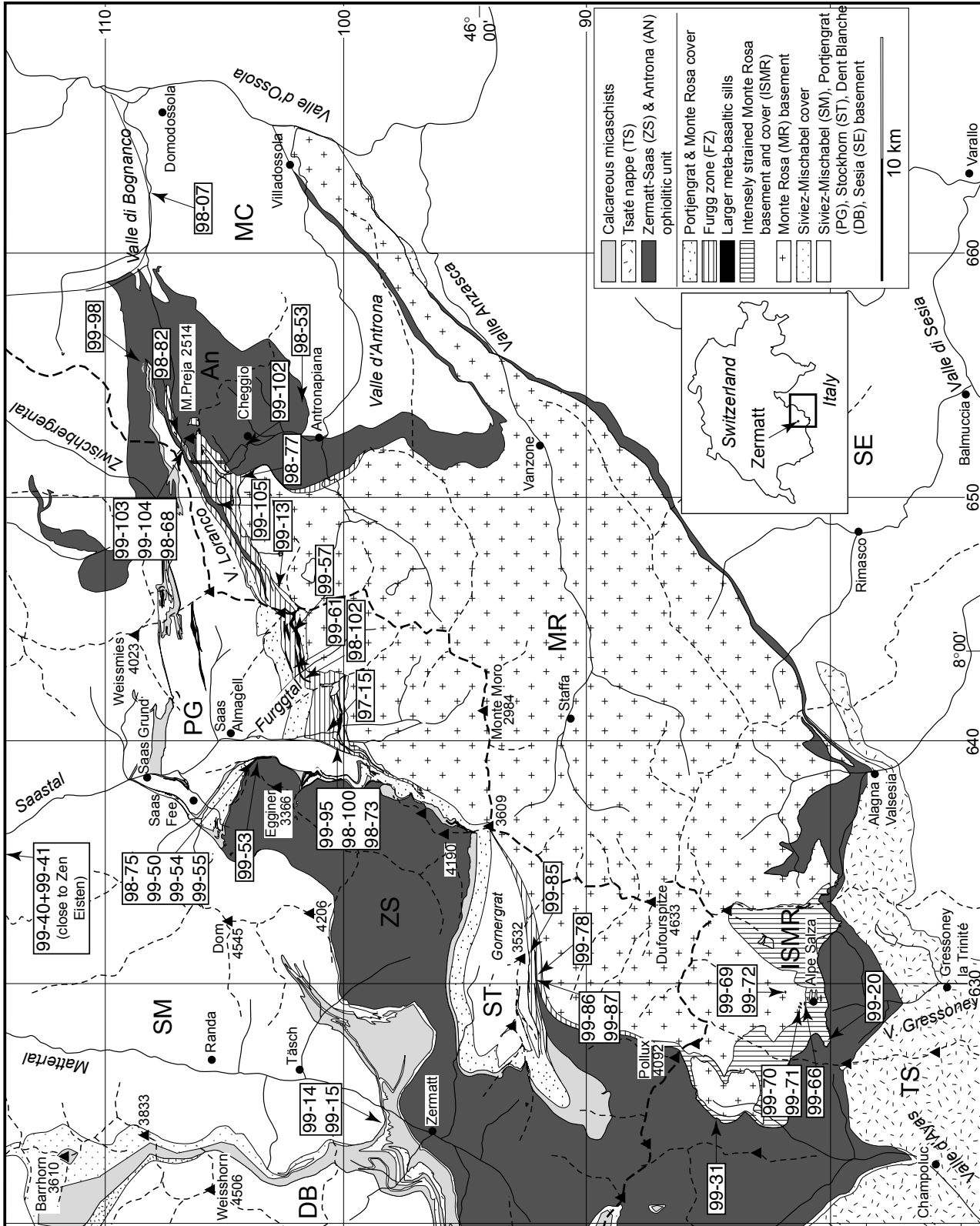
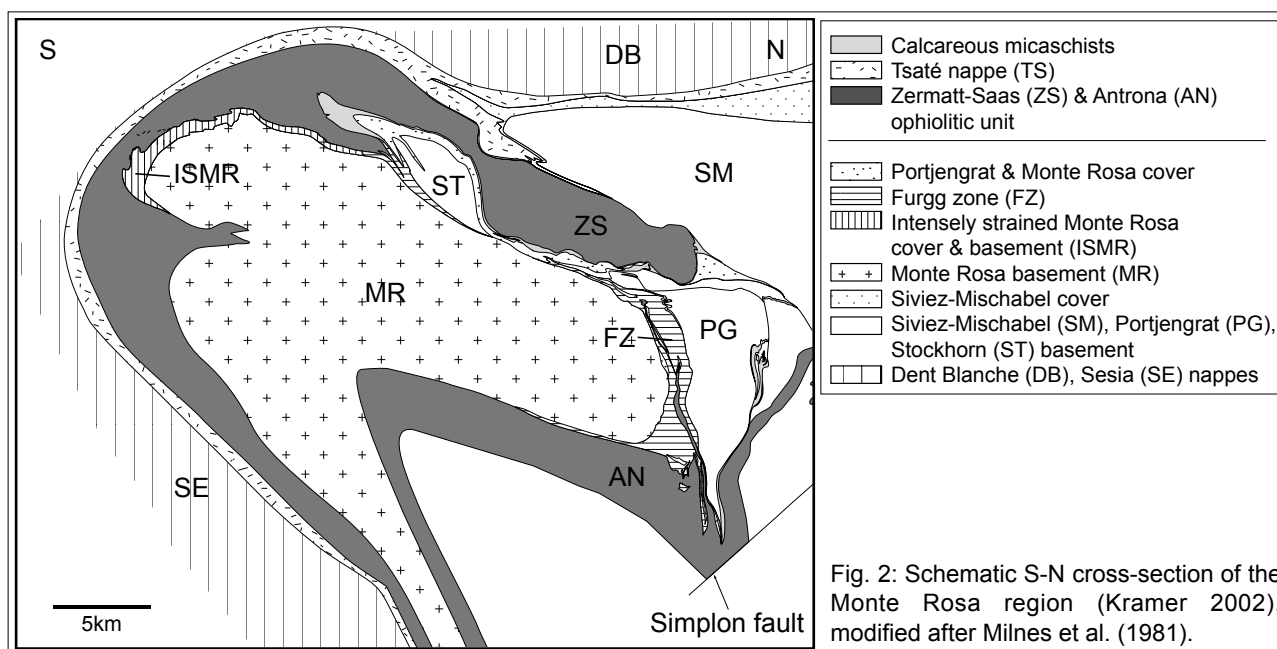


Fig. 1: Sample locations in a simplified geological sketch map of the Monte Rosa region, compiled from Dubach (1998), Keller (2000), Rössler (2000), Weber (2001), Bacher (2002), Bearth (1953a, 1954 a, b), Steck et al. (1999), and mapping by Kramer (2002).

previously published data (Beccaluva et al. 1984, Pfeifer et al. 1989) shed light on magma sources and evolution, and on the paleogeographic relations among the tectonic units in the Monte Rosa region.



2 Geological setting

The Monte Rosa nappe forms the “backbone” of the Penninic nappe edifice west of the Lepontine dome. It is comprised of large masses of Permian granitoids and orthogneisses, which were derived from granitoid intrusions (Frey et al. 1976). These granitoids were emplaced into pre-Permian, primarily meta-pelitic paragneisses with subordinate mafic rocks (Hunziker 1970). The present-day geometry of the Monte Rosa nappe is largely controlled by a large-scale SSE-facing D4 fold, referred to as “Vanzone backfold” by Milnes et al. (1981) and Escher et al. (1988, 1997). The ophiolitic Zermatt-Saas and Antrona units form an almost complete envelope around the continental Monte Rosa nappe, except for the area between Gornergrat and Monte della Preja, where only isolated slivers of ophiolites are present (Fig. 1).

The Furgg zone (FZ in Figs. 1 and 2) and the intensely strained Monte Rosa cover and basement (ISMR in Figs. 1 and 2) represent up to one km thick mylonitic shear zones found north and south of the Monte Rosa main crest, respectively. They overprinted basement-cover contacts of the continental tectonic units, as well as nappe contacts between ophiolitic and continental tectonic units during WNW-directed nappe stacking (deformation phases D1 and D2; Kramer 2002). Mylonitic shearing resulted in the superposition of two phases of isoclinal and/or sheath folding affecting the nappe contacts between Zermatt-Saas unit and Monte Rosa nappe in case of the ISMR, and between Portjengrat and Stockhorn unit, Monte Rosa nappe and Antrona unit in case of the FZ, respectively (see Fig. 2; Kramer 2002).

Subsequent reactivation of the Furgg zone during syn-D3 and syn-D4 shearing partly led to the imbrication of isoclinal D1 and D2 folds, now forming isolated fold cores that consist of a variety of rocks of different provenance which are embedded within a highly strained matrix. D3 and D4 deformation also accounted for large-scale SE-directed folding and dextral oblique thrusting (e.g. Keller and Schmid 2001, Kramer 2002), in the course of which both the Furgg zone and the intensely strained Monte Rosa and cover were tilted into their present-day structural position enveloping the Monte Rosa nappe.

Several larger coherent imbricates of ultramafic and mafic rocks represent mappable units and were therefore not regarded as part of the Furgg zone, but assigned to the Zermatt-Saas (at Gornergrat) and the Antrona units (at Monte della Preja and in Furggtal), respectively. On structural grounds the numerous smaller mafic boudins found in both Furgg zone and intensely strained Monte

Rosa basement and cover, however, are considered as intrusions of former dykes and sills into continental lithosphere, that were overprinted by mylonitic shearing later. Hence, these mafic boudins are regarded as part of both shear zones (FZ and ISMR) overprinting continental tectonic units. It is one of the aims of this publication to test this structural interpretation by adding geochemical data. Note that our structural interpretation differs from the view of Froitzheim (2001), who considers both the large imbricates of ultramafics and the small mafic boudins as ophiolitic imbricates and defines the Furgg zone as an ophiolitic subduction mélange (Froitzheim 2001).

The intensely strained Monte Rosa basement and cover on the southern side of the Monte Rosa massif (ISMR) was, however, not reactivated during D3 and D4 shearing. There, syn-D1- and D2-shearing mainly resulted in a complex superposition of two mylonitic folding phases on basement and cover of the Monte Rosa nappe. Because of the abundant occurrence of mafic boudins in a highly strained matrix, the ISMR strongly resembles the Furgg zone in the field. However, the two shear zones differ in respect to their tectonic significance, and, as will be shown, also geochemically. Therefore, we distinguish between these two shear zones, although some authors consider the ISMR as part of the FZ (Dal Piaz 1964, Froitzheim 2001). In the following we will treat the ISMR as part of the Monte Rosa nappe.

The Portjengrat unit, as well as its southern equivalent, the Stockhorn unit, consists of continental basement and a cover series interpreted to represent Permo-Triassic sediments. The Portjengrat unit is either interpreted as part of the Grand St. Bernhard nappe system (e.g. Bearth 1956) or as a derivative of the Monte Rosa nappe (e.g. Bearth 1957, Keller and Schmid 2001). The Siviez-Mischabel nappe forms the central part of the Grand St. Bernhard nappe system. Whereas its cover comprises only Permo-Triassic rocks in most parts of the region, a complete sedimentary sequence of up to Eocene age is preserved in the "Barrhorn series" in Matteredal (Sartori 1987, 1990). Since the mafic rocks that were analysed in this study were sampled in the Furgg zone, the ophiolitic Zermatt-Saas and Antrona units, the continental Monte Rosa and Siviez-Mischabel nappes, as well as in the continental Portjengrat unit, these units will be described here in more detail.

2.1 Furgg zone

The Furgg zone comprises the following rock types derived from the neighbouring tectonic units (Monte Rosa nappe and Portjengrat – Stockhorn unit): para- and orthogneisses of Paleozoic age, along with the adjoining meta-sedimentary cover consisting of garnet micaschists, meta-arkoses, quartzites, and marbles of inferred Permo-Triassic age (Bearth 1954 a, b, 1957; Klein 1978; Jaboyedoff et al. 1996; Rössler 2000; Keller and Schmid 2001; Bacher 2002; Kramer 2002). The abundant mafic intercalations, which typically take the form of disrupted layers and boudins are a remarkable feature of the Furgg zone. In some places these mafics represent more than 50 % of the rock volume on outcrop scale. In some of the mafic boudins, eclogitic assemblages are preserved (Wetzel 1972, Liati et al. 2001). As described in the previous section, several larger coherent slivers comprising ultramafics and mafics were mapped as ophiolitic imbricates derived from the Zermatt-Saas or the Antrona ophiolitic unit, and not as part of the Furgg zone (Keller and Schmid 2001, Bacher 2002, Kramer 2002). Between Gornergrat and Monte della Preja (Fig. 1), the Furgg zone overprints the nappe contacts of the Monte Rosa nappe with the Stockhorn and Portjengrat units, respectively (Bearth 1953 a, b, 1954 b, 1957; Escher and Sartori 1991; Escher et al. 1997).

Within less deformed portions of the Furgg zone rock types with a stratigraphy similar to that of the Permo-Triassic meta-sediments in the adjacent Portjengrat – Stockhorn unit and Monte Rosa nappe were mapped (Jaboyedoff et al. 1996, Keller and Schmid 2001, Bacher 2002, Kramer 2002). Such a stratigraphic sequence is particularly well preserved in the Passo della Preja area (Fig. 1), where Triassic dolomite and calcite marbles are associated with rauhwackes, quartzites, and meta-arkoses. These Triassic marbles were intruded by well preserved mafic dykes (see Fig. 5 in Jaboyedoff et al. 1996), which were collected for chemical analysis ("F4: Furgg zone marbles" in Tab. 1).

2.2 Zermatt-Saas ophiolitic unit

The Zermatt-Saas unit largely consists of metamorphosed ultramafic and mafic rocks (Bearth and Stern 1971, 1979; Pfeifer et al. 1989) with a late Jurassic formation age (166-160 Ma,

Gebauer 1999). The associated meta-sediments are manganese-rich quartzites (meta-radiolarites), marbles and calcareous micaschists ("Bündnerschiefer" or "schistes lustrés"; Bearth 1976, Bearth and Schwander 1981) of probably late Jurassic to late Cretaceous age (Marthaler 1981, 1984). The calcareous micaschists may contain meta-basalt boudins. High-pressure peak metamorphic conditions of 2.6 - 2.8 GPa and 590 - 630° C are recorded by meta-radiolarites (Reinecke 1991, 1998; van der Klauw et al. 1997) while conditions of 1.75 - 2.0 GPa and 550 - 600° C are reported from the ophiolites (Barnicoat and Fry 1986). Peak metamorphic conditions were reached during the Middle Eocene, i.e. at 44 Ma (Amato et al. 1999, Rubatto and Gebauer 1999, Gebauer 1999) while the retrograde greenschist facies overprint occurred during the early Oligocene (Müller 1989, Barnicoat et al. 1995, Gebauer 1999).

2.3 Antrona ophiolitic unit

The Antrona unit consists of metamorphosed ultramafic and mafic rocks and associated marbles and calcareous micaschists (Carrupt and Schlup 1998, Colombi 1989, Pfeifer et al. 1989). So far, no radiometric formation ages have been reported for the meta-basic rocks. Recently discovered eclogites (Keller, pers. comm.) probably represent the remnants of a high-pressure metamorphic event. Engi et al. (2001) related the peak metamorphic conditions found within the eastern Monte Rosa nappe to the emplacement of this nappe into the surrounding units at 35-40 Ma ago, hence the high pressure metamorphic peak within the adjacent Antrona unit might fall into the same time span. The Oligocene retrograde greenschist facies overprint as a result of the exhumation of the nappe pile, and a prograde amphibolite facies metamorphic overprint in the area of the Lepontine dome were described by Pfeifer et al. (1989) and by Colombi (1989).

2.4 Monte Rosa nappe

The basement of the Monte Rosa nappe consists of pre-Carboniferous paragneisses and calc silicate rocks (Bearth 1952, 1954 a, b, 1957; Dal Piaz 1966, 1971; Escher et al. 1997), which were intruded by late Carboniferous to Permian granites (310 - 260 Ma; Hunziker 1970, Frey and Hunziker 1976, Engi et al. 2001). Peak metamorphic conditions of 2.3 GPa and 520° C were inferred from white schists within the Monte Rosa basement (Le Bayon et al. 2001) and dated at 35 - 40 Ma (Hunziker 1970, Gebauer 1999).

Meta-sedimentary strata of inferred Permo-Triassic age are rare, but partly preserved in upper Valle d'Ayas, Valle di Gressoney and Valle di Loranco (Keller 2000, Kramer 2002). These meta-sediments consist of garnet micaschists, meta-arkoses and quartzites as well as calcite and dolomite marbles. They contain numerous mafic layers and boudins. These meta-sediments are similar to the Permo-Triassic cover of the Portjengrat unit. Yet, they were interpreted as Paleozoic in age by Dal Piaz (1966, 2001). With respect to their spectrum of rock types, boudin-rich parts of the Monte Rosa basement and its meta-sedimentary cover are rather similar to the Furgg zone and referred to as "intensely strained Monte Rosa cover and basement" (ISMR) in Fig. 1.

2.5 Siviez-Mischabel nappe

The Siviez-Mischabel nappe consists of a Paleozoic polymetamorphic basement (Bearth 1945, Thélin et al. 1993, Escher et al. 1997) and its relatively well-preserved Permo-Mesozoic cover (i.e. Barrhorn series; Marthaler 1984, Sartori 1990). In contrast to all the other tectonic units described in this contribution, no eclogite facies event is documented. Nappe emplacement occurred under greenschist facies conditions, estimated at 350° - 450° C and 0.4 - 0.6 GPa by Sartori (1990) in late Eocene times (Markley et al. 1998). The basement rocks contain numerous mafic layers and boudins (see Thélin et al. 1990, Eisele et al. 1997).

2.6 Portjengrat and Stockhorn units

The Portjengrat unit comprises basement of Paleozoic age, consisting of calc-silicates, paragneisses and orthogneisses (Huang 1935 a, b; Bearth 1945; Escher et al. 1997) and a cover of presumed Permo-Mesozoic age (Dubach 1998). Both basement and Permo-Triassic cover contain numerous mafic layers and boudins. In Valle di Loranco, the abundance of mafic layers and boudins, as well as strain intensity, gradually increase towards the Furgg zone (Keller and Schmid

2001). This is one of the reasons, why we regard the Furgg zone as a shear zone that overprints continental crust, in this case the Portjengrat unit (see Kramer 2002). Note, however, that further west (in Furggtal and Saastal), the basement of the Portjengrat unit contains far fewer mafic dykes and boudins (Rössler 2000, Weber 2001, Bacher 2002).

The cover of the Portjengrat unit, which is well preserved e.g. at the Mittaghorn in Saastal and at the Zwischbergen pass in Almagellertal - Zwischbergental (Huang 1935 a, b; Bearth 1954 b, 1957; Dubach 1998) consists of a sequence of garnet micaschists, meta-conglomerates, meta-arkoses, quartzites, marbles, and rauhwackes. Boudinaged meta-basalt layers are oriented parallel to the main foliation. As the metasediments of presumed Permo-Triassic age have been continuously traced all the way to Gornergrat in Matteredal, the Portjengrat and Stockhorn units are correlated (Kramer 2002). Near the Stockhorn at Gornergrat, a prograde eclogite facies mineral assemblage of early Oligocene age (34.9 ± 1.4 Ma) is preserved in Permo-Mesozoic quartzites ("Gornergrat series") for which conditions of $P < 1.4 - 1.5$ GPa, $T < 500 - 550^\circ$ C were estimated by Rubatto and Gebauer (1999).

3 Sample descriptions

Metabasalts sampled for geochemical analysis were taken from the Furgg zone and all adjacent units described above. Sample localities are shown in Fig. 1 and brief sample descriptions are listed in Tab. 1. Based on their lithologic-tectonic setting, the metabasalts are divided into 9 classes. These classes may be grouped into three broad categories: (1) metabasalts from ophiolitic units (Antrona and Zermatt-Saas units); (2) mafic sills, dykes and boudins, found within continental basement and associated meta-sedimentary cover series (Siviez-Mischabel nappe, Portjengrat-Stockhorn unit and Monte Rosa nappe); (3) metabasalts from the Furgg zone.

3.1 Metabasalts from the Antrona ophiolitic unit (O1)

Three samples were taken from the main body of the Antrona unit (sample 99-98 near Alpe Varallo in Valle di Bognanco; sample 99-102 at Cavalli lake in Valle d'Antrona), one of them close to the contact with the Moncucco-Camughera unit (sample 98-53; Antronapiana in Valle d'Antrona). A large coherent imbricate of the Antrona unit, situated near the Simplon shear zone, was sampled at San Marco in Valle d'Antrona (sample 98-07). The "Loranco-Lappen" (Bearth 1954 b, 1957) was sampled close to Alpe Campolamana in Valle di Loranco (sample 99-105). Here the Antrona ophiolites occur within the core of an isoclinal antiform (Kramer 2002), which refolds a mappable tectonic contact between Antrona unit and Furgg zone (Keller 2000, Bacher 2002).

3.2 Metabasalts from the Zermatt-Saas ophiolitic unit (O2)

The Zermatt-Saas unit was sampled close to the contact with the Portjengrat-Stockhorn unit (sample 99-53 from Mittaghorn in Saastal) and with the Monte Rosa nappe (sample 99-31 from Rifugio Mezzalama in Valle d'Ayas), respectively. Sample 99-53 stems from the northern limb of the D3 Mittaghorn synform, 50 m south of the contact with the calcareous micaschists. Sample 99-31 was collected ten meters west of the contact with the highly strained sedimentary cover of the Monte Rosa nappe.

3.3 Meta-basalt sills from the continental basement of the Siviez-Mischabel nappe (C1)

Samples were taken at localities in Matteredal and Saastal. The sampling sites are structurally located in the core of the D3 "Mischabel backfold", a south-facing kilometer-scale antiform. Samples 99-14 and 99-15 (near Zermatt in Matteredal) were collected approximately 60 m north of the basement-cover contact. Samples 99-40 and 99-41 (near Zen Eisten in Saastal) were collected within basement far off any tectonic or sedimentary contact. All samples stem from up to 1.5 m thick, partly boudinaged and/or isoclinally folded foliation-parallel layers. They are interpreted as early (pre-Alpine?) sills, which intruded the paragneisses of the Siviez-Mischabel nappe and were boudinaged and folded during subsequent deformation.

3.4 Isolated meta-basalt boudins from basement and cover of the southwestern Monte Rosa nappe (C2)

This group comprises samples from the intensely strained Monte Rosa cover and basement in the southwestern part of the Monte Rosa massif (ISMR), which was considered as part of the Furgg zone by some authors (i.e. Dal Piaz 1964, Froitzheim 2001). Meta-basalt boudins frequently occur in paragneisses whereas they are scarce in meta-granites. Since one of the metabasalt boudins was found to be intruded by a granite of supposed late Paleozoic age (Kramer 2002) near the Mezzalama refuge in upper Valle d'AYas, at least some of these boudins are probably Paleozoic in age. Furthermore, paragneisses occasionally contain pre-Alpine sillimanite, oriented parallel to the foliation and the principal extension direction of the embedded mafic boudins (Dal Piaz 1966, 1971). This also suggests a Paleozoic age for these metabasalts. Since mafic boudins are abundant within paragneisses of the Monte Rosa nappe, and particularly so near the tectonic contact with the Zermatt-Saas unit, field evidence does not allow us to exclude the possibility that they may represent ophiolitic imbricates incorporated during nappe stacking .

Metabasalts from this group were sampled in Valle di Gressoney at the Alpe Bettolina (sample 99-20) and at the Plateau del Lys (samples 99-66, 99-69, 99-70, 99-71, 99-72). The Bettolina sample (99-20) stems from a 0.3 m thick boudin, whereas sample 99-69 stems from a large imbricate of approximately 25 by 12 meters in size. The other samples were collected from 3 m thick boudins. Except for sample 99-66, all sampled boudins occur in a matrix of garnet micaschists, which are believed to represent Permo-Mesozoic cover. Sample 99-66 occurs in an intensely strained matrix of isoclinally folded orthogneisses, garnet micaschists and meta-arkoses. As the sample localities are structurally situated in the flat hinge region of the D4 Vanzone antiform, the distance to the nappe contact of the overlying Zermatt-Saas unit, as inferred from cross-section (Kramer 2002), is probably less than 100 meters. Hence the boudins could also represent tectonically incorporated ophiolitic imbricates.

3.5 Meta-basalt sills from the Permo-Triassic cover of the Portjengrat-Stockhorn unit and northern Monte Rosa nappe (C3)

This group of samples comprises meta-basalt occurrences, which represent intrusions into Permo-Triassic country rocks, for which *mélange* formation can be excluded. Metabasalts taken from the cover of the Portjengrat-Stockhorn unit were sampled in tectonically relatively undisturbed meta-arkoses and marbles below the Mittaghorn in Saastal (samples 98-75, 99-50, 99-54, 99-55). The samples were collected from 0.6 to 1 m thick, partly boudinaged foliation-parallel layers, interpreted as sills or parallelized dykes.

One amphibolite was collected from the Monte Rosa unit in Valle di Loranco, i.e. from an approximately 3 m thick, boudinaged foliation-parallel layer, found in carbonate-bearing meta-arkoses of inferred Permo-Triassic age (sample 99-13 at Bottarello glacier).

3.6 Metabasalts from the Furgg zone at Gornergrat (F1)

Here the Furgg zone consists of an association of paragneisses and calc silicates of supposed Paleozoic age and a cover sequence, including garnet micaschists, meta-arkoses, quartzites and calcite-dolomite marbles of inferred Permo-Triassic age. The meta-basalt samples from this part of the Furgg zone were collected in the Stockchnubel area (samples 99-78, 99-86, 99-87) and east of P. 3223 (sample 99-85; see Tab. 1 for exact location). Sample 99-78 was collected from an approximately 30 by 10 m large boudin, while the other samples are from smaller boudins up to 1 m in thickness. The boudins in the vicinity of the Stockchnubel are embedded in a matrix of garnet micaschists and quartzites; the sample east of P. 3223 (sample 99-85) is surrounded by a matrix of dolomite marble.

3.7 Metabasalts from the Furgg zone in Saastal (F2)

Here the Furgg zone consists of an assemblage of highly strained, fine-grained orthogneisses and the presumed Permo-Triassic cover of garnet micaschists and subordinate meta-arkoses (see Bearth 1954 b, 1957; Rössler 2000; Weber 2001). It contains metabasalts, which were sampled near the Allalin glacier (samples 98-73, 98-100, 99-95) and at the river Saaser Vispa (sample 97-15).

Samples from the Allalin glacier area were collected from two up to 0.5 m thick boudins (samples 98-73 and 98-100) and one 3 m thick boudin (sample 99-95), all embedded in garnet micaschists and meta-arkoses. Sample 97-15 (river Saaser Vispa) was collected from a 0.8 m thick boudinaged layer embedded in meta-arkoses.

3.8 Metabasalts from the Furgg zone in Furggtal and in Valle d'Antrona (F3)

Here the Furgg zone mostly comprises the same lithologies as described for Saastal. However, in Valle d'Antrona quartzites occur less and marbles more frequently in the Furgg zone. Mafic boudins are particularly abundant, and some of them are several tens of meters long.

Metabasalts from Furggtal were collected from up to 1.5 m thick boudins embedded in a matrix of meta-arkoses (sample 99-57), garnet micaschists (sample 98-102) and orthogneisses (sample 99-61). The meta-arkoses are intercalated with garnet micaschists, at least partly due to isoclinal folding. One meta-basalt sample collected from Valle d'Antrona (sample 98-77 from west of Lake Cavalli) stems from a 1 m thick boudin in a matrix of garnet micaschists. It was collected 100 m east of and structurally below the contact to the basement of the Monte Rosa nappe.

3.9 Dykes and sills in marbles of the Furgg zone (F4)

This group of Furgg zone samples comprises metabasalts found in marbles of the Furgg zone in the Monte della Preja area. Samples stem from Alpe Preja (sample 98-82) and from the core of a synform at the Passo della Preja between Valle di Loranco and Valle di Bognanco (samples 98-68, 99-103, 99-104). Here the metabasalts may readily be interpreted as representing sills or parallelized dykes, which intruded Triassic marbles.

The post-Triassic intrusion age is particularly evident for sample 99-104, which was collected from a 0.3 m thick discordant dyke described by Jaboyedoff et al. (1996, see her Fig. 5), obviously post-dating the Triassic marbles. Samples 98-82 and 98-68 were collected from 0.8 - 1.5 m thick foliation-parallel boudins, sample 99-103 from a 0.6 m thick foliation-parallel layer.

4 Mineralogical composition of metabasalts

All samples are fine-grained, foliated amphibolites, with a grain size of generally less than 2 mm. Mineral parageneses (see Tab. 1) include yellow and green actinolitic hornblende (act), albitic plagioclase (ab), clinozoisite (cz), zoisite (zo), epidote (ep), chlorite (chl), white mica (wm) and titanite (ttn) +/- biotite (bt). This assemblage is interpreted to have formed during retrograde greenschist facies overprint. Accessory minerals are rutile (rt), ilmenite (ilm), +/- hematite (hem), +/- pyrite (py), +/- zircon (zr), +/- quartz (qtz), +/- calcite (cc).

Relics of an earlier high-pressure metamorphic event could only be identified in amphibolites collected from the Permo-Mesozoic sedimentary cover of the Portjengrat-Stockhorn unit and the Monte Rosa nappe, where abundant garnet is found. This garnet is partly retrogressed to blue-green hornblende and/ or chlorite. Wetzel (1972) and Liati et al. (2001) also describe relics of high-pressure assemblages within amphibolites of the Furgg zone (see below). Two generations of albitic plagioclase and actinolitic hornblende are common. A first generation of plagioclase and hornblende (ab 1, act 1) forms symplectites which partly replace blue-green hornblende and, probably more commonly, former omphacite (see Kramer 2002). These symplectites are replaced by a second generation of synkinematically grown albite and actinolitic hornblende (ab 2, act 2), or by post-kinematic clinozoisite and zoisite. The retrograde breakdown of garnet produced chlorite, zoisite/ clinozoisite and more rarely blue-green or yellow-green hornblende. Titanite is commonly the breakdown product of ilmenite and rutile, but also occurs as xenoblastic grains in the matrix.

5 Whole rock chemistry

5.1 Analytical methods

Samples were carefully selected to avoid cracks or veins, and weathered crusts were removed. The samples were crushed in a jawbreaker and ground in an agate mill to grain sizes < 60 μm . For major element analyses 300 mg of ignited powder were mixed with 4700 mg of dried $\text{Li}_2\text{B}_4\text{O}_7$ and

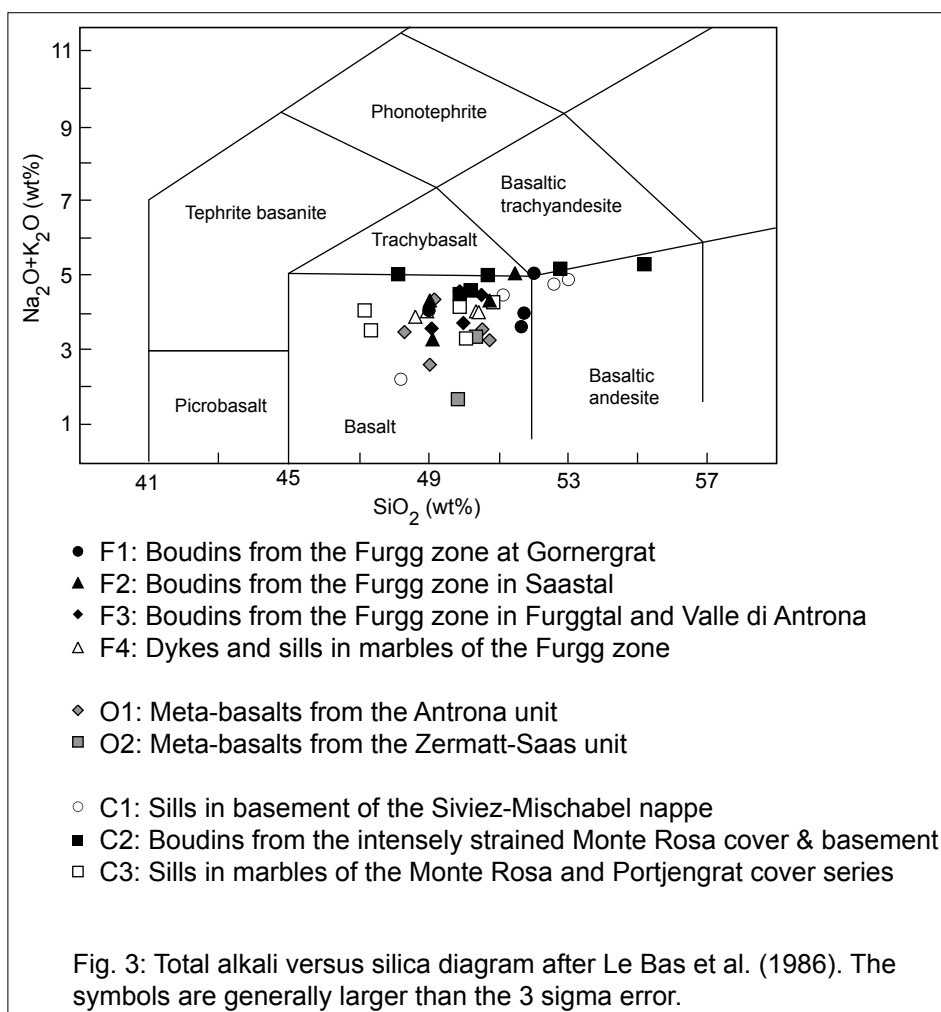
fused to glass discs. The XRF analyses (SRS-3400 Bruker-AXS) were done at the geochemical laboratory of the University of Basel. The statistical uncertainty at the 3 sigma-level is less than 2 relative % for all major elements, except for K_2O (5-10 relative %) and TiO_2 (2-20 relative %). Trace elements were analyzed by ICP-MS at the CNRS in Nancy, France. For this purpose, 300 mg of sample powder were fused with $LiBO_2$ and dissolved in HNO_3 . Detection limits range from 0.01 to 6 ppm (Tab. 2). Uncertainties are usually less than 10 relative % except for values close to the detection limit.

5.2 Major and trace element composition

The major and trace element compositions of the amphibolites are given in Tab. 2. Additional analyses from the Zermatt-Saas and Antrona ophiolitic units may be found in Pfeifer et al. (1989). The SiO_2 concentrations generally fall into a range between 46 and 52 wt%. In the total alkali versus silica (TAS) diagram after Le Bas et al. (1986), the analyses plot into the basalt and basaltic andesite fields (Fig. 3). However, all samples are amphibolites and it is therefore likely that alkali metals were affected to some degree by either ocean floor (hydrothermal) and/or regional metamorphism (Pearce 1976, MacGeehan and MacLean 1980, Gelinis et al. 1982, Mottl 1983, Rollinson 1983, Saunders and Tearney 1984). The same is true for other large ion lithophile elements (LILE; Cs, Rb, Ba, Pb and Sr), which is reflected by large concentration variations in the different samples (see Tab. 2 and Fig. 7). This makes it difficult to use major elements and especially the alkali metals to decipher the igneous history of the amphibolites. Therefore we mainly rely on trace elements in the following discussion, which are considered to be less mobile during alteration and metamorphism (Dostal and Capedri 1979, Grauch 1989, Gelinis et al. 1982, Humphris 1984).

The large range of MgO (4.06 – 8.62 wt %) coupled with relatively low Ni contents (< 140 ppm, Tab. 2, see also Fig. 8) indicates that all amphibolites are derived from differentiated magmas and do not represent unmodified liquids that were in equilibrium with the mantle. This is illustrated in Fig. 4. Mg# (molar Mg/(Mg+Fe_{tot})) are less than 65 and decrease with increasing incompatible element contents.

Harker diagrams of selected major and trace elements (Fig. 5) show that incompatible elements (Ti, Y, V) are positively correlated with Zr. These correlations are well defined for the samples from the Furgg zone, but less clear for the ophiolitic units and the C1 and C2 units. This suggests that the Furgg zone amphibolites were derived from a single cogenetic magma suite, whereas a more heterogeneous magma source and/or a more heterogeneous magma evolution was associated with mafic magmatism in the



ophiolitic units.

The Zr/Nb ratio in metabasalts from the ophiolitic units is about 30 (Fig. 5). Samples from the Furgg zone generally plot at somewhat lower Zr/Nb ratios indicating a higher T-type MORB affinity than the classical N-type MORB of the ophiolitic units (Wood et al. 1979).

In MORB the REE concentrations may vary from less than 10 times chondritic in primitive basalts to about 50 times chondritic in more evolved basalts (Schilling et al. 1983, Venturelli et al. 1981, Pearce 1982, Cullers and Graf 1984, Henderson 1984, Saunders 1984, Rollinson 1993, Desmurs et al. 2002). Low-pressure fractional crystallization leads to an overall enrichment of the incompatible elements, but does not change the slope of the REE pattern (Schilling 1983, Frey et al. 1976). This is why the shape of REE patterns observed in evolved basalts largely reflects the REE chemistry of the parent liquid, and REE are particularly useful for discrimination between different MORB magma types. With respect to the relative abundance of light, intermediate and heavy REE, the investigated samples fall into two broad categories (Fig. 6).

A first group shows relatively flat REE patterns with 10 to 20 times chondritic concentrations, typical for T-type MORB, with (Ce/Yb) between 1.00 and 1.76 (Tab. 2). This group includes all samples from the two ophiolitic units (O1 and O2), all samples from the Furgg zone (F1 - F4) and the basalts of group C3 (Fig. 6). Primitive mantle-normalized trace element patterns (Fig. 7; after Sun and MacDonough 1989) indicate a consistent positive Zr anomaly, with the exception of two samples, which probably represent former gabbro cumulates (see below). Such a trace element pattern is not uncommon in basalts and is a characteristic feature of low-degree melts generated in the spinel peridotite field (e.g. Casey 1997). Sr (and Rb, which is not shown) is highly variable and may reflect alteration processes related to the breakdown of plagioclase.

A second group of samples comprises dykes and sills from the Siviez-Mischabel basement unit (C1) and isolated boudins found within the southwestern part of the Monte Rosa basement and cover (C2). These samples have highly variable REE patterns and slopes (Fig. 6). The compatible/incompatible element ratios (Fig. 8) are different from those of the first group. As can be seen from Figure 8,

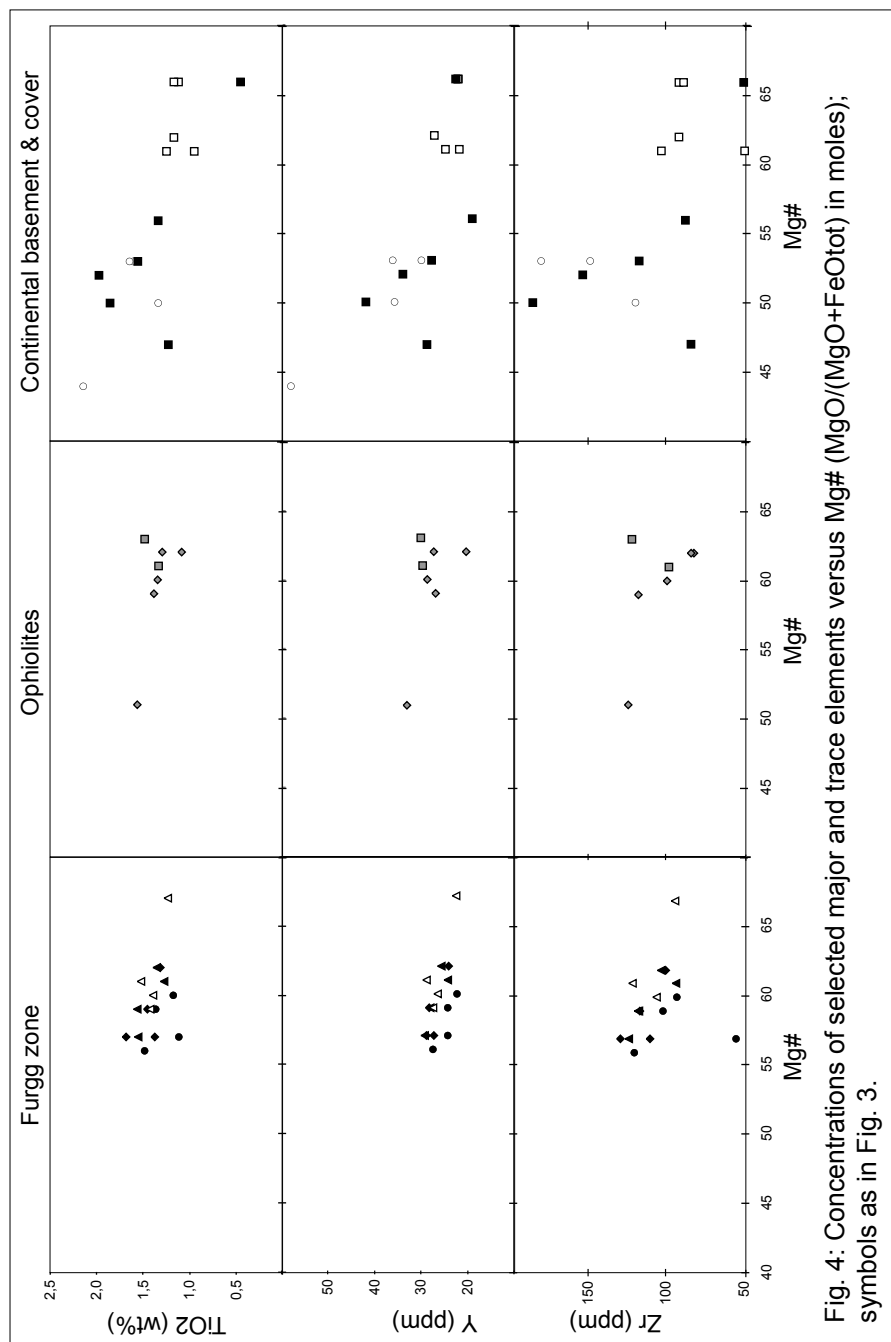


Fig. 4: Concentrations of selected major and trace elements versus Mg# (MgO/(MgO+FeOtot) in moles); symbols as in Fig. 3.

the C1 and C2 samples show different Ce/Ni ratios and highly variable Nb contents. These features indicate that the C1 and C2 samples have another origin than all the other samples.

6. Discussion and conclusions

6.1 Gabbro or basaltic precursors of the amphibolites?

It is often difficult to decide from whole rock analyses of amphibolites whether they were derived from basaltic or gabbroic precursor rocks. This problem is particularly difficult to tackle if the metamorphosed mafic rocks are differentiated, because Fe-Ti-oxide gabbros are often fine-grained and resemble metamorphosed basalts. Compatible element (Ni) versus incompatible elements (Ce, Nb) covariation trends may provide a chemical criterion for the distinction between different protoliths (see Fig. 8). If samples represent a single suite of crystallized liquids (e.g. basaltic rocks), smooth negative correlations between compatible and incompatible elements are expected. As can be seen from Fig. 8, all samples from the ophiolites, the Furgg zone (with one exception) and the Portjengrat unit (with one exception) show a smooth increase of incompatible Ce and Nb with decreasing Ni

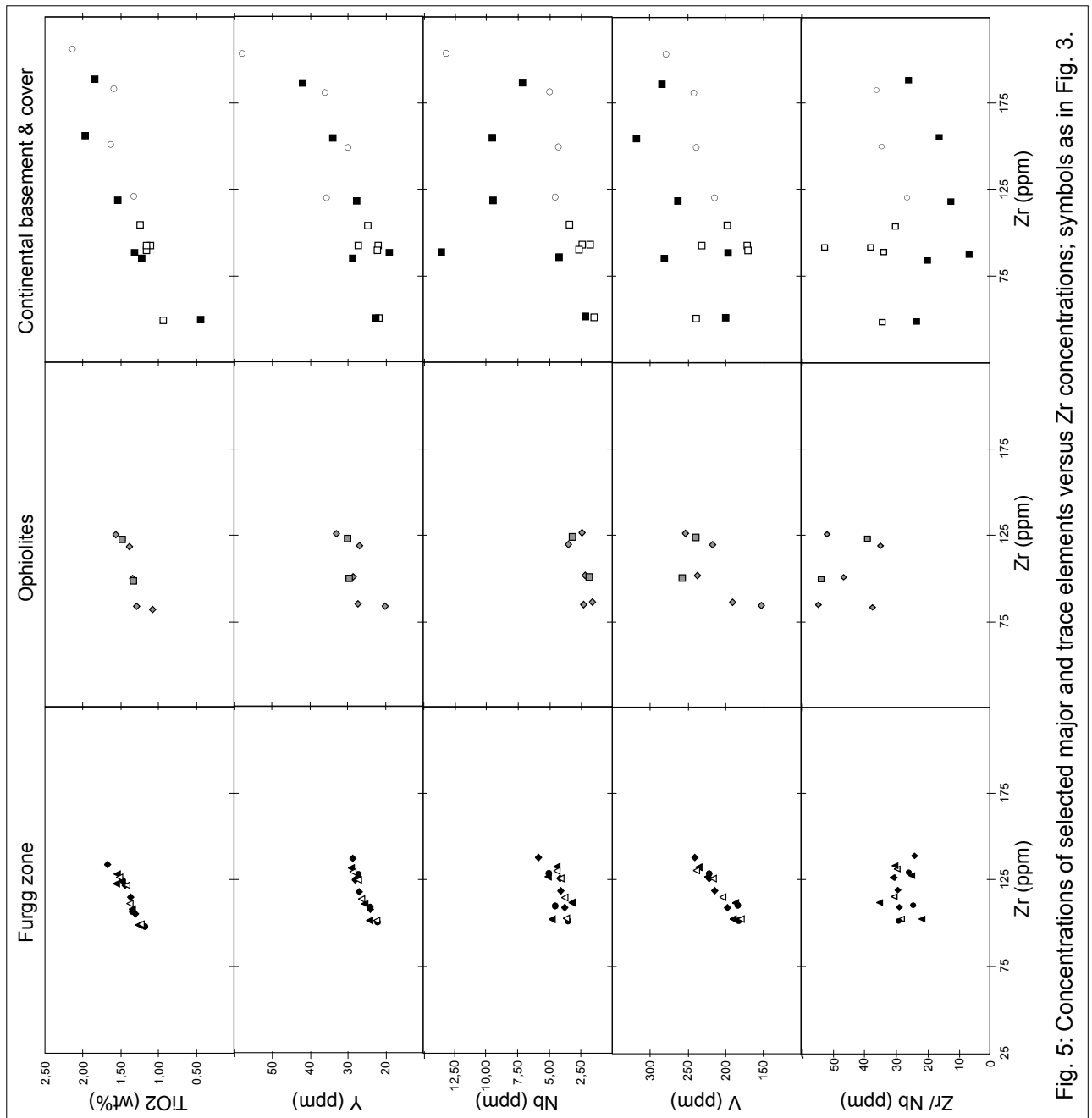
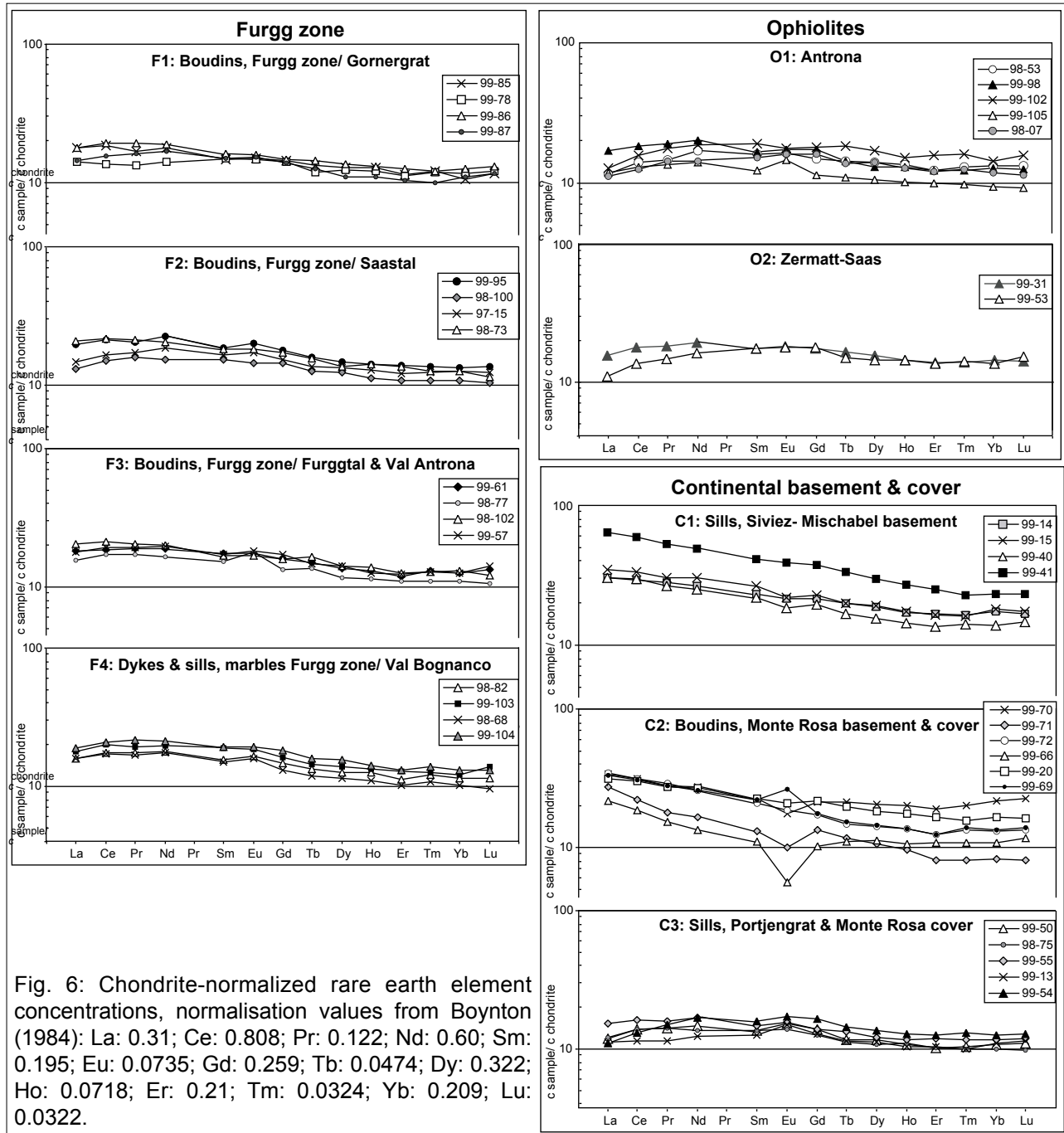


Fig. 5: Concentrations of selected major and trace elements versus Zr concentrations; symbols as in Fig. 3.

content. The samples falling off the trend most probably represent cumulates. These samples are not further considered in the discussion¹.

Compared to the samples from the ophiolitic units, the Furgg zone and the Portjengrat unit, the samples from the Siviez-Mischabel basement (C1) and the southwestern Monte Rosa nappe (C2) exhibit generally higher LREE contents at comparable Ni (Fig. 8) and REE spectra with higher LREE/HREE ratios (Fig. 6). In addition, in the C2 group Nb is highly variable, which probably reflects different proportions of Fe-Ti oxides in these samples. The smooth REE spectra from the Siviez-



¹ U-Pb dating of zircons from sample 99-13 (Monte Rosa cover) yielded a Paleozoic age (Liati et al. 2001), which was interpreted to represent the time of crystallisation of the igneous (gabbroic?) protolith by these authors. However, the chemistry of this sample (Figs. 6, 8) is indicative of a cumulate precursor, and hence the sample is not representative of the suite of amphibolites in Furgg zone (group F1-F4), Portjengrat unit and northern Monte Rosa nappe (group C3). Since we do not regard the sample as part of the same magmatic suite, its Paleozoic age is not considered as representative of the other samples. Furthermore, we doubt that the dated zircons necessarily represent the age of the igneous protolith of sample 99-13, as the zircons might be inherited.

Mischabel basement (C1) may indicate enriched MORB (e.g. Bill et al. 2000) derived from a source with initially high incompatible element content. The samples from the southwestern Monte Rosa nappe (C2) do not show any systematics with respect to incompatible elements (Fig. 8). In addition, field relations indicate a possible Paleozoic origin for some of the amphibolites from the southwestern Monte Rosa nappe. This is why we think that the C1 and C2 amphibolites cannot be directly compared with the amphibolites from the ophiolites, the Furgg zone and the Portjengrat unit.

6.2 Possible sources of the MORB magmatism in the Furgg zone, the Portjengrat unit and adjacent ophiolitic units

In Fig. 9a, the Nb_n/Zr_n and the Ce_n/Sm_n ratios of samples from the Furgg zone, the Portjengrat unit, the Antrona ophiolites and the Zermatt-Saas ophiolites are plotted and compared to basalts from Piemont-Ligurian ophiolites from outside the study area. The Ce_n/Sm_n and the Nb_n/Zr_n ratios of the Antrona and Zermatt-Saas ophiolites cluster in two different groups, one with $Ce_n/Sm_n < 1$ and $Nb_n/Zr_n < 0.4$, and one with $Ce_n/Sm_n > 1$ and $Nb_n/Zr_n > 0.4$, respectively (Fig. 9 a). The latter are very similar to the Furgg zone metabasalts and are intermediate between T-MORB from the Gets and upper Platta nappe, and T-MORB from the external Ligurides and Corsica (Fig 9 b). This suggests that the Furgg zone metabasalts are T-MORB from a single homogenous magma source while in the metabasalts from the adjacent ophiolitic units the source was more heterogeneous, producing basalts of T- to N-MORB composition. All metabasalts from the Furgg zone and from the Antrona and Zermatt-Saas ophiolites show a positive anomaly in Zr (Zr^*). This probably indicates a low degree of melting in the spinel field (Casey 1997). The Zr^* decreases from T- to N-MORB in Corsica and the Ligurides. This indicates that they are the products of variable degrees of partial melting (higher for N- than T-MORB). Taken together, these data show that partial melting of a slightly enriched (lithospheric?) mantle source led to the formation of the metabasalts from the Furgg zone (group F1 – F4) and Portjengrat unit (group C3), whereas partial melting of a more depleted mantle source accounted for the formation of the metabasalts of the ophiolitic units (group O 1 and O2).

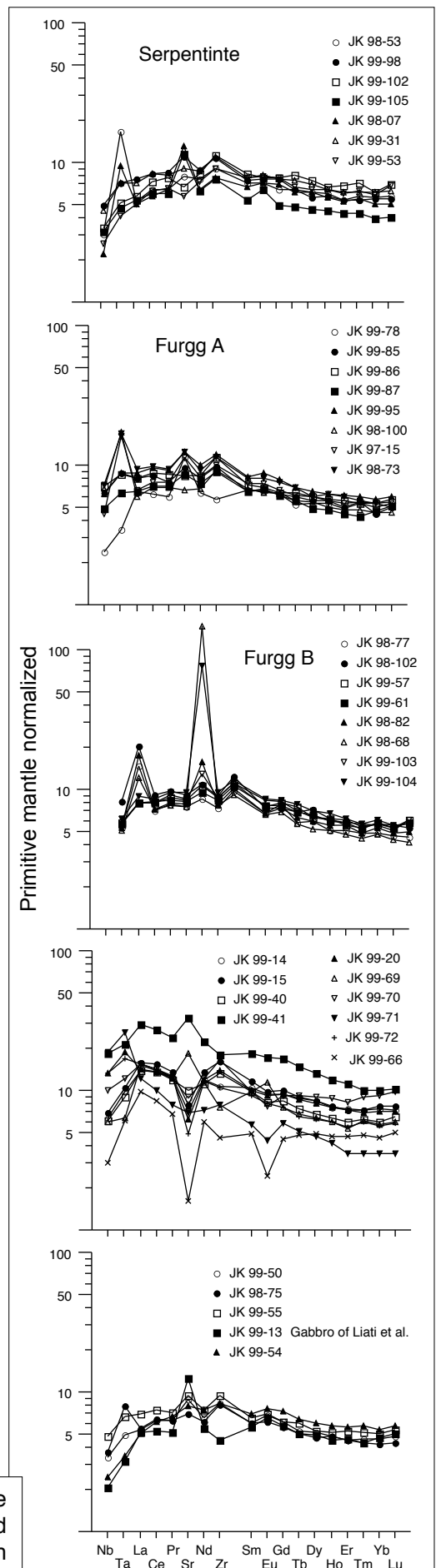


Fig. 7: Primitive mantle-normalized diagrams of selected trace elements of amphibolites from the Monte Rosa region and surrounding areas (normalization after Sun and McDonough 1989).

6.3 Tectonic implications of the geochemical data

The geochemical data discussed above suggest that the abundant small metabasaltic boudins of the Furgg zone (group F1-F4) are T-MORB type intrusives that were derived from a slightly enriched (lithospheric?) and single cogenetic magma suite. In this respect they differ from the ophiolitic units that exhibit a tendency towards a more depleted, T- to N-MORB type and towards a more heterogeneous magma source. If the Furgg zone metabasalts were derived from ophiolitic units, one would expect a complete overlap of the chemistry of the Furgg zone metabasalts with that of the metabasalts from the ophiolitic units. This is, however, not supported by our data (Figs. 8, 9). Furthermore, the Zr, Y, V, and Ti inter-element correlations are significantly higher in the Furgg zone metabasalts than in the mafic rocks from the ophiolitic units. This excludes the possibility that the Furgg zone metabasalts were derived through tectonic incorporation of adjacent ophiolitic components. In summary, these data indicate that the Furgg zone cannot be interpreted as an ophiolitic mélangé, as proposed by Froitzheim (2001).

Given the geochemical similarities of the metabasaltic boudins of the Furgg zone with those of the Portjengrat unit (group C3), the main difference between the two units seems to be the continuous increase in strain intensity towards the Furgg zone. Since the Portjengrat unit is undoubtedly a fragment of continental upper crust, the Furgg zone may conclusively be interpreted as an intracontinental shear zone that overprints both Portjengrat unit and adjacent Monte Rosa nappe. This is consistent with structural evidence indicating that the Monte Rosa nappe and the Portjengrat-Stockhorn units were originally connected to form a single Portjengrat – Stockhorn – Monte Rosa continental fragment, separating the Antrona ophiolites from the Zermatt-Saas ophiolites (Keller and Schmid 2001, Kramer 2002). This is again in marked contrast to the model proposed by Froitzheim (2001), who considers the Furgg zone, together with the Antrona ophiolitic unit, as representing North Penninic oceanic crust, which separates the Briançonnais microcontinent (= Portjengrat-Stockhorn unit) from the European plate (= Monte Rosa nappe). However, the geochemical data presented above do not exclude the possibility that the Antrona and Zermatt-Saas units were an originally continuous unit forming part of the Piemonte-Ligurian ocean, as was proposed by Escher et al. (1997).

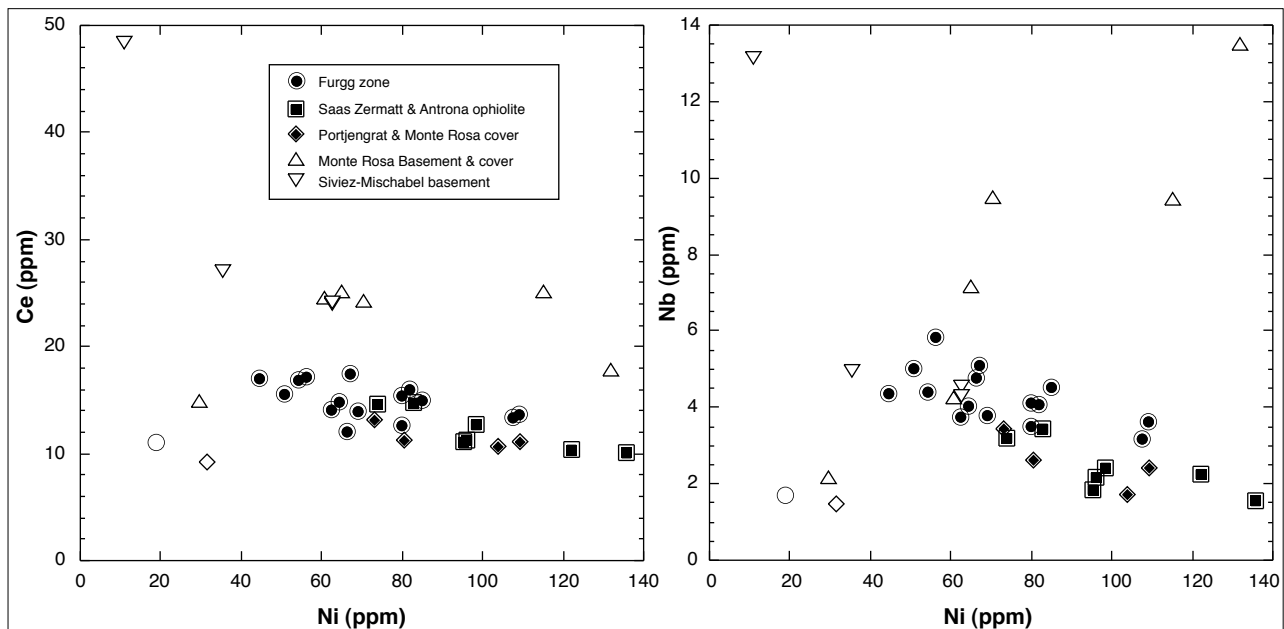


Fig. 8: Compatible (Ni) versus incompatible element (Nb, Ce) plots. All samples (filled symbols) from the Furgg zone (except one, open circle), the Zermatt-Saas and Antrona ophiolitic units and the Portjengrat unit (except one, open diamond) indicate a coherent chemical trend with decreasing Ni and increasing incompatible elements (Ce, Nb). Open symbols show either low incompatible elements at low Ni content or high incompatible element content at variable Ni content (all samples from the Monte Rosa basement, and the Siviez-Mischabel nappe). These samples are probably not metabasalts but gabbro cumulates or gabbros with high proportions of trapped interstitial liquid or (in the case of the Siviez Mischabel nappe) metabasalts with a source enriched in incompatible elements.

The different geochemical signatures of the metabasaltic boudins from the intensely strained Monte Rosa cover and basement of the southwestern Monte Rosa nappe (ISMR, group C2) preclude a direct correlation with the Furgg zone, as was proposed by Dal Piaz (1966). Furthermore, their derivation from the Zermatt-Saas ophiolitic unit can also be excluded on geochemical arguments. Hence, the chemical data presented in this study do not support the idea that the ISMR represents the prolongation of the Furgg zone in terms of an ophiolitic mélangé (Froitzheim 2001). On the other hand, larger mappable ophiolitic slivers containing ultramafic rocks, which are surrounded by the Furgg zone, do exist. However, they demonstrably are either isoclinal D3 fold cores of the Zermatt-Saas unit (at Gornergrat) or fold cores of the Antrona unit (in the Monte della Preja region) that were fragmented during D3 overprint (Kramer 2002) and that are not regarded as part of the Furgg zone (Keller and Schmid 2001, Kramer 2002).

6.4 Paleogeographic implications of the geochemical data

Based on the geochemistry of the metabasalts, two stages of mafic magmatism are inferred. An early stage is recorded by the samples of groups C1 and C2. The amphibolite boudins of group C2 are embedded in the basement of the southwestern Monte Rosa nappe (ISMR), as well as in garnet micaschists of its supposedly Permo-Triassic meta-sedimentary cover. The boudins are parallel to the foliation of the basement rocks, which is, at least in part, defined by pre-Alpine sillimanite (Dal Piaz 1966). Hence, Dal Piaz concluded, that foliation and embedded boudins are Paleozoic in age. This view is corroborated by the observation of amphibolite boudins, which are intruded by granites of probably Permian (or Late Carboniferous) age (Kramer 2002). Late Carboniferous to

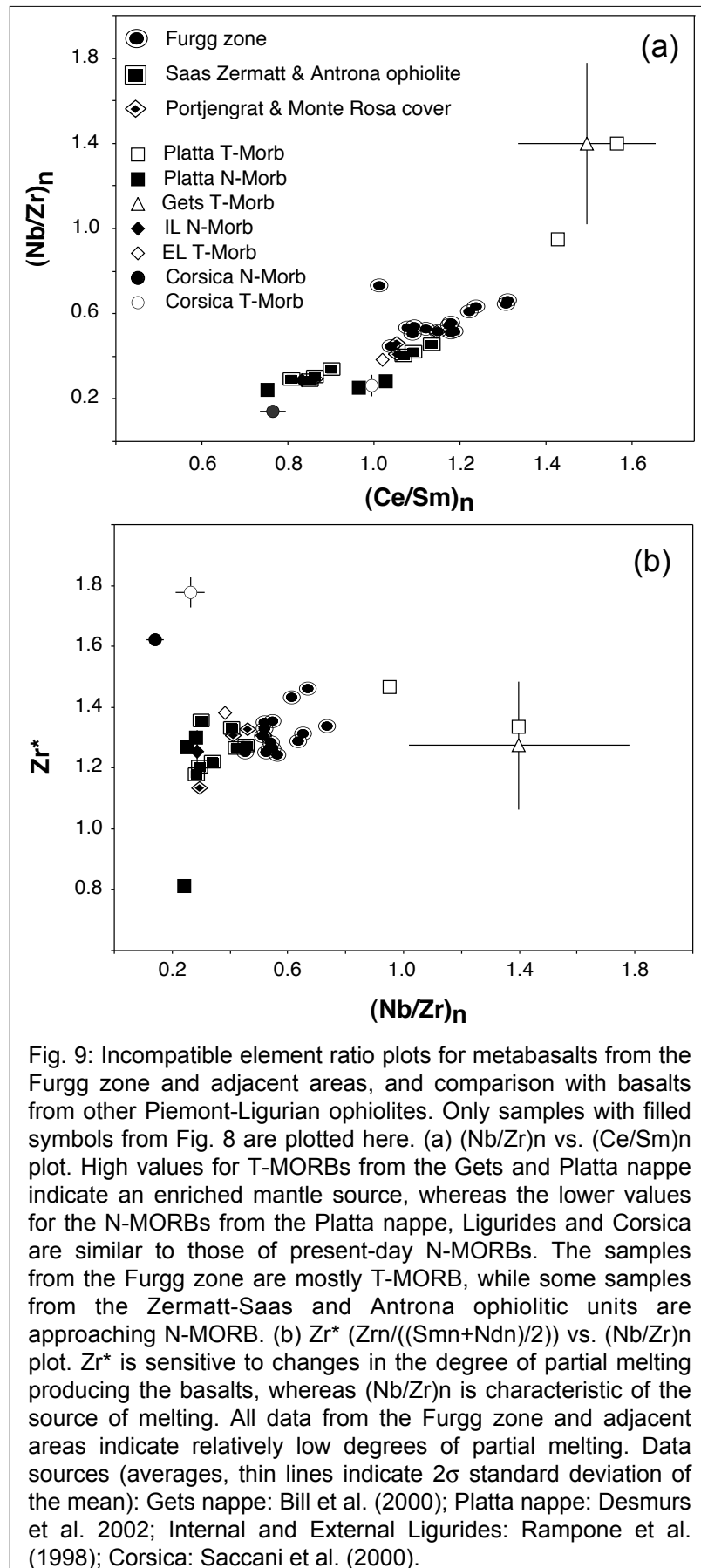


Fig. 9: Incompatible element ratio plots for metabasalts from the Furgg zone and adjacent areas, and comparison with basalts from other Piemont-Ligurian ophiolites. Only samples with filled symbols from Fig. 8 are plotted here. (a) $(\text{Nb/Zr})_n$ vs. $(\text{Ce/Sm})_n$ plot. High values for T-MORBs from the Gets and Platta nappe indicate an enriched mantle source, whereas the lower values for the N-MORBs from the Platta nappe, Ligurides and Corsica are similar to those of present-day N-MORBs. The samples from the Furgg zone are mostly T-MORB, while some samples from the Zermatt-Saas and Antrona ophiolitic units are approaching N-MORB. (b) Zr^* ($\text{Zr}/((\text{Sm}_n + \text{Nd}_n)/2)$) vs. $(\text{Nb/Zr})_n$ plot. Zr^* is sensitive to changes in the degree of partial melting producing the basalts, whereas $(\text{Nb/Zr})_n$ is characteristic of the source of melting. All data from the Furgg zone and adjacent areas indicate relatively low degrees of partial melting. Data sources (averages, thin lines indicate 2σ standard deviation of the mean): Gets nappe: Bill et al. (2000); Platta nappe: Desmurs et al. 2002; Internal and External Ligurides: Rampone et al. (1998); Corsica: Saccani et al. (2000).

Permian igneous activity, producing MORB-type and also more differentiated magmas has been described from several regions in the Alps (e.g. von Raumer et al. 1990). A pre-Triassic age is also likely for the amphibolites of group C1 from the Siviez-Mischabel nappe, which were collected within basement only.

A later, presumably post-Triassic age is proposed for all T-type MOR basalts. The main reasoning is that some of the metabasalts of groups C3 (Portjengrat and Stockhorn units) and F4 (parts of the Furgg zone) intruded Triassic meta-arkoses and/or marbles (Jaboyedoff et al. 1996, Kramer 2002). Our geochemical data and field relations suggest that this post-Triassic MORB-type magmatism affected pericontinental as well as oceanic units. This has recently been described from other ocean-continent transition zones in the Eastern Central Alps (e.g. Puschnig 2000, Desmurs et al. 2002) and in the Gets nappe (Bill et al. 2000). However, in none of these regions were comparable volume proportions of mafic rocks found within continental upper crustal basement, including its Triassic cover.

The question whether the Furgg zone magmatism was linked in space and time with the magmatism in the ophiolitic Antrona or with that of the Zermatt-Saas unit cannot be answered unequivocally with the existing geochemical data alone. In case of the existence of only one single oceanic basin in the working area, as proposed by Escher et al. (1997), all ophiolitic units would have belonged to the Piedmont-Ligurian ocean. According to this tectonic model, this single oceanic suture derived from South Penninic oceanic crust would separate Austroalpine units from the Briançonnais microcontinent, the southern margin of which would be represented in our working area.

In case of the existence of two oceanic basins in the working area, the Antrona and Zermatt-Saas units would have been part of the Valais and Piedmont-Ligurian oceans, respectively (e.g. Keller and Schmid 2001). Those metabasalts that pertained to the Valaisan ocean, would be Late Jurassic or younger in age. The fact that the adjacent Portjengrat unit and Furgg zone were intruded by dykes and sills with T- to N-MORB compositions similar to the ophiolites suggests that both units may have been derived from the same distal continental margin within the Briançonnais, that was stacked between the Valaisan and Piedmont-Ligurian oceanic sutures. According to this scenario the Portjengrat - Stockhorn - Monte Rosa continental fragment (including the Furgg zone) represents the eclogitic part of the Briançonnais microcontinent, as proposed by Keller and Schmid (2001) and Kramer (2002).

Structural studies indicate that the distal margin of the Briançonnais, represented by the Portjengrat unit and the Furgg zone, may have been located adjacent to the more external Valaisian oceanic basin (Keller and Schmid 2001). In this context it is interesting to note that T-type MORB dykes have neither been reported from the sedimentary cover of the Siviez-Mischabel nappe (internal Briançonnais), nor from the southwestern part of the Monte Rosa nappe (most internal Briançonnais situated directly adjacent to undisputed Piedmont-Ligurian ophiolites, i.e. the Zermatt-Saas unit; see Figs. 1 and 2). Together with the fact that ophiolitic imbricates derived from the Antrona unit (Valaisan according to Keller and Schmid 2001) can be found in the Furgg zone, these structural and field arguments may indicate that the basaltic intrusions into distal continental margin units occurred in the context of Late Jurassic to Early Cretaceous opening of the Valais ocean.

Notwithstanding the different paleotectonic interpretations, an important finding of this study is that T-type MOR basalts are not only found in ophiolitic units but also in (thinned) distal continental margin units. The volume of mafic rocks intruding the Briançonnais distal continental margin adjacent to the Valais ocean or, alternatively, to the Piedmont-Ligurian ocean, is distinctly higher than the volume of mafic rocks found in the Adriatic distal continental margin (e.g. Puschnig, 2000, Desmurs et al. 2002). This 'asymmetry' in the distribution of mafic rocks along continental margins is consistent with asymmetric low angle detachment faulting during the latest stages of rifting. The finding of T-MORB basalts intruding distal parts of the continental crust is similar to the evolution of the Red Sea rifting system (e.g. Voggenreiter et al. 1988).

Acknowledgements

The authors gratefully acknowledge the contributions of all the members of the Basel, Bonn and Mainz "Monte Rosa group" (Nikolaus Froitzheim, Ronan Le Bayon, Katharina Dubach,

Christiane Rössler, Lukas Keller, Andreas Weber, Corinne Bacher, Lukas Baumgartner, Sabine Pawlig). Furthermore, we benefited from discussions with and/or reviews from Hans-Rudolf Pfeifer, Philippe Monjoie, Dieter Gebauer, and Martin Engi.

J. Kramer acknowledges support from the Werenfels-Fonds, Freiwillige Akademische Gesellschaft, Basel. S. Schmid acknowledges support from NF-projects Nr. 20-61814.00 and 2000-068020/1, initiated by the late Martin Frey. The authors are grateful for Martin's initiative and support during the initial stages of this study.

References

- Amato, J.M., Johnson, C.M., Baumgartner, L.P. and Beard, B.L. (1999): Rapid exhumation of the Zermatt-Saas ophiolite deduced from high-precision Sm-Nd and Rb-Sr geochronology. *Earth Planet. Sci. Lett.* 171/3, 425-438.
- Bacher, C. (2002): Strukturen und Metamorphose in der Furggzone (Furggtal bei Saas Almagell, Wallis). Unpubl. diploma thesis, University of Basel, 83 pp.
- Barnicoat, A.C. and Fry, N. (1986): High-pressure metamorphism of the Zermatt-Saas ophiolite zone, Switzerland. *J. Geol. Soc. London* 143/4, 607-618.
- Barnicoat, A.C., Rex, D.C., Guise, P.G. and Cliff, R.A. (1995): The timing of and nature of greenschist facies deformation and metamorphism in the upper Pennine Alps. *Tectonics* 14/2, 279-293.
- Bearth, P. (1945): Über das Verhältnis von Kristallisation und Bewegung in der Monte Rosa-Bernhard-(Mischabel)-Decke. *Schweiz. Mineral. Petrog. Mitt.* 25/2, 537-538.
- Bearth, P. (1952): Geologie und Petrographie des Monte Rosa. *Beitr. Geol. Karte Schweiz (Neue Folge)* 96, 1-94.
- Bearth, P. (1953a): Blatt Zermatt, Geologischer Atlas der Schweiz, Nr. 29. 1:25'000. Basel, Schweiz. Geol. Kommission.
- Bearth, P. (1953b): Erläuterungen Blatt Zermatt, Geologischer Atlas der Schweiz. Nr. 29. 1:25'000. Basel, Schweiz. Geol. Kommission.
- Bearth, P. (1954a): Blatt Monte Moro, Geologischer Atlas der Schweiz, Nr.30. 1:25'000. Basel, Schweiz. Geol. Kommission.
- Bearth, P. (1954b): Blatt Saas, Geologischer Atlas der Schweiz, Nr.31. 1:25'000. Basel, Schweiz. Geol. Kommission.
- Bearth, P. (1956): Geologische Beobachtungen im Grenzgebiet der lepontinischen und penninischen Alpen. *Eclogae geol. Helv.* 49/2, 279-290.
- Bearth, P. (1957): Erläuterungen Blatt Saas und Monte Moro, Geologischer Atlas der Schweiz. Nr. 30, 31. Basel, Schweiz. Geol. Kommission.
- Bearth, P. (1976): Zur Gliederung der Bündnerschiefer in der Region von Zermatt. *Eclogae geol. Helv.* 69/1, 149-161.
- Bearth, P. and Schwander, H. (1981): The post-Triassic sediments of the ophiolite zone Zermatt-Saas Fee and the associated manganese mineralizations. *Eclogae geol. Helv.* 74/1, 189-205.
- Bearth, P. and Stern, W. (1971): Zum Chemismus der Eklogite und Glaukophanite von Zermatt. *Schweiz. Mineral. Petrogr. Mitt.* 51/3, 349-359.
- Bearth, P. and Stern, W. (1979): Zur Geochemie von Metapillows der Region Zermatt-Saas. *Schweiz. Mineral. Petrogr. Mitt.* 59/3, 349-373.
- Beccaluva, L., Dal Piaz, G.V. and Macciotta, G. (1984): Transitional to normal MORB affinities in ophiolitic metabasites from Zermatt-Saas, Combin and Antrona units, Western Alps. *Geol. En Mijnbouw* 63, 165-177
- Bill, M., Nägler, T.F. and Masson, H. (2000): Geochemistry, Sm-Nd and Sr isotopes of mafic rocks from the earliest oceanic crust of Alpine Tethys. *Schweiz. Mineral. Petrogr. Mitt.* 80, 131-145.
- Boynton, W.V. (1984): Cosmochemistry of the rare earth elements: meteorite studies. In: Henderson, P. (ed.): *Developments in Geochemistry 2 - Rare Earth Element Geochemistry*. Elsevier, Amsterdam, 63 - 114.

- Carrupt, E. and Schlup, M. (1998): Métamorphisme et tectonique du versant sud du Val Bognanco (Pennique, Alpes italiennes). *Bull. Soc. Vaud. Sci. Nat.* 86/1, 29-59.
- Casey, J.F. (1997): Comparison of major- and trace element geochemistry of abyssal peridotites and mafic plutonic rocks with basalts from the MARK region of the Mid-Atlantic Ridge. *Proc. Ocean. Drill. Prog. Sci. Res.* 153,181-241.
- Colombi, A. (1989): Métamorphisme et géochimie des roches mafiques des Alpes ouest-centrales (géoprofil Viège-Domodossola-Locarno). *Mém. Géol.* 4. Imprive S.A., Lausanne, 216 pp.
- Cullers, R.L. and Graf, J.L. (1984): Rare earth elements in igneous rocks of the continental crust: predominantly basic and ultrabasic rocks. In: Henderson, P. (ed.): *Developments in Geochemistry 2 - Rare Earth Element Geochemistry*. Elsevier, Amsterdam, 237 - 274.
- Dal Piaz, G.V. (1964): Il cristallino antico del versante meridionale del Monte Rosa paraderivati a prevalente metamorfismo alpino. *Rendiconti Soc. Min. Italiana Anno XX*, 101-135; 4 Tav.
- Dal Piaz, G.V. (1966): Gneiss ghiandoni, marmi ed anfiboliti antiche del ricoprimento Monte Rosa nell'alta Valle d'Ayas. *Boll. Soc. Geol. Italiana* 85/1, 103-132.
- Dal Piaz, G.V. (1971): Nuovi ritrovamenti di cianite alpina nel Cristallino antico del Monte Rosa. *Rend. Soc. Italiana Min. Petrol.* 27/2, 437-477.
- Dal Piaz, G.V. (2001): Geology of the Monte Rosa massif: historical review and personal comments. *Schweiz. Mineral. Petrogr. Mitt.* 81, 275-303.
- Desmurs, L., Müntener, O. and Manatschal, G. (2002): Onset of magmatic accretion within a magma-poor rifted margin: A case study from the Platta ocean-continent transition, Eastern Switzerland. *Contrib. Mineral. Petrol.* 144, 365-382.
- Dostal, J. and Capedri, S. (1979): Rare earth elements in high-grade metamorphic rocks from the Western Alps. *Lithos* 12, 41 - 49.
- Dubach, K. (1998): Die Grenzzone von Portjengrat- Einheit und Siviez-Mischabel-Decke im Almagellertal, Wallis. Unpubl. diploma thesis, University of Basel, 61 pp.
- Eisele, J., Geiger, S. and Rahn, M. (1997): Chemical characterization of metabasites from the Turtmann Valley (Valais, Switzerland): implications for their protoliths and geotectonic origin. *Schweiz. Mineral. Petrogr. Mitt.* 77/3, 403-417.
- Engi, M., Scherrer, N.C. and Burri, T. (2001): Metamorphic evolution of pelitic rocks of the Monte Rosa nappe: Constraints from petrology and single grain monazite age data. *Schweiz. Mineral. Petrogr. Mitt.* 81, 305-328.
- Escher, A., Hunziker, J.-C., Marthaler, M., Masson, H., Sartori, M. and Steck, A. (1997): Geologic framework and structural evolution of the western Swiss-Italian Alps. In: Pfiffner, O.A., Lehner, P., Heitzmann, P., Müller, S. and Steck, A. (ed.): *Deep structure of the Swiss Alps: Results from NRP 20*. Birkhäuser, Basel, 205-221.
- Escher, A., Masson, H. and Steck, A. (1988): Coupes géologiques des Alpes occidentales suisses. *Mém. Géol. Lausanne, Rapp. géol. serv. hydrog. géol. natl.* 2, 1-11, incl. 1 map, 2 tables, 1 plate.
- Escher, A. and Sartori, M. (1991): The geology of the Zermatt - Gornergrat area. *NFP 20 Bull.* 9, 5 - 11.
- Frey, M., Hunziker, J.C., R, O.N.J. and Schwander, H.W. (1976): Equilibrium-disequilibrium relations in the Monte Rosa Granite, Western Alps; petrological, Rb-Sr and stable isotope data. *Contrib. Mineral. Petrol.* 55/2, 147-179.
- Froitzheim, N. (2001): Origin of the Monte Rosa nappe in the Pennine Alps - A new working hypothesis. *Geol. Soc. Am. Bull.* 113/5, 604 - 614.
- Gebauer, D. (1999): Alpine geochronology of the Central and Western Alps: new constraints for a complex geodynamic evolution. *Schweiz. Mineral. Petrogr. Mitt.* 79/1, 191-208.
- Gelinas, L., Mellinger, M. and Trudel, P. (1982): Archaean mafic metavolcanics from the Rouyn-Noranda district, Abitibi greenstone belt, Quebec. 1. Mobility of the major elements. *Canad. J. Earth Sci.* 19, 2258-2275.
- Grauch, R.I. (1989): Rare earth elements in metamorphic rocks. In: Lipin, B.R. and McKay, G.A. (ed.): *Geochemistry and mineralogy of rare earth elements*. 21. Mineralogical Society of America, Washington D.C., 147 - 167.
- Henderson, P. (1984): General geochemical properties and abundances of the rare earth elements. In: Henderson, P. (ed.): *Developments in Geochemistry 2 - Rare Earth Element Geochemistry*. Elsevier, Amsterdam Oxford New York Tokyo,

1-32.

Huang, T.-K. (1935a): Carte géologique de la région Weissmies-Portjengrat (Valais). 1:25'000. Basel, Schweiz. Geol. Kommission.

Huang, T.-K. (1935b): Etude géologique de la région Weissmies-Portjengrat (Valais). Bull. Soc. Neuchât. Sci. Nat. 60, 3-76.

Humphris, S.E. (1984): The mobility of the rare earth elements in the crust. In: Henderson, P. (ed.): Developments in Geochemistry 2 - Rare Earth Element Geochemistry. Elsevier, Amsterdam, 317 - 342.

Hunziker, J.C. (1970): Polymetamorphism in the Monte Rosa, Western Alps. *Eclogae geol. Helv.* 63/1, 151-161.

Jaboyedoff, M., Béglé, P. and Lobrinus, S. (1996): Stratigraphie et évolution structurale de la zone de Furgg, au front de la nappe du Mont-Rose. Bull. Soc. Vaud. Sci. Nat. 84/2, 191-210.

Keller, L. (2000): Kinematik der duktilen Scherung an der Front der Monte Rosa Decke (Val Loranco, Italien). Unpubl. diploma thesis, University of Basel, 90 pp.

Keller, L. and Schmid, S.M. (2001): On the kinematics of shearing near the top of the Monte Rosa nappe and the nature of the Furgg zone in the Val Loranco (Antrona valley, N. Italy): tectono-metamorphic and paleogeographical consequences. *Schweiz. Mineral. Petrogr. Mitt.* 81, 347-367.

Klein, J.A. (1978): Post-nappe folding southeast of the Mischabelrückfalte (Pennine Alps) and some aspects of the associated metamorphism. *Leidse geol. Medel.* 51/2, 233-312.

Kramer, J. (2002): Structural evolution of the Penninic units in the Monte Rosa region (Swiss and Italian Alps). PhD thesis No. 23, University of Basel, 147 pp, 2 maps, 2 encl.

Le Bas, M.J., Le Maître, R.W., Streckeisen, A. and Zanettin, B. (1986): A chemical classification of volcanic rocks based on the total alkali-silica diagram. *J. Petrol.* 27, 745-750.

Le Bayon, R., Schmid, S.M. and De Capitani, C. (2001): The metamorphic evolution of the Monte Rosa nappe and its relation to exhumation by fore- and back-thrusting in the Western Alps. *Geol. Paläont. Mitt. Innsbruck* 25, 132-133.

Liati, A., Gebauer, D., Froitzheim, N. and Fanning, M. (2001): U-Pb SHRIMP geochronology of an amphibolitized eclogite and an orthogneiss from the Furgg zone (Western Alps) and implications for its geodynamic evolution. *Schweiz. Mineral. Petrogr. Mitt.* 81, 379-393.

MacGeehan, P.J. and MacLean, W.H. (1980): An Archaean sub-seafloor geothermal system, 'calc-alkali' trends, and massive sulphide genesis. *Nature* 286, 767-771.

Markley, M.J., Teyssier, C., Cosca, M.A., Caby, R., Hunziker, J.C. and Sartori, M. (1998): Alpine deformation and ⁴⁰Ar/³⁹Ar geochronology of synkinematic white mica in the Siviez-Mischabel nappe, Western Pennine Alps, Switzerland. *Tectonics* 17/3, 407-425.

Marthaler, M. (1981): Découverte de foraminifères planctoniques dans les "schistes lustrés" de la pointe de Tourtemagne (Valais). Bull. Soc. Vaud. Sci. Nat. 75, 171-178.

Marthaler, M. (1984): Géologie des unités penniniques entre le Val d'Anniviers et le Val de Tourtemagne (Valais, Suisse). *Eclogae geol. Helv.* 77/2, 395-448.

Mattirolo, E., Novarese, V., Franchi, S. and Stella, A. (1912): Foglio Monte Rosa, Carta Geologica d' Italia. No. 29. 1:100 000. Novara, Serv. Geol. Ital.

Milnes, A.G., Grellier, M. and Müller, R. (1981): Sequence and style of major post-nappe structures, Simplon-Pennine Alps. *J. Struc. Geol.* 3/4, 411-420.

Mottl, M.J. (1983): Metabasalts, axial hot springs, and the structure of hydrothermal systems at mid-ocean ridges. *Geol. Soc. Am. Bull.* 94, 161-180.

Müller, C. (1989): Albitisation of the Zermatt area, Western Alps. PhD thesis, University of Basel, 285 pp.

Pearce, J.A. (1976): Statistical analysis of major element patterns in basalts. *J. Petrol.* 17, 15 - 43.

Pearce, J.A. (1982): Trace element characteristics of lavas from destructive plate boundaries. In: Thorpe, R.S. (ed.):

Andesites - Orogenic andesites and related rocks. John Wiley and Sons, Chichester, 525-548.

Pfeifer, H.R., Colombi, A. and Ganguin, J. (1989): Zermatt-Saas and Antrona Zone: A petrographic and geochemical comparison of polyphase metamorphic ophiolites of the West-Central Alps. *Schweiz. Mineral. Petrogr. Mitt.* 69/2, 217-236.

Puschign, A.R. (2000): The oceanic Forno Unit (Rhetic Alps). *Eclogae Geol. Helv.* 93: 103-124.

Rampone, E., Hofmann, A.W. and Raczek, I. (1998): Isotopic contrasts within the Internal Liguride Ophiolite (N. Italy): the lack of a genetic mantle-crust link. *Earth Planet. Sci. Lett.* 163, 175-189.

Reinecke, T. (1991): Very-high-pressure metamorphism and uplift of coesite-bearing metasediments from the Zermatt-Saas zone, Western Alps. *Europ. J. Mineral.* 3/1, 7-17.

Reinecke, T. (1998): Prograde high-to ultrahigh-pressure metamorphism and exhumation of oceanic sediments at Lago di Cignana, Zermatt-Saas Zone, western Alps. *Lithos* 42/3-4, 147-189.

Rollinson, H.R. (1993): Using geochemical data: evaluation, presentation, interpretation. Longman, Singapore, 352 pp.

Rössler, C. (2000): Transport und Faltung in der Furggzone und in den angrenzenden Einheiten (südliches Saastal, Wallis, Schweiz). Unpubl. diploma thesis, University of Basel, 74 pp.

Rubatto, D. and Gebauer, D. (1999): Eo/Oligocene (35 Ma) high-pressure metamorphism in the Gornergrat Zone (Monte Rosa, Western Alps): implications for paleogeography. *Schweiz. Mineral. Petrogr. Mitt.* 79/3, 353-362.

Saccani, E., Padoa, E. and Tassinari, R. (2000): Preliminary data on the Pineto gabbroic massif and Nebbio basalts: Progress toward the geochemical characterization of Alpine Corsica ophiolites. *Ofioliti* 25, 75-85.

Sartori, M. (1987): Structure de la zone du Combin entre les Diablons et Zermatt (Valais). *Eclogae geol. Helv.* 80, 789-814.

Sartori, M. (1990): L'unité du Barrhorn (Zone pennique, Valais, Suisse). PhD thesis, University of Lausanne, 156 pp.

Saunders, A.D. (1984): The rare earth element characteristics of igneous rocks from the ocean basins. In: Henderson, P. (ed.): *Developments in Geochemistry 2 - Rare Earth Element Geochemistry*. Elsevier, Amsterdam Oxford New York Tokyo, 205 - 236.

Saunders, A.D. and Tearney, J. (1984): Geochemical characteristics of basaltic volcanism within back-arc basins. In: Kohelaar, B.P. and Howells, M.F. (ed.): *Marginal basin geology*. Spec. Publ. 16. Geol. Soc. London, 59-76.

Schilling, J.-G., Zajac, M., Evans, R., Johnston, T., White, W., Devine, J.D. and Kingsley, R. (1983): Petrologic and geochemical variations along the Mid-Atlantic Ridge from 27°N to 73°N. *Am. J. Sci.* 283, 510-586.

Schmid, S.M. and Kissling, E. (2000): The arc of the western Alps in the light of geophysical data on deep crustal structure. *Tectonics* 19/1, 62-85.

Stampfli, G.M. and Marchant, R.H. (1997): Geodynamic evolution of the Tethyan margins of the Western Alps. In: Pfiffner, O.A.e.a. (ed.): *Deep structure of the Swiss Alps: results of NRP 20*. Birkhäuser, Basel, 223-239.

Steck, A., Epard, J.-L., Escher, A., Gouffon, Y. and Masson, H. (1999): Carte tectonique des Alpes de Suisse occidentale et des régions avoisinantes. Feuille Monte Rosa, No. 47. 1:100000. Bern, Serv. hydrol. géol. nat.

Sun, S.S. and McDonough, W.F. (1989): Chemical and isotopic systematics of oceanic basalts: implications for mantle composition and processes. In: Saunders, A.D. and Norry, M.J. (ed.): *Magmatism in ocean basins*. Spec. Pub. 42. Geol. Soc. London, 313-345.

Thélin, P., Sartori, M., Burri, M., Gouffon, Y. and Chessex, R. (1993): The Pre-Alpine Basement of the Briançonnais (Wallis, Switzerland). In: von Raumer, J.F. and Neubauer, F. (ed.): *Pre-Mesozoic Geology in the Alps*. Springer, Berlin, 297-315.

Thélin, P., Sartori, M., Lengeler, R. and Schaerer, J.P. (1990): Eclogites of Paleozoic or early Alpine age in the basement of the Penninic Siviez-Mischabel Nappe, Wallis, Switzerland. *Lithos* 25/1-3, 71-88.

van der Klauw, S.N.G.C., Reinecke, T. and Stöckhert, B. (1997): Exhumation of ultrahigh-pressure metamorphic oceanic crust from Lago di Cignana, Piemontese zone, western Alps: the structural record in metabasites. *Lithos* 41, 79-102.

Venturelli G., Thorpe R.S., Potts P.J. (1981): Rare earth and trace element characteristics of ophiolitic metabasalts from

the Alpine-Apennine belt. *Earth Planet. Sci. Lett.* 53, 109-123.

von Raumer, J.F., Galetti, G., Pfeifer, H.R. and Oberhänsli, R. (1990): Amphibolites from Lake Emosson/ Aiguilles Rouges, Switzerland: tholeiitic basalts of a Paleozoic continental rift zone. *Schweiz. Mineral. Petrogr. Mitt.* 70, 419-435.

Weber, A. (2001): Zur strukturellen und metamorphen Entwicklung der Furgg-Zone und angrenzender Einheiten im südlichen Saastal, Wallis, Schweiz. Unpubl. diploma thesis, University of Bonn, 85 pp.

Wetzel, R. (1972): Zur Petrographie und Mineralogie der Furgg-Zone (Monte Rosa-Decke). *Schweiz. Mineral. Petrogr. Mitt.* 52/2, 161-236.

Wood, D.A., Joron, J.-L. and Treuil, M. (1979): A re-appraisal of the use of trace elements to classify and discriminate between magma series erupted in different tectonic settings. *Earth Planet. Sci. Lett.* 45, 326-336.

Table 1: Sample descriptions of the studied amphibolites. For locations see Fig. 1.				
Sample	Petrography of meta-basaltic sample	Host rock	Swiss coordinates	Location
F1: Boudins, Furgg zone Gornergrat				
99-78	Very fine-grained symplectite of Ab + Act; late stage large poikiloblastic, hypidiotomorph Czo/ Czo/ Ep; Rt and Ilm rimmed by Ttn; Chl; Bt; poikiloblastic Ab	Garnet mica schists	630 425/ 92 025	Mattertal, Gornergrat, below Stockknubel
99-85	Hypidiotomorph to idiomorphic Act defining mineral lineation; Rt rimmed by Ttn; Fe-bearing carbonate; eye-shaped, deformed Zo/ Czo; Bt from Act; Chl	Dolomitic marbles	631 250/ 92 300	Mattertal, Gornergrat, east of P. 3223
99-86	Idiomorphic, poikiloblastic Grt randomly retrogressed to yellow-green Hbl and symplectite from Ab + yellow-green Act; large grains of Czo/ Zo growing on expense of symplectite; Ilm rimmed by Rt rimmed by Ttn; large grains of Ttn; WM rimmed by Czo/ Zo/ Ep; Hem	Quartzites	630 225/ 92 075	Mattertal, Gornergrat, above Stockknubel
99-87	Fine-grained symplectite from Ab + yellow-green Act; large grains of Czo/ Zo growing on expense of symplectite; Ilm rimmed by Rt rimmed by Ttn; large grains of Ttn; WM rimmed by Czo/ Zo/ Ep; Hem	Garnet mica schists	630 225/ 92 075	Mattertal, Gornergrat, above Stockknubel
F2: Boudins, Furgg zone Saastal				
99-95	Hypidiomorph to xenomorph, zoned, yellow-green, actinolitic Hbl; poikiloblastic, xenomorph Ab; Rt with reaction seams of Ttn; Hem, zoned Czo + Ep; Bt; Chl	Meta- arkoses	639 725/ 100 250	Saastal, below Allalin glacier
98-100	Latest phase: xenomorph Ab; large zoned, hypidiotomorph, unaligned Czo; Bt, partly replacing zoned Act (rim Mg-rich, core Fe-rich); Chl growing on expense of Bt; Hem; Ttn	Meta- arkoses	639 825/ 100 225	Saastal, below Allalin glacier
97-15	Latest phase: xenomorph Ab; zoned, hypidiotomorph, unaligned Czo; Bt, partly replacing zoned Act (rim Mg-rich, core Fe-rich); Chl growing on expense of Bt; Hem; Rt rimmed by Ttn	Meta- arkoses	640 350/ 100 675	Saastal near Mattmark
98-73	Latest phase: large poikiloblastic, hypidiotomorph zoned Zo/Czo; fine-grained symplectite from Ab+ Act, Act partly crystallized to larger idiomorphic grains, defining mineral lineation; Bt retrogressed to pale Chl; Ilm rimmed by Rt rimmed by Ttn, Hem; small, poikiloblastic, idiomorph Grt, large poikiloblastic WM	Garnet mica schists	639 750/ 100 025	Saastal, below Allalin glacier
F3: Boudins, Furgg zone Furggtal & Valle d' Antrona				
98-77	Fine-grained symplectite from Ab+ Act, Act mostly recrystallized to larger hypidiomorph grains; Ab partly recrystallized to small idiomorph grains; Bt growing at expense of Act; Rt rimmed by Ttn; Hem	Garnet mica schists	650 825/ 104 275	Valle d' Antrona, W' Lake Bacino dei Cavalli
98-102	Idiomorph, poikiloblastic Grt randomly retrogressed to blue-green Hbl; blue-green Hbl retrogressed to symplectite from Ab + yellow-green Act; large grains of Czo/ Zo growing on expense of symplectite; Ilm rimmed by Rt rimmed by Ttn; WM; Hem	Garnet mica schists	642 550/ 101 625	SW-side Furggtal
99-57	Fine-grained symplectite of Ab + Act; Act partly recrystallizing to larger grains; late stage large poikiloblastic, hypidiotomorph Zo/ Czo/ Ep; Rt rimmed by Ttn; opaques Ilm?; Chl; Bt	Meta- arkoses	644 450/ 102 075	NE-side Furggtal
99-61	Very fine-grained symplectite from Ab + yellow-green Act; large grains of Czo/ Zo growing on expense of symplectite; Ilm; Rt rimmed by Ttn; WM; Hem	Orthogneisses	642 950/ 102 100	NE-side Furggtal, Augstkummenrinne
F4: Dykes & sills, Furgg zone marbles, Valle di Loranco & Valle di Bognanco				
98-82	Latest phase: poikiloblastic, hypidiotomorph zoned Zo/ Czo; fine-grained symplectite from Ab + Act, Act partly recrystallized to larger idiomorph grains, defining mineral lineation; Bt retrogressed to pale Chl; Ilm rimmed by Rt rimmed by Ttn, Hem	Calclitic marbles	652 600/ 106 875	Valle di Bognanco, W' Alpe Preja
98-68	Latest phase: poikiloblastic albitic plagioclase, partly polysynthetic twinned, overgrowing hypidiotomorph and idiomorph Zo + Czo; Rt rimmed by Ttn; WM; Ank?; hypidiomorph to idiomorph, zoned, yellow-green, actinolitic Hbl defining mineral lineation; Hem partly retrogressed to Bt; Bt retrogressed to pale Chl	Calclitic marbles	652 075/ 106 500	Passo della Preja, Valle di Loranco - Valle di Bognanco
99-103	Poikiloblastic albitic plagioclase, overgrowing hypidiotomorph and idiomorph Zo + Czo; hypidiomorph to idiomorph, zoned, yellow-green, actinolitic Hbl; Hem partly retrogressed to Bt; Bt retrogressed to Chl; Rt rimmed by Ttn; WM	Calclitic & dolomitic marbles	652 025/ 106 525	Passo della Preja, Valle di Loranco - Valle di Bognanco
99-104	see 99-103	Calclitic & dolomitic marbles	652 025/ 106 525	Passo della Preja, Valle di Loranco - Valle di Bognanco
O1: Antrona unit				
98-53	Hypidiomorph to idiomorph, zoned, yellow-green, actinolitic Hbl defining mineral lineation; polysynthetic twinned Pl + poikiloblastic, xenomorph, eye-shaped, untwinned Ab with inclusions of Ttn + Ep; zoned Czo + Ep; Rt with reaction seams of Ttn; Hem		653 925/ 101 600	Valle d' Antrona, near Antronapiana
99-98	see above; additionally some Fe-bearing carbonate, late-stage hypidiomorph Ep/ Czo/ Zo		655 450/ 108 250	Valle di Bognanco, Alpe Vallaro
99-102	Very fine-grained symplectite of Ab + Act; Act partly recrystallized to larger grains; late-stage large poikiloblastic, hypidiotomorph Zo/ Czo/ Ep; Rt and Ilm rimmed by Ttn; very fine-grained cubic opaques Py?; Fe-poor carbonate		652 200/ 104 300	Val Antrona, NE-side Lake Bacino dei Cavalli
99-105	see 98-53, additionally large Ep/ Zo/ Czo; Chl	"Loranco amphibolite"	649 725/ 105 200	Valle di Loranco, path to Andolla refuge, near Alpe Campolamana
98-7	Hypidiotomorph to xenomorph Ep + Czo; Pl, simple and polysynthetic twinned, sericitized; hypidiomorph to idiomorph, zoned, yellow-green, actinolitic Hbl defining mineral lineation; hypidiotomorph to xenomorph Ttn; Chl; late carbonatic sealed cracks	WM-Bt-Qtz-Kfs Orthogneiss	662 500/ 107 900	Valle di Bognanco, 1.5 km E' San Marco, at Simplon shear zone
O2: Zermatt-Saas unit				
99-31	Hypidiotomorph to idiomorph Act and also Zo/ Czo defining strong mineral lineation; Ab; Ilm rimmed by Rt and Ttn; Rt rimmed by Ttn; WM; Fe-bearing carbonate		624 675/ 84 675	Valle d'Ayas, Mezzalama refuge
99-53	see 99-31, no pronounced mineral lineation, higher amount of idiomorph Czo/ Zo		639 225/ 103 625	Saastal, path from Plattjen to Britannia refuge

Table 1 continued: Sample descriptions of the studied amphibolites. For locations see Fig. 1.				
C1: Sills, Siviez-Mischabel basement				
99-14	Poikiloblastic, hypidio- to idiomorphic zoned Zo/ Czo symplectically intergrown with Ab; fine-grained symplectite from Ab + Act, Act partly crystallized to larger idiomorphic grains; Act retrogressed to Bt; Ttn, Hem	Czo-Ep-Grt-Chl-Bt-WM-Rt-Ilm-Ttn-Apt-Hem-Qtz paragneiss	624 250/ 98 350	Mattertal, NNW' Zermatt, Luegelbach
99-15	see 99-14	Grt-Chl-Bt-WM-Ttn-Apt-Hem-Qtz paragneiss	624 250/ 98 350	Mattertal, NNW' Zermatt, Luegelbach
99-40	see 99-14, no symplectite, but Ab + Act; Ilm rimmed by Ttn	Para- and orthogneiss	635 575/ 115 350	Lower Saastal, near Zen Eisten
99-41	see 99-14, large amounts of idiomorphic Czo/ Zo/ Ep; Bt retrogressed to Chl	Grt-WM-Chl-Bt-Qtz paragneiss	635 575/ 115 350	Lower Saastal, near Zen Eisten
C2: Boudins, Monte Rosa cover & basement				
99-20	Idiomorphic, poikiloblastic Grt randomly retrogressed to yellow-green Hbl and symplectite from Ab + yellow-green Act; large grains of Czo/ Zo grown on expense of symplectite; Ilm rimmed by Rt rimmed by Ttn; large grains of Ttn; WM rimmed by Czo/ Zo/ Ep; Hem; Qtz	Garnet mica schists; Monte Rosa cover	627 875/ 80 025	Valle di Gressoney, Alpe Bettolina
99-69	Idiomorphic, poikiloblastic Grt randomly retrogressed to blue-green Hbl and partly replaced by Chl + Bt; blue-green Hbl retrogressed to symplectite from Ab + yellow-green Act; poikiloblastic Ab strongly grown on expense of symplectite; Ilm rimmed by Rt rimmed by Ttn; Czo/ Zo; WM; Hem; more intense retrogression than samples above	Meta-arkoses & garnet mica schists; Monte Rosa cover	629 750/ 81 825	Valle di Gressoney, Plateau del Lys
99-70	Poikiloblastic Grt randomly retrogressed to blue-green Hbl and partly replaced by Chl + Bt; blue-green Hbl retrogressed to symplectite from Ab + yellow-green Act; poikiloblastic Ab strongly grown on expense of symplectite; Ilm rimmed by Rt rimmed by Ttn; Czo/ Zo; WM; Hem	WM-Qtz-garnet mica schists; Monte Rosa cover	629 125/ 81 300	Valle di Gressoney, Plateau del Lys
99-71	Yellow-green Act partly symplectitic; poikiloblastic Ab; Rt rimmed by Ttn; Ilm; Hem; Bt; Chl; Fe-poor carbonate	Act-WM-Ab-Grt-Qtz garnet mica schists; Monte Rosa cover	629 125/ 81 300	Valle di Gressoney, Plateau del Lys
99-72	Symplectite of Ab + Act; Act commonly recrystallized to larger grains; poikiloblastic Ab; hypidiomorphic Zo/ Czo/ Ep; Rt and Ilm rimmed by Ttn; Chl; Bt	WM-Grt-Act-Chl-Qtz garnet mica schists & meta-arkoses; Monte Rosa cover	629 750/ 81 850	Valle di Gressoney, Plateau del Lys
99-66	Very fine-grained symplectite of Ab + Act; some larger Act; late-stage, large, poikiloblastic, hypidio- to idiomorphic Zo/ Czo/ Ep; Rt rimmed by Ttn	Garnet mica schists, meta-arkoses and orthogneisses; Monte Rosa cover & basement	629 150/ 81 025	Valle di Gressoney, Plateau del Lys
C3: Sills, Portjengrat & Monte Rosa cover				
99-50	Large, poikiloblastic Ab; Ep/ Czo often as inclusions in Ab; Act; Rt rimmed by Ttn; Chl partly intercalated with minor amounts of Bt; Hem; Fe-bearing carbonate	Calcitic & dolomitic marbles; Portjengrat cover	639 200/ 103 725	Saastal, path to Mittaghorn
98-75	Poikiloblastic xenomorphic Ab; mostly small xenomorphic Czo/ Zo/ Ep; Act; Rt rimmed by Ttn; Fe-poor carbonate	Calcitic & dolomitic marbles; Portjengrat cover	639 200/ 104 800	Saastal, path from Plattjen to Britannia refuge
99-55	Act defining mineral lineation; poikiloblastic Ab; hypidio- to idiomorphic Czo/ Ep; Rt rimmed by Ttn; Chl partly intercalated with minor amounts of Bt	Calcitic & dolomitic marbles; Portjengrat cover	639 100/ 103 700	Saastal, below Mittaghorn
99-13	Idiomorphic, poikiloblastic Grt randomly retrogressed to blue-green Hbl; blue-green Hbl retrogressed to symplectite from Ab + yellow-green Act; large grains of Czo/ Zo grown on expense of symplectite; Ilm rimmed by Rt rimmed by Ttn; WM; Hem	Meta-arkoses; Monte Rosa cover	646 250/ 102 650	Val Loranco, S-side Bottarello glacier
99-54	Idiomorphic, poikiloblastic Grt internally replaced by Ep/Czo and randomly retrogressed to yellow-green Hbl; symplectite from Ab + yellow-green Act; large grains of Czo/ Zo grown on expense of symplectite; Ab recrystallized to larger poikiloblastic grains; Ilm rimmed by Rt rimmed by Ttn; WM; Hem; Chl; stronger retrogressed than 99-13	Meta-arkoses; Portjengrat cover	639 050/ 103 750	Saastal, path to Mittaghorn

Table 2: Analytical data, Mg# number, Zr/Y ratio and Ce_n/Yb_n ratio. For the Ce_n/Yb_n ratio, the Ce and Yb values are chondrite-normalized; normalisation values were taken from Boynton (1984).

Tectonic unit	Sample	SiO ₂	Al ₂ O ₃	Fe ₂ O ₃	MnO	MgO	CaO	Na ₂ O	K ₂ O	TiO ₂	P ₂ O ₅	LOI	Total	V 51	Cr 53	Co 59	Ni 60	Cu 63	Rb 85	Sr 86	Y 89	
		%	%	%	%	%	%	%	%	%	%	%	%	ppm	ppm							
F1: Boudins, Furgg zone	JK 99-78	51.75	15.61	9.82	0.16	6.57	9.64	3.73	0.31	1.12	0.12	1.03	99.86	252.26	125.47	37.06	18.64	15.55	6.84	238.04	24.24	
	JK 99-85	49.00	16.83	9.35	0.15	6.71	8.81	3.80	0.33	1.36	0.22	3.26	99.82	184.34	229.85	38.64	84.72	57.66	9.31	203.23	24.16	
	JK 99-86	51.67	16.13	9.46	0.14	6.18	10.24	3.48	0.21	1.48	0.26	0.73	99.96	222.35	254.61	31.18	50.49	32.44	4.60	177.67	27.25	
	JK 99-87	52.02	16.06	8.68	0.14	6.48	8.81	4.97	0.16	1.18	0.19	1.22	99.91	182.90	234.22	31.84	79.66	26.03	1.27	179.98	22.16	
	JK 99-95	50.74	15.24	9.67	0.16	6.34	10.44	3.58	0.82	1.55	0.22	1.11	99.87	235.87	247.21	38.56	44.36	81.08	34.04	260.52	29.18	
	JK 98-100	51.49	15.72	8.38	0.15	6.50	9.99	3.18	1.94	1.27	<0.08	1.24	99.86	190.53	267.42	51.97	66.03	74.13	131.19	141.17	24.23	
	JK 97-15	49.02	16.97	9.12	0.15	7.41	10.10	3.19	1.21	1.35	<0.08	1.36	99.87	187.09	208.05	54.09	107.41	38.99	52.78	239.39	25.56	
	JK 98-73	49.11	17.11	9.53	0.15	6.99	10.83	3.25	0.11	1.56	<0.08	1.18	99.82	224.00	261.14	48.87	66.84	78.49	1.46	260.21	27.85	
	JK 98-77	49.09	16.89	9.42	0.16	7.74	10.47	3.08	0.57	1.31	<0.08	1.14	99.87	197.81	257.89	52.38	68.78	54.75	18.84	180.12	23.99	
	JK 98-102	49.90	16.35	10.24	0.15	6.95	9.90	4.08	0.55	1.68	<0.08	0.61	100.41	240.98	248.53	52.45	58.08	52.03	24.46	228.25	28.63	
Furggtal & Valle di Antrona	JK 99-57	50.00	16.67	9.27	0.15	6.70	10.52	3.30	0.50	1.45	0.19	1.13	99.88	222.15	251.08	38.47	79.58	87.63	15.02	225.55	28.16	
	JK 99-61	50.52	16.06	9.33	0.14	6.32	10.08	4.13	0.40	1.37	0.23	1.07	99.66	214.11	263.43	39.62	64.16	86.74	15.84	202.74	27.10	
	JK 98-82	48.94	16.67	9.40	0.17	7.09	11.07	3.62	0.49	1.39	<0.08	0.93	99.77	203.82	251.50	56.03	62.20	95.11	12.21	330.30	26.33	
	JK 98-68	48.61	17.18	8.22	0.06	8.58	9.73	3.34	0.62	1.24	<0.08	1.88	99.46	179.32	235.97	49.66	108.84	66.34	23.90	3138.67	22.36	
Bognanco	JK 99-103	50.35	16.68	9.20	0.15	6.80	9.99	3.76	0.34	1.42	0.22	0.99	99.90	216.23	250.30	36.98	81.64	85.14	9.60	272.82	27.24	
	JK 99-104	50.43	15.81	9.52	0.13	7.49	7.71	3.78	0.29	1.52	0.23	2.77	99.67	238.29	271.61	38.97	54.01	75.38	10.40	1639.41	28.65	
O1: Antrona unit	JK 98-53	50.74	16.02	9.30	0.15	6.96	11.29	3.16	0.17	1.35	<0.08	0.68	99.82	236.72	260.49	60.70	96.01	69.04	1.13	167.14	28.64	
	JK 99-98	50.54	16.49	8.86	0.13	6.38	10.92	3.46	0.16	1.39	0.24	1.29	99.85	216.93	252.77	37.55	82.76	69.75	1.60	229.81	26.82	
	JK 99-102	49.02	15.58	9.43	0.13	4.91	13.90	2.54	0.14	1.57	<0.08	2.75	99.98	253.47	273.17	37.14	98.58	64.75	2.49	140.90	32.95	
	JK 99-105	49.15	18.61	8.35	0.11	6.91	8.95	4.15	0.28	1.09	<0.08	2.37	99.97	153.18	208.89	38.51	122.28	97.67	4.27	240.93	20.13	
	JK 98-07	48.30	16.21	8.97	0.15	7.54	12.79	2.80	0.74	1.30	<0.08	1.00	99.80	190.46	310.67	50.48	135.55	12.72	17.50	272.44	27.29	
	JK 99-31	50.35	15.82	9.27	0.16	8.05	9.36	3.09	0.33	1.49	0.21	1.64	99.76	238.78	271.99	37.34	74.10	82.82	3.67	191.22	29.97	
	JK 99-53	49.84	14.98	9.48	0.15	7.42	12.70	1.68	0.08	1.34	0.20	1.70	99.55	257.28	360.53	38.30	95.16	19.15	<L.D.	120.96	29.52	
	C1: Sills, Siviez-Mischabel basement	JK 99-14	52.60	14.49	10.43	0.15	5.23	7.61	3.67	1.17	1.33	0.26	3.03	99.98	213.99	219.50	33.50	62.64	26.54	43.86	186.40	35.68
		JK 99-15	53.03	15.30	10.45	0.15	5.94	7.55	4.26	0.68	1.60	0.25	2.28	101.49	241.67	194.87	35.30	35.40	47.81	18.65	167.19	36.01
		JK 99-40	51.15	14.73	11.45	0.18	6.62	7.31	3.33	1.22	1.64	0.24	2.05	99.91	238.77	102.50	39.47	62.44	10.16	49.83	210.08	29.86
JK 99-41		48.19	14.44	10.25	0.21	4.06	1.49	1.70	0.58	2.14	1.09	2.21	86.36	278.32	233.63	31.61	10.90	7.40	22.51	695.46	57.91	
JK 99-20		52.80	13.99	11.96	0.15	6.59	6.09	5.01	0.23	1.97	0.42	0.77	99.98	317.48	219.61	43.36	70.30	43.58	2.93	130.20	33.87	
C2: Boudins, Monte Rosa cover & basement	JK 99-69	50.21	18.02	10.40	0.14	4.74	9.03	3.59	1.09	1.23	0.19	1.21	99.84	280.19	144.22	34.82	60.75	281.55	48.91	388.82	28.71	
	JK 99-70	50.71	15.52	11.29	0.19	5.59	7.48	4.48	0.59	1.85	0.19	1.83	99.71	284.23	194.88	38.30	65.03	21.82	16.31	149.94	41.89	
	JK 99-71	48.10	15.29	10.37	0.15	6.74	8.81	3.23	1.87	1.33	0.17	3.73	99.78	196.12	443.48	41.47	131.71	13.30	62.72	146.90	19.03	
	JK 99-72	49.90	15.59	10.17	0.18	5.83	10.63	3.05	1.50	1.55	0.26	1.33	99.99	262.33	282.22	30.48	115.10	8.24	62.72	103.33	27.71	
	JK 99-66	55.22	14.66	6.80	0.10	6.62	9.38	4.02	1.35	0.45	0.08	1.22	99.89	200.04	463.09	32.74	29.56	<5.00	44.29	34.25	22.59	
C3: Sills, Portjengrat & Monte Rosa cover	JK 99-50	47.33	16.89	8.28	0.00	7.97	7.44	3.18	0.40	1.12	0.17	7.08	99.86	171.48	232.90	38.59	109.18	85.51	13.40	186.50	22.05	
	JK 98-75	47.14	16.61	8.83	0.14	8.69	7.71	4.03	0.13	1.17	<0.08	5.48	99.90	170.15	242.55	43.01	80.40	65.93	2.27	147.00	22.16	
	JK 99-55	49.88	16.62	9.24	0.11	7.36	9.26	3.98	0.23	1.25	0.17	1.77	99.87	197.97	271.66	42.40	73.13	85.11	5.91	197.37	24.65	
	JK 99-13	50.86	16.92	8.13	0.13	6.50	10.03	4.26	0.08	0.95	<0.08	2.10	99.97	238.29	103.37	33.52	31.69	13.41	1.68	261.09	21.83	
	JK 99-54	50.06	17.24	8.88	0.16	7.42	9.71	3.27	0.11	1.17	0.15	2.04	100.20	231.37	311.26	36.40	104.02	14.06	1.51	165.55	27.15	

4 Structural geology

The present-day geometry of the Penninic nappe pile in the Monte Rosa region is largely the result of four superposed phases of folding and thrusting that evolved under eclogite to greenschist facies metamorphic conditions and during the exhumation of the nappe pile. The prograde structural evolution is only locally preserved, usually in relict minerals (see e.g. Dal Piaz, 1966, 1971; Gebauer, 1999; Keller, 2000; Pawlig & Baumgartner, 2001; Le Bayon et al., 2001). The particular structural characteristics of each deformation phase were investigated in micro- and outcrop-scale and will be introduced in chapter 4.1 and summarized in Table 4.1. Chapter 4.2 discusses the large-scale structures that are illustrated in the geologic-tectonic map (Encl. 1 & 2) and 13 N-S cross-sections (Encl. 3 & 4). In chapter 4.3 the major shear zones will be discussed. Chapter 4.4 presents a composite cross-section illustrating the geometric relationship of the large-scale structures. Together with the kinematic indicators from mylonitic shear zones discussed in chapter 4.5, all these structural data form the basis of the discussion on the large-scale kinematics in chapter 5.

4.1 Characterization of deformation phases and associated metamorphism

The investigated area comprises a variety of rock types with differing rheological properties and viscous strength that strongly influence the style of deformation. Since strength is primarily a function of bulk rock chemistry, temperature and metamorphic grade, the geometrical characteristics of a particular deformation phase at a given time may vary depending on rock type. Where necessary, the deformation phases will therefore be discussed separately for the two major rheological units - Furgg zone & Permo-Mesozoic sedimentary cover, and ophiolitic & granitic continental basement. Since the structures in the Furgg zone were studied in greater detail than in the remaining units (cf. chapter 4.2), equivalent structures cannot be presented for each unit. Table 4.1 provides an overview of the structures observed. Lower hemisphere stereographic projections of all the observed structures are compiled in Figs. 4.2.2, 4.2.9, 4.2.18, 4.2.25, and Figs. 4.5.4 and 4.5.5.

4.1.1 Pre-D1 structures

Although generally scarce, several pre-D1 structures can be observed.

Locally, a **pre-Alpine foliation** is preserved in the paragneisses of the continental basement units. Dal Piaz & Lombardo (1986) described fibrous sillimanite defining a pre-Alpine foliation in paragneisses of the Monte Rosa nappe. Sillimanite is often replaced by unaligned kyanite that is therefore interpreted to have grown in a period of tectonic quiescence prior to Alpine deformation. Chadwick (1974), Rössler (2000) and Keller & Schmid (2001) also described the unaligned growth of kyanite from paragneisses of the Monte Rosa nappe and its Alpine deformation in anastomosing shear zones.

At the following three localities, **discordant intrusive contacts** of Pre-Alpine age are preserved. (1) At Lake Mattmark in Saastal, granites intruded paragneisses of the Monte Rosa nappe. (2) Below the Allalin glacier in Saastal, a basaltic dyke intruded garnet micaschists of the Portjengrat unit (Fig. 4.3.1 B). (3) At Passo della Preja in Valle di Loranco - Valle di Bognanco, a basaltic dyke intruded marbles of the Portjengrat unit (Fig. 4.3.1 A). All other lithological contacts are transposed into the foliation (see section 4.1.2).

Although overprinted by the successive deformation, the **sedimentary bedding** of the Permo-Mesozoic sediments can often be recognized as a compositional layering. It usually consists of an alternation of mica- (and eventually garnet-) rich and mica- poor layers, or - in the marbles - of an alternation of calcite and dolomite marble. Other sedimentary structures are not preserved.

A first penetrative Alpine-age foliation (s₀) was formed under supposedly eclogite facies conditions (see below and chapter 4.1.2). As it was isoclinally refolded during successive deformation phases, it forms part of a composite foliation which is composed of the foliations formed during D₀,

Table 4.1: Characteristics of deformation phases.

Note that the two major movement directions, i.e. top to the WNW thrusting (D1 & D2) and top to the S/SE dextral transpression (D3 & D4) both form continuous processes in the sense of progressive deformation. Hence D1 and D2 (or D3 and D4) may overlap in time and space (see chapter 5).

Cycle	Event	Permo-Mesozoic sedimentary cover		Continental crystalline units (SM, PG, ST, MR)		Ophiolitic units (ZS, An)	
		Structures	Metamorphism	Structures	Metamorphism	Structures	Metamorphism
Variscan				Remnants of pre-Alpine nT-foliation in MR paragneisses.	Foliation defined by sillimanite, often retrogressed to kyanite. Further unaligned growth of kyanite.		
Alpine	Sedimentation during continental break-up	Sedimentary bedding ss partly preserved as compositional layering.					
	Sea-floor spreading	Intrusion of basaltic dykes & sills		Intrusion of basaltic dykes & sills (all units)		Magmatic pillow structures preserved in ZS unit. Sedimentary bedding ss preserved as compositional layering in calcareous micaschists.	
	Nappe stacking, D0	Penetrative foliation s0 ?	Eclogite to upper greenschist facies.	Penetrative foliation s0	Eclogite to upper greenschist facies.	Penetrative foliation s0	Eclogite to upper greenschist facies.
	Nappe stacking, D1	Isoclinal folding of s0 and sedimentary bedding ss. Penetrative foliation s1 developed as axial plane cleavage of isoclinal folds.	Eclogite to upper greenschist facies.	First mylonitic foliation s1. Synkinematic isoclinal folding of s1 and compositional layering ss.	Eclogite to upper greenschist facies.	First mylonitic foliation s1. Synkinematic isoclinal folding of s1 and compositional layering s0.	Eclogite to upper greenschist facies.
	Nappe stacking, D2 (Ragnor-Randa phase)	Isoclinal folding of ss, s0 and s1. Penetrative foliation s2 developed as axial plane cleavage in the isoclinal folds. ss, s0, s1 and s2 define the composite main foliation. Stretching lineation with associated top to the NW/W sense of shear developed on the composite foliation planes.	Eclogite to upper greenschist facies. Locally until lower greenschist facies (e.g. Gornegrat).	Isoclinal folding of s0 and s1. Penetrative foliation s2 developed as axial plane cleavage in the isoclinal folds. ss, s0, s1 and s2 define the composite main foliation. Stretching lineation with associated top to the NW/W sense of shear developed on the composite foliation planes.	Eclogite to upper greenschist facies. Locally down to lower greenschist facies (e.g. Gornegrat).	Isoclinal folding of s0 and s1. Penetrative foliation s2 developed as axial plane cleavage in the isoclinal folds. ss, s0, s1 and s2 define the composite main foliation. Stretching lineation with associated top to the NW/W sense of shear developed on the composite foliation planes.	Eclogite to upper greenschist facies. Lower conditions not observed.
	Post-nappe stacking, D3 (Mischabel phase) "back-folding"	Open to isoclinal folding of the composite foliation. Locally s3 foliation developed in the D3 fold hinges. Penetrative s3 foliation s3 restricted to major D3 shear zones. Stretching lineation with associated top to the SE/E sense of shear developed on s3 foliation planes.	Upper greenschist facies to semi-brittle.	Open to isoclinal folding of the composite foliation. Locally s3 foliation developed in the D3 fold hinges. Penetrative s3 foliation s3 restricted to major D3 shear zones. Stretching lineation with associated top to the SE/E sense of shear developed on s3 foliation planes.	Upper greenschist facies to semi-brittle.	Open to isoclinal folding of the composite foliation. Locally s3 foliation developed in the D3 fold hinges. Penetrative s3 foliation s3 restricted to major D3 shear zones. Stretching lineation with associated top to the SE/E sense of shear developed on s3 foliation planes.	Upper to lower greenschist facies. Lower conditions not observed.
	Post-nappe stacking, D4 (Vanzone phase)	Open folds.	Upper greenschist facies to semi-brittle.	Open folds. Gentle crenulation.	Upper greenschist facies to semi-brittle.	Open shear folds (all lithologies) and box folds (in serpentinites). Gentle crenulation.	Upper greenschist facies to semi-brittle.

D1 and D2. The minerals defining this foliation and the associated metamorphic conditions are described in detail in chapter 4.1.2. In some of the meta-basaltic boudins in the Furgg zone below the Allalin glacier in Saastal, a compositional layering of supposed Alpine-age tectono-metamorphic origin (D0) was observed (s0 in Fig. 4.3.2 d). It consists of a layering of coarse- and fine-grained symplectite (intergrowth of actinolite and albitic plagioclase, see Fig. 4.1.3 A + B). Eclogite facies formation conditions are indicated by the symplectites as they are considered as recrystallization products of omphacite and garnet (see chapter 4.1.2 for a detailed discussion).

4.1.2 D1 and D2 deformation phases

The first two deformation phases D1 and D2 are related to NNW- to NW-directed nappe stacking (e.g. Stampfli & Marchant, 1997; Schmid & Kissling, 2000). They are characterized by high strains presumably related to high strain rates. In the course of straining, all the planar and linear structural elements like sedimentary bedding, lithological contacts, foliation, fold axes and stretching lineations were parallelized. Hence, a structure can only be unequivocally assigned to D1 or D2 if overprinting relationships are preserved. As this is often not the case, the two deformation phases and the associated metamorphic conditions are described together.

D1 deformation phase

During the first deformation phase (D1), the foliation s0 (and eventually the sedimentary bedding ss) was refolded by a **first generation of isoclinal folds** (Figs. 4.1.1 A, B, C; see also Fig. 4.3.2 f and Fig. 4.2.19). Due to the high strain rates, their limbs were often thinned out strongly and intrafolial folds developed (Figs. 4.1.1 D). Contemporaneously with folding, the **foliation s1** developed as axial plane cleavage of the isoclinal D1 folds (Fig. 4.1.1 A & C). The minerals defining the foliation are described below (section "metamorphic conditions"). Due to the isoclinal nature of folding, D1 fold axial planes are parallel to the foliation s1.

D2 deformation phase

During the second deformation phase (D2), the foliations s0 and s1 (and eventually the sedimentary bedding ss) were refolded by a **second generation of isoclinal folds** (Figs. 4.1.1 B; see also Fig. 4.3.2 f & g and Figs. 4.2.20 & 4.2.22). High strain rates again accounted for strongly thinned fold limbs. Contemporaneously with folding, the **foliation s2** developed as axial plane cleavage of the isoclinal D2 folds (Figs. 4.1.1 B; see also Fig. 4.5.2 A & B). The minerals defining the foliation are described below (section "metamorphic conditions"). Due to the isoclinal nature of folding, D2 fold axial planes are parallel to the foliation s2. Fold axes of both D1 and D2 folds range in orientation from SW to NNW-plunging (see Figs. 4.2.2, 4.2.9, 4.2.18, 4.2.25). However, many of them were reoriented by D3 folding and thrusting (see section 4.1.3 and chapter 4.5).

Composite foliation composed of s0, s1, s2, and eventually ss

Due to the isoclinal nature of D1 and D2 folding, the three mylonitic foliations s0, s1 & s2 and, where present, the sedimentary bedding, are oriented parallel to each other in the limbs of the isoclinal folds. As such they define a penetrative composite foliation (e.g. Fig. 4.1.1 E & F) that, in outcrop, is recognized as the main foliation throughout the investigated area. The pervasiveness of the foliation varies with the amount of sheet silicates in a rock and/ or with the degree of grain size reduction during mylonitization.

For example, the granites of the Monte Rosa nappe cover all stages of mylonitization, ranging from undeformed granites with preserved magmatic texture to ultramylonitic textures in shear zones. In the Monte Rosa granites, the shear zones are usually narrow (cm to dm in width). Some of them were repeatedly reactivated, especially those associated with fluid enhanced metasomatism (see Pawlig & Baumgartner, 2001).

Stretching lineation

On the foliation planes, a stretching lineation has developed that moderately plunges from the SW to the NNW (see maps in Figs. 4.5.7 & 4.5.8). The minerals defining the stretching lineation

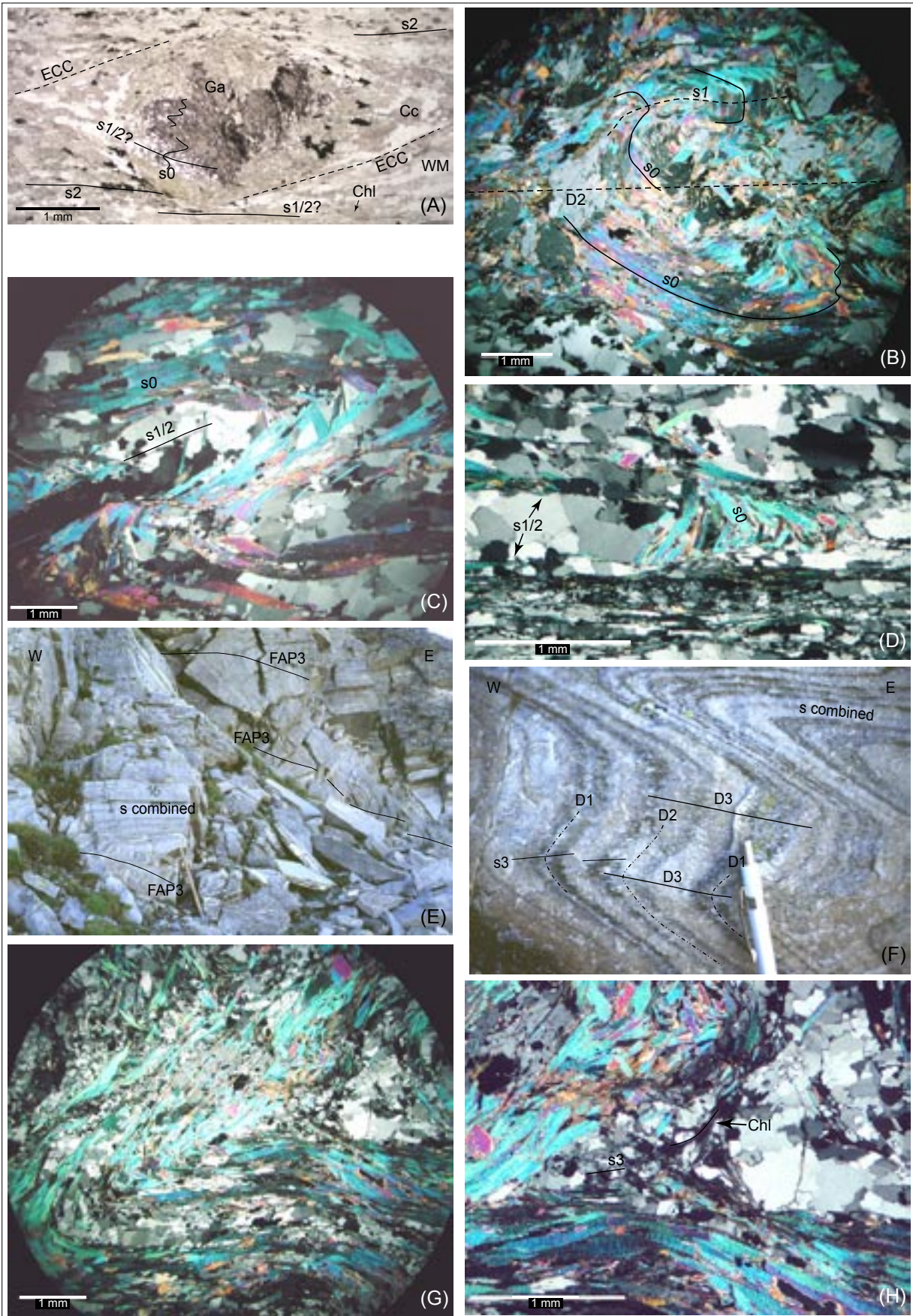


Fig. 4.1.1: Development of foliation in thin section and outcrop. Figure captions see next page.

are described below (section “metamorphic conditions”). The associated kinematic indicators exhibit a top to the SW to NNW (downplunge direction) sense of shear (see chapter 4.5).

Fold interference patterns

The superposition of first- and second-generation folds usually led to type 3 interference patterns (after Ramsay & Huber, 1987, Vol. II). This requires subparallel D1 and D2 fold axes and D1-D2 fold axial planes at a high angle to each other. The orientation of the regional stress field, however, did not necessarily change from D1 to D2. Initially upright D2 folds may have simply been superposed onto previously flat-lying or recumbent D1 folds. Later, also D2 folds were rotated into a flat-lying position due to ongoing D2 deformation.

The kilometer-scale "Hangende Gletscher fold" (see chapter 4.2.3) was described as a single-phase structure, i.e. as a D2 sheath fold, by Lacassin & Mattauer (1985) and Rössler (2000). However, for comparable, less spectacular geometric structures unequivocal evidence for a single-phase formation was not found. Such structures were therefore rather interpreted as basin and domes formed by a superposition of D3 folds onto D1/ D2 folds (see chapter 4.1.3).

Minerals defining the composite s₀/s₁/s₂ foliation & stretching lineation and interpreted metamorphic conditions

In the investigated area, pT-paths suggest either a direct transition from eclogite to greenschist facies conditions (Le Bayon et al., 2001), or via epidote-amphibolite facies or blueschist facies to greenschist facies (Zermatt-Saas unit; Meier, 1987; for further references see chapter 2.2.1). The detailed investigation of the tectono-metamorphic evolution, however, was not the primary aim of this study. The conditions derived from mineral assemblages observed in thin section are usually greenschist facies. The following description is therefore not comprehensive and only describes the findings of this study (see Le Bayon et al., 2001, for further details regarding the tectono-metamorphic evolution).

In metapelites and metacarbonates, the composite s₀/s₁/s₂ foliation is generally defined by the shape-preferred orientation (SPO) of sheet silicates (usually white mica and/ or chlorite) and/ or by a compositional layering. For the formation of the latter, metamorphic segregation processes as well as the original sedimentary bedding probably played a role. Eclogite facies conditions have previously been deduced from the high phengite content of white mica that define the (composite) main foliation in Permo-Mesozoic quartzites at the Gornergrat in Mattertal (Rubatto & Gebauer, 1999). However, the formation of the foliation was a continuous process that prevailed until lower metamorphic conditions, as can also be concluded from lower phengite contents described from white mica by Rössler (2000) and Keller (2000).

The stretching lineation in metapelites is usually defined by stretched aggregates of quartz and sheet silicates and possibly garnet. In metacarbonates, the stretching lineation is only rarely developed, defined by the SPO of acicular tremolite (Fig. 4.1.2). According to Spear (1993), the observed assemblage of tremolite + dolomite + calcite (+ quartz) is indicative of epidote-amphibolite to middle amphibolite facies, as the formation of tremolite starts at pressures of 0.5 GPa and temperatures > 500°C. As those are the conditions reached throughout the investigated area, and since no amphibolite facies overprint has been described so far, the presence of tremolite can be explained by passing from eclogite through epidote-amphibolite facies metamorphic conditions before the greenschist facies overprint. The tremolite-producing retrograde reaction could not be

Fig. 4.1.1: Development of foliation in thin section or outcrop.

(A) Isoclinally refolded s₀ foliation defined by quartz preserved in garnet (Ga). The fold axial planes (s₁/s₂?) are subparallel to the external foliation defined by white mica (WM) and chlorite (Chl). Shear bands (ECC) developed during D3. Calcareous micaschists. **(B)** Superposition of isoclinal D1 and D2 microfolds. Meta-arkoses. **(C)** Isoclinal D1 or D2 fold with a weak D1 or D2 axial plane cleavage. Garnet micaschists. **(D)** More penetratively developed D1/ D2 fold axial plane cleavage defined by white mica and small recrystallized quartz grains. Quartzite. **(E) & (F)** Combined foliation (s combined) in Mesozoic quartzites is the product of sedimentary bedding (compositional layering of quartz- and mica-rich layers) and two isoclinal folding phases D1 and D2 (systematic doubling of mica-rich layers). During D3 folding, a weak axial plane cleavage s₃ has locally developed in the fold hinges. At Plattjen in Saastal. **(G)** Thin section of a D3 fold hinge as seen in (E) & (F). **(H)** Enlargement of (G). S₃ is defined by white mica (WM) and chlorite (Chl). Plane polarized light in (A), crossed polarized light in (B), (C), (D), (G) and (H).

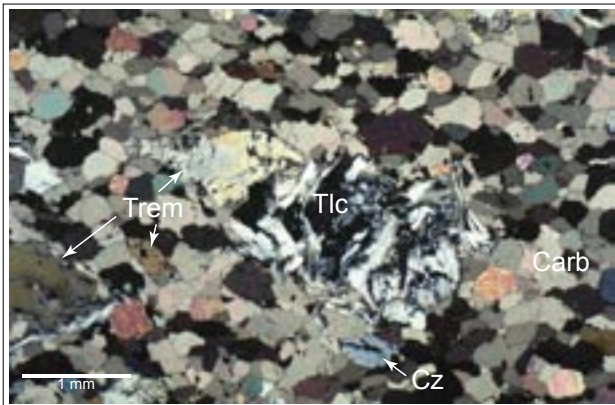


Fig. 4.1.2: Photomicrograph of tremolite (Trem) that is retrogressed to talc (Tlc) in Mesozoic marbles.

The tremolite needles define a stretching lineation. Cz: clinozoisite, Carb: calcite and dolomite. At Passo P. 2325, near Monte della Preja in Val Loranco. For discussion see text.

unraveled as no relict mineral assemblages were found (see Spear, 1993, p. 452 and Bucher & Frey, 1994, p. 173 for possible reactions). The further retrogression of tremolite to talc (tremolite + dolomite + H₂O + CO₂ = 3 calcite + 2 talc in the present dolomite- rich compositions) indicates the transition to upper greenschist facies conditions. Unfortunately, tremolite or talc could never be used as kinematic indicators and a sense of shear could not be derived.

In metagranites, the development of a deformation fabric is very heterogeneous and corresponds to shear zones of different width, intensity and age (D1/D2 or D3). The s1/s2 composite foliation is usually defined by flattened feldspar-clasts that now form elongate augen in mylonitized zones, and by aligned tourmaline needles, white mica and/ or chlorite.

The semi-brittle flattening of feldspar simultaneously with a ductile deformation of quartz requires temperatures between 550° and 350°C (Tullis & Yund, 1977 & 1980) that prevailed during D2 and D3 alike. Additionally, the parallelisation of aplitic dykes contribute to the foliation.

The stretching lineation is usually defined by stretched aggregates of quartz and feldspar and the SPO of acicular black tourmaline.

In metabasites, the composite foliation is usually defined by the SPO of chlorite, actinolite and by deformed albite blasts, or, by an alternation of fine- and coarse-grained symplectites of actinolite and albite (cf. Fig. 4.1.3; no symplectites found in the metabasaltic dykes of the Siviez-Mischabel nappe). The present mineral assemblage of chlorite + albite + epidote + actinolite + quartz +/- carbonate (calcite, dolomite or ankerite) +/- titanite is diagnostic for greenschist facies conditions (Spear, 1993). The symplectitic intergrowth of actinolite and plagioclase, ranging in composition from oligoclase to albite, is probably the result of the decomposition of omphacite that was stable during eclogite facies conditions (not observed in the Siviez-Mischabel nappe). As the plagioclase series displays a pronounced miscibility gap between albite and oligoclase (Peristerite gap), retrograde metamorphic reactions enforce a jump in plagioclase composition from

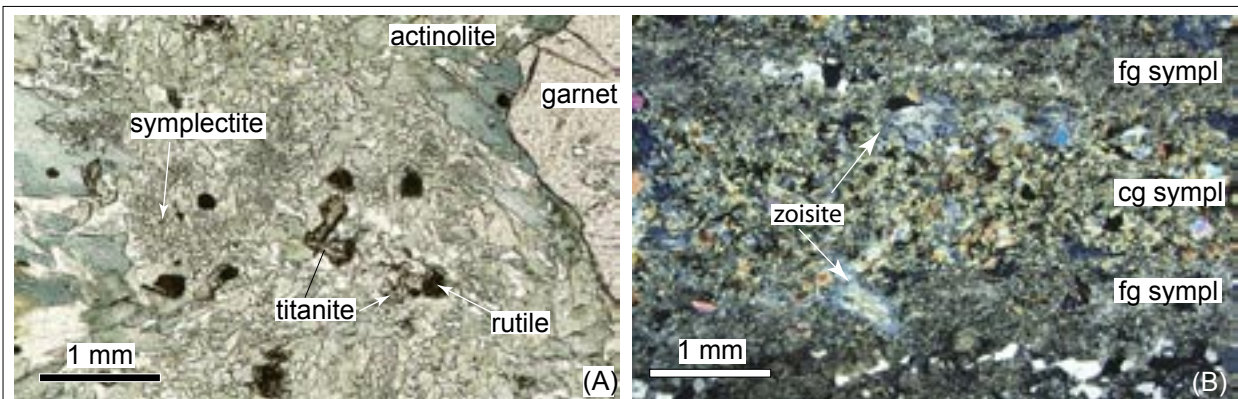


Fig. 4.1.3: Photomicrograph of the symplectitic intergrowth of actinolite and albite.

(A) Symplectitic intergrowth of actinolitic hornblende and albitic plagioclase as supposed recrystallisation products of omphacite, indicating the retrogression from eclogite to upper greenschist facies conditions. Metabasaltic boudin from the Furgg zone in Furggtal (crd. 642 550/ 101 625). Plane polarized light.

(B) Fine- and coarse-grained symplectite defining the first penetrative foliation s0. Discussion see text. Metabasaltic boudin from the Furgg zone below the Allalin glacier in Saastal (crd. 639 825/ 100 225). Crossed polarized light.

approximately An_{18} to An_3 . This decalcification led to the formation of zoisite or epidote, as it can be observed in Fig. 4.1.3 B. As this reaction involves a hydration of the anorthite component (anorthite + H_2O = zoisite + quartz; unbalanced), water needs to be introduced into the system.

A stretching lineation is only scarcely developed and, if so, defined by the shape-preferred orientation of acicular actinolitic hornblende. This leads to the conclusion that the formation of actinolite generally post-dates the nappe stacking (D1 & D2). Evidence that it occurred late during the successive deformation phase D3 will be provided in chapter 4.3.1.

4.1.3 D3 deformation phase (Mischabel phase)

The third deformation phase (Mischabel phase) is related to dextral oblique SE- to E-directed thrusting of the nappe stack, and is generally referred to as "post-nappe stacking" or "backfolding" phase (e.g. Milnes et al., 1981; Escher et al, 1997; Ring & Merle, 1992). D3 is characterized by the development of dextral oblique shear zones of up to kilometer-width and by S- to SE-facing large-scale folds that largely define the present-day geometry of the nappe stack (see chapter 4.2 for a detailed discussion of the structures). As deformation was accompanied by cooling to lower greenschist facies and semi-brittle conditions, the rheological differences became prominent during later stages of D3, leading to a partitioning of strain. Hence, the geometry of the D3 structures strongly depends on the rock type.

Foliation s3

The formation of a new penetrative foliation s3 and associated stretching lineation is largely restricted to three major shear zones: the Portjengrat-, Gornergrat-Furggtal- and Saas shear zones (described in detail in chapter 4.3). Within those shear zones, the s3 foliation is mainly defined by shear bands (see Figs. 4.3.5, 4.3.7 and 4.5.1 D-G). In the augengneisses situated in the Portjengrat shear zone (see Fig. 5.1), s3 is additionally defined by flattened feldspar clasts, aligned tourmaline, white mica and biotite (see Fig. 4.5.1 D).

Outside those three shear zones, a weak s3 foliation was locally observed in the fold hinges of the D3 folds, parallel to the D3 fold axial planes (Figs. 4.1.1 E - H).

Style of folding

The style of D3 folding depends on the rock composition. The more isotropic feldspar-, pyroxene- or amphibole-rich rocks (**ophiolites and continental granites**) behave as relatively rigid bodies that accommodate straining by the formation of open folds (e.g. Mittaghorn synform, Fig. 4.2.21) or along mm- to m-scale discrete shear zones.

The well-foliated and fine-grained, or the quartz- and calcite-rich rocks (**paragneisses of the continental basement and Permo-Mesozoic sediments**) are still relatively weak even at low temperatures. This led to the formation of tight to isoclinal folds (e.g. Figs. 4.1.1 E & F and 4.3.7 A) or to tens or hundreds meter-sized shear zones (e.g. Saas shear zone, see chapter 4.3).

Gently bowed domes and basins of decimeters in diameter (type 1 interference pattern according to Ramsay & Huber, 1987) can exceptionally be observed, for example at the Gornergrat in Mattertal and at the Längflue in Saastal in calcite marbles, and at the Nollenhorn in Saastal in Monte Rosa orthogneisses. This interference pattern requires fold axes at a high angle and subparallel fold axial planes and was interpreted as a superposition of D3 onto D1/ D2 folds.

4.1.4 D4 deformation phase (Vanzone phase)

The fourth deformation phase (Vanzone phase) succeeds the Mischabel phase and is also related to S- to SE-directed folding and dextral oblique thrusting. On a larger scale, it is responsible for the folding of the Monte Rosa nappe around the kilometer-scale S-facing Vanzone antiform (see discussion in chapter 4.2.1; Milnes et al., 1981; Escher et al, 1988 & 1997). In the investigated area, outcrop-scale D4 folds are either developed as open shear folds (Fig. 4.2.3) or as box folds, or, on a smaller scale, as a gentle crenulation of the combined foliation (Fig. 4.2.4 A). In contrast to the

steeply NNW-ward dipping D4 fold axial plane of the large-scale Vanzone antiform, many of the smaller-scale D4 fold axial planes steeply dip to the S to SSW (average 194/66; Fig. 4.2.4 B). D4 fold axes range from moderately SW- to W-ward plunging. This leads to the formation of basin and dome structures, especially in the hinge region of the Vanzone antiform in Valle d'Ayas and Valle di Gressoney.

4.2 Meso- and large-scale structures

In this chapter, the field relationships between meso- and large-scale structures observed in the investigated area will be discussed with the help of geologic-tectonic maps and cross-sections. The geologic-tectonic maps are presented in Enclosures 1 & 2, the cross-sections are presented in Enclosures 3 & 4. The location of the cross-sections is given in Fig. 4.2.1. The projection techniques used for the construction of the cross-sections are described in detail at the beginning of each subchapter. They are also summarized in Tab. 4.2.1.

The nappe contacts were investigated in detail at a scale of 1:10'000 or, in parts of the Saas and Zwischbergen areas, 1:2'500. The scale was then reduced to 1:25'000. Data from the following diploma theses were included: Dubach (1998), Keller (2000), Rössler (2000), Weber (2001), and Bacher (2002). The Swiss topographic maps (Landeskarte der Schweiz 1:25'000: 1308 St. Niklaus, 1309 Simplon, 1328 Randa, 1329 Saas, 1348 Zermatt, 1349 Monte Moro; and 1:50'000: 285 Domodossola, 294 Gressoney) form the topographic basis. Names and spellings are adopted from the maps. The reader is advised to refer to these maps to find the described localities. The refuges on the southern slope of the Monte Rosa massif are shown only on the Italian topographic map 1:35'000, sheet Monte Rosa, edition 1999.

The more internal parts of the basement nappes have been investigated in less detail at a scale of 1:25'000. For their presentation, data from the following geological maps and publications were included: Geologischer Atlas der Schweiz 1:25'000, sheets 29 Zermatt, 43 Randa, 71 St. Niklaus, 61 Simplon, 31 Saas, 30 Monte Moro (all mapped by Bearth 1953 a+b, 1954 a+b, 1957, 1964 a+b, 1972, 1973, 1978 a+b); Carte geologique 1:25'000 Weissmies-Portjengrat (mapped by Huang, 1935 a+b); Carte tectonique des Alpes de Suisse occidentale 1:100'000, sheet 47 Monte Rosa (mapped by Steck et al., 1999); Carta geologica d'Italia, 1:100'000, sheets 29 Monte Rosa and 30 Varallo (mapped by Mattiolo et al., 1912, 1927) and sheet 15 Domodossola (mapped by Novarese & Stella, 1913); and maps included in Klein (1978).

Geologic-tectonic maps

The geologic-tectonic maps (Enclosures 1 & 2) are presented as interpreted maps and all quarternary cover has been removed. Because lakes, glaciers, moraines and alluvium cover large parts of the investigated area, the exact location of lithological contacts across the Quarternary cover remains unknown. Due to the complexity of the structures, mappable and inferred contacts could not be distinguished graphically in Enclosures 1 & 2. The retreat of the glaciers has exposed new outcrops since the last correction of maps in some places. This is the case below the tongue of the Allalin glacier in the upper Saastal (exposed to approximately 2450 m elevation) and at the northern rim of the Zwischbergen glacier in the upper Zwischbergental (a band of 50 additional meters is exposed). Glaciers and lateral moraines were treated as even topographic surfaces onto which the lithological boundaries were projected.

Cross-sections

13 N-S cross-sections whose location is indicated in Fig. 4.2.1 were constructed perpendicular to the major D3 and D4 fold axes (Enclosures 3 & 4). The numbers of the cross-sections refer to the corresponding N-S coordinate of the Swiss topographic map. In addition, three E-W cross-sections, found in Fig. 4.2.1, were constructed for the Gornergrat in Mattertal. All cross-sections are exclusively based on surface geological data.

Thickness of strata

Due to polyphase folding and ductile deformation during nappe stacking and subsequent deformation the thickness of the Permo-Mesozoic sedimentary strata varies considerably throughout the region. Thus the thickness of strata at hand in a given area was used for the construction of the cross-sections. At places covered with Quarternary sediments, the thickness of the strata of the

closest outcrops was extrapolated.

Thicknesses m were computed after the following equation:

$$m = x \sin \alpha$$

where x is the width of outcrop perpendicular to the composite main foliation $s_0/s_1/s_2$, and the angle α is the average dip of the composite main foliation.

Projection techniques

Projection of tectonic contacts

As the structures are highly non-cylindrical, structure contour maps have been drawn for all major tectonic contacts. They consider strike and dip of nearby foliations and the intersection lines of outcrops and topography.

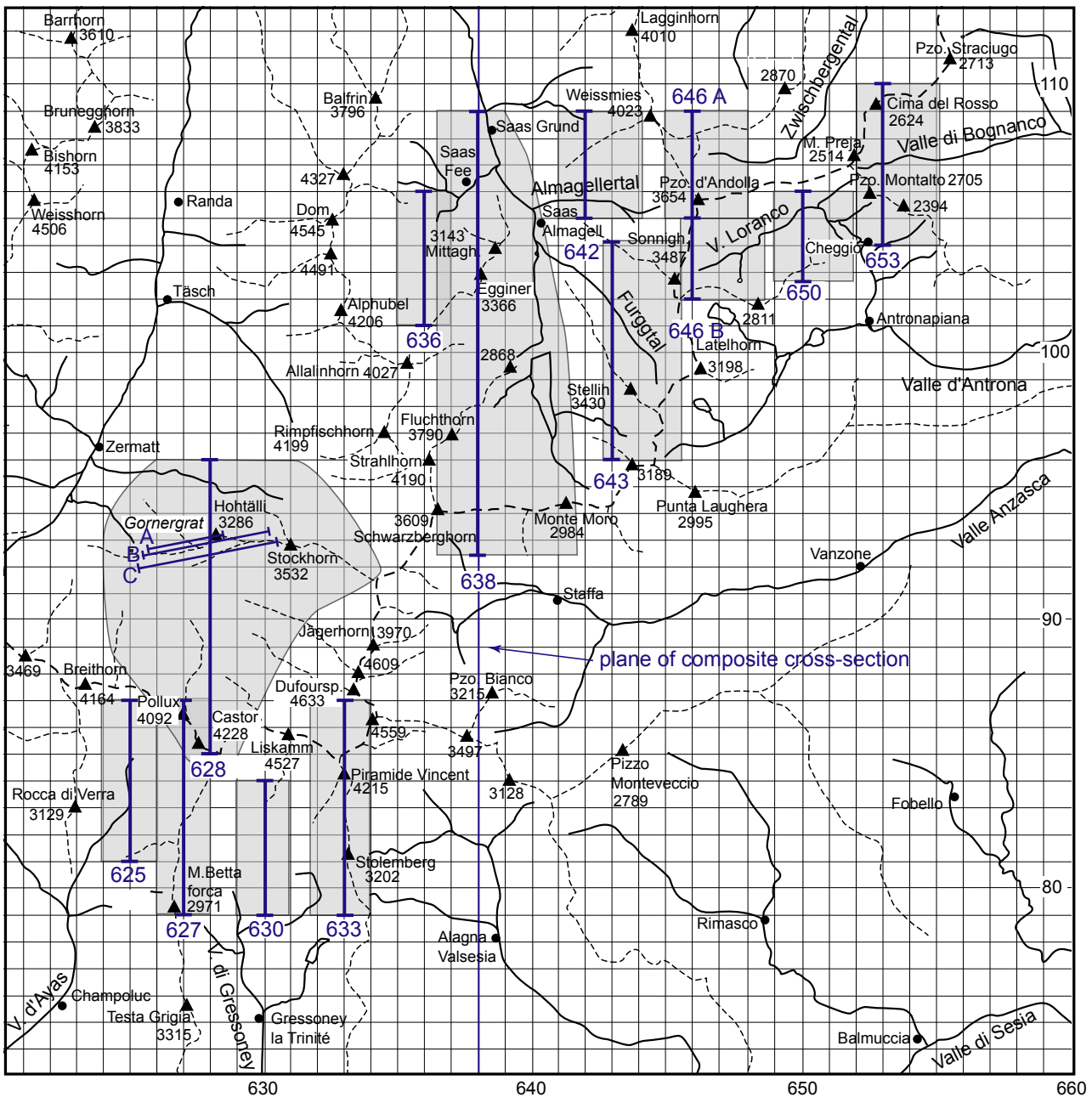


Fig. 4.2.1: Geographic overview of the field area and location of the cross-sections. The gray boxes indicate the approximate catchment area of the structures projected into the individual cross-sections.

Projection of single points

Single points were projected into the section plane along the major fold axes, which are D3 or D4 structures. These fold axes were calculated by stereographic projection as π -poles from the measured composite main foliations (s0/s1/s2; Fig. 4.3.2). Where necessary, subareas were defined and projected with different projection values into the same cross-section. In some of the areas, the calculated fold axes are not in agreement with the structural contour maps and the measured meso-scale fold axes. In this case, a best fitting value (indicated as "best fit" in Tab. 4.2.1) was introduced, considering that lithological boundaries are not allowed to intersect. The axial plunge was assumed to be constant over short distances. The maximum distance of projection is 1.5 km.

The difference in height Δh between the elevation of a point in the map and its elevation in the cross-section is given by the following equation:

$$\Delta h = x \tan \alpha,$$

where x is the distance of a point from the section plane measured along the azimuth of the fold axis, and α is the plunge of the fold axis.

As the D3 and D4 fold axes roughly plunge to the W, points situated W of a N-S cross-section are projected in up-plunge direction. Thus their elevation in the section is equal to Δh + their elevation in the map. Points situated E of the section are projected in down-plunge direction, thus their elevation in the section is equal to their elevation in the map - Δh .

Recalculation of measured foliations

The true dip α of the measured foliations was converted to the apparent dip α' in the section plane by the following equation:

$$\tan \alpha' = \tan \alpha \sin \beta,$$

where β is the angle between the section plane and the azimuth of the foliation.

Tab. 4.2.1: Projection values of cross-sections.

„Best fit“ means that an average projection value was chosen, which is usually a combination of the orientation of the calculated large-scale and the measured small-scale fold axes. Additionally, structure contour lines were constructed for the major nappe contacts. They defined the framework, into which the internal structures had to fit. For a detailed discussion see the respective section in chapter 4.2.

Section & N- S coord.	E- W coord.	Projection value		Projection value used for projection into the plane of cross- section 628 (see ch. 4.4)	Distance from section 628 in m measured along projection value	Total height of cross-section in m in the composite section plane
625	81 - 86	270/33	best fit	not projected		
627	79 - 87	250/27 + 250/10	best fit	285/27	1000	4550
630	79 - 84	264/31	D4- FA Lys antiform	not projected		
633	79 - 86	266/17	best fit	not projected		
				Projection value used for projection into the plane of composite cross- section 638 (see ch. 4.4)	Distance from section 638 in m measured along projection value	Total height in m relative to 638
628	85 - 96	285/30	best fit	285/30	10300	9950
636	101 - 106	280/33	Average of D3- FA Spiel-	288/25	2000	3820
638	93.5 - 109	289/25	D3- FA Mittaghorn synform			
642	105 - 109	270/29	best fit	262/29	4000	660
643	96 - 104	255/12	best fit	259/22	5020	970
646	102 - 105	250/30	Meso- scale D3- FA			
646	105 - 109	266/33 + 266/30	D3- FA Zwischbergen anti- form + meso- scale D3- FA	262/33	8000	-2350
650	102.5 - 106	250/30	Meso- scale D3- FA	253/31	12350	-5220

4.2.1 Upper Valle d'Ayas and Valle di Gressoney

Cross-sections 625, 627, 630, and 633

Projection methods

The sections at the southern slope of the Monte Rosa massif are situated in the hinge region of the D4 Vanzone antiform (cf. Fig. 4.4.2). Due to the heteroaxial superposition of D4 onto D3 folds (E-W-striking D4 fold axial planes onto N-S-striking D3 axial planes, and a small angle between D4 and D3 fold axes), elongate structural basins and domes arise. The resulting axial culminations and depressions make a cylindrical projection method for the construction of cross-sections impossible. As, however, the exposure of the area is insufficient to collect enough structural data, the structures were still cylindrically projected over short distances. Because of the non-cylindricity of structures, however, the cross-sections at the southern slope of the Monte Rosa massif cannot be reasonably projected into a single plane (see ch. 4.4).

Due to the absence of a D3 axial plane cleavage, π -poles used for the projection were calculated from the composite foliation. Also, because the azimuths of D4 and D3 fold axes are subparallel, the calculated projection values are the product of both D3 and D4 folding. The values used for projection are therefore usually best fitting averages of the calculated π -poles and measured D3 and D4 fold axes.

625, in Valle d'Ayas

Monte Rosso - Mezzalama refuge - Guide d'Ayas refuge

Coordinates: N-S: 625, E-W: 81-86; length: 5 km

A projection value of 270/33 was used. This is the mean of the π -pole of the composite foliation (281/30, D3 and D4; Fig. 4.2.2 A) and the measured D3 small-scale fold axes (258/35).

627, at the crest between Valle d'Ayas and Valle di Gressoney

Alpe Bettolina - Quintino Sella refuge - Pollux

Coordinates: N-S: 627, E-W: 79-87; length: 8 km

Two different values were used for projection: 250/27 for the interface ophiolites/metasediments, and 250/11 for the metasediments situated north of that interface.

The average azimuth of 250° had to be used for the two subareas in order to avoid the intersection of lithological contacts. It was calculated from the two π -poles of the composite foliation and the two maxima of D3 small-scale folds. These are for the ophiolites: π -pole: 267/33, small-scale fold axes maximum: 250/11 (Fig. 4.2.2 B), and for the metasediments: π -pole: 233/16, small-scale fold axes maximum: 247/11 (Fig. 4.2.2 C). The projection value was chosen such as to avoid offsets of identical lithologies.

630, in Valle di Gressoney

Alpe Salza - Plateau del Lys - Naso del Liskamm

Coordinates: N-S: 630, E-W: 79 - 84; length: 5 km.

The projection value 264/31 corresponds to the π -pole of the composite foliation of the D4 Lys antiform (Fig. 4.2.2 D).

633, at the crest between Valle di Gressoney and Valle di Sesia

Rifugio Gulielmina - Corno del Camoscio - Pyramide Vincent

Coordinates: N-S: 633, E-W: 79 - 86; length: 7 km.

A projection value of 266/17 was used. This value slightly deviates from the calculated π -pole of the s1-/s2 foliation (262/15; Fig. 4.2.2 E) and the maximum of the D3 small-scale folds (263/17).

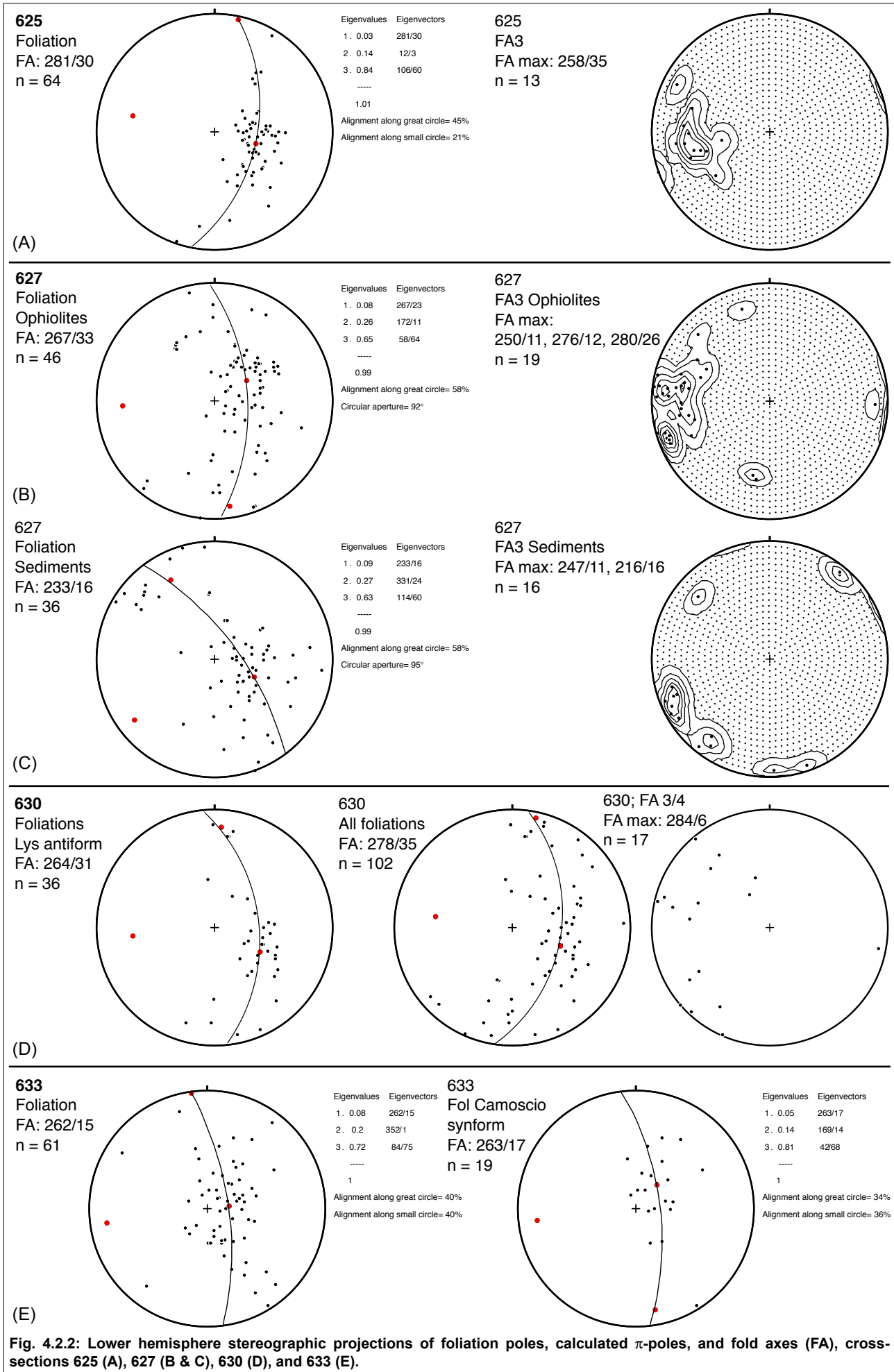


Fig. 4.2.2: Lower hemisphere stereographic projections of foliation poles, calculated π -poles, and fold axes (FA), cross-sections 625 (A), 627 (B & C), 630 (D), and 633 (E).

Discussion

D4 structures

The **D4 Vanzone antiform** is a SSE-facing large-scale fold (cf. Laduron & Merlyn, 1974; Milnes et al., 1981; Escher et al., 1993, 1997; Steck et al., 1999) that formed together with dextral transpressive shearing at the Insubric line (Schmid et al., 1989). Its overturned southern limb is part of the adjoining shear zone ("Southern steep belt") that is responsible for the marked asymmetry of the fold.

In the upper Valle d'Ayas and Valle di Gressoney, the hinge region of the D4 Vanzone antiform is exposed (Fig. 4.2.3, see also Fig. 4.3.6 and cross-sections 625 & 627). It is defined as a broad structural dome that is characterized by the heteroaxial superposition of D3 and D4 folding. The style of D4 folding is open and does not pervasively overprint D3 structures. As a result, basin and dome structures arise, leading to a wide variety in axial azimuths and plunge of both D3 (Fig. 4.2.2 A) and D4 folds (Fig. 4.2.4 B). They range between a moderate SW- to NW-ward plunge to a shallow NE- to E-ward plunge. For this reason, the structures are highly non-cylindrical and cannot be connected from one cross-section to another.

Extensive glaciation and the lack of asymmetric parasitic D4 folds prohibits an exact localisation of the trace of the axial plane of the Vanzone antiform. In the Valle d'Ayas, it strikes in an E-W-direction and is situated approximately 1 km N' of the Mezzalama refuge. From there, it passes eastwards to Castor. Its exact location depends on the interpretation of the Punta antiform (see below; Fig. 4.2.5). If the Punta antiform is interpreted as a D4 structure, it represents the SSE part of an M-shaped Vanzone antiform. The fold axial plane trace of the Vanzone antiform would then be located N of it and would pass through the south face of Castor. If the Punta antiform is a D3 structure, however, the axial plane trace of the Vanzone antiform would be located around 100 m S of the south face of Castor. From there, it is supposed to continue S of Liskamm and to cross the border to Switzerland at the Lisjoch. However, the area is glaciated.

On a large scale (cf. Escher et al., 1988) the fold axial plane of the Vanzone antiform dips steeply to the NNW. In the investigated hinge region, however, some of the meso-scale fold axial planes (see below) and the D4 crenulation cleavages of parasitic small-scale folds (Fig. 4.2.4) dip steeply to the S (average 194/66).

The parasitic D4 folds described below, are exposed in the Valle di Gressoney (cross-sections 627 & 630). Where they do not obviously re-fold D3 folds, the main criteria for their interpretation as D4 folds are their steeply dipping fold axial planes and their open style of folding.

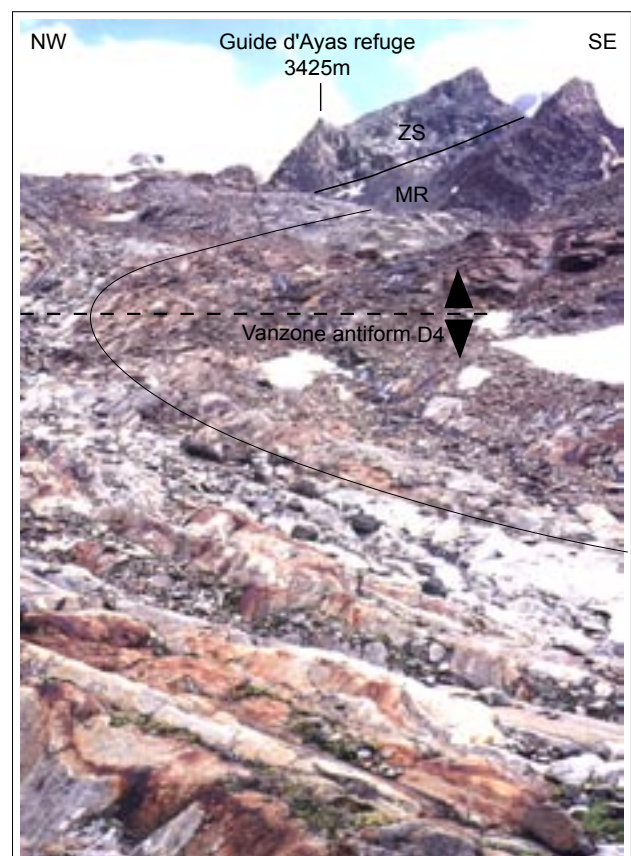


Fig. 4.2.3: Hinge region of the D4 Vanzone antiform as seen from near the Mezzalama refuge, Valle d'Ayas, towards the N (crds. 624 900/ 084 700).

The Vanzone antiform refolds the composite foliation (s1/s2; thin black lines) and the tectonic contact of the Zermatt-Saas unit (ZS) and the Monte Rosa nappe. Its fold axial plane, as inferred from the cross-section (see section 625) dips steeply to the N. Its fold axis plunges moderately to the W. Distance from the viewer to the Guide d'Ayas refuge: 1 km.

The **D4 Bettolina antiform and Bettolina synform** are situated on the southern limb of the D4 Vanzone antiform. They can be discontinuously traced from Colle di Bettaforca to the Alpe Bettolina (cross-section 627) and to Alpe Salza (cross-section 630). Their interlimb angle tightens from W (cross-section 627) to E (cross-section 630), suggesting the accommodation of a larger amount of shortening in the E. Accordingly, their fold axial planes, as inferred from the cross-sections, change from a steeply S-dipping orientation in the W (cross-section 627) to steeply N or NW-dipping in the E (cross-section 630). The fold axis of the Bettolina antiform, as calculated from the composite foliation at the Alpe Bettolina, is 250/11 (Fig. 4.2.4 B).

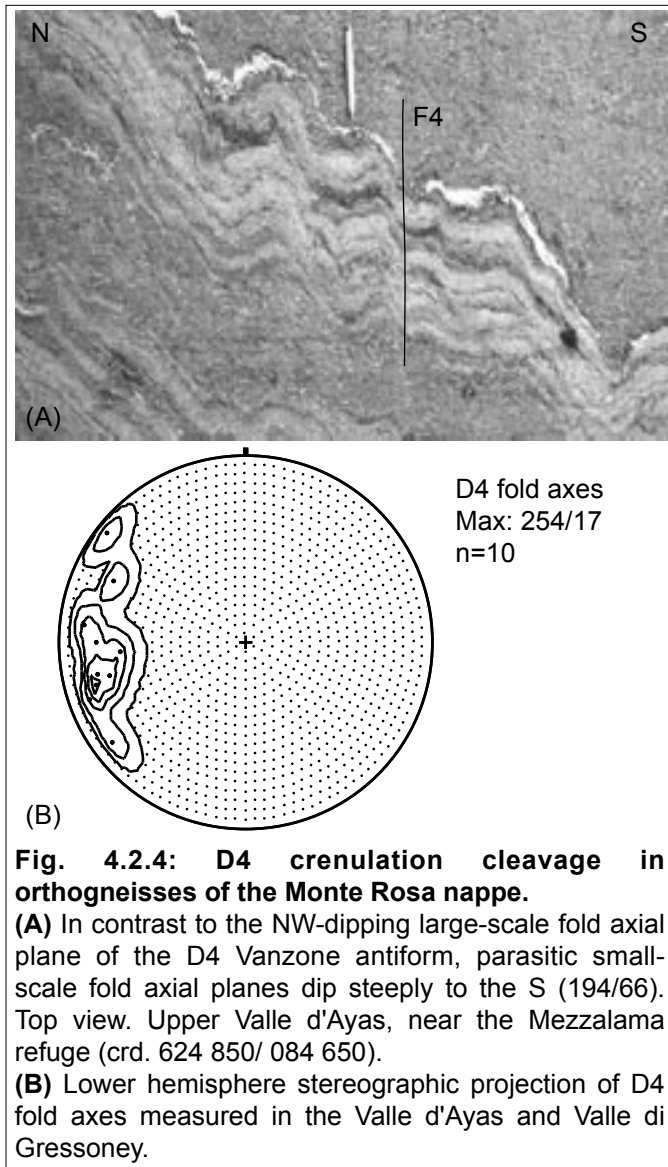


Fig. 4.2.4: D4 crenulation cleavage in orthogneisses of the Monte Rosa nappe.

(A) In contrast to the NW-dipping large-scale fold axial plane of the D4 Vanzone antiform, parasitic small-scale fold axial planes dip steeply to the S (194/66). Top view. Upper Valle d'Ayas, near the Mezzalama refuge (crd. 624 850/ 084 650).

(B) Lower hemisphere stereographic projection of D4 fold axes measured in the Valle d'Ayas and Valle di Gressoney.

The **D4 Felik antiform** (cross-section 627, Fig. 4.2.5) is a parasitic located on the upper limb of the D4 Vanzone antiform. The Felik antiform is exposed in the wall below the Quintino Sella refuge, where it bends the fold axial planes of the parasitic minor folds of the D3 Perazzi antiform (see below). The fold axial plane of the Felik antiform dips moderately to the W (cf. insert in Fig. 4.2.5).

The M-shaped **D4 Zwilling synform** (cross-section 627) results from the projection of the contact of granitic basement to strained Monte Rosa basement and cover. However, the exact shape of the fold, as well as the exact location and orientation of its fold axial plane, cannot be inferred as the crucial area is glaciated. Its fold axial plane, as inferred from the cross-section, dip steeply to the NNW.

The **D4 Lys antiform** (cross-section 630) is exposed at the Plateau del Lys, but it could not be traced further along strike. Its fold axial plane dips steeply to the N, its fold axis, as calculated from the composite foliation, is 264/31 (Fig. 4.2.2 D). The Lys antiform is characterized by numerous parasitic folds on both limbs.

South of the Lys antiform, numerous M-shaped meso-scale D4 folds are exposed. In the serpentinites of a small tectonic window at the Alpe Salza (D1/D2 Salza thrust, see below), they are developed as box folds.

D3 structures

The lower limb of the recumbent south-closing **D3 Verra fold** (cross-section 625) is exposed W of Alpe Pian di Verra (2382 m) in the Valle d'Ayas. There, garnet micaschists of intensely strained Monte Rosa cover and basement are situated structurally below metagranites of the Monte Rosa basement. This locality has been interpreted to be situated in the lower limb of a recumbent fold. The upper limb of this fold is represented by the intensely strained cover and basement of the Monte Rosa nappe at the Mezzalama refuge. The fold axial plane of the Verra fold, as inferred from the cross-section, is subhorizontal. Its trace probably runs along the western lateral moraine of the Piccolo Ghiacciaio di Verra glacier.

The SE-facing **D3 Mezzalama antiform** (cross-section 625) was interpreted to represent a parasitic fold of the D3 Perazzi antiform (see below) in accordance with the facing directions of the Perazzi antiform parasitic folds in cross-sections 627 and 633. It is exposed around 350 m W of the Mezzalama refuge. It refolds the contact of the ophiolites with the intensely strained Monte Rosa basement and cover, as well as the composite foliation. Measured fold axial planes dip moderately to the NW (in average 328/40), small-scale fold axes plunge moderately to the W (in average 272/28, included in Fig. 4.2.2 A).

The recumbent north-closing **Ayas fold** (cross-section 625) is exposed N of the Guide d'Ayas refuge at the edge of the Grande Ghiacciaio di Verra glacier. It refolds the contact of the ophiolites with the intensely strained Monte Rosa basement and cover. As in the adjacent cross-section 627 all the parasitic D3 folds point towards a D3 antiform in the N (D3 Perazzi antiform, see below), the Ayas fold, the vergence of which necessitates an antiformal hinge in the opposite direction, is interpreted as an older **D1 or D2** structure. Its fold axial plane dips moderately to the NNW (342/49), fold axes plunge moderately to the W (in average 267/32).

At the west face of P. 3992, the **D3 Punta antiform** (cross-section 627, Fig. 4.2.6) refolds magmatic dykes that are parallel to the composite foliation. The Punta antiform represents a parasitic minor fold of the D3 Perazzi antiform (see below). Its fold axial plane dips moderately to the NNW, its fold axis plunges moderately to the W.

The north-vergent large-scale **D3 Perazzi antiform** was inferred from the asymmetry of parasitic meso-scale D3 folds. This asymmetry is persistent throughout the investigated area (cross-sections 627 & 633). The asymmetry indicates that these cross-sections are located in the overturned lower limb of a N-closing antiform. Due to the lack of parasitic folds with a reverse asymmetry, the axial plane trace of this antiform could not be located exactly. It was assumed to follow the Grande Ghiacciaio di Verra glacier and is indicated with question marks in the cross-sections. The antiformal hinge of the Perazzi antiform must therefore be located on the northern slope of the Monte Rosa massif. As the



Fig. 4.2.6: 270°- panoramic view of the border crest between Italy and Switzerland in the upper Valle d'Ayas. View from P.2730 towards the N and E.

The nappe contact of the Zermatt-Saas unit (ZS) and the Monte Rosa nappe (MR) runs along the eastern side of the Grande Ghiacciaio di Verra glacier (left-hand side), passes below the Guide d'Ayas refuge and disappears below the Piccolo Ghiacciaio di Verra glacier between Castor and Pollux. The bending of the contact from moderately W-dipping on the left-hand side to NW-dipping near Pollux is caused by the D4 Vanzone antiform (Fig. 4.2.3). At the west face of the Punta Perazzi, the asymmetry of the parasitic D3 folds exposed indicates an antiformal hinge to north (D3 Perazzi antiform; cf. cross-section 627 and discussion in the text). The D3 Punta antiform, at the W face of P.3992, is located one scenery farther to the E (cf. Enclosure 1). As it exhibits the same facing direction, it was also interpreted to be a parasite of the D3 Perazzi antiform (see text). MR basement: Para- and orthogneisses of the Monte Rosa nappe; MR cover and basement: Intensely strained basement and cover of the Monte Rosa nappe.

D3 Perazzi antiform was refolded by the D4 Vanzone antiform at the border crest between Switzerland and Italy, its fold hinge appears as a synform farther in the north (referred to as Stockchnubel synform in Enclosure 1; see also ch. 4.2.2, cross-section 628 and Fig. 4.4.2)

The **parasitic folds of the Perazzi antiform** are exposed in the wall below the Quintino Sella refuge (crest between Valle d'Ayas and Valle di Gressoney; Figs. 4.2.5, 4.2.6 & 4.2.7; cross-section 627) and along the crest between Valle di Gressoney and Valle di Sesia (Figs. 4.2.7 & 4.2.8; cross-section 633). The fold axial planes dip moderately to the NW (in average 315/27). Their fold axes plunge moderately to the WSW (average 233/16) in cross-section 627 and moderately to the W (268/19) in cross-section 633.

The **D3 Camoscio synform** (cross-section 633) is a parasitic fold of the D3 Perazzi antiform and is exposed at the Corno del Camoscio (3026 m) at the crest between Valle di Gressoney and Valle di Sesia (Fig. 4.2.8). It refolds the contact of the Zermatt-Saas ophiolites with the intensely strained cover and basement of the Monte Rosa nappe, as well as the composite foliation. Its fold axial plane dips moderately to the NW (322/20). Its fold axis, as calculated from the composite foliation, plunges moderately to the W (263/17; Fig. 4.2.2 E).

Additional parasitic D3 folds are exposed along strike of the contact at the crest between Valle di Gressoney and Valle di Sesia. However, since they do not display special features they are not described here.

D1 & D2 structures

The recumbent north-closing **D2 Mantova antiform** (cross-section 633) is exposed below the Mantova refuge. This antiform isoclinally refolds orthogneisses (meta-granites and -diorites) of the Monte Rosa basement and quartzites of the intensely strained Monte Rosa cover and basement. Its fold axial plane dips shallowly to the NW (324/15). Because the orthogneisses were not found to be connected with the basement situated at a deeper structural level, they are interpreted to form the

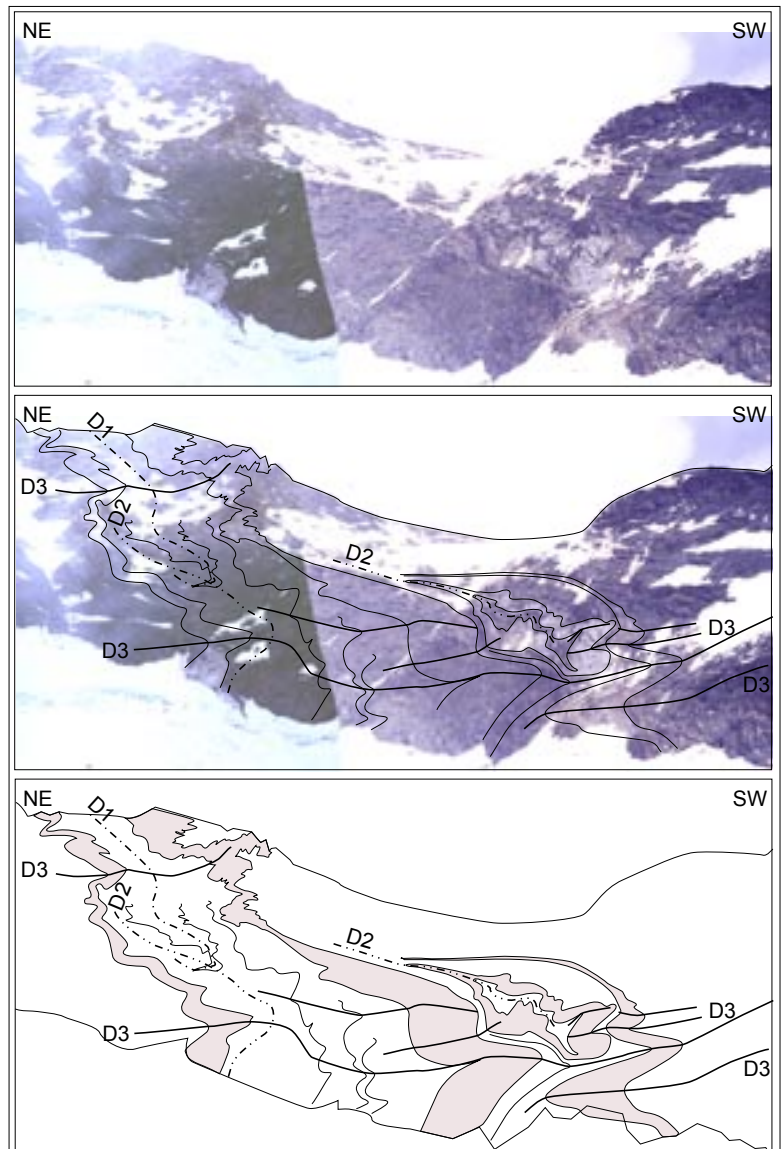


Fig. 4.2.7: View of the SW crest of the Vincentpiramide, i.e. the crest between Valle di Gressoney and Valle di Sesia, from approximately 3800 to 4000 m elevation. View from the Lys glacier towards the SE.

Palaeozoic basement and Permo-Mesozoic meta-arkoses and quartzites of the Monte Rosa nappe are refolded by three fold generations - D1, D2, and D3. The asymmetry of the parasitic D3 folds indicates an antiformal hinge in the north and structurally above (D3 Perazzi antiform; cf. cross-section 627). The D3 fold axial planes dip shallowly to the WNW, the D3 fold axes plunge shallowly to the W.

core of a fold that was detached from the lower structural level of basement.

The **Salza thrust** is exposed at the Alpe Salza Superiore in the Valle di Gressoney (cross-section 630). The thrust strikes E-W and is interpreted as a N-directed syn-D1/D2 ramp thrust, along which a slice of serpentinites of the Zermatt-Saas unit has been sandwiched between meta-granites of the Monte Rosa nappe and garnet micaschists and quartzites of the intensely strained Monte Rosa basement and cover.

Serpentinites in a similar structural position were found in the lower limb of the D3 Camoscio synform at the Corno del Camoscio (cross-section 633). There, a 10 m thick serpentinite of the Zermatt-Saas unit is sandwiched between garnet micaschists of the intensely strained Monte Rosa basement and cover. As the serpentinite is largely covered by moraine debris, it is not possible to decide whether it represents a thrust slice, or the core of an isoclinal D1/D2 fold, that is still connected with the Zermatt-Saas unit.

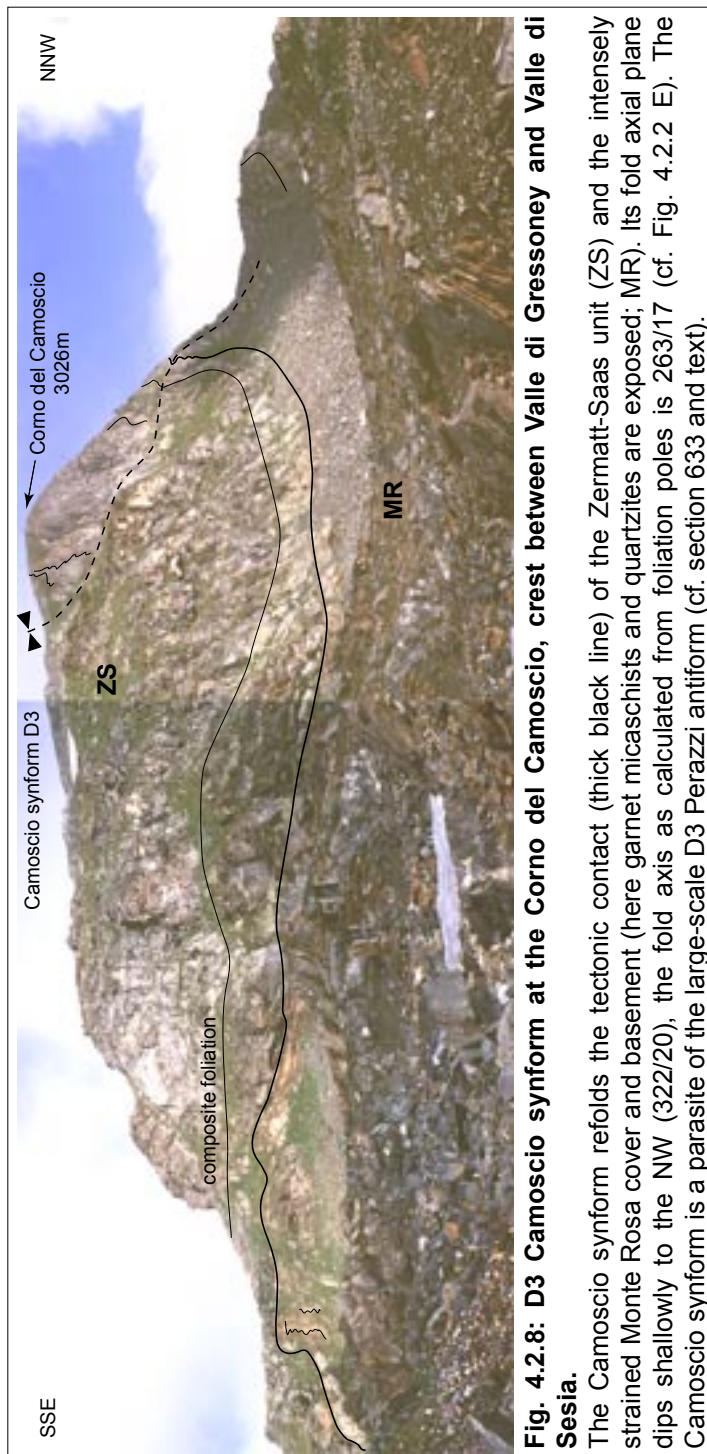


Fig. 4.2.8: D3 Camoscio synform at the Corno del Camoscio, crest between Valle di Gressoney and Valle di Sesia.

The Camoscio synform refolds the tectonic contact (thick black line) of the Zermatt-Saas unit (ZS) and the intensely strained Monte Rosa cover and basement (here garnet micaschists and quartzites are exposed; MR). Its fold axial plane dips shallowly to the NW (322/20), the fold axis as calculated from foliation poles is 263/17 (cf. Fig. 4.2.2 E). The Camoscio synform is a parasite of the large-scale D3 Perazzi antiform (cf. section 633 and text).

4.2.2 Gornergrat, Mattertal

Cross-sections 628 & 628 E-W

Projection methods

628, Gornergrat in Mattertal

Felekjoch - Hohtälli - Stellisee

Coordinates: N-S: 628, E-W: 85-96; length: 11 km

A projection value of 285/30 was used. This deviates from the π -pole of the composite foliation calculated to be 312/29 (i.e. the fold axis of the D3 Stockhorn antiform, see Fig. 4.2.9) and the maximum of the D3 small-scale folds of 309/31. In a projection using this azimuth of around 310°, lithological interfaces located at large distances from the section plane would be "stretched" and become relatively flat. However, the structure contours necessitate a steeper dip of lithological interfaces than would result from a projection with the constructed and measured values for the D3-fold axes. An average azimuth best meeting the requirements was therefore used for projection.

The reason for the difference in the azimuth of the projection might be due to the rotation of the fold axes during D3 by synkinematic dextral transpressive shearing along the Saas shear zone and Gornergrat-Furggtal shear zone (see ch. 4.3 and 5). Such a rotation is also suggested by the wide range of measured D3 small-scale fold axes (azimuths ranging from 270 - 360°).

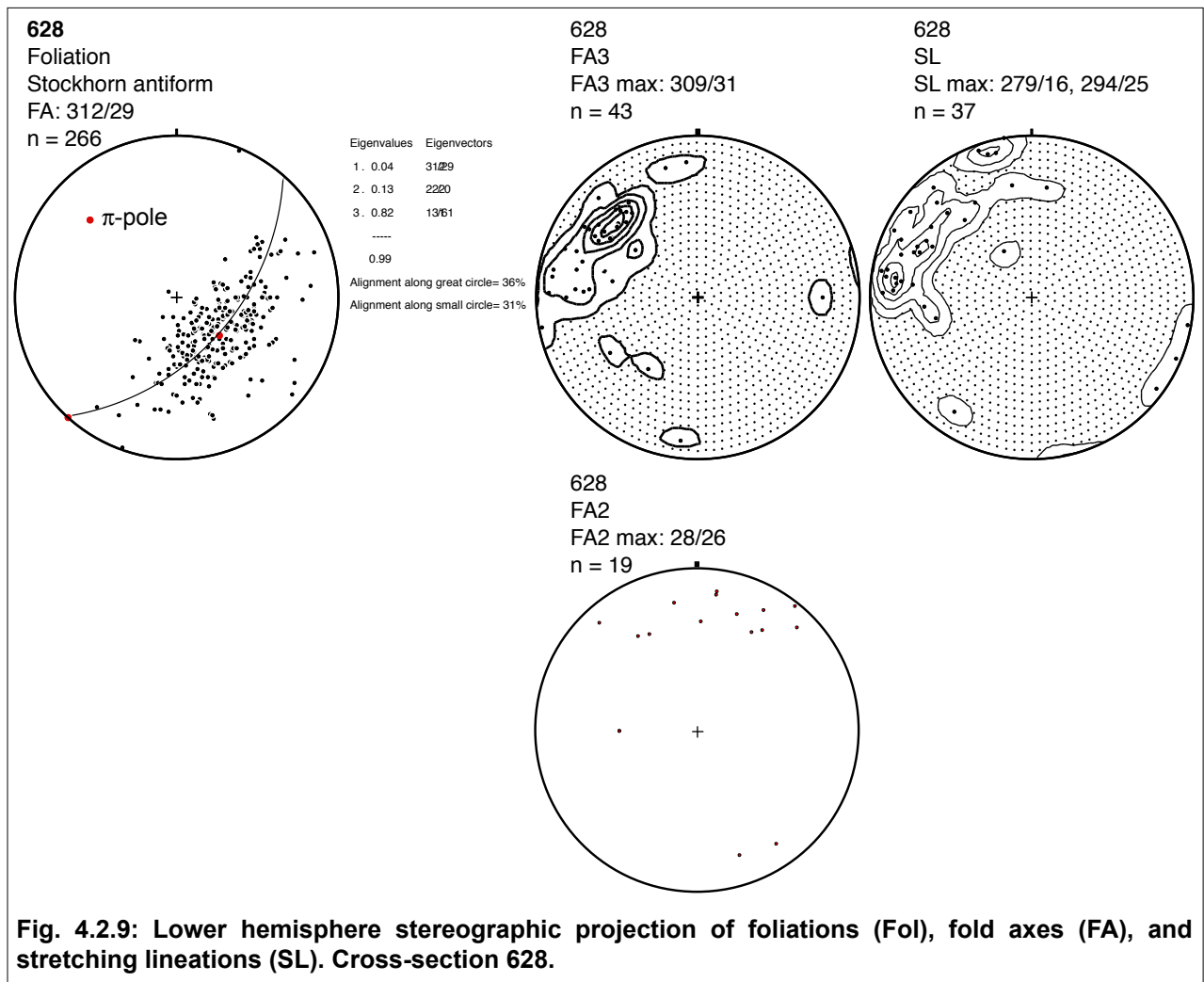


Fig. 4.2.9: Lower hemisphere stereographic projection of foliations (Fol), fold axes (FA), and stretching lineations (SL). Cross-section 628.

Discussion

Along the northern slope of the Monte Rosa massif, D4 folding is generally less pronounced and either developed as gentle buckling at a larger scale or as a crenulation at outcrop-scale.

D3 structures

The south-facing, tight **D3 Stockhorn antiform** (Fig. 4.2.10) occupies the entire Gornergrat and the northern slope of the Breithorn massif. On a large scale, it has an amplitude of approximately 11.5 km and a width of about 3 km (see Fig. 4.4.2). Its fold axial plane varies in orientation from a moderate W-ward dip at the Breithorn massif to a steep NW-ward dip at the western Gornergrat (approximately 55°, inferred from the cross-section), and a steep NNW-ward dip at the eastern Gornergrat. This variation in orientation is caused by the D4 Vanzone antiform (see ch. 4.2.1), which refolds the D3 Stockhorn antiform. The fold axis of the Stockhorn antiform, as calculated from the composite foliation, is 312/29 (Fig. 4.2.9).

The style of parasitic folding is open within the northern upright limb of the Stockhorn antiform. In contrast, numerous parasitic D3 small-scale folds in the fold hinge (Fig. 4.2.11) and within the southern overturned limb of the Stockhorn antiform are tight to isoclinal. Fold axial planes dip moderately to the NW (average 330/29), while their fold axes plunge moderately to the NW (average 309/31). The difference in fold style on the upright and overturned limb of the D3 Stockhorn antiform is the result of a pervasive overprint of the overturned limb by syn-D3 dextral transpressive shearing along the D3 Saas and Gornergrat-Furggtal shear zone (see ch. 4.3). This shearing is also responsible for the parallelisation of D3 and D2 fold axes and fold axial planes in the overturned limb of the D3 Stockhorn antiform. Therefore, a clear distinction of D2 and D3 structures is often difficult in this region.

The isoclinal **D3 Stockchnubel synform** is exposed in the Stockchnubel area. There, the fold axial plane, as inferred from the cross-section, dips with 55° to the N. The Stockchnubel synform is detached along the late-stage D3 Saas shear zone (see ch. 4.3 and Fig. 4.4.2). The location of the fold axial plane is indicated by parasitic folds. In the northern overturned limb such asymmetric parasitic folds are located around 150 m W of P. 3223 (see Enclosure 1). Folds with an M-symmetry indicate the location of the hinge of the Stockchnubel synform (Fig. 4.2.12). The persistent asymmetry of the parasitic folds located 50 m S' of the Stockchnubel at P. 3047 (Fig. 4.2.13) indicates the southern limb of the D3 Stockchnubel synform. The D3 Schalbetter fold (see below) also represents one of these parasitic folds. The fold axial plane trace changes orientation from an E-W strike at the Stockchnubel to a N-S-strike west of the Stockchnubel. The axial trace probably follows the western edge of the Zwilling glacier and continues into cross-section 627, adjacent to cross-section 628 in the south (see Enclosure 3 and Fig. 4.4.2). At the border crest between Switzerland and Italy, the Stockchnubel synform is refolded by the D4 Vanzone antiform and therefore appears as an antiform farther in the south (referred to as D3 Perazzi antiform in Enclosure 1; see also ch. 4.3.1 and cross-section 627). The Perazzi antiform and Stockchnubel synform are therefore a single D3 fold that was subsequently refolded by the D4 Vanzone antiform.

The **D1/D2/D3 Schalbetter fold** (Fig. 4.2.14) is exposed at the Schalbetterflue (N-crest of Pollux). There, three folding phases are superimposed within amphibolites of the Zermatt-Saas unit. The asymmetry of D3 folds indicates the location of the Schalbetter fold in the overturned upper limb of the D3 Stockchnubel synform. The associated major D3 fold axial plane dips to the W.

D2 structures

At the Gornergrat, the nappe stack is refolded by numerous isoclinal D2 folds. Because all D2 folds are refolded by the D3 Stockhorn antiform, the fold axial planes change orientation from a N-ward dip in the overturned southern limb of the D3 Stockhorn antiform to a NW- or W-ward dip in its normal limb. Due to glaciation and moraine debris, only a few D2 folds could be traced over larger

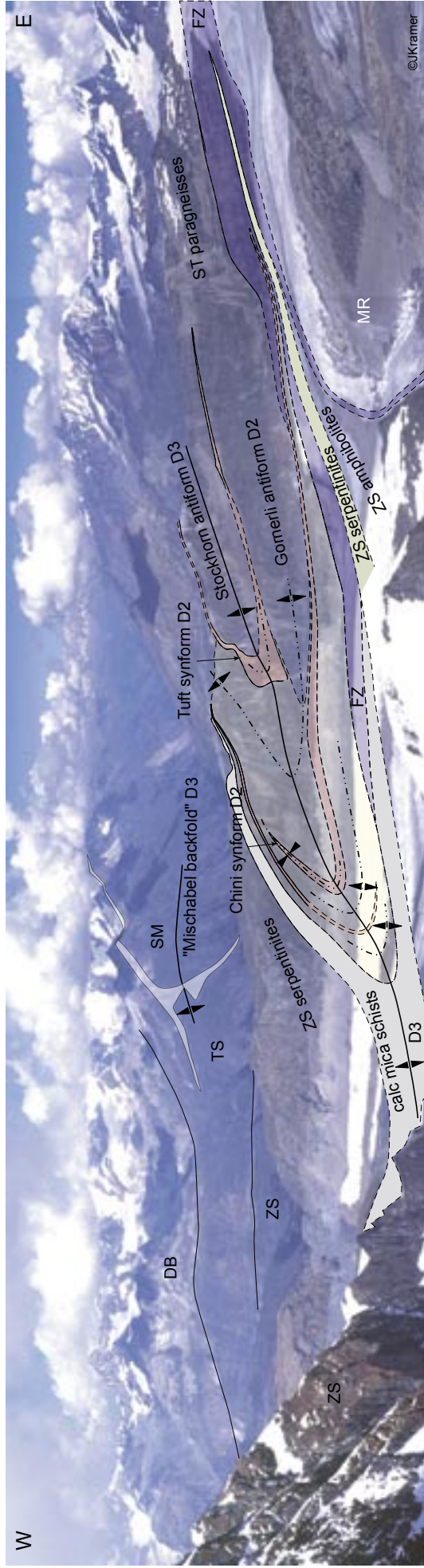
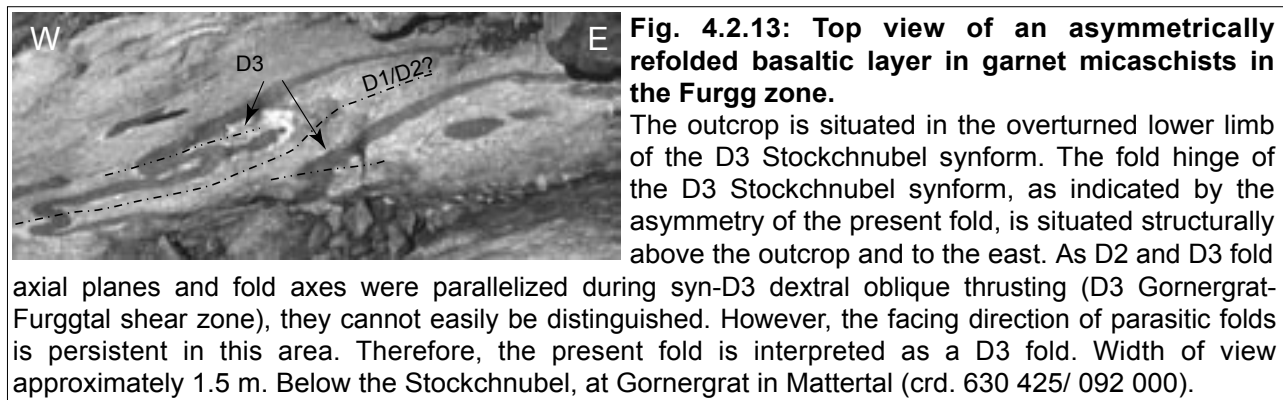
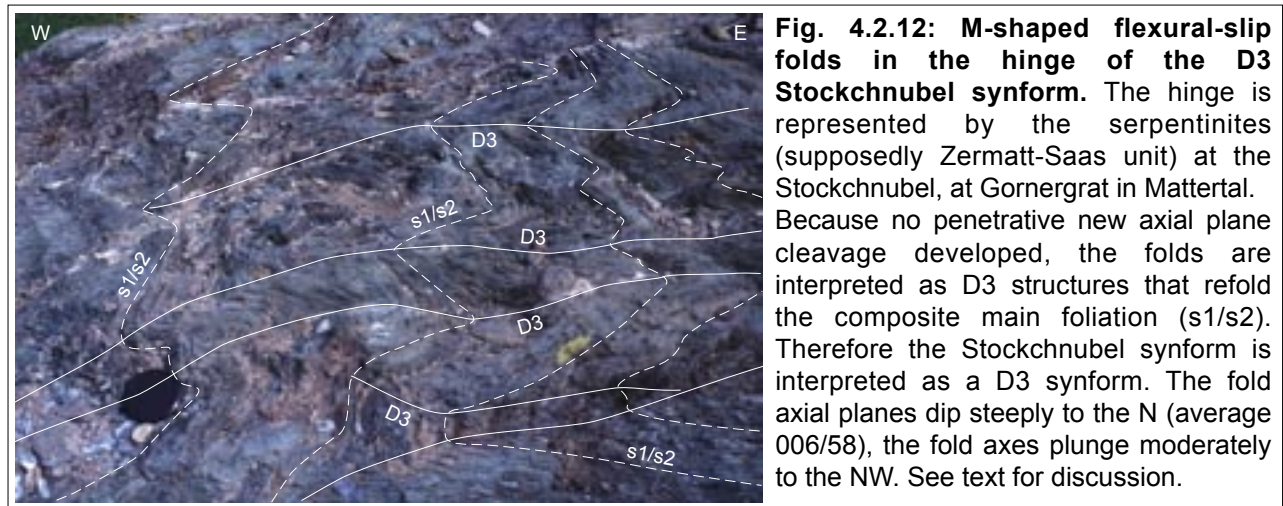
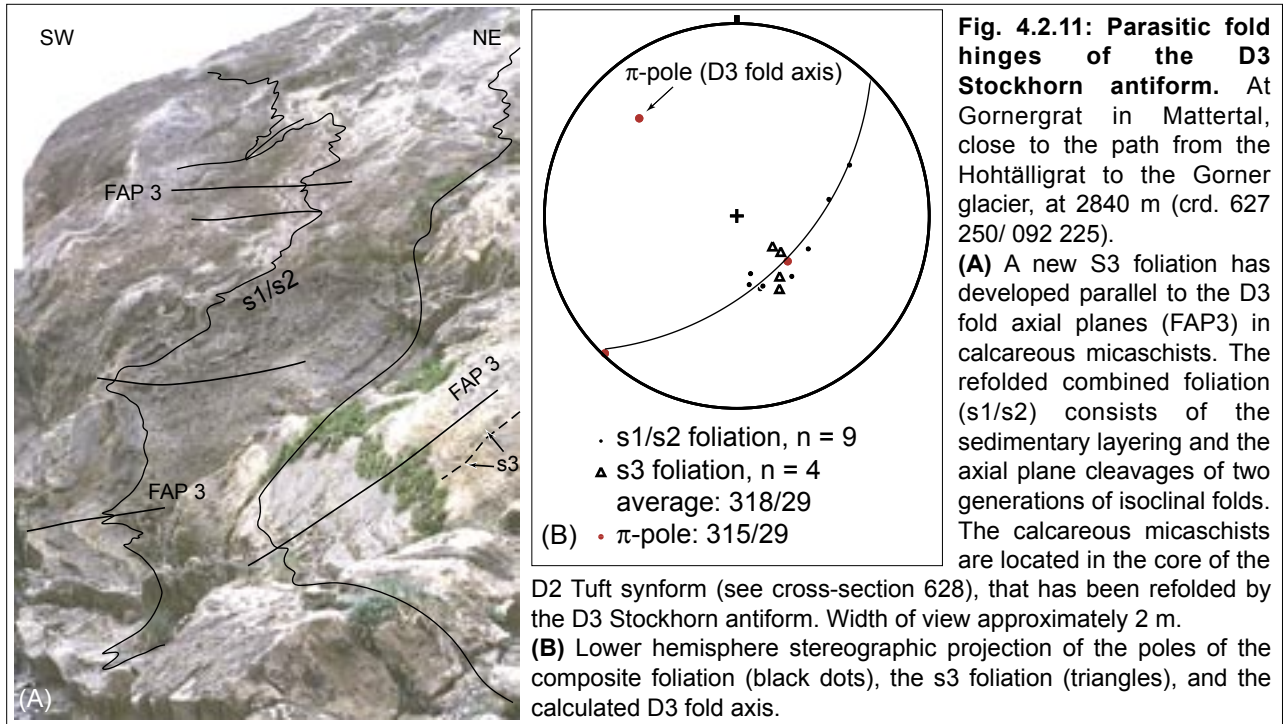


Fig. 4.2.10: View of Gornegrat from Pollux towards the N.
 DB: Dent Blanche nappe, FZ: Furgg zone, MR: Monte Rosa nappe, SM: Siviez-Mischabel nappe, ST: Stockhorn unit, TS: Tsaté nappe, ZS: Zermatt-Saas unit.
 Yellow: meta-conglomerates, meta-arkoses, quartzites; pink: marbles, rauhwackes, calcareous mica schists.



distances. Therefore only the major D2 folds will be named and described below.

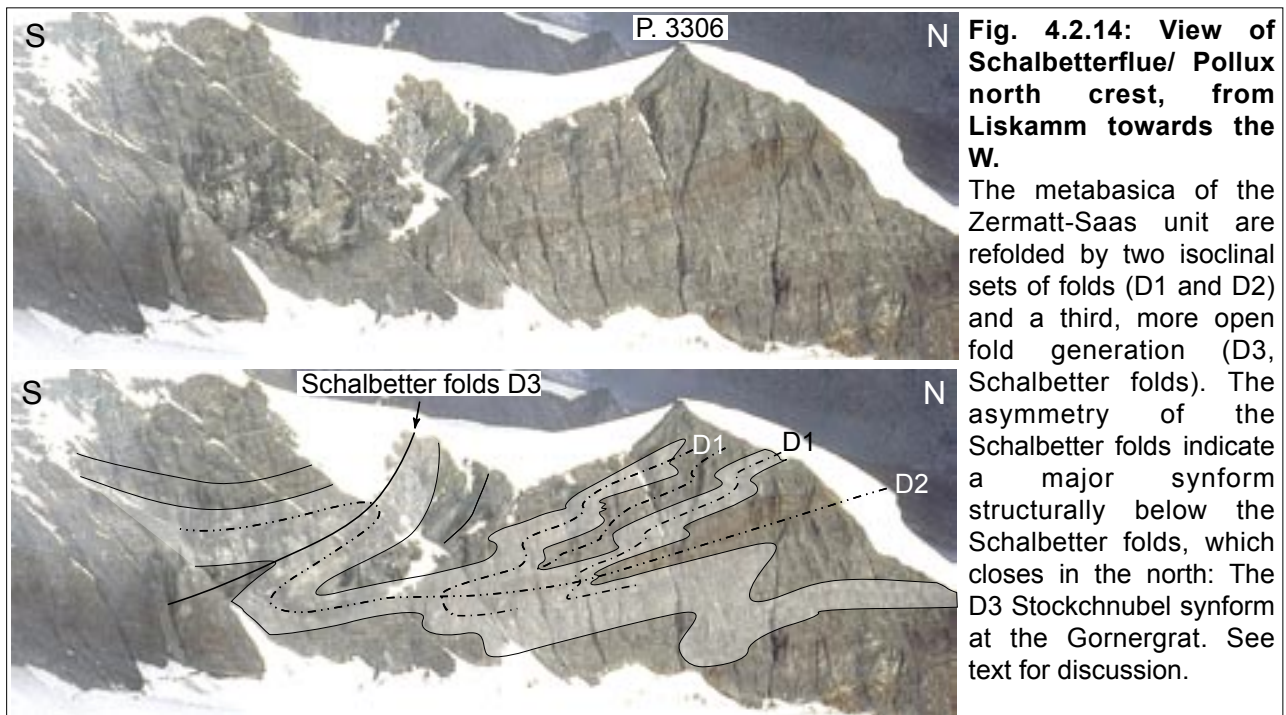


Fig. 4.2.14: View of Schalbetterflue/ Pollux north crest, from Liskamm towards the W.

The metabasica of the Zermatt-Saas unit are refolded by two isoclinal sets of folds (D1 and D2) and a third, more open fold generation (D3, Schalbetter folds). The asymmetry of the Schalbetter folds indicate a major synform structurally below the Schalbetter folds, which closes in the north: The D3 Stockchnubel synform at the Gornergrat. See text for discussion.

The isoclinal **D2 Chini synform** (Fig. 4.2.15, cf. Fig. 4.2.10) is well exposed in the Chinischlucht. Northwards it continues into the wall situated below the Gornergrat observatory and at the Hohtälligrat. At the Hohtälligrat, its fold axial plane is situated at least 50 m E of P.3135, as indicated by the asymmetry of parasitic D2 folds in marbles (Fig. 4.2.16). The axial trace can be followed to the Ritzengrat further to the north. Southwards the Chini synform disappears below the Gorner glacier. It is interpreted to appear again north of the Stockchnubel, i.e. in the southern overturned limb of the D3 Stockhorn antiform, where synformally folded calcite and dolomite marbles are interpreted to define the core of the Chini synform.

In the Chinischlucht, the fold axial plane of the Chini synform is roughly parallel to the W- to NW-dipping foliation (Fig. 4.2.15C). Due to the intense overprint by the D3 Gornergrat-Furggtal shear zone (cf. ch. 4.3.2), D2 fold axes (measured average in the northern Chinischlucht: 316/33) have been rotated into parallelism with D3 fold axes (average 311/34). The attempt to calculate the D2 fold axes from the poles of layering and s_1 foliation reveals values of 353/17 in the northern part of the Chinischlucht and 276/47 in the southern part of the Chinischlucht. This is interpreted as the result of the increasing intensity of overprint by the D3 Gornergrat-Furggtal shear zone. As the northern part of the D2 Chini synform is situated farther apart from the D3 Gornergrat-Furggtal shear zone, the N-plunging value is supposedly closer to its original orientation prior to D3 overprint. The fact, that a calculation of the fold axis from the poles of the two subareas leads to a value that is similar to the calculated D3 fold axis of the Stockhorn antiform, indicates that D3 overprint is incomplete.

The Chini synform isoclinally refolds the Permo-Mesozoic cover of the Stockhorn unit (Fig. 4.2.15 A & B). In the Chinischlucht, its core consists of calcite and dolomite marbles. Towards the hinges the marbles are followed by rauhwackes, then by a second layer of marbles and a second, strongly thinned layer of rauhwackes (10 cm thick). Then follow quartzites and quartzitic conglomerates. The overall younging direction is therefore towards the core, suggesting a stratigraphic contact with the Stockhorn basement. The repetition of stratigraphy is interpreted to be the effect of isoclinal D1 folding.

The isoclinal **D2 Tuft synform** (see Fig. 4.2.10) is exposed at the Tuftgrat, at the Hohtälligrat and at the Ritzengrat. At the Tuftgrat, the core of the Tuft synform consists of intercalated rauhwackes and calc micaschists. The intercalation is probably due to D1 folding and/ or thrusting. At the Hohtälligrat and Ritzengrat, the core consists of rauhwackes. The limbs of the synform consist of quartzites that are thinned to a thickness of 20 m at the Tuftgrat and to 0.5 m at the path from the Hohtälligrat to the Gorner glacier. At the Ritzengrat, the rauhwackes are in direct contact with

the paragneisses of the Stockhorn basement. From there, they can be traced towards the Hohtälli summit, which is capped by quartzites and quartzitic conglomerates of the upper limb of the Tuft synform.

Evidence for the **D2 Gornerli antiform** (cf. Fig. 4.2.10) is found at the "Roter Zug" situated below the Stockhorn cable car station. There, the paragneisses of the Stockhorn basement are refolded by S-vergent tight to isoclinal parasitic folds, indicating their location in the upright limb of the Gornerli antiform.

The SSE-vergent **D2 Gadmen folds** (Fig. 4.2.17) are exposed near Gadmen below the Tuftgrat, i.e. close to the Gorner glacier. The asymmetry of these parasitic folds (i.e. the refolded part of the D2 Chini synform) indicates a synform situated structurally above this locality, but below the Gornerli antiform. Due to glaciation, however, the fold axial plane trace cannot be traced further along strike.

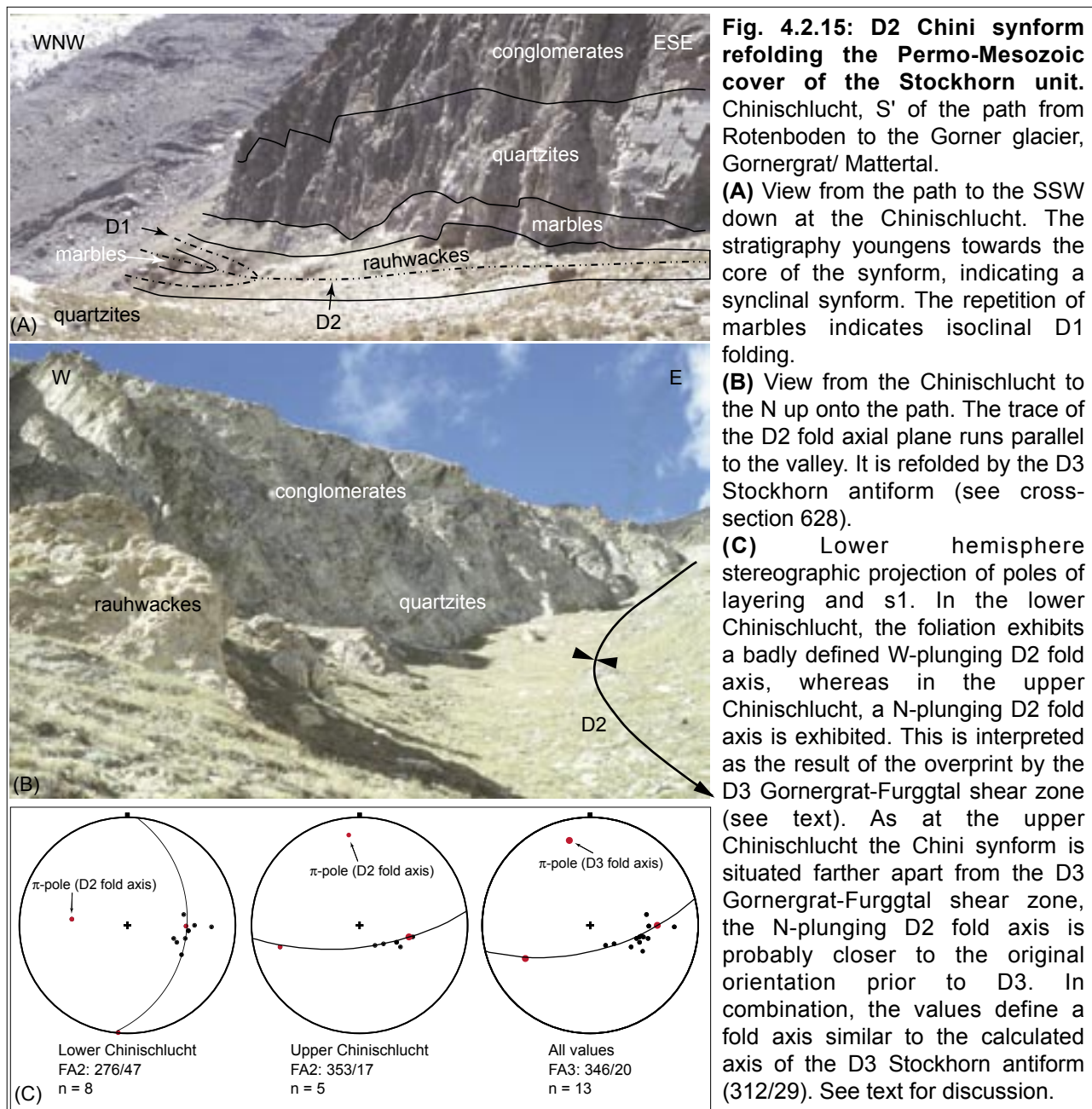




Fig. 4.2.16: Mesozoic calcite and dolomite marbles of the Stockhorn unit.

The marbles are situated 20 m below the tectonic contact with the calcareous micaschists of the Zermatt-Saas unit. They are isoclinally refolded by two superposed fold generations (D1 and D2). The asymmetry of the parasitic D2 folds indicates the location of the D2 Chinisynform to the east. As the outcrop is located in the northern upright limb of the D3 Stockhorn antiform, the D2 fold axial planes are reoriented. They dip with approximately 40° to the WNW, the fold axes plunge with 30° to the NW. the width of view is approximately 3 m. Close to P. 3135/ Gornergrat observatory, at Gornergrat in Mattertal (crd. 626 850/ 092 475).

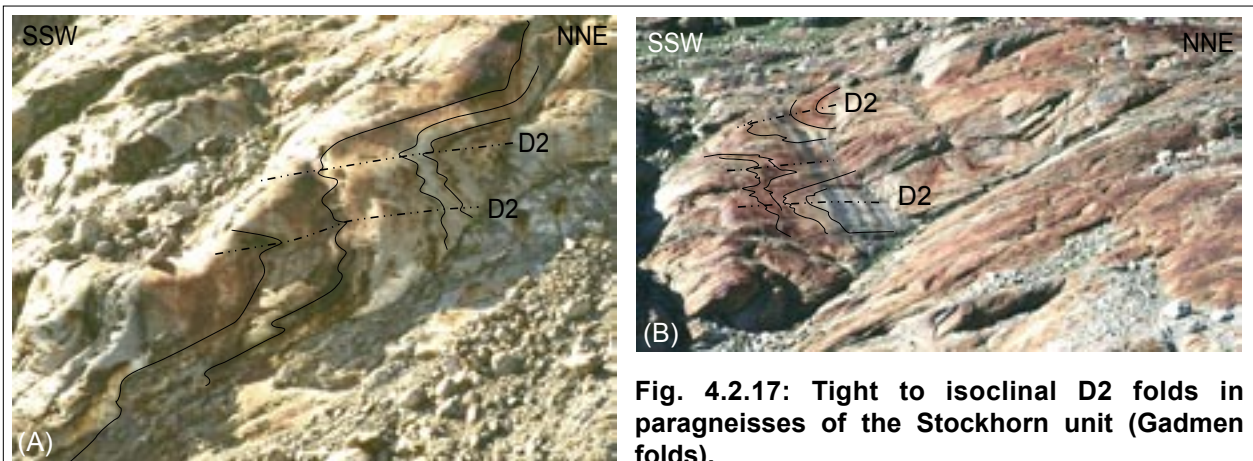


Fig. 4.2.17: Tight to isoclinal D2 folds in paragneisses of the Stockhorn unit (Gadmen folds).

The folds are situated in the overturned southern limb of the D3 Stockhorn antiform (see section 628 Gornergrat). Therefore the D2 fold axial planes were reoriented by D3 and dip with $25-40^\circ$ to the WNW. Their asymmetry indicates a synformal, N-closing hinge situated structurally above. Width of view approximately 3 m in (A), and 15 m in (B). Below the Tufgrat near Gadmen, at 2740m, at Gornergrat in Mattertal (crds. 628 625/ 092 200).

4.2.3 Saastal

Cross-sections 636 and 638

Projection techniques

636, at Spielboden in Saastal

Mittelallalin - Gletscheralp

Coordinates: N-S: 636, E-W: 101 - 106; length: 5 km.

A projection value of 280/34 was used. This corresponds to the mean value of the π -pole, as calculated from the composite foliation (277/36, fold axis of the D3 Spielboden antiform, Fig. 4.2.18 D) and the maximum of the D3 small-scale fold axes (283/31).

638, in Saastal

Roffelhörner - Egginer - Saas Fee

Coordinates: N-S: 638, E-W: 93.5 - 110; length: 16.5 km.

Structure contour maps of the nappe contacts were constructed in a first step. The projection value for single points (289/25) corresponds to the fold axis of the D3 Mittaghorn synform, as calculated from the composite foliation (Fig. 4.2.18 A). Cross-section also integrates cross-section 636, which was projected with a value of 288/25 into cross-section 638 (see Enclosure 4).

Discussion

Due to widespread superpositions of folding, the folds will not be described by their relative age but from south to north and from top to bottom.

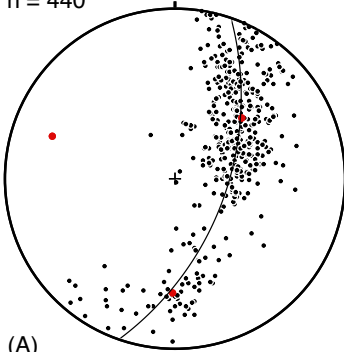
The **D1/ D3 Fluchthorn fold** (Fig. 4.2.19) is exposed at the bottom of the SE face of Fluchthorn, at 3040 m elevation. Two fold generations - D1 and D3 - are superimposed within marbles (in the core) and quartzites/ meta-conglomerates of the cover of the Portjengrat unit. The D1 fold axial plane of the isoclinal south-closing D1 fold is parallel to the foliation (316/17). The band of marble can be traced to the Hangende Gletscher glacier, where it is refolded by an isoclinal D2 fold. Further to the N, this D2 fold axial plane continues into the Hangende Gletscher fold (see below). To the south and east, and structurally below the Fluchthorn fold, this D2 fold axial plane is refolded by several isoclinal D3 folds (see Fig. 4.3.7 A). There, D3 folds exhibit an M-symmetry and therefore define the hinge of a SE-facing antiform. This larger antiform is interpreted as a parasitic fold of the major D3 Stockhorn antiform (cross-section 628) which is situated in the upper normal limb of the Stockhorn antiform. This interpretation is based on the observation that farther to the south, i.e. along the Schwarzberg glacier, the foliation dips again uniformly to the NW (see Enclosure 4). The fold axial planes of the D3 M-folds dip moderately to the NW (on average 320/23); their fold axes plunge shallowly to the NW (on average 325/9). The parasitic SE-facing D3 fold that overprints the D1 Fluchthorn fold (Fig. 4.2.19), is the uppermost of those D3 folds. Its fold axial plane dips moderately to the NW (328/27). All these observations indicate that hinge and lower limb of the D3 Stockhorn antiform, including the D3 Stockhobel synform, are totally cut off by the D3 Saas shear zone (see ch. 4.3.3).

The **D2/D3 Hangende Gletscher fold** is exposed below the Hangende Gletscher. It has previously been described as a (D2) sheath fold, associated with a WNW-directed transport direction by Lacassin (1984, 1987), Lacassin & Mattauer (1985), and Rössler (2000). It refolds marbles (in the core) and quartzites of the Portjengrat unit. The closing direction of the D2 fold cannot be inferred.

Below the Innere Turre (3381m), a parasitic SE-verging D3 fold overprints the Hangende Gletscher fold, confirming its location in the northern upright limb of the D3 Stockhorn antiform (see ch. 4.2.2). However, its fold axial plane trace cannot be traced farther to the north. D2 and D3 fold axes are parallel and plunge shallowly to the W (average 280/15).

638 Foliation; Mittaghorn synform

FA: 289/25
n = 440



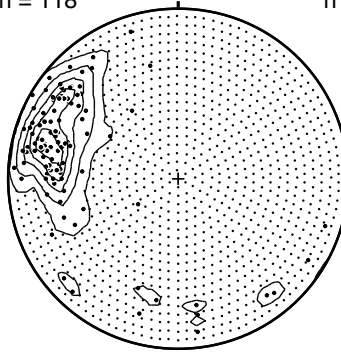
Eigenvalues	Eigenvectors
1. 0.03	289/25
2. 0.26	181/33
3. 0.71	48/46

1	

Alignment along great circle= 72%
Circular aperture= 92°

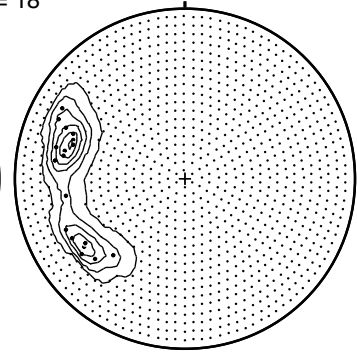
Mittaghorn synform FA

FA3 max: 285/21
n = 118



Mittaghorn synform SL

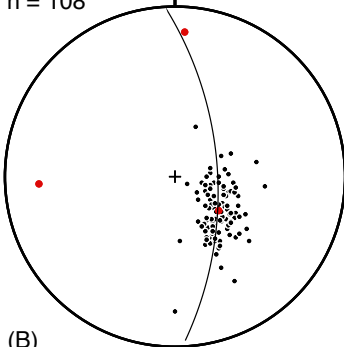
SL max: 287/31, 236/31
n = 18



(A)

Saas Fee Foliation

FA: 267/21
n = 108



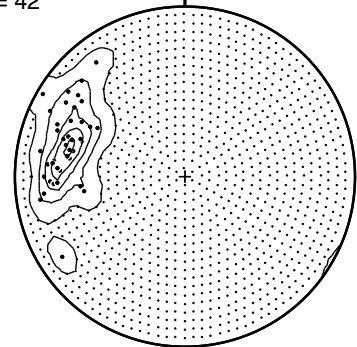
Eigenvalues	Eigenvectors
1. 0.01	267/21
2. 0.05	4/16
3. 0.94	128/63

1	

Alignment along great circle= 32%
Alignment along small circle= 20%

Saas Fee SL

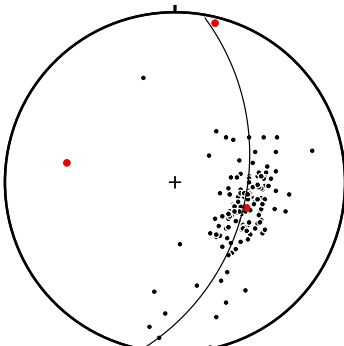
SL max: 283/31
n = 42



(B)

Mattmark W Foliation

FA: 280/36
n = 145



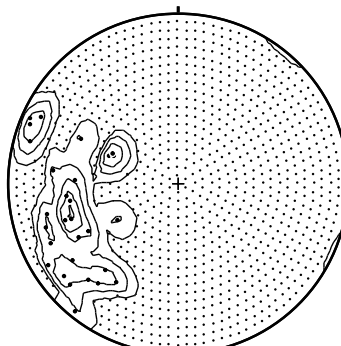
Eigenvalues	Eigenvectors
1. 0.02	280/36
2. 0.1	14/4
3. 0.88	110/53

1	

Alignment along great circle= 41%
Alignment along small circle= 20%

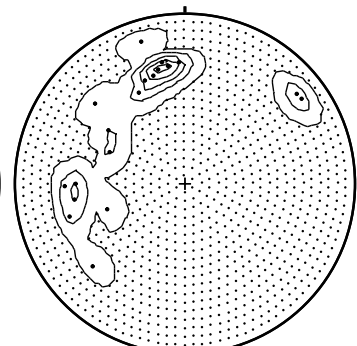
Mattmark W FA3

FA max: 254/35, 294/6
n = 30



Mattmark W SL

SL max: 347/31, 266/35
n = 20

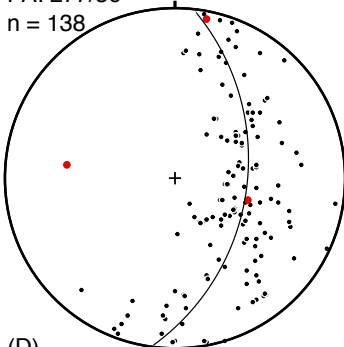


(C)

636

Foliation

FA: 277/36
n = 138



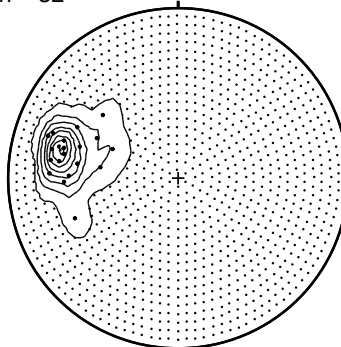
Eigenvalues	Eigenvectors
1. 0.06	277/36
2. 0.35	11/5
3. 0.59	107/53

1	

Alignment along great circle= 82%
Circular aperture= 114°

FA3

FA max: 283/31
n = 32



(D)

Fig. 4.2.18: Lower hemisphere stereographic projections of foliations, fold axes (FA), and stretching lineations (SL), cross-sections 638 (A, B & C) and 636 (D).

For comparison, the subareas Saas Fee and Mattmark West (both section 638 Saas) are also presented. As, however, the Mittaghorn synform is the dominant structure in section 638, its fold axis was used as a projection value.

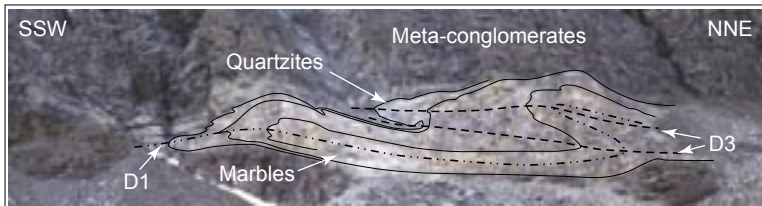


Fig. 4.2.19: D1/D3 fold superposition in metasediments of the Portjengrat unit (D1/D3 Fluchthorn fold).

Mapping revealed, that D2 folding is responsible for the multiple repetition of lithologies such as found structurally below the outcrop depicted in the figure (see cross-section 638). For this reason, the south-closing fold hinge of the Fluchhorn fold must be a D1 structure. The D1 fold axial plane is parallel to the foliation (316/17); the D3 fold axial planes dip moderately to the NW (328/27). Note that the D3 fold axial plane traces do not cross the lithological boundaries on the right-hand side of the picture, where the fold is covered by debris. Below the Fluchthorn, Saastal, at 3040 m (crd. 637 475/ 096 525). Width of view approximately 40 m.

Gletscher fold from SW to NE and farther to the N-closing D2 hinge of the Schwarzberg fold (see Enclosure 2 and cross-section 638). The upper one follows the quartzites above the marbles of the Hangende Gletscher fold and passes into the S-closing hinge of the Schwarzberg fold. The D2 fold axial planes dip moderately to shallowly to the NW. D2 fold axes plunge moderately to the W (average 282/27).

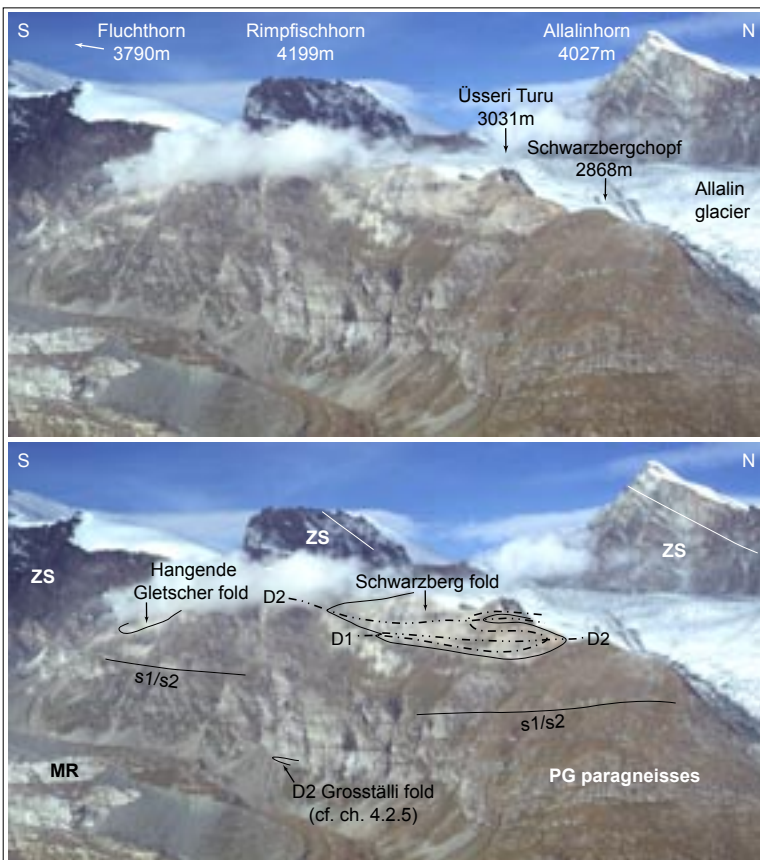


Fig. 4.2.20: View of Schwarzbergchopf, west of the Schwarzberg glacier in Saastal, from the Nollenhorn.

The Schwarzberg fold exhibits two superposed folding phases - D1 and D2. The fold hinge (edged in black) consists of marbles of the Portjengrat unit. MR: Monte Rosa nappe, PG: Portjengrat unit, ZS: Zermatt-Saas unit.

The **D1/D2 Schwarzberg fold** (Fig. 4.2.20) is exposed at the Schwarzberg SE face. It has previously been described by Lacassin (1987) and Rössler (2000). An interference pattern of two fold generations - D1 and D2 - is formed by Permo-Mesozoic metasediments of the Portjengrat unit. The marbles are found in the core of this interference pattern. Rössler (2000) found the D1 fold hinge (her fold U4) to be located in the SE face of the Schwarzberg, and not at its NW crest as described by Lacassin (1987). Two D2 fold axial planes can be traced from the Hangende Gletscher fold to the Schwarzberg fold. The lower one crosses the core of the Hangende

The **D2 Grosställi fold** will be described in chapter 4.2.5.

Only the limbs of the **D3 Allalin antiform** are exposed, i.e. north and south of the Allalin glacier. Therefore, the amplitude of the Allalin antiform is unknown and might be less than indicated in cross-section 638. However, the connection of the orthogneisses of the Portjengrat unit south of the Allalin glacier with the orthogneisses north of it necessitates an antiformal structure. Its fold axial plane as inferred from the cross-section, dips moderately to the NW.

The isoclinal **D1/ D2 Britannia folds** (D1 and D2 cannot be distinguished) are exposed at the crest of the Hinter Allalin, between the Britannia refuge and Kleiner Allalin (3069 m), as well as at the Chessjen glacier. They are characterized by the intercalation of bands of calcareous micaschists and subordinate serpentinites of the Zermatt-Saas unit and basement and cover of the Portjengrat unit. Isoclinal folding and

syn-D2 boudinage of more competent layers (e.g. dolomitic marbles in a matrix of calcitic marbles) are well exposed east of the Chessjen glacier. The Britannia folds are gently refolded by asymmetric parasitic D3 folds, indicating the D3 Mittaghorn synform to be structurally situated above and to the north, e.g. in the SSE face of the Kleiner Allalin or south of the Britannia refuge.

The **D3 Chessjen antiform and synform** are exposed east of the Chessjen glacier. The fold axial plane trace of the **Chessjen antiform** is contained between steeply W- and steeply N-dipping foliations of the Zermatt-Saas unit at the Egginerjoch. From there, the axial trace can be followed to the east along steeply N-dipping foliations in calcareous micaschists. The Chessjen antiform has a cusped geometry (see cross-section 638) reflecting the competence contrast between the weak calcareous micaschists and the more competent ophiolites. This agrees with the lobate shape of the adjacent D3 Mittaghorn synform (see below).

The fold axial plane trace of the **Chessjen synform** is contained between steeply and moderately N-dipping foliations of intercalated calcareous micaschists and Portjengrat orthogneisses. The intercalation is the result of isoclinal D1 and D2 folding (D1/ D2 Britannia folds, see above).

The **D3 Mittaghorn synform** (Fig. 4.2.21) has an open lobate shape and is exposed at the east face of the Mittaghorn and below the Egginer. It has previously been described by several authors (Güller, 1947; Bearth, 1954b, 1957, 1964, 1967; Klein, 1978, Milnes et al., 1981). The D3 Mittaghorn synform refolds the nappe contact between the Zermatt-Saas unit and the Portjengrat unit. The hinge of the D3 Mittaghorn synform is not the deepest point of the structure, as this synform refolds a pile of sediments that wedge out towards the south and north. This wedging-out is the result of earlier folding and/ or nappe stacking. The fold axial plane, as inferred from the cross-section, dips moderately to the NW (310/30). The fold axis as calculated from the poles of the composite foliation is 289/25 (Fig. 4.2.18 A). Towards the north, the fold axial plane trace follows the SSE-crest of the Mittaghorn, where it is indicated by the M-symmetry of refolded calcareous micaschists. From

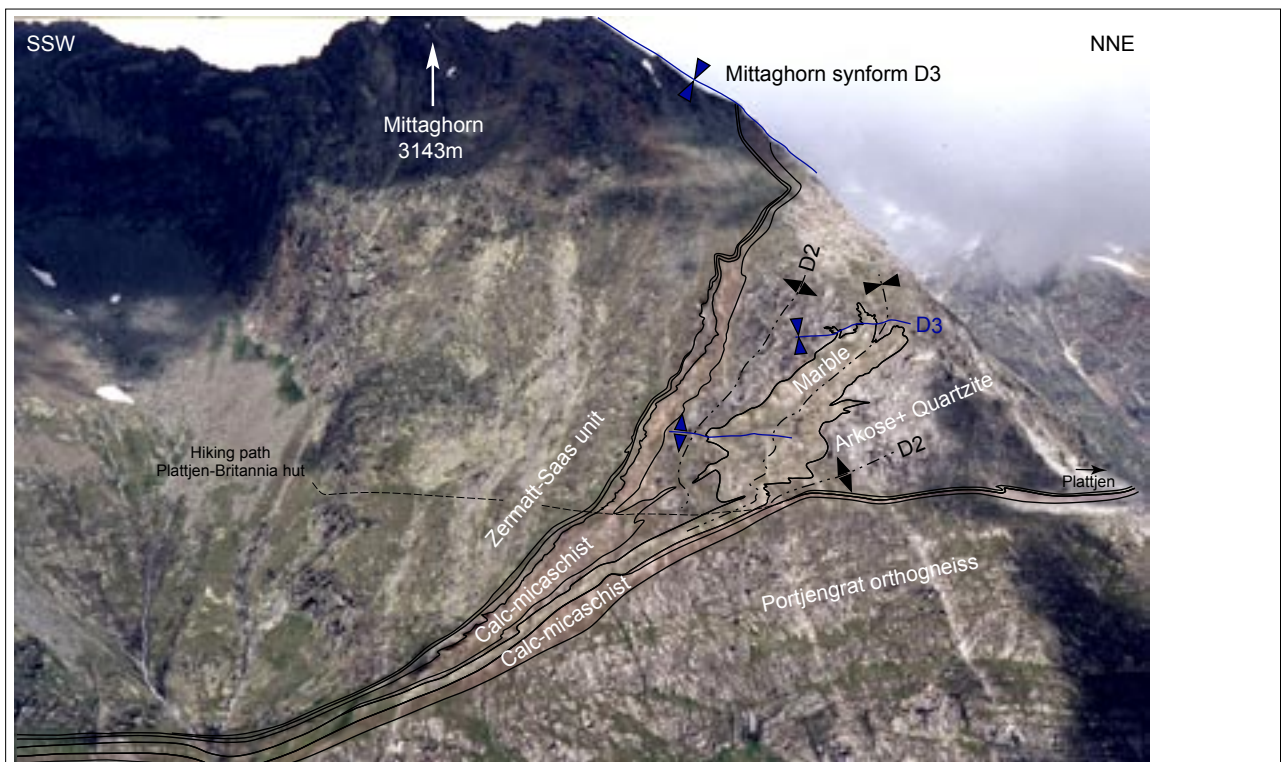


Fig. 4.2.21: View of the Mittaghorn, Saastal, from Furggtal.

The D3 Mittaghorn synform refolds the nappe contact of the Zermatt-Saas unit (on top) and the Portjengrat unit. Its fold axial plane trace is located at the crest on the right-hand side of the picture, indicated by folds with an M-symmetry (not visible in the picture) as well as by the asymmetry of the parasitic D3 folds in the metasediments of the southern limb. The metasediments are additionally refolded by two older isoclinal folding phases (cf. Fig. 4.2.22). The hinge of the Mittaghorn synform is not the deepest point of the structure, as it refolds a pile of sediments that wedge out towards the south. The wedging-out has probably evolved during nappe stacking.

there, it can be followed into the meta-arkoses of the NNE face of the Mittaghorn, right below the calcareous micaschists. Considering the intersection of the fold axial plane with the topography, the fold axial plane trace should turn to the NNE at Oberer Schopfen (covered by moraine debris), and pass through the lower band of calcareous micaschists near Bifig (see Enclosure 2). There, it is supposedly cut off by the Saas shear zone (see ch. 4.3 and 5).



Fig. 4.2.22: Superposition of three folding phases in the Permo-Mesozoic metasedimentary cover of the Portjengrat unit.

Basaltic sills or dykes frequently occur throughout the sequence (arrows). Below the Mittaghorn, Saastal; at the hiking path from Plattjen to the Britannia refuge, close to the turning of the path to the Mittaghorn (crds. 639 200/103 760).

The **D2 Plattjen folds** are exposed in the S face of the Mittaghorn (Figs. 4.2.21 & 4.2.22). They isoclinally re-fold marbles (in the core of D2 synforms), and quartzites, meta-arkoses and -conglomerates of the Portjengrat unit. Numerous asymmetric parasitic D3 folds are superimposed on the D2 folds. The D3 parasitic folds confirm that the hinge of the D3 Mittaghorn synform is located to the north and above this locality.

The **D1/ D2 Gletscheralp folds** comprise all the isoclinal D1/ D2 folds that are exposed at the Gletscheralp and Spielboden west of Saas Fee (e.g. Fig. 4.2.23). As they are located in the hinge region of the D3 Spielboden antiform (see below), three fold generations (D1, D2, D3) are superimposed within the metasedimentary cover and the basement of the Portjengrat unit and within the calcareous micaschists and serpentinites

of the Zermatt-Saas unit. D1 and D2 folding is isoclinal and responsible for the multiple repetition of lithologies, that are exposed in roughly SE-NW striking bands. At a larger scale, the lithologies of the Portjengrat unit are situated in the core of these D2 synforms. They are enveloped by calcareous micaschists of the Zermatt-Saas unit.

The overturned southern limb of the SE-facing **D3 Spielboden antiform** is exposed at the Gletscheralp and Spielboden west of Saas Fee, where it re-folds the D1/ D2 Gletscheralp folds described above. The D3 Spielboden antiform has an amplitude of 3 km and a width of approximately 1.5 km. Its fold axial plane, as inferred from the cross-section, dips with approximately 60° to the NW. The location of the fold axial plane trace of the Spielboden antiform is indicated by the abrupt change of the azimuth of the foliations at the NE edge of the Gletscheralp at approximately 2000 m elevation. There, the foliations abruptly change from a SW-ward to a NW-ward dip. As the foliations farther in the north (north of the Fee glacier at Trift and Hannigalp) continue to dip to the W or NW, this change in orientation cannot be interpreted as a deflection caused by another D3 parasitic fold.

The kilometer-scale, S-facing **D3 Mischabel "backfold"** is an antiform adjacent in the N and W of the D3 Mittaghorn synform (see above). This D3 Mischabel backfold is exposed from the western slope of the Mattertal N of Zermatt to Saas Fee and further north to Zen Eisten in Saastal (cf. Fig. 4.2.1 D; for its illustration in cross-section see Escher et al., 1988, 1997; for a schematic cross-section see Fig. 5.2). The D3 Mischabel backfold is situated N of the area investigated in this study (see Fig. 5.1) and it will, therefore, not be described in detail (for a detailed description see Escher et al., 1997; Steck et al. 1989; and also Güller, 1947; Bearth, 1964 a+b; Klein, 1978; Milnes et al., 1981; Müller, 1983). Towards the E (at the eastern slope of Saastal and in Zwischbergental),

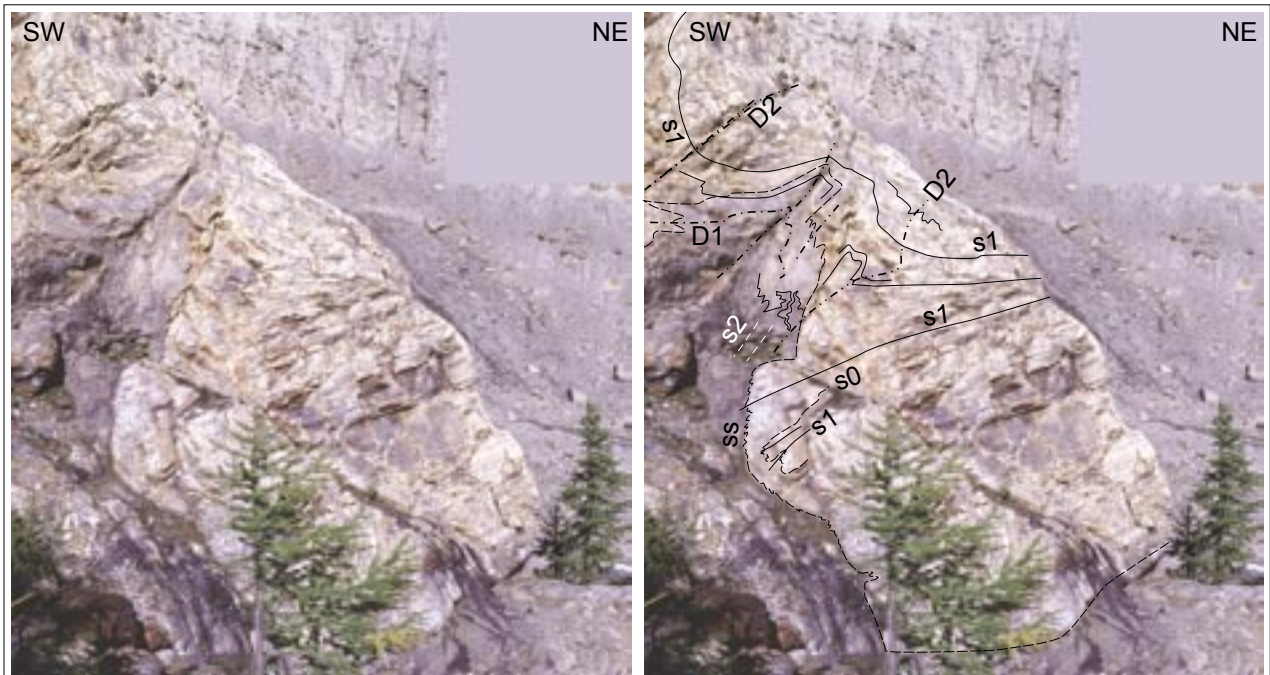


Fig. 4.2.23: Superposed folding in quartzites (yellow, on top) and quartzitic conglomerates (grey) of the Portjengrat unit.

The sedimentary layering *ss* and a first foliation *s0* are isoclinally folded (*D1*), and a penetrative new axial plane cleavage *s1* has developed. It is refolded by a second generation of tight to isoclinal folds (*D2*). Parallel to the *D2* fold axial planes (average value 228/56; *D2* fold axes 288/30) a new axial plane cleavage *s2* has developed. There is no displacement along the joints that run parallel to the *D2* fold axial planes. The outcrop is situated in the hinge region of the large-scale *D3* Spielboden antiform (see cross-section 636). SW of Saas Fee, at the hiking path from Lake Gletschersee (P. 1904) to Längflue, at 1960 m (crds. 636 470/ 105 320).

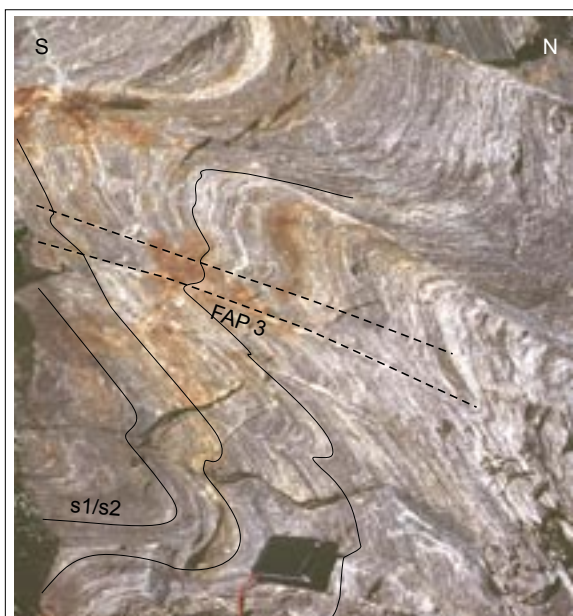


Fig. 4.2.24: Asymmetric parasitic folds in the overturned northern limb of the *D3* Gabbio synform.

The axial plane trace is situated structurally below and in the south. Oriented parallel to the fold axial planes (FAP3), a new axial plane cleavage has sporadically developed in paragneisses of the Monte Rosa basement. At the dam on the W-side of Lake Mattmark, Saastal (crds. 639 900/ 099 675).

the overturned lower limb of the *D3* Mischabel backfold was probably cut off by the S- to SE-directed ***D3* Mischabel thrust** that separates the Siviez-Mischabel nappe from the Portjengrat unit (see ch. 4.3 and 5).

The ***D3* Trifflhorn antiform** and the ***D3* Trifflhorn thrust** will be described in chapter 4.2.4.

The ***D3* Gabbio synform** is exposed from Lake Mattmark in Saastal (cross-section 638) to Furggtal (cross-section 643), Valle di Loranco (cross-section 650), and the uppermost Valle di Bognanco (cross-section 653). The *D3* Gabbio synform has previously been described by several authors (Blumenthal, 1952, as “Antronamulde”, Bearth, 1957; Klein, 1978; Escher et al., 1988, 1997; Froitzheim, 2001; Keller & Schmid, 2001). From Saastal to Valle di Loranco, the fold axial plane trace is located within the Monte Rosa nappe, close to the contact with the Furgg zone. Farther east, it passes into the Antrona unit. The different rheological behaviour of the well-foliated paragneisses and the isotropic granites of the Monte Rosa nappe (cf. ch. 4.1), however, led to a different style of folding associated with the same folding phase. This often complicates the

unequivocal attribution of folds to D2 or D3, and therefore the localisation of the fold axial plane trace of the Gabbio synform is sometimes difficult.

Close to the dam, on the W-side of Lake Mattmark, asymmetric parasitic folds of the overturned northern limb of the Gabbio synform (Fig 4.2.24) are exposed. On the E-side of Lake Mattmark, near the dam, numerous parasitic isoclinal folds are exposed. These exhibit either an M-symmetry, or an asymmetry indicating the location of the fold axial plane further to the south. Approximately 370 m south of the dam, the first parasitic folds exhibiting a reverse asymmetry appear. As they re-fold the main foliation of the paragneisses, they are interpreted as parasitic D3 folds. Therefore the fold axial plane trace of the Gabbio synform was located about 350 m south of the dam.

In Furggtal, at the bottom of the Nollenhorn SW face and below P. 2962, migmatites of the Monte Rosa nappe are overprinted by parasitic D3 folds, which indicate the location of the fold axial plane trace farther to the south. As no parasitic folds were found in the mylonitised metagranites south of the base moraine of the Nollen glacier, the fold axial plane trace is interpreted to be located under the debris of the moraine. However, the fold axial plane trace could not be traced to the NE-side of the Furggtal. Klein (1978) suggests its location north of the Kehrenrück.

In Valle di Loranco, the fold axial plane trace of the Gabbio synform is located approximately 1 km N of the Punta Turiggia, passing through a nearly undeformed granite to the N-crest of the Cime di Pozzuoli S' of P.2485, and crossing into the Furgg zone N of Lake Bacino Alpe dei Cavalli (Keller, 2000; Klein, 1978). At the Alpe del Gabbio, the orientation of the foliation abruptly changes from W-dipping to NNW-dipping. This has been interpreted as hinge collapse by Keller (2000).

At the Monte della Preja, several parasitic D3 folds are exposed in the hinge of the Gabbio synform (see also Fig. 4.2.35, ch. 4.2.6). Their fold axial planes dip moderately to the NW (352/55), while fold axes plunge moderately to the W (320/45). The major fold axial plane trace of the Gabbio synform is contained between two bands of marble in the W-slope of the Monte della Preja. They unify to a single, steeply NW-dipping band (330/83), that descends to the E-slope of Monte della Preja. From there, the fold axial plane trace passes to the "Monte Pasquale" (see also Figs. 4.2.36 and 4.2.38, ch. 4.2.6). The axial plane trace of the D3 Gabbio synform was not followed farther E into the Valle Bognanco.

4.2.4 Almagellertal, Zwischbergen pass, and Zwischbergental

Cross-sections 642 & 646 A

Projection methods

642, in Almagellertal

Stafelalp - Trifflhorn - Schwarzalm

Coordinates: N-S: 642, E-W: 105 - 109; length: 4 km.

A projection value of 270/29 was used. It represents the mean of the π -pole, as calculated from the composite foliation of the D3 Trifflhorn antiform (269/28; see Fig. 4.2.25 A) and the maximum of the D3 small-scale fold axes (270/31).

646 A & B

These two sections run along the same N-S coordinate. Two separate cross-sections were constructed because the structures at the southern rim of the Portjengrat unit strike with 250° (646 B), whereas the structures at its northern rim strike with 266° (646 A; see also Fig. 4.2.25 B and Enclosure 2). Therefore, the structures had to be projected with different azimuths and hence two separate cross-sections were constructed. Cross-section 646 B will be discussed in chapter 4.2.5.

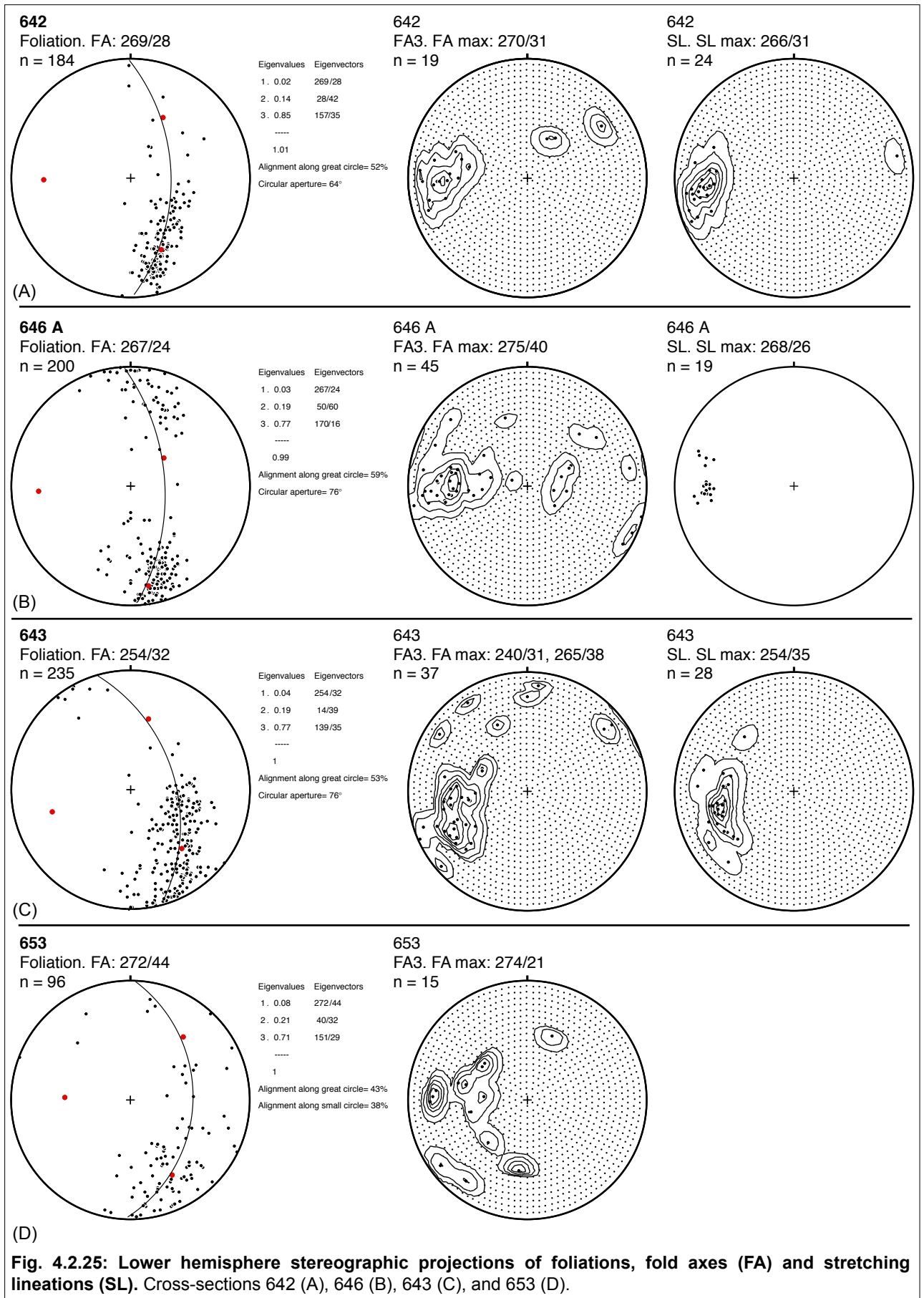
646 A, E' of the Zwischbergen pass in Zwischbergental

Pizzo d'Andolla - Tällhorn

Coordinates: N-S 628, E-W: 105 - 109; length: 4 km.

Two different plunges were used for projection: 266/33 for structures situated E of the Zwischbergen pass, and 266/30 for structures situated W of this pass. The azimuth is equal for both,

so that lithological interfaces do not intersect. Since t azimuth was calculated from the composite foliation poles (Fig. 4.2.25 B). The plunge of the D3 fold axes steepens discontinuously from W to E



(from 24° to 42°). An average value was therefore chosen for the structures situated W (30°) and E (33°) of the Zwischbergen pass in order to avoid the intersection of lithological interfaces.

Discussion

D3 & D2 structures

The SSE-facing **D3 Trifhorn antiform** (cross-section 642) is structurally situated below the Mittaghorn synform (see Enclosure 2). Therefore, its structural position is similar to that of the Stockhorn antiform. The D3 Trifhorn antiform is exposed in the E face of the Trifhorn. Its northern upright limb contains the calcareous micaschists which can be followed to the Farwald (east of Saas Grund) and into the cliffs situated below Saas Fee (see Enclosure 2 and Fig. 4.2.26). The Trifhorn antiform has previously been described by Bearth (1957), Klein (1978), and Dubach (1998). It has an amplitude of 3 km and a width of approximately 1.5 km. The fold axis, as calculated from the composite foliation, plunges moderately to the W (269/28; Fig. 4.2.25 A). The fold axial plane, as inferred from the cross-section, dips moderately to the NNW (around 50°). The fold axial plane trace is exposed at the E and S face of the Trifhorn. Further to the west, it probably follows the southern edge of the belt of calcareous micaschists which extend from the Farwald to Saas Fee (Fig. 4.2.26).

The core of the Trifhorn antiform consists of paragneisses of the Portjengrat unit and it tightens towards the west (at the Saaser Vispa below Saas Fee). At the Farwald, the northern limb contains an up to 90 m thick band of calcareous micaschists, and several small thrust slices of rauhwackes and quartzites, structurally situated both above and below the calcareous micaschists. Below Saas Fee, at Hannig, the northern limb consists of intercalated calcareous micaschists and marbles (Fig. 4.2.27). The southern overturned limb is only exposed in the E face of the Trifhorn. It was cut off by the D3 Trifhorn thrust (see ch. 4.3).

The tight **D3 Zwischbergen antiform** (cross-section 646 A; Figs. 4.2.29, 4.2.30, 4.2.31) is well exposed in the upper Zwischbergental, 350 m east of the Zwischbergen pass. It refolds calcareous micaschists and the cover and basement of the Portjengrat unit. Its fold axial plane trace is contained in a band of calcareous micaschists, that can be followed towards the east to P.2939 at the Tällihorn S crest, and farther east to P.2697 and south of P.2176. At the Zwischbergen pass and in the Almagellertal, the trace of the fold axial plane runs within the calcareous micaschists, exposed along the hiking path to the Allmageller refuge. The fold axial plane of the Zwischbergen antiform, as inferred from the cross-section, is bent (see cross-section 646 A): its lower part (south of the Tällihorn S crest) dips with 50-60° to the N, its upper part (at the Zwischbergen pass) steepens up to 70-80° N-dip (see ch. 4.3.4 and 5 for a kinematic interpretation). The fold axis, as calculated from the composite foliation (Fig. 4.3.29 B) plunges moderately to the W (267/24). The values measured east of the Zwischbergen pass are 266/42. The vergences of the D3 Zwischbergen antiform and synform indicate the location of the D3 Trifhorn antiform to the N.

The **D3 Zwischbergen synform** (cross-section 646 A; Figs. 4.2.29, 4.2.30, 4.2.31) is well exposed at the Tällihorn S crest. There, it refolds several isoclinal D1/D2 folds that are responsible for an intercalation of calcareous micaschists, amphibolites and the metasedimentary cover of the Portjengrat unit (see D2/D3 Weissmies folds; Figs. 4.2.30, 4.2.31). Because of these interference patterns, its fold axial plane trace cannot easily be traced to the Zwischbergen pass. At the Zwischbergen pass, the Zwischbergen synform splits into several parasitic folds. The major fold axial plane trace is contained in a parasitic antiform, refolding garnet-bearing calcareous micaschists south of the pass. It probably crosses the crest to the Dri Horlini at approximately 3250 m elevation. Like the Zwischbergen antiform, its fold axial plane is bent and steepens from a dip of 50-60° to the N at the Tällihorn S crest to a dip of 70-80° to the N at the Zwischbergen pass (see ch. 4.3.4 and 5 for a kinematic interpretation). The fold axis plunges moderately to the W.

The **D2/D3 Weissmies folds** (cross-section 646 A; Figs. 4.2.29, 4.2.30, 4.2.31) comprise all

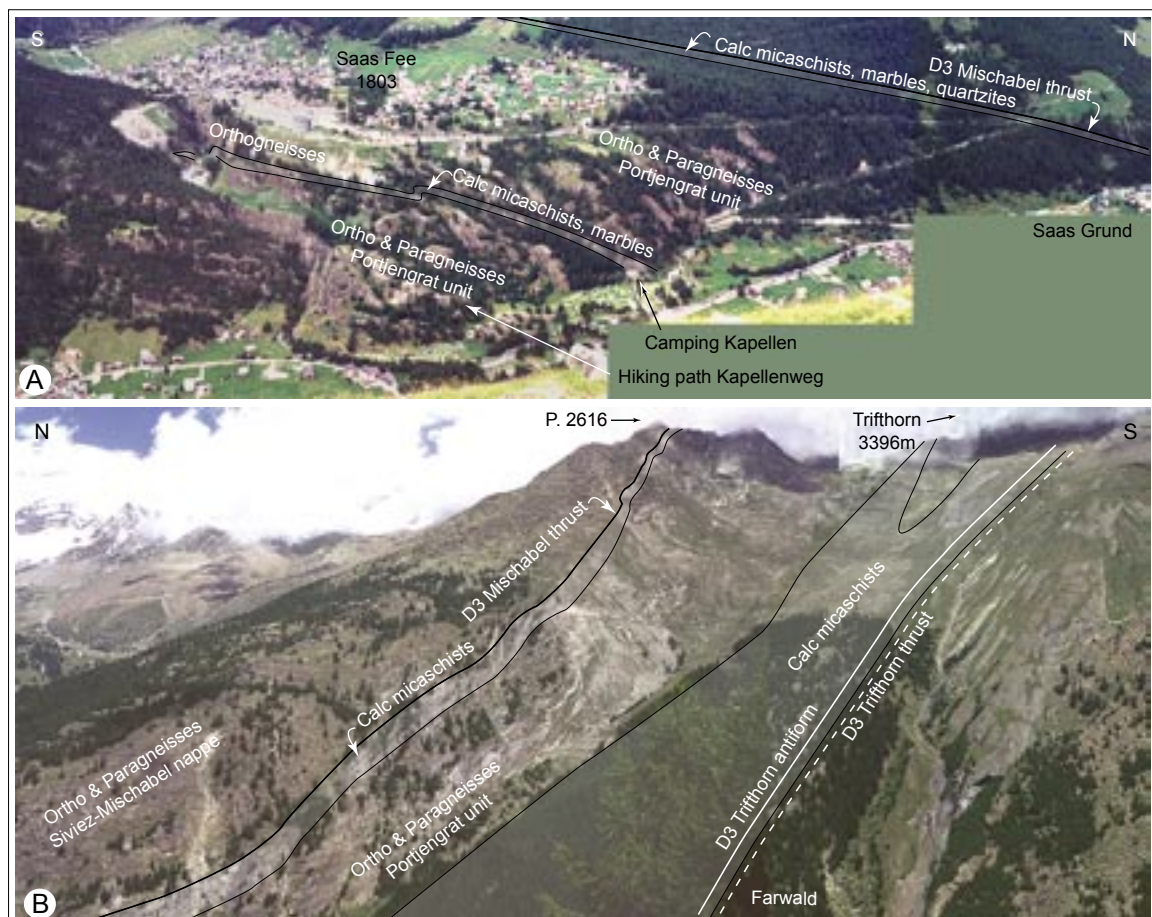


Fig. 4.2.26: Metasedimentary belts between ortho- and paragneisses of the Portjengrat unit at Saas Fee and Saas Grund in Saastal.

(A) View of Saas Fee, western side of Saastal, from the Grundberg. Two belts of metasediments can be recognized, both dipping with approximately 35° to the NW. The lower one consists of calcareous micaschists and minor marbles (cf. Fig. 4.2.27). The thickness is up to approximately 70 m. On the eastern side of Saastal (B), the lower belt can be connected with the calcareous micaschists of Farwald. Structurally, this belt is situated in the northern normal limb of the D3 Trifhorn antiform (cf. cross-sections 638 & 642).

The upper metasedimentary belt consists of calcareous micaschists and minor marbles near Saas Grund, and can be connected with the upper belt of calcareous micaschists on the eastern side of the Saastal (B). Above Saas Fee, the upper belt predominantly consists of quartzites and marbles and only minor calcareous micaschists. There, the upper belt can be traced to the metasediments at the Gletscheralp and the Mittaghorn. Its thickness is up to approximately 40 m. The D3 Mischabel thrust is supposedly located on top of the upper metasedimentary belt, marking the contact to the gneisses of the Siviez-Mischabel nappe.

(B) View of the Grundberg, eastern side of the Saastal, from Plattjen. The lower metasedimentary belt consists of calcareous micaschists and minor rauhewackes and quartzites. It can be traced to P. 3227 south of the Trifhorn, where it is cut off by the D3 Trifhorn thrust (see text). The upper metasedimentary belt consists of calcareous micaschists and minor rauhewackes and can be traced towards the Triftgratij and the Schwarzemies.

the folds exposed along the S crest of the Weissmies, north of the Zwischbergen pass. The folds affect the calcareous micaschists and the sedimentary cover of the Portjengrat unit. D3 folding is isoclinal and the D3 fold axial planes dip steeply to the N or S. The two most prominent folds will be described below.

The E-W-striking trace of the fold axial plane of the **D2/D3 Weissmies antiform** (Fig. 4.2.31) can be traced from the Weissmies S crest to the Tällihorn S crest. At the Weissmies S crest, its core consists of quartzites. Towards the Tällihorn S crest, one passes through stratigraphy that repeatedly changes the younging direction (quartzites - marbles - rauhewackes - calcareous micaschists). This



Fig. 4.2.27: Contact of augengneisses (Portjengrat unit; on top), marbles (light) and calcareous micaschists (grey).

The outcrop is located at the chapel at the end of the hiking path "Kapellenweg" below Saas Fee (P. 1748, crds. 638 300/ 106 600). The metasediments are situated in the normal northern limb of the D3 Trifhorn antiform (cf. cross-section 638). They continue to the Grundberg/ Saas Grund (cf. Fig. 4.2.26, lower band of metasediments) and the Trifhorn in the E, where they are cut off by the late-D3 dextral oblique Trifhorn thrust (cf. cross-section 642). The contact is parallel to the foliation and dips moderately to the NW (300/25). In the augengneisses, asymmetric feldspar clasts associated with the stretching lineations (277/22) indicate a top to the E sense of shear. For discussion of the affiliation of the metasediments see chapter 5. Height approximately 7 m.

is interpreted to result from D2 folding with a transverse strike of the D2 fold axial planes. The quartzites are interpreted as the cores of such D2 folds. However it remains unclear, whether they were originally antiformal cores, in which case the stratigraphy rests in a normal upright position on the Portjengrat basement; or whether they originally were synformal cores, in which case the stratigraphy is turned upside down.

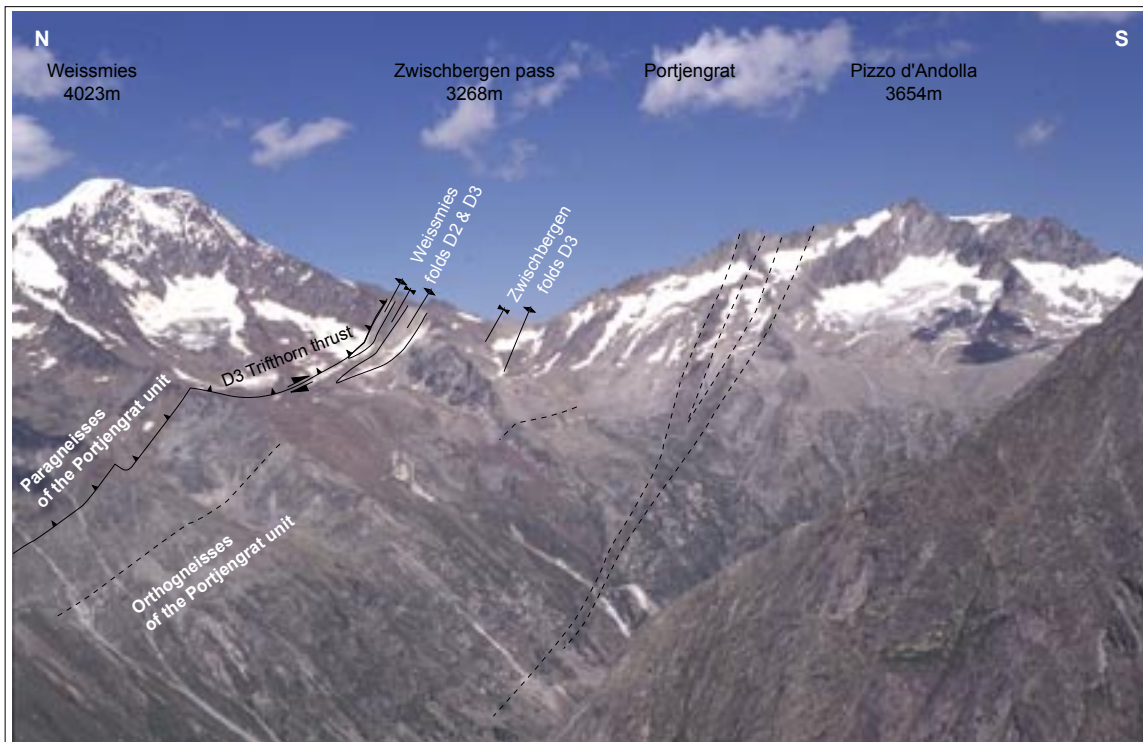


Fig. 4.2.28: View of Almagellertal, Zwischbergen pass and Portjengrat from the Mittaghorn towards the east.

The light bands at the SSE-crest of the Weissmies and at the Zwischbergen pass are refolded Permo-Mesozoic metasediments. The fold axes of the D2/D3 Weissmies and D3 Zwischbergen folds plunge with 30 - 40° to the west and therefore disappear below the surface south of the Weissmies summit. The D3 Trifhorn thrust is a dextral oblique thrust, along which the Portjengrat unit was thrust over itself. For discussion of the affiliation of the metasediments see text.

Rauhwackes are exposed adjacent to the the Weissmies antiform. These form the core of the **D3 Weissmies synform** (Fig. 4.2.31). As they can be connected with several other exposures of rauhwackes between the Weissmies S crest and the Tällihorn S crest (see Enclosure 2), they are interpreted as the northern limb of the D2/D3 Weissmies antiform discussed above (cf. cross-section 646 A).

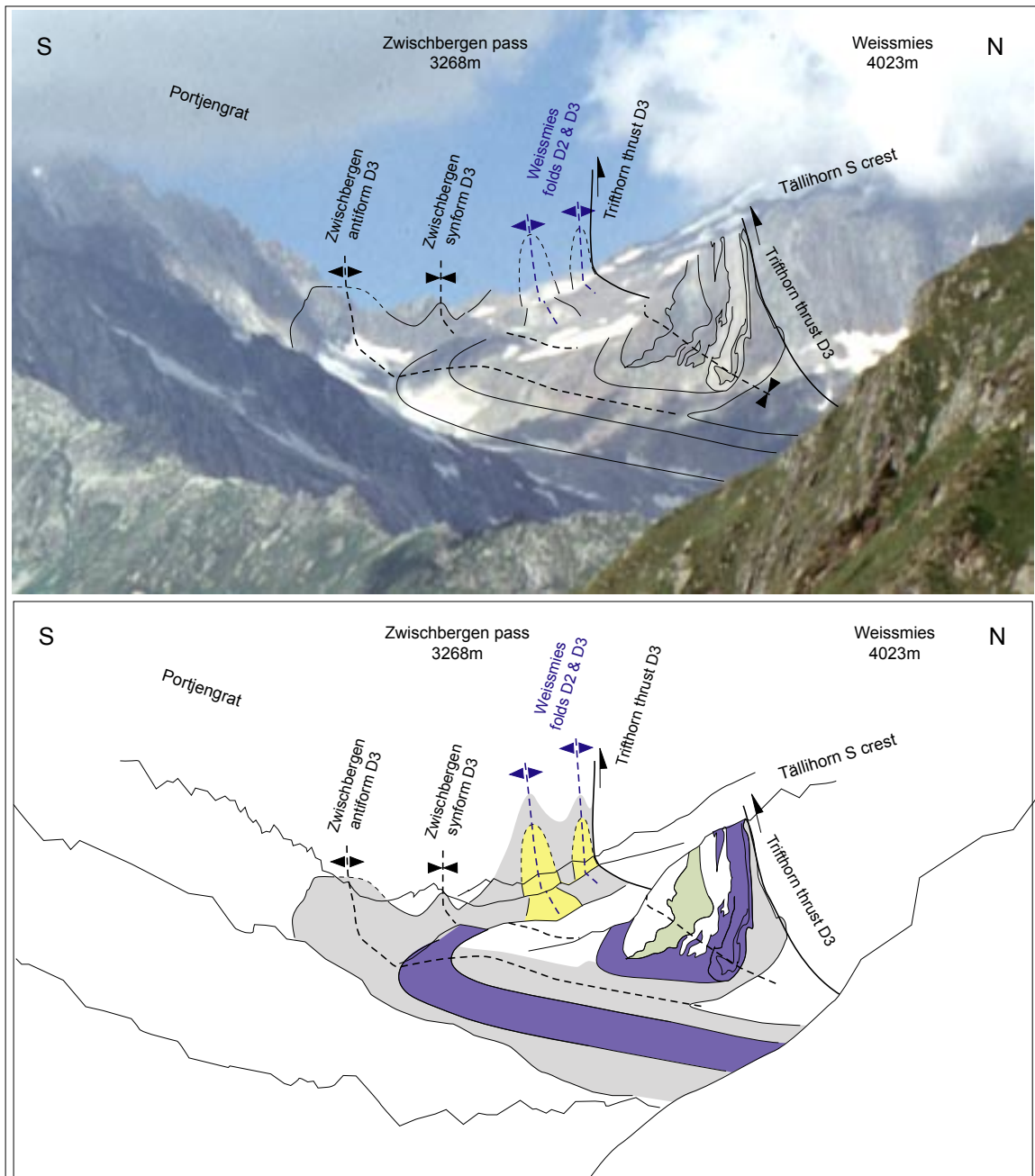
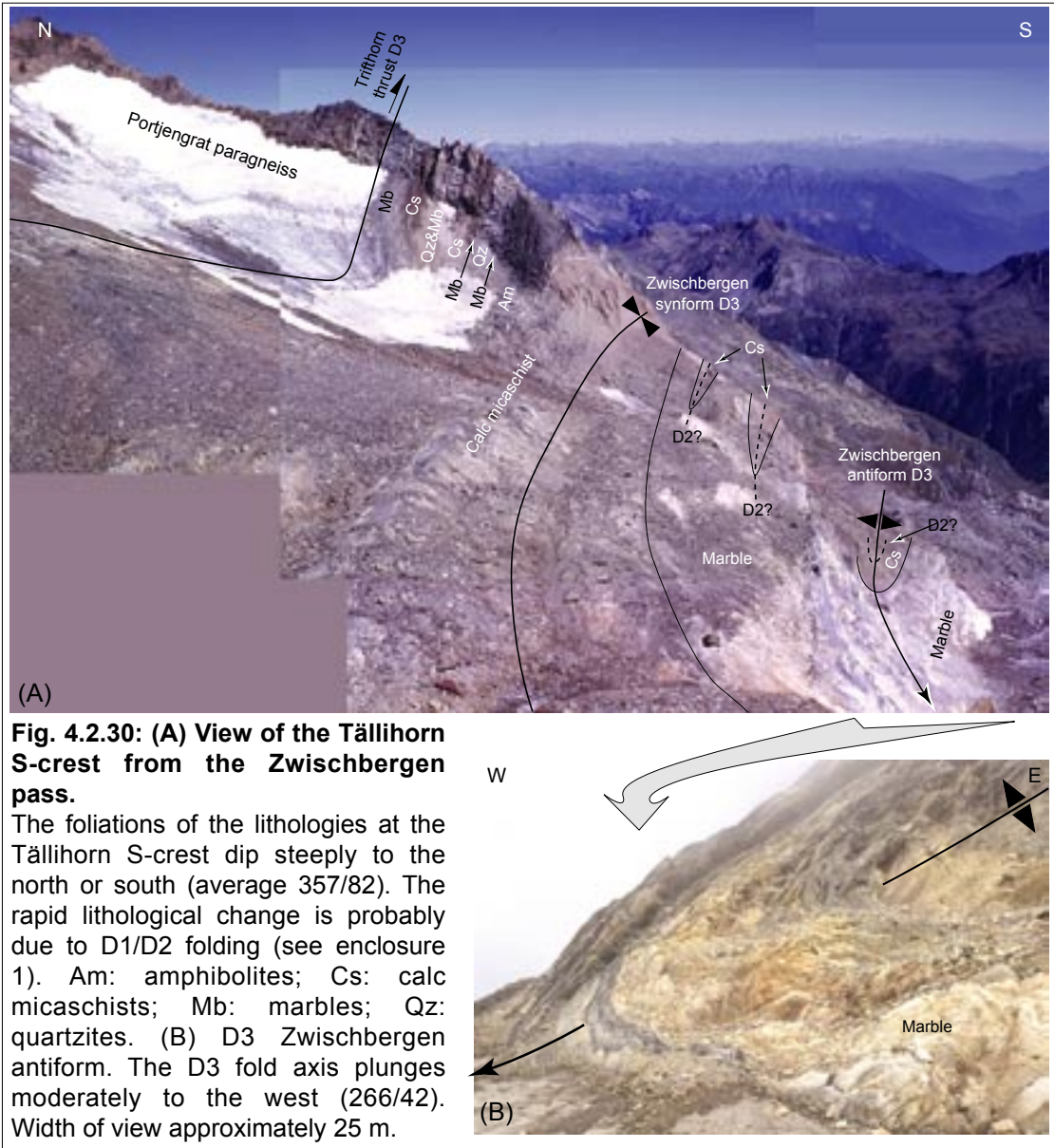


Fig. 4.2.29: View of the Permo-Mesozoic metasediments of the Zwischbergental from Pizzo del Büsin towards the WNW.

The fold axes of the major D3 structures plunge with 30 - 40° to the west. The fold axial planes of both the D3 Zwischbergen synform and D3 Zwischbergen antiform are bent (see cross-section 646). In their lower part, they dip with 50 - 60° to the north (inferred from the cross-section). In their upper part - towards the Zwischbergen pass - they steepen to 70 - 80°. The Portjengrat paragneisses were thrust over the Portjengrat metasediments and orthogneisses along the dextral oblique Trifhorn thrust, a late D3 structure. Grey: calcareous mica schists; purple: marbles; yellow: quartzites, marbles and rauhwackes; green: metabasica.



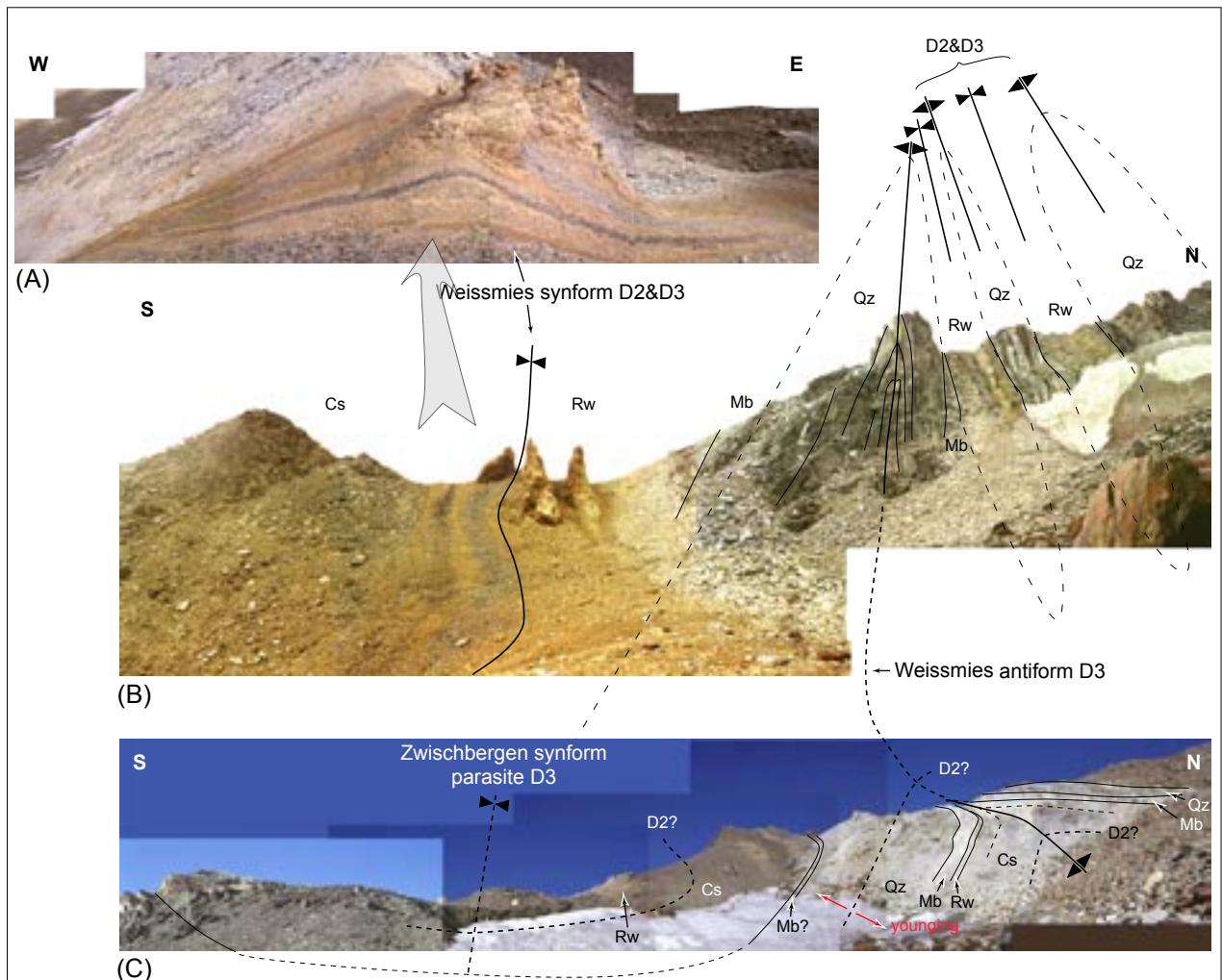


Fig. 4.2.31: View towards the W onto the metasediments at the Zwischbergen pass, Almagellertal - Zwischbergental.

(A) The core of the D2/3 Weissmies synform consists of rauhwackes. The dark bands are chlorite and white mica-rich layers. View along the SSE crest of the Weissmies. Width of view approximately 30 m.

(B) D2 and D3 folds at the SSE crest of the Weissmies. The foliation was rotated into a steeply south or north-dipping position (average 176/81) by isoclinal D3 folding. The D3 fold axes plunge moderately to the west (average 269/25). Cs: calcareous micaschists; Mb: marbles; Qz: quartzites; Rw: rauhwackes. Width of view approximately 100 m.

(C) Metasediments along strike of (B), 300 m further in the east, at 3225 m elevation (crds. 645 200/ 107 500). The existence of D2 folds is inferred from the repetition of lithologies (see Enclosure 2 & text). Width of view approximately 250m. □

4.2.5 Furggtal and western Valle di Loranco

Cross-sections 643 & 646B

Projection methods

643, in Furggtal

Spechhorn - Stellihorn - Almagellhorn

Coordinates: N- S 643, E- W: 96 - 104; length: 8 km.

A projection value of 255/12 was used. It represents a compromise between an average azimuth of D3 folds and a plunge which avoids intersection of lithological interfaces. The azimuth of 255° represents the mean value of the π -pole as calculated from the composite foliations (254/32; see Fig. 4.2.25 C) and the two maxima of the D3 small-scale fold axes (240/31; 265/38). The chosen plunge of 12° is much smaller than that of the calculated or measured D3 fold axes. However, steeper plunge would result in the intersection of lithological interfaces.

646 B, in Val Loranco

Coronette di Camposecco - Pizzo di Loranco - Pizzo d'Andolla

Coordinates: N-S: 646, E-W: 102 - 105; length: 3 km.

A projection value of 250/30 was used. This corresponds to the maximum of the measured D3 small-scale fold axes.

For cross-section 646 A see chapter 4.2.4.

Discussion

In Furggtal, as seen in cross-section 643, the foliations and fold axial planes generally change in orientation towards higher structural levels from a steeply NW- to a shallowly W-dipping orientation. This change is caused by the overprint of the SE-directed D3 Saas shear zone (see chapter 4.3 and Fig. 4.4.2). D3 fold axes plunge moderately to the WSW with shallower values at the top and steeper values at the bottom of the folds (in average 248/35, Fig. 4.2.25 C).

D3 folds

The isoclinal **D3 Sonnighorn antiform** (cross-section 643, Fig. 4.2.32) is well exposed along the Sonnigrat and in the Steintälli. The Sonnighorn antiform refolds basement and cover of the Portjengrat unit, as well as garnet-micaschists and meta-arkoses of the Furgg zone, situated adjacent to the SE. At the Sonnigrat, the rocks are refolded by parasitic folds with a M-symmetry, indicating the hinge of the antiform. At the wall on the backside of the Steintälli, the Portjengrat basement is exposed in the core of the Sonnighorn antiform.

The fold axial plane trace of the Sonnighorn antiform runs from the Sonnighorn along the Sonnigrat, passes into the Steintälli at P.3339 and can be traced into the Plattenhorn E face. From Kanzilti towards the bottom of the Furggtal and farther to the Saastal, the fold axial plane trace could not be located with accuracy anymore.

The **D3 Steintälli synform** (cross-section 643, Fig. 4.2.32) is exposed along the SW face of P.3080 (NE-side of Furggtal), and at the Nollenhorn NE face (SW-side of Furggtal). At the southwestern side of Furggtal, it refolds meta-arkoses (in the core) and garnet micaschists of the cover of the Portjengrat unit. Its fold axial plane can be traced along the northern and southern side of the crest that runs from P.3080 to P.3339, and to the S face of the Plattenhorn. From Kanzilti towards the bottom of Furggtal, its approximate location is indicated by parasitic D3 folds at around 2500 m elevation (see Fig. 4.2.32).

On the SW-side of Furggtal, three fold generations (D1, D2, and D3) are superimposed within orthogneisses of the Monte Rosa nappe and garnet-micaschists and meta-arkoses of the Furgg zone. The D2-fold is called the "D2 Grosställi fold" (see below). This D2 fold is overprinted by an isoclinal

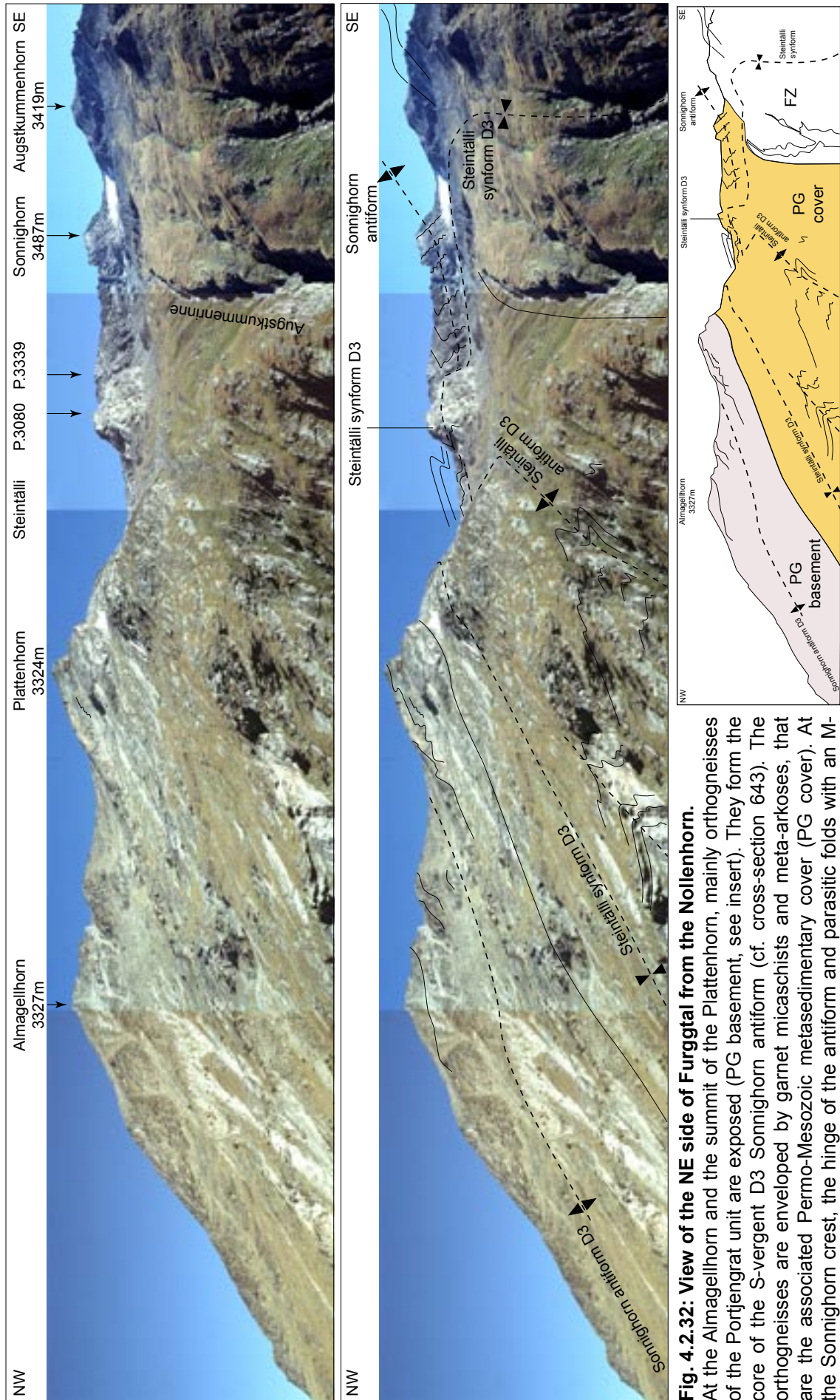


Fig. 4.2.32: View of the NE side of Furggtal from the Nollenhorn. At the Almageilhorn and the summit of the Plattenhorn, mainly orthogneisses of the Portjengrat unit are exposed (PG basement, see insert). They form the core of the S-vergent D3 Sonnighorn antiform (cf. cross-section 643). The orthogneisses are enveloped by garnet micaschists and meta-arkoses, that are the associated Permo-Mesozoic metasedimentary cover (PG cover). At the Sonnighorn crest, the hinge of the antiform and parasitic folds with an M-symmetry are exposed. The fold axial plane is bent - along the crest, it dips moderately to the W (269/24), and it steepens towards the bottom of the valley (approximately 254/82). FZ: Meta-arkoses and garnet-micaschists with basaltic boudins in Furgg zone.

D3 synform. The D3 fold axial plane dips moderately to the W (270/35). D3 small-scale folds plunge moderately to the WSW (245/32). The fold axial plane trace of the Steintälli antiform can be traced from the Nollenhorn to north of Lake Mattmark in the Saastal (Weber, 2001). From there, a band of mylonitized orthogneisses passes below the Allalin glacier to the bottom of the Schwarzbergchopf and ends in an antiformal S-closing hinge W of P. 2513 (Rössler, 2000; see Fig. 4.2.20). Due to the same closing direction, this hinge is interpreted to be the hinge of the D2 Grosställi fold, whereas the hinge of the D3 fold is supposed to be obscured by mylonitisation. At the NE-side of Furggtal, the fold axial plane trace passes south of the Augstkummenrinne to the southern edge of the Augstkummen glacier.

The **D2 Grosställi fold** (cross-sections 643 & 646 B, Fig. 4.2.33) is exposed at the Nollenhorn NE face. D1- and D2-folding results in meso-scale intercalations of Monte Rosa orthogneisses and meta-arkoses of the Furgg zone. The D2 fold hinge is supposed to be located below the moraine debris at the bottom of the Nollenhorn (Grosställi). For the location of the fold axial plane trace in Saastal see D3 Steintälli synform.

The **D3 Steintälli antiform** (cross-section 643, Fig. 4.2.32) is exposed below Kanzilti. It refolds basement (in the core) and cover of the Portjengrat unit. Its fold axial plane trace can be traced from the termination of the Kanzilti SW crest to the SW at approximately 2500 m elevation, where several parasitic D3 folds with a M-symmetry are exposed (see Fig. 4.2.33).

The overturned southern limb of the **D3 Börterrück antiform** (cross-section 643 & 646 B, Fig. 4.2.34) is exposed at the Börterrück. It refolds garnet-micaschists, meta-arkoses and amphibolites of the Furgg zone. At the Börterrück, its fold axial plane dips moderately to the WSW. Its fold axial plane trace can be traced from the Cimone di Camposecco to the SW along the amphibolite at the Börterrück. From there, it probably passes into the marbles. At the SW side of the Furggtal, it cannot be located exactly, as the crucial area in the Grosställi is covered by moraine debris. However, it appears again at the crest to the Saastal, where it is indicated by several parasitic M-folds. From there, it probably passes between a band of meta-basalts and the Monte Rosa gneisses in the core of the D2 Grosställi fold.

The **D3 Gabbio synform** is structurally positioned below the above described folds and it is described in chapter 4.2.3.

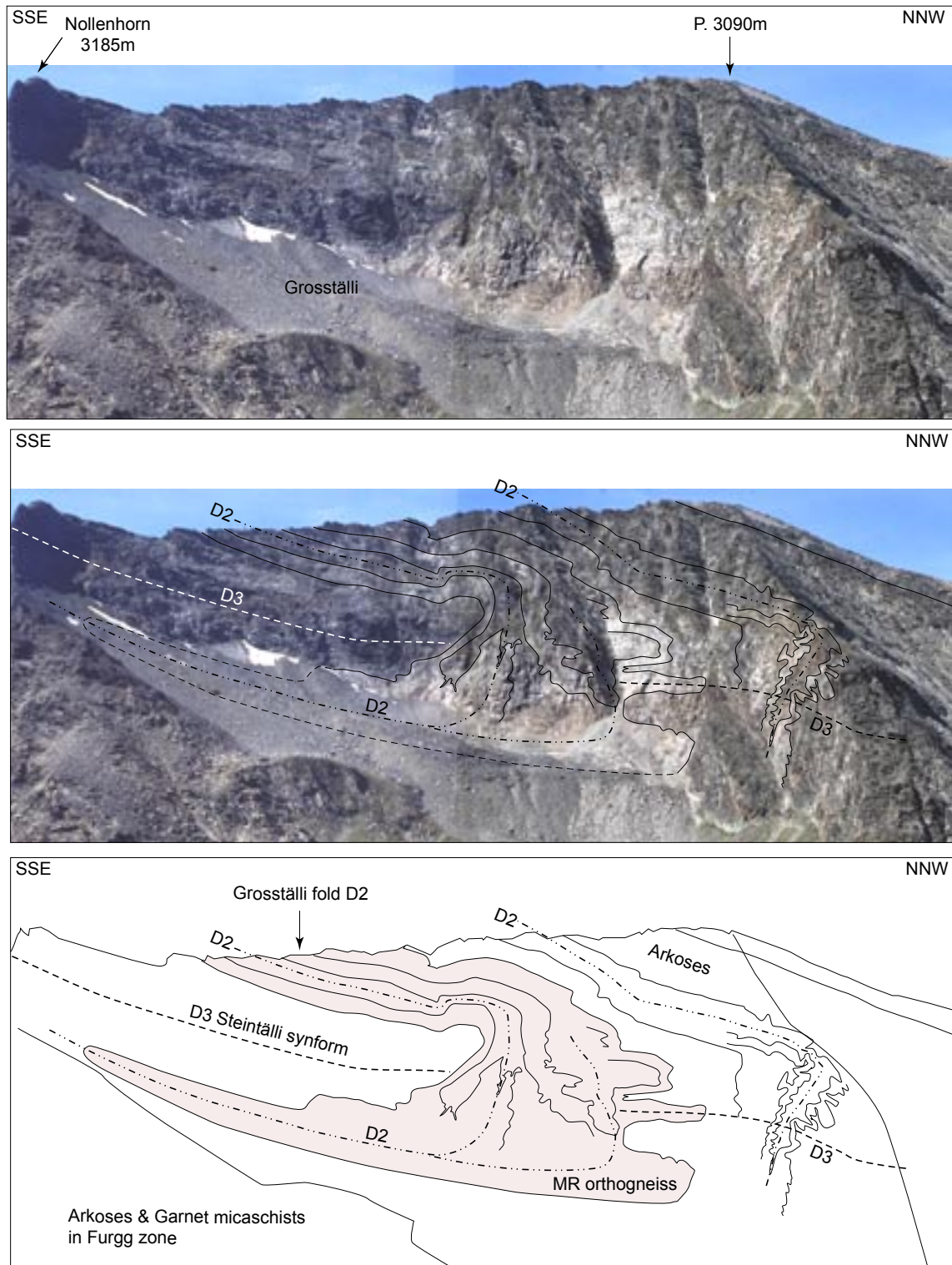


Fig. 4.2.33: View of the NW side of Furggtal onto the Nollenhorn N-crest, the crest between Furggtal and Saastal, from the Börterrück, Furggtal.

Two folding phases (D2 and D3) can be recognized. D2 isoclinally refolds the contact of fine-grained orthogneisses of the Monte Rosa nappe (MR orthogneiss) and Permo-Mesozoic metasediments (meta-arkoses and garnet micaschists with basaltic boudins in the Furgg zone). The hinge of the D2 fold is not exposed. However, the orthogneisses can be traced along strike at the western flank of the Nollenhorn to Lake Mattmark, Saastal, and further to P.2513 west of the Schwarzberg glacier (see Enclosure 2). There, a south-closing hinge is exposed, assumed to be the corresponding D2 fold hinge. The D2 fold is refolded by the isoclinal D3 Steintälli synform. The D3 fold axial plane dips moderately to the W (270/35); small-scale fold axes plunge moderately to the WSW (245/32).

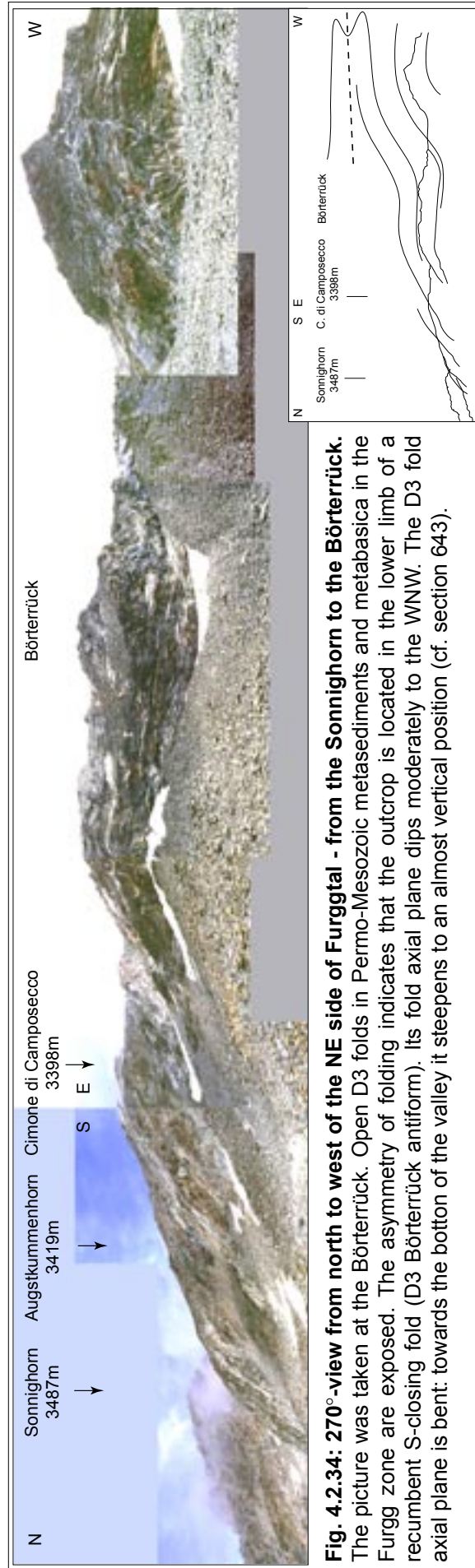


Fig. 4.2.34: 270°-view from north to west of the NE side of Furggtal - from the Sonnighorn to the Börterrück. The picture was taken at the Börterrück. Open D3 folds in Permo-Mesozoic metasediments and metabasica in the Furgg zone are exposed. The asymmetry of folding indicates that the outcrop is located in the lower limb of a recumbent S-closing fold (D3 Börterrück antiform). Its fold axial plane dips moderately to the WNW. The D3 fold axial plane is bent: towards the bottom of the valley it steepens to an almost vertical position (cf. section 643).

4.2.6 Eastern Valle di Loranco, Passo della Preja, and Valle di Bognanco

Cross-sections 650 & 653

Projection methods

650, W of lake Bacino Alpe dei Cavalli, Valle di Antrona

Cime di Pozzuoli - Monte Forcolaccia

Coordinates: N-S: 650, E-W: 102.5 - 106; length: 3.5 km.

A projection value of 250/30 was used. This corresponds to the maximum of the D3 small-scale fold axes.

653, E of the Monte della Preja pass in Valle di Bognanco

Pizzo Straciugo - Alpe Preja - Alpe Cheggio

Coordinates: N-S: 628, E-W: 104 - 110; length: 6 km.

Two different projection values were used: 250/44 for structures situated W, and 270/44 for structures situated E of the section plane, respectively. The strike of the structures changes orientation across the plane of the section. The plunge is that of the π -pole, as calculated from the composite foliations (Fig. 4.2.25 D). It is steeper than the maximum of the D3 small-scale fold axes (21°). However, any other projection value would result in the intersection of lithological interfaces.

Discussion

D3 structures

The **D3 Gabbio synform** and its parasitic folds are described in chapter 4.2.3.

The **D3 Preja thrust** (Fig. 4.2.35 B) is exposed at a small unnamed pass (2440m) between the N-summit (2485m) and the main summit (2514m) of the Monte della Preja. The thrust plane dips steeply to the NW (323/65) and is parallel to the foliation of the meta-arkoses of the Furgg zone in the footwall. In the hangingwall, serpentinites of the Antrona unit with a subvertical, steeply N- or S-ward dipping foliation (185/71, 350/85) are exposed. As the thrust cross-cuts the composite s1/s2 main foliation of the serpentinites, it has been interpreted as a D3 structure. The sense of movement could not be inferred from the thrust. However, SE-directed dextral oblique thrusting is likely, as similarly oriented D3 shear zones in the vicinity exhibit a top to the SE sense of shear (stretching lineations: 330/44; Fig. 4.2.35). As there is another angular unconformity between the foliations of the serpentinites and the amphibolites adjacent to the north, a second thrust must limit the serpentinites to the north. All of those thrust planes are considered to form part of the large-scale **D3 Gornergrat-Furggtal shear zone** (ch. 4.3.2), that extends from the Gornergrat in M Mattertal to Valle di Bognanco.

Between the D3 Gabbio synform and the D3 Passo della Preja synform, a D3 antiform is suspected (**D3 Passo della Preja antiform**). It is indicated on the map, but it was not investigated in detail.

The **D3 Passo della Preja synform** (Fig. 4.2.36) is continuously exposed from Alpe Roncalli in Valle di Loranco, to Passo della Preja, and to Alpe Agrosa in Valle di Bognanco. It refolds rauhewackes (in the core, at the hiking path from Alpe Preja/ Val Bognanco to "Monte Pasquale"), marbles (elsewhere in the core), quartzites, meta-arkoses and garnet micaschists of the Furgg zone. At the Monte della Preja pass, the fold axial plane dips steeply to the NNW (in average 349/69), the fold axes plunge moderately to the W (in average 273/35). At coordinate 653, the fold axial plane changes orientation to a NNW dip.

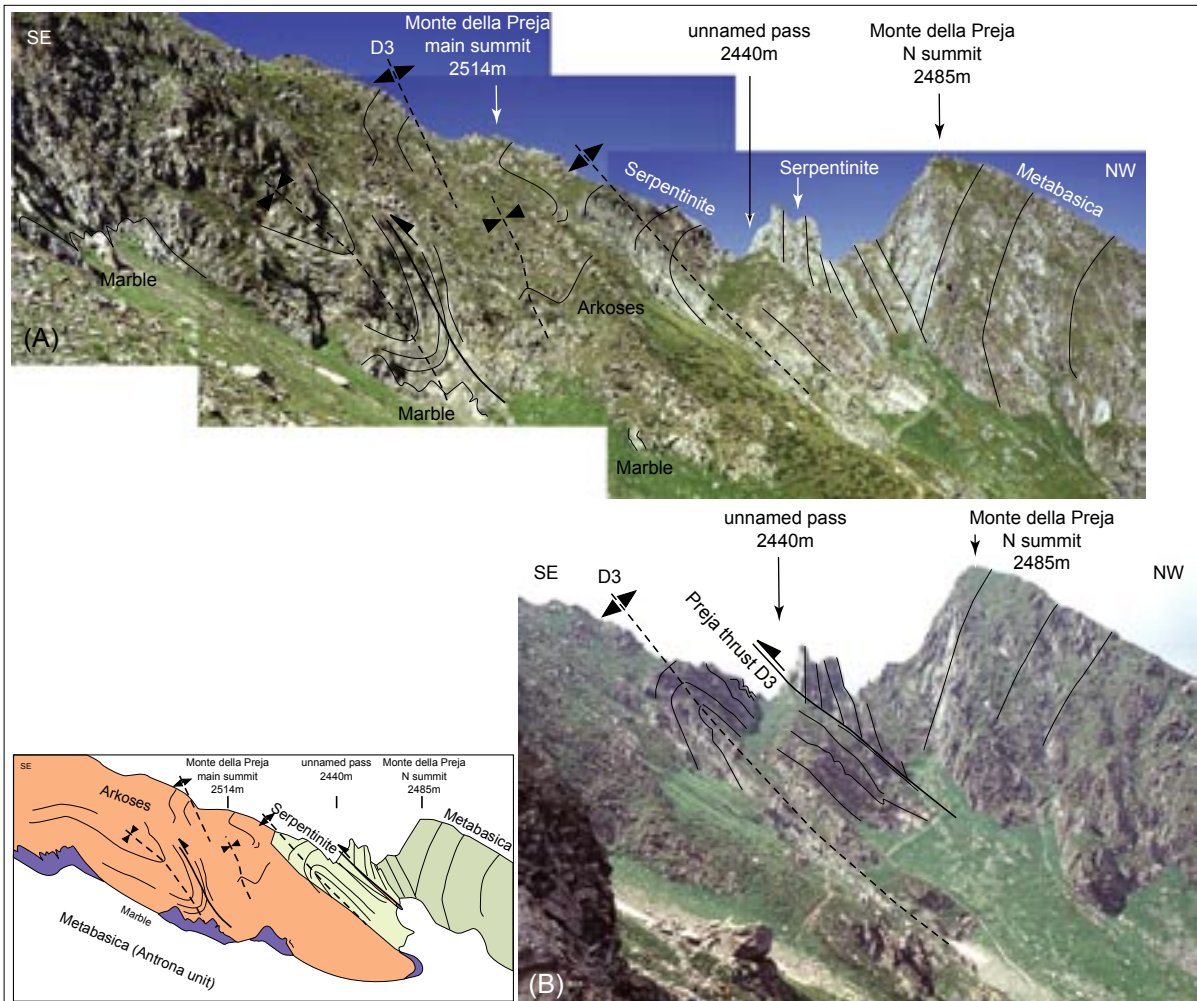


Fig. 4.2.35: View of Monte della Preja NE face and the small unnamed pass (2440 m) between its main and north summit.

Picture B is a detail as seen from a slightly different perspective from the "Monte Pasquale". The insert shows the lithologies and interpretation. Arkoses: Meta-arkoses and minor quartzites with basaltic boudins in the Furgg zone; Marbles, Metabasica, and Serpentinites: Antrona unit. Several D3 folds re-fold the composite main foliation (s1/s2). The fold axial planes dip moderately to the north (in average 352/55). The fold axes plunge moderately to the NW (320/45). The folds are parasites in the hinge of the large-scale D3 Gabbio synform (see Enclosure 2). Additionally, several shear zones can be recognised. On the left-hand side of picture A, the foliation is sigmoidally dragged along a shear zone. Associated stretching lineations plunge moderately to the NW (330/44), suggesting a syn-D3 top to the SE displacement direction. At the unnamed pass, the Preja thrust marks the contact of serpentinites and meta-arkoses (hidden in the picture). The thrust plane is parallel to the foliation of the meta-arkoses left of the pass and dips steeply to the NW (323/65). On the right side of the pass, the foliation of the serpentinites is nearly vertical (185/71, 350/85). A sense of shear could not be inferred. However, as the shear zone cross-cuts the main foliation of the serpentinites, a syn-D3 development and therefore a top to the SE movement is likely.

D1 & D2 structures

The **D2 "Preja SE summit synform"** and the **D2 Pasquale synform** (Fig. 4.2.37) are exposed at the SE summit of Monte della Preja and "Monte Pasquale", respectively. Their fold axial planes dip steeply to the NW (on average 310/65). The two folds exhibit opposite facing directions (see insert Fig. 4.2.38). This indicates that the Antrona rocks represent the core of a D1 fold that has been refolded by D2. The fold axial plane of the D2 Preja SE summit synform is situated in a structurally higher position in respect to the axial plane of the Pasquale synform. The D2 fold axial planes are refolded by the D3 Gabbio synform (Fig. 4.2.38; cf. chapter 4.2.3).

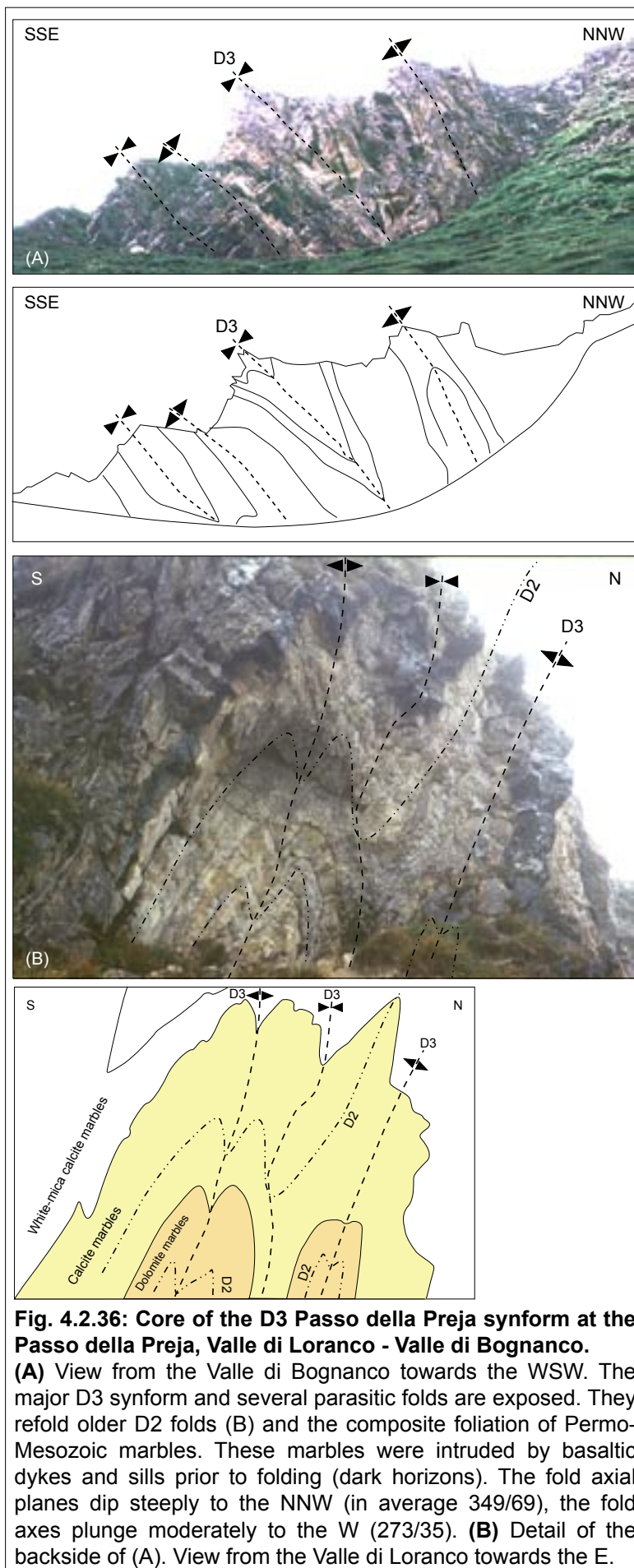


Fig. 4.2.36: Core of the D3 Passo della Preja synform at the Passo della Preja, Valle di Loranco - Valle di Bognanco.

(A) View from the Valle di Bognanco towards the WSW. The major D3 synform and several parasitic folds are exposed. They refold older D2 folds (B) and the composite foliation of Permo-Mesozoic marbles. These marbles were intruded by basaltic dykes and sills prior to folding (dark horizons). The fold axial planes dip steeply to the NNW (in average 349/69), the fold axes plunge moderately to the W (273/35). **(B)** Detail of the backside of (A). View from the Valle di Loranco towards the E.

The insert in Fig. 4.2.38 is a simplified three-dimensional sketch of the Monte della Preja region. Exposed at the Monte della Preja are the structures SE of the D3 fold axial plane. The band of serpentinite exhibited NW of the D3 fold axial plane ("serpentinite at Monte Forcolaccia") illustrates, that the slices of serpentinites found in the Furgg zone (cf. Steck et al., 1997; Keller, 2000) might be derived from detached isoclinal pre-D3 folds.

The **D1 Loranco antiform** ("Loranco- Lappen" of Beath, 1957 a+b) consists of amphibolites, serpentinites and marbles of the Antrona unit, that can continuously be traced from the Valle di Bognanco into the Portjengrat E face in Valle di Loranco, where serpentinites and amphibolites wedge out. The associated marbles, however, can be traced farther to the WSW into the Furggtal. There the amphibolites and serpentinites appear again in a D1 antiformal core (cf. cross-section 643 and Fig. 4.4.2). At the Portjengrat E face, the marbles are refolded by a D2 synform and a D2 antiform (Keller, 2000, p. 60, his folds 4 & 5). The Loranco antiform has a width of up to 300 m and an amplitude of at least 8 km.

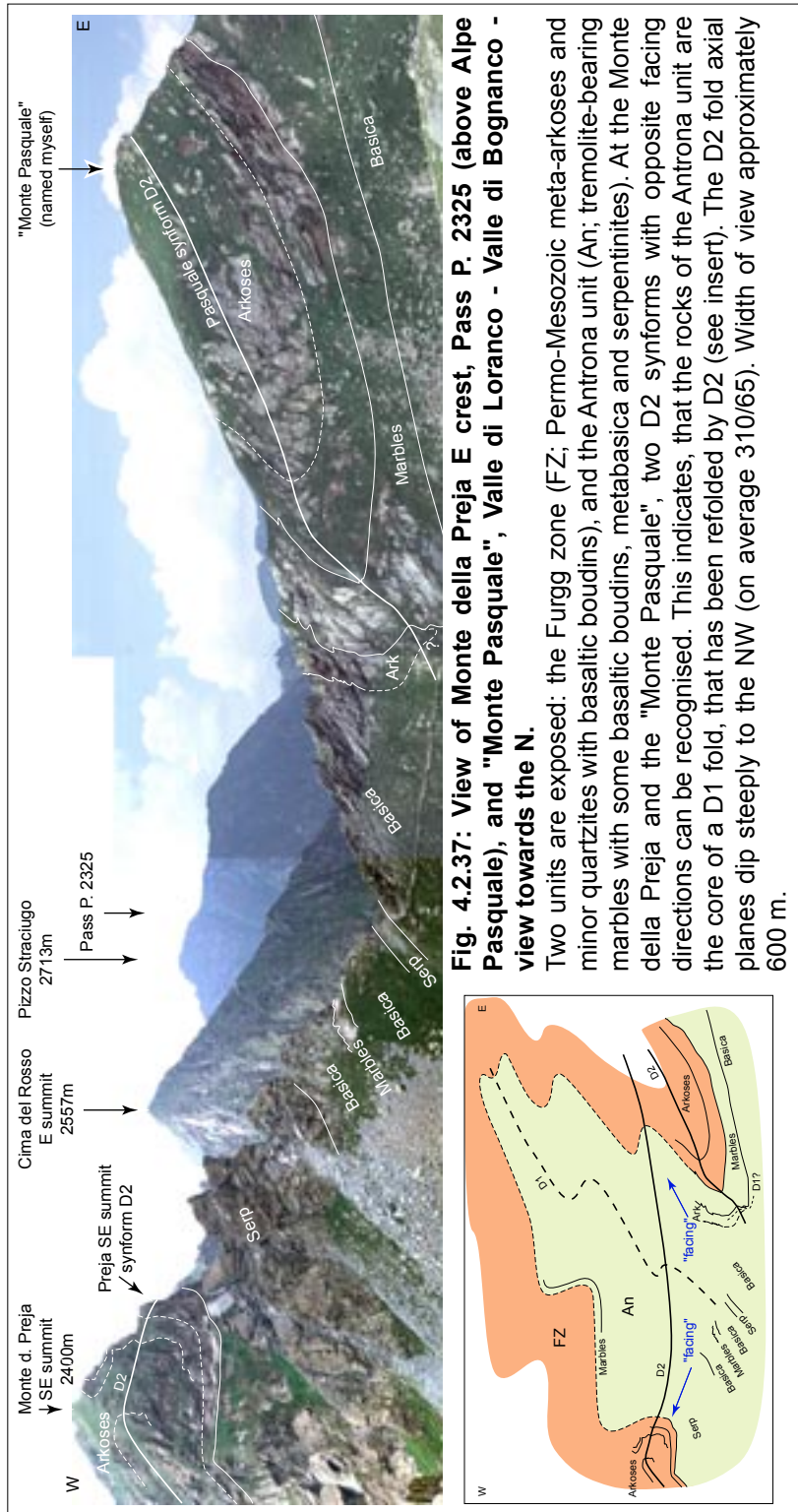
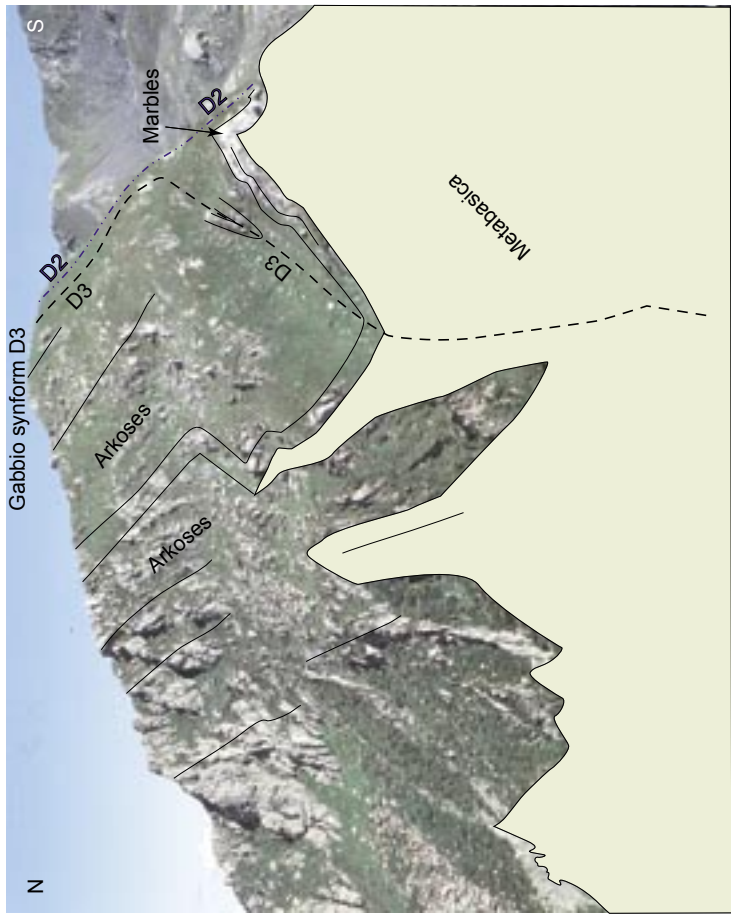
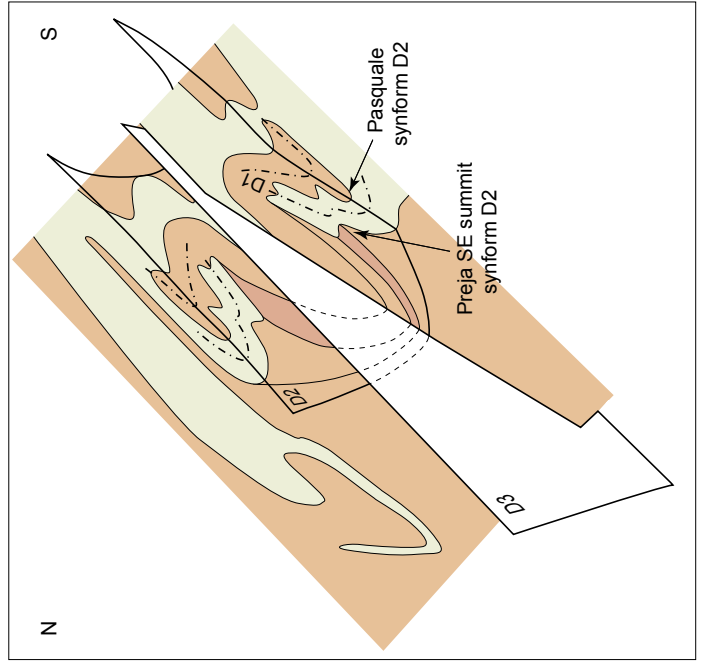


Fig. 4.2.37: View of Monte della Preja E crest, Pass P. 2325 (above Alpe Pasquale), and "Monte Pasquale", Valle di Loranco - Valle di Bognanco - view towards the N.

Two units are exposed: the Furgg zone (FZ; Permo-Mesozoic meta-arkoses and minor quartzites with basaltic boudins), and the Antrona unit (An; tremolite-bearing marbles with some basaltic boudins, metabasica and serpentinites). At the Monte della Preja and the "Monte Pasquale", two D2 synforms with opposite facing directions can be recognised. This indicates, that the rocks of the Antrona unit are the core of a D1 fold, that has been refolded by D2 (see insert). The D2 fold axial planes dip steeply to the NW (on average 310/65). Width of view approximately 600 m.

Fig. 4.2.38: Third dimension of the "Monte Pasquale" - view towards the E from Monte della Preja.

The foliation north of the summit dips to the SSE, whereas south of the summit, it dips to the NW (see Fig. 4.2.37). This indicates the superposition of D3 (Gabbio synform) on the D2 Pasquale synform. The insert shows a three-dimensional sketch of the deformation phases in the Monte della Preja region. See text for discussion.



4.3 Major shear zones

4.3.1 D1/ D2 Furgg zone (FZ) and intensely strained Monte Rosa cover and basement (ISMR)

Lithological composition

Both FZ and ISMR are defined by two superposed phases of synmylonitic isoclinal folding (D1 and D2; see ch. 2.3.4) which deform the contact between crystalline basement and sedimentary cover. The lithological association affected by this intense straining and folding was already complex prior to nappe stacking. The two earliest Alpine deformation phases, however, added complex interference patterns of folds and thrusts within the present rock association. Obviously, the FZ and ISMR did not escape successive overprint by D3- and D4-folding and straining. However, it is emphasized, that FZ and ISMR are primarily defined as D1-/ D2 shear zones in this study. For reasons of terminological clarity, D3-straining and folding is ascribed to the overprint by the syn-D3 "Gornergrat-Furggtal shear zone" (ch. 4.3.2).

The Monte Rosa nappe and the Stockhorn-Portjengrat unit comprise pre-Alpine paragneisses and calc silicate rocks that contain abundant meta-basaltic layers and boudins (ch. 2.3.2, 2.3.3, and 3.2; see also Fig. 4.3.1 D). These Palaeozoic rocks represent the erosional basis onto which the Permo-Mesozoic sediments were deposited. The Permo-Carboniferous granitic intrusions of the Monte Rosa nappe only locally form the depositional basis of the sediments. For this reason, straining and folding of the basement-cover contact of the Monte Rosa nappe usually affected a complex pre-Alpine paragneiss rock association, including some aplitic dykes associated with the Permo-Carboniferous granite intrusion, and a thin Permo-Mesozoic sedimentary cover. Supposedly in Jurassic times, mafic dykes and sills associated with oceanic spreading of the Piemont-Ligurian and/ or Valaisian oceans (ch. 3.2), intruded cover and basement of the Monte Rosa nappe, as well as the Stockhorn-Portjengrat unit (Fig. 4.3.1 A, B, C; see ch. 3.2). Their imbrication, folding and boudinage during subsequent Alpine straining led to the characteristic appearance of the affected parts of the involved continental tectonic units in the Furgg zone (Figs. 4.3.2 a & b) and the adjacent intensely strained Monte Rosa basement and cover (Fig. 4.3.2 f).

As D1- and D2- straining and folding also affects the ophiolitic tectonic units adjacent to the Monte Rosa nappe and the Stockhorn-Portjengrat unit, serpentinitic ophiolitic slivers are also interbedded within the FZ and ISMR (see below). However, these slivers were separately mapped out as meta-ultrabasica.

Occurrences of serpentinites

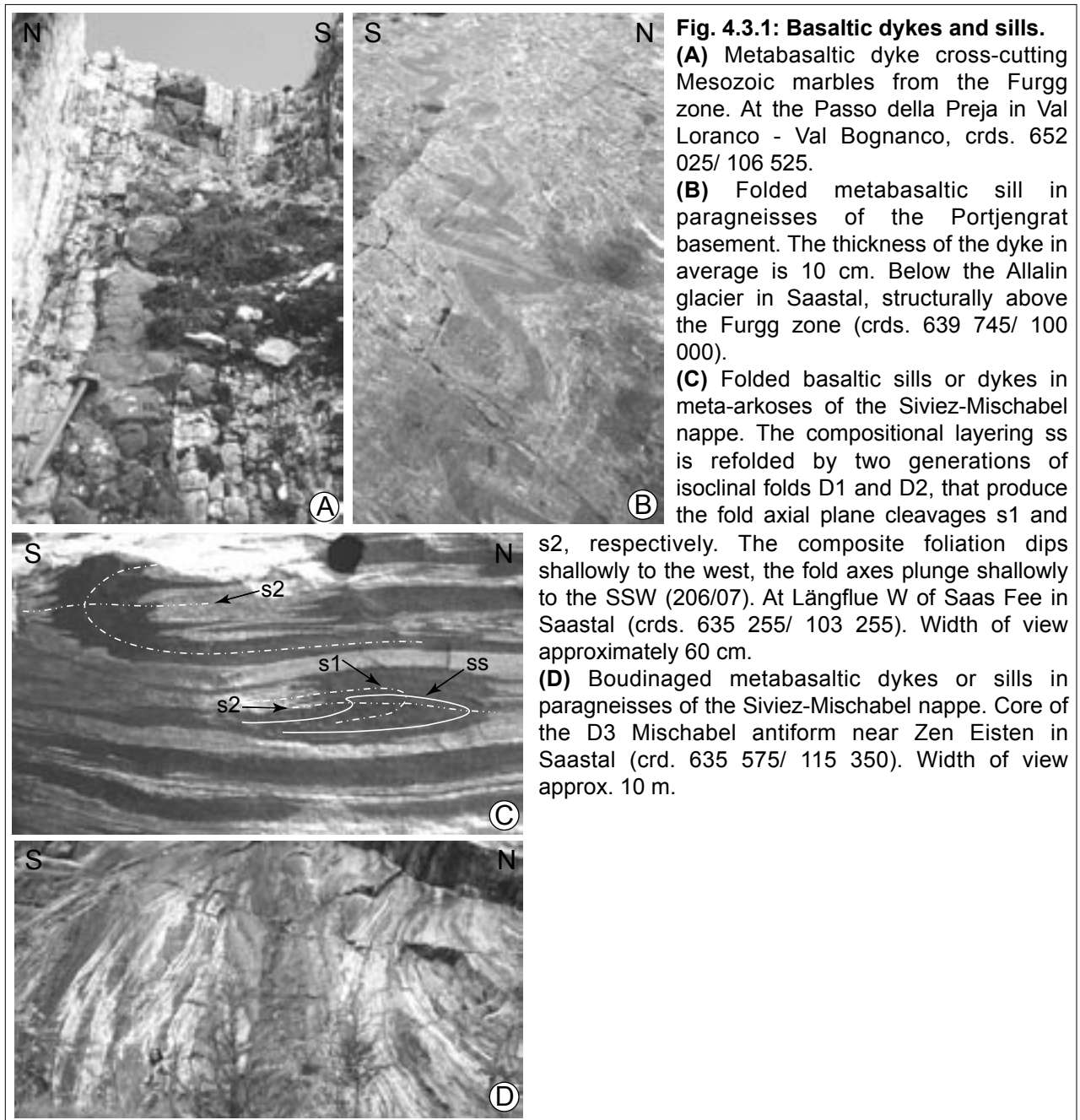
Two larger slices of serpentinites of 1.5 km in length, and numerous smaller occurrences between them, can be found in the Furgg zone at the Gornergrat in Matteredal, south of the Stockhorn. These serpentinites are considered to be derived from the Zermatt-Saas unit. The northern and structurally higher serpentinitic slice is exposed near P. 3223 and defines the contact between the Stockhorn unit and the Furgg zone (Enclosure 1). The structurally lower serpentinitic slice is exposed at the Stockchnubel and represents the core of the D3 Stockchnubel synform (see ch. 4.2.2) and it is therefore supposedly connected to the main body of the Zermatt-Saas unit.

In Valle d'Ayas and Valle di Gressoney, thin slices of serpentinites embedded in the intensely strained Monte Rosa cover and basement are exposed at the Corno del Camoscio and at the Alpe Salza (see ch. 4.2.1). These serpentinites are also considered to be derived of the Zermatt-Saas unit.

In Valle di Loranco and Furggtal, serpentinites, amphibolites and marbles of the Antrona unit form the isoclinal D1 Loranco antiform (for details see ch. 4.2.5). The antiform is also subjected to intense D3 overprint by the Gornergrat-Furggtal shear zone (see ch. 4.3.2). Additional thin slices of serpentinites within the Furgg zone are exposed at the Monte Forcolaccia, west of lake Bacino Alpe dei Cavalli. There, they define the contact between intensely strained Monte Rosa basement and cover and the Monte Rosa paragneisses (Keller, 2000; Steck et al., 1999).

In Valle d' Antrona, from Lago di Antrona towards the north (towards Alpe Ronco), numerous slices of serpentinites are exposed in the intensely strained Monte Rosa basement and cover. As this high

strain zone is situated adjacent to the Antrona unit, the serpentinites are considered as derived from the Antrona unit.



Meso-scale structures of FZ and ISMR

The glacier-polished outcrops below the Allalin glacier in Saastal and at Gornergrat in Mattertal offer the opportunity to study the meso-scale structural evolution of the Furgg zone in more detail. This structural evolution will be discussed with the aid of Fig. 4.3.2. Table 4.1 summarizes the structures observed.

D0

The first deformation phase recorded corresponds to a first boudinage event (D0), during which the more competent mafic layers, which are situated in a matrix of less competent quartz- and carbonate-rich rocks, were imbricated. The mineral assemblage in the boudin necks is albitic plagioclase, +/- chlorite, +/- zoisite, +/- actinolite and +/- Fe- carbonate (Fig. 4.3.2 c, d,

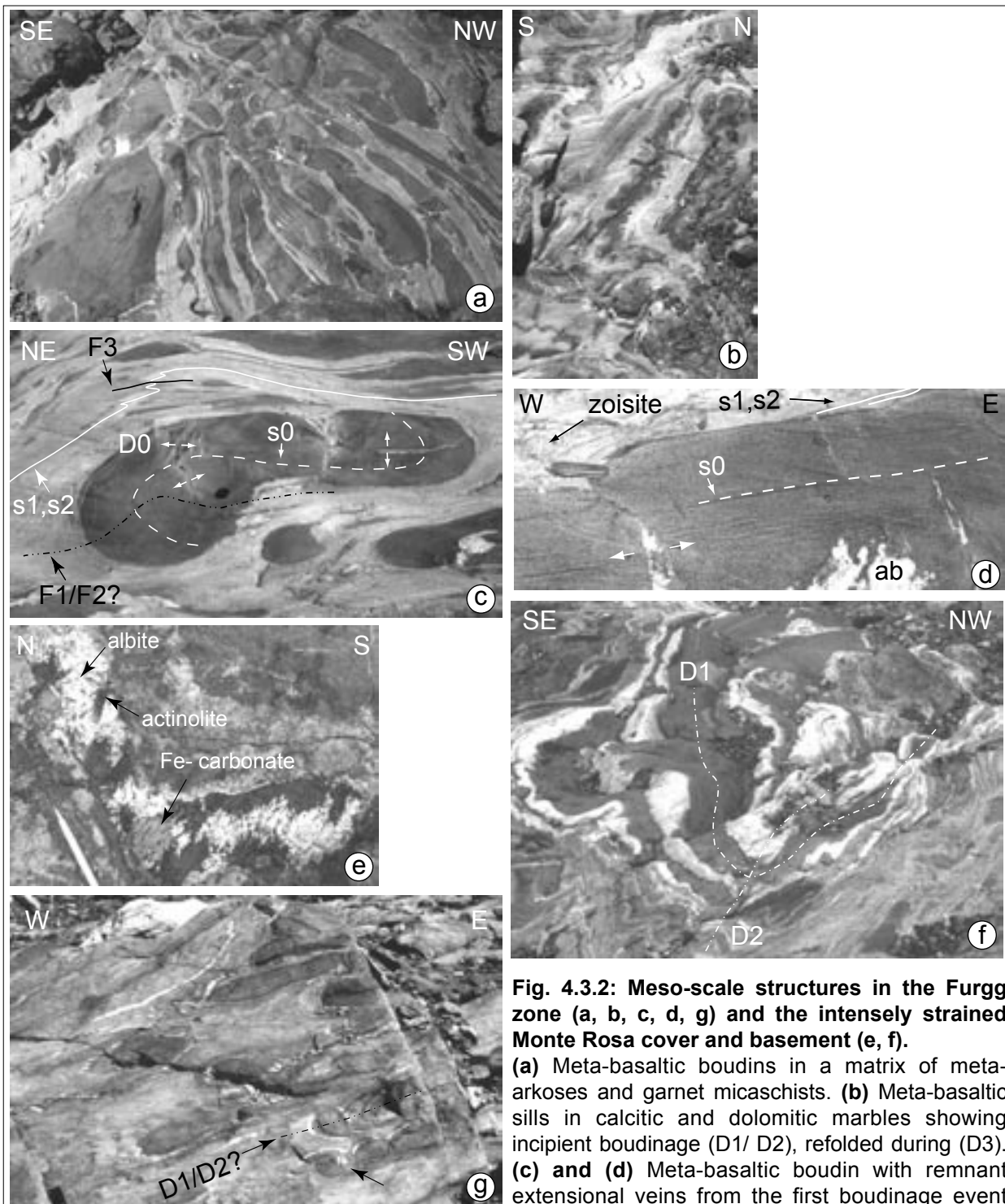


Fig. 4.3.2: Meso-scale structures in the Furgg zone (a, b, c, d, g) and the intensely strained Monte Rosa cover and basement (e, f).

(a) Meta-basaltic boudins in a matrix of meta-arkoses and garnet micaschists. (b) Meta-basaltic sills in calcitic and dolomitic marbles showing incipient boudinage (D1/ D2), refolded during (D3). (c) and (d) Meta-basaltic boudin with remnant extensional veins from the first boudinage event D0. The veins are filled with albitic plagioclase, zoisite and chlorite. The foliation inside the boudin (s0) is considered to be associated to the boudinage, as it formed parallel to the opening direction of the cracks. In (c), the folding of the boudin is considered to be associated to D1 or D2, as the vergence of younger parasitic D3 folds (e.g. in the upper left of the figure) does not change when passing across the D1/ D2 fold axial plane. (e) Greenschist facies mineral assemblage (albitic plagioclase, actinolitic hornblende, Fe- carbonate) in a vein boudinaging a meta-basaltic sill. (f) Superposition of two phases of folding (D1 and D2) in meta-arkoses (white), meta-basaltic sills (dark) and garnet micaschists (gray). (g) Boudinage of D1 or D2 fold hinges during a second boudinage event. Meta-basaltic sills in a matrix of garnet micaschists. For discussion see text.

Locations: (a), (c), (d): Below Allalin glacier in Saastal, crds. 639 825/100 225. (b) At eastern termination of Gornergrat/ Mattertal, crds. 631 375/ 092 350. (e) At Plateau del Lys in Valle di Gressoney, crds. 629 750/ 081 850. (f) Near Mezzalama refuge in Valle d' Ayas, crds. 624 700/ 084 675. (g) Below Stockchnubel at Gornergrat/ Mattertal, crds. 630 430/ 092 025.

e), suggesting greenschist facies conditions during the final stages of boudinage. However, the mineral assemblage within the mafic boudins evidences higher metamorphic conditions during their boudinage. Microscopic symplectites of albite and actinolite (Fig. 4.1.3) supposedly represent the greenschist facies reaction products of omphacite. The alternation of these coarse- and fine-grained symplectites (Fig. 4.1.3 B) defines a first foliation s_0 (represented by a light- and dark-colored layering in Fig. 4.3.2 d), which formed synkinematically with the boudinage, as it is oriented parallel to the opening direction of the extensional veins. The mineral assemblage of the boudinaged mafic rocks therefore supposedly was in disequilibrium with the prevailing metamorphic conditions indicated by the mineral assemblage in the boudin necks, thereby causing the competence contrast necessary for a boudinage of the mafic rocks.

D1 & D2

The mylonitic foliations s_1 and s_2 define axial plane cleavages of the two superposed phases of isoclinal folding F1 & F2 (Figs. 4.3.2 c & f). As a result of the isoclinal nature of folding, the observed main foliation is a combination of pre-D1, s_1 and s_2 (see also chapter 4.2.1 and 4.1.2). A second boudinage event took place during D1 and/ or D2 (Fig. 4.3.2 g) and it is responsible for the boudinage of pre-existing F1- or F2- fold hinges. Since both D1 and D2 folds are isoclinal, they can only be distinguished where they clearly overprint each other.

Large-scale structures of the Furgg zone

The Furgg zone, which extends from the Gornergrat in Mattertal to the Valle di Bognanco, is not continuous, but interrupted at the Schwarzberg-Weisstor (see Enclosures 1 + 2). It is not clear, if this interruption is an effect of D2 and D3 folding (see discussion below) or if the Furgg zone was cut off by the Saas shear zone (ch. 4.3.3). This open question will be discussed below.

At the eastern Gornergrat in Mattertal, the Furgg zone (FZ) forms the synformal core of the D3 Stockchnubel synform (see cross-section 628 on Enclosure 3, and ch. 4.2.2). As the FZ disappears below the Gorner glacier, it cannot be traced farther to the E to the Schwarzberg-Weisstor (see Enclosures 1 + 2). Further along strike, the FZ appears to be exposed in two branches found below the Allalin glacier in Saastal (see Encl. 1 + 2; Bearth, 1954b, 1957; Wetzel, 1972; Rössler, 2000). The upper branch ("FZ" in Fig. 4.3.3) wedges out towards the SW at the Schwarzbergchopf (Rössler, 2000). In this upper branch the Furgg zone is refolded by several D2 antiforms (Fig. 4.3.3). The

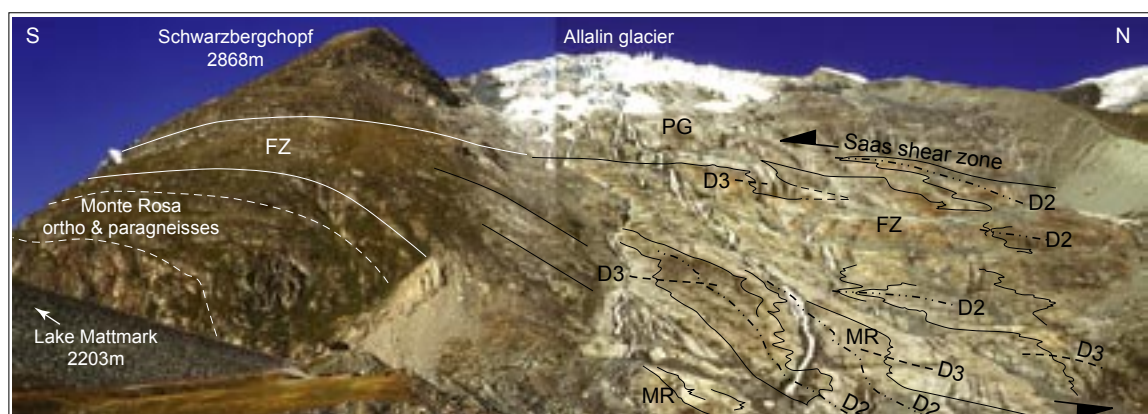


Fig. 4.3.3: Late-D3 Saas shear zone overprinting older structures.

The foliations of the three units - orthogneisses of the Monte Rosa nappe (MR), Furgg zone (FZ), and garnet micaschists of the Portjengrat unit (PG) - are reoriented from a moderate northwest-dip on the right-hand side of the picture (in average 327/30) to a moderate west-dip on the left-hand side (in average 284/32). This apparent flattening towards the Schwarzbergchopf suggests large-scale top to the left shearing associated to SE-directed thrusting along the Saas shear zone.

The contacts of the three tectonic units (MR, FZ and PG) are refolded by two superposed meso-scale fold generations - D2 and D3. The asymmetry of the D3 folds indicates the closure of the D3 Stockhorn antiform structurally above and in the south, and the closure of the D3 Gabbio synform structurally below. For discussion see text. View towards the W onto Schwarzbergchopf and Allalin glacier, at Lake Mattmark in upper Saastal.

termination of the upper branch of Furgg zone at the Schwarzbergchopf might therefore be due to a large-scale D2 antiformal hinge. The termination of the lower branch of the Furgg zone, however, cannot be studied as it disappears below the Schwarzberg glacier. Whether this lower branch of Furgg zone terminates in an antiformal D2 hinge and consequently was never connected with the Furgg zone at the Gornergrat, or whether the Furgg zone in Saastal was continuous with the Furgg zone at Gornergrat prior to its cut-off by the Saas shear zone (see ch. 4.3.3), can therefore not be proven.

4.3.2 D3 Gornergrat-Furggtal shear zone

The SE-directed, dextral transpressive D3 Gornergrat-Furggtal shear zone roughly follows and overprints the D1-/ D2- Furgg zone between the Gornergrat/ M Mattertal and the Valle di Bognanco (see Enclosures 1 & 2 and Fig. 4.4.2).

D3-straining along the Gornergrat-Furggtal shear zone was accommodated in two ways and presumably more or less contemporaneously: by thrusting along numerous discrete thrust planes (see Figs. 4.3.4 & 4.3.5; cf. ch. 4.2.6, "D3 Preja thrust") and by shear folding (e.g. the D3 Stockhorn antiform in Fig. 4.2.10, see also the formation of the Gabbio synform in Keller & Schmid, 2001). Fig. 4.3.6 a & b show an outcrop-scale example for such synkinematic folding. In this example, straining parallel to the fold axial planes was accommodated by the opening of semi-ductile tension gashes. The mullion structures in D3 fold hinges in Fig. 4.3.6 c & d indicate a higher competence of the quartz-rich meta-arkoses compared to the meta-basaltic boudins. This is in contrast to early D1/ D2 structures in the Furgg zone (see ch. 4.3.1 and Fig. 4.3.2). The driving force for this reversal in relative competence is a successive greenschist facies re-equilibration of the mineral assemblage of the meta-basaltic boudins during late D3. It is indicated by the poikiloblastic growth of zoisite at the expense of the albite- actinolite-symplectite (Fig. 4.1.3 B).

At a large scale, the Gornergrat-Furggtal shear zone acted as a SE-directed, dextral transpressive forelimb thrust of the emerging SE-facing Stockhorn antiform. Along this forelimb thrust both the Stockhorn unit, which represents the core of the Stockhorn antiform, and the Portjengrat unit were thrust to the SE over the Monte Rosa nappe (cf. Fig. 4.4.2). During late D3 straining, the Gornergrat-Furggtal shear zone was cut off by the younger Saas shear zone (ch. 4.3.3; see also Fig. 4.4.2 and ch. 5). Thereby, it was rotated from a relatively steep position (55° northward dip at Gornergrat, up to 80° northwestward dip in Furggtal and Valle di Loranco) into a relatively flat-lying position in Saastal (30° westward-dip; cf. 4.4.2 and Enclosures 1 & 2). Fig. 4.3.3 illustrates the overall bending of the lithologies and smaller shear zones associated to the Gornergrat-

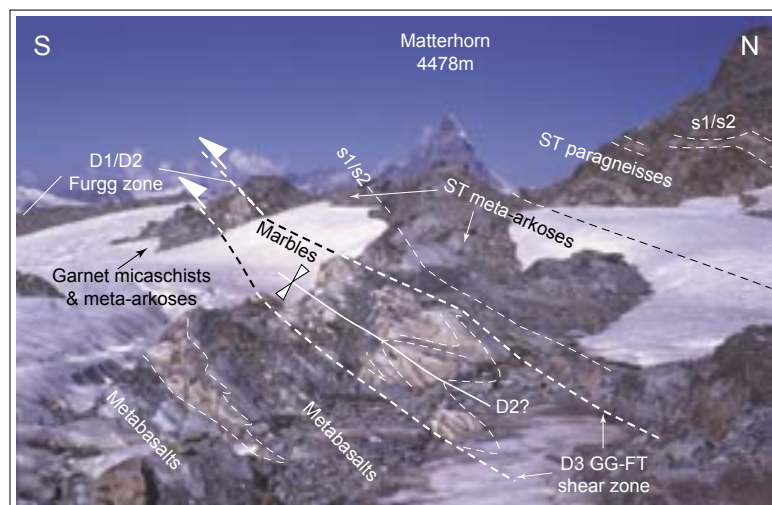


Fig. 4.3.4: D3 Gornergrat-Furggtal shear zone (GG-FT) overprinting older structures.

Several SE-directed D3 thrusts associated to the Gornergrat-Furggtal shear zone overprint the D1/ D2 Furgg zone. The D3 thrusts cross-cut an older, folded contact of marbles and meta-arkoses and of marbles and meta-basalts, respectively. The facing upwards direction of the stratigraphy indicates, that the sedimentary succession rests in a normal position in respect to the Stockhorn basement (ST paragneisses), which is interpreted as the associated basement. Whereas the lithologies in the Furgg zone (marbles, meta-arkoses and garnet micaschists) contain numerous basaltic boudins, the meta-arkoses north of the Furgg zone do not contain any basaltic boudins. Foliations dip moderately to the NNW, and fold axes plunge moderately to the NW (see Enclosure 1). Eastern termination of Gornergrat/ Mattertal (crds. 631 375/ 092 350). View towards the W.

Furggtal shear zone into the direction of shearing.

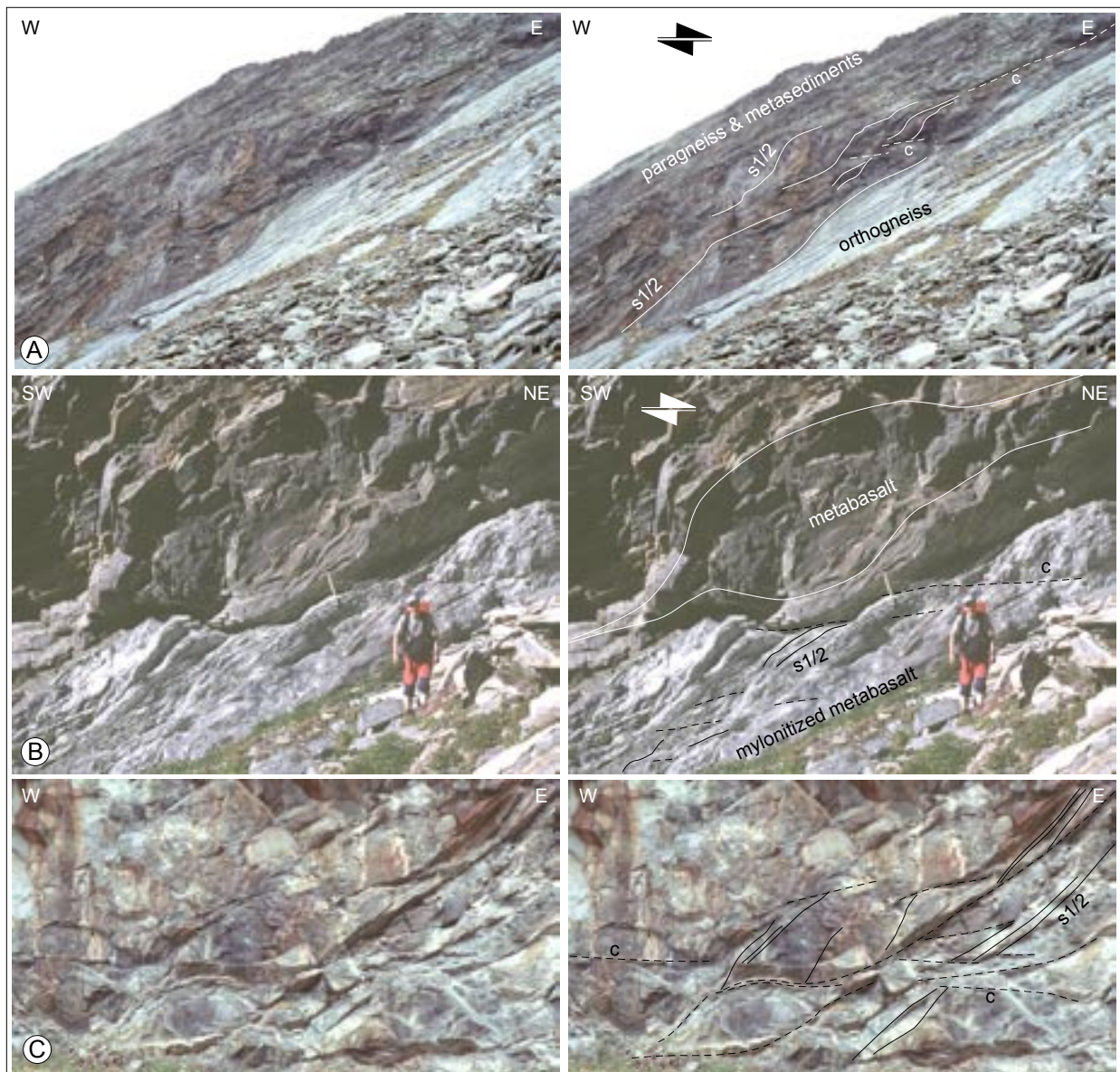


Fig. 4.3.5: Gornergrat-Furggtal shear zone in (A) Saastal, (B) Furggtal, and (C) Valle Antrona.

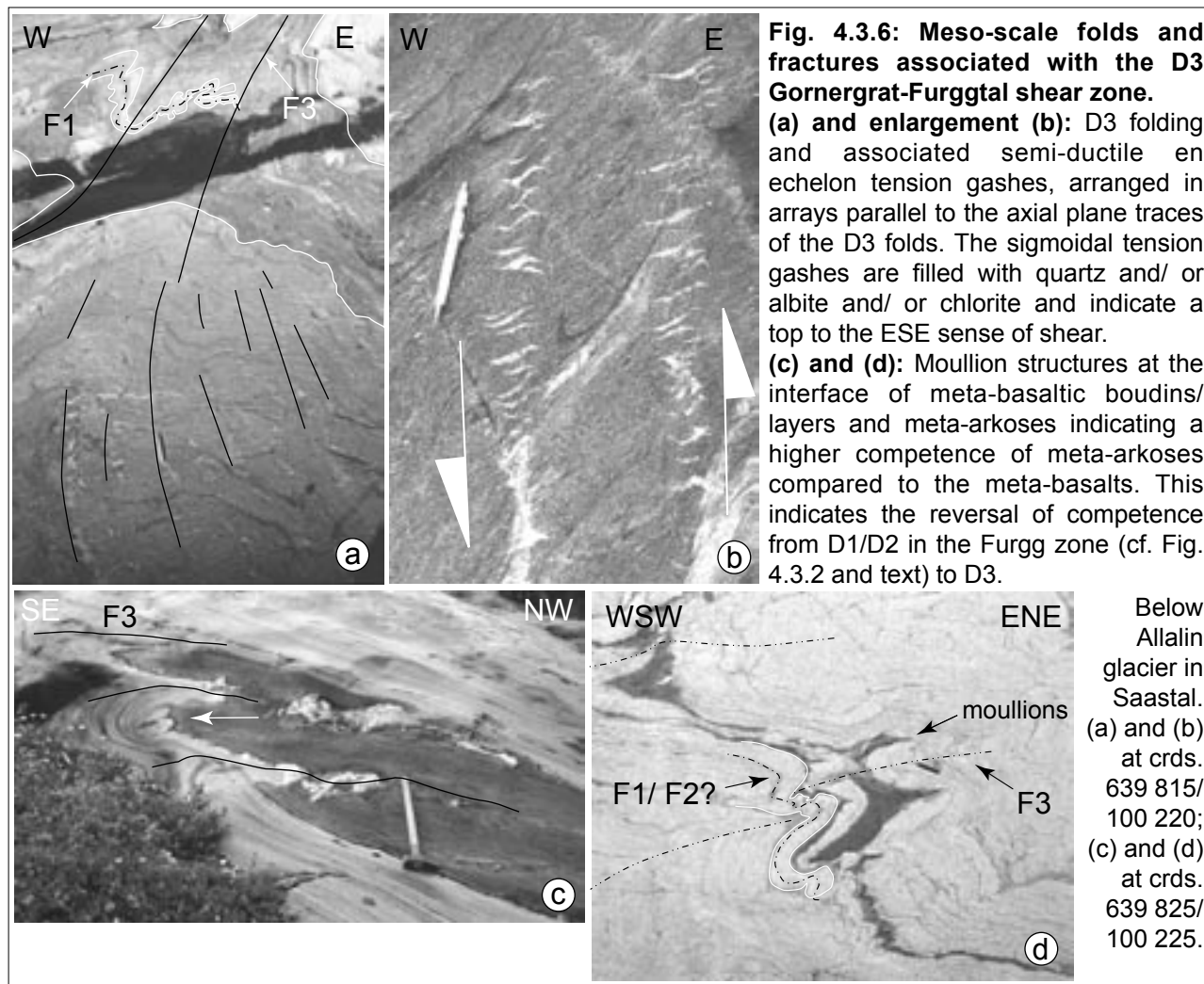
(A) Outcrop-scale shear bands *c* (dashed lines) and syn-D3 reactivated composite main foliation *s*1/2 (solid lines), indicating a top to the E sense of shear. At the contact of Monte Rosa orthogneisses (bottom) and Furggtal zone (on top), N of Nollenhorn at the W-side of Saastal (crds. 642 000/ 100 510).

(B) Outcrop-scale σ -clast in weaker deformed metabasalts of the Antrona unit situated on top of a zone of mylonitized metabasalts. Within the latter, shear bands *c* (dashed lines) have evolved, indicating a top to the E sense of shear. The metabasalts represent the core of the D1/D2 Loranco fold (cf. ch. 4.2.5 & 4.2.6). At the base of Mount Cimone di Camposecco (3398m) at the NE-side of Furggtal (crds. 645 125/ 101 925).

(C) Shear bands *c* (dashed lines) crosscutting the main foliation in metabasalts of the Antrona unit. At the northern termination of Lake Bacino Alpe dei Cavalli (crds. 652 200/ 104 300).

4.3.3 D3 Saas shear zone

The SE-directed dextral transpressive D3 Saas shear zone is exposed on the W-side of Saastal (cf. Enclosure 2, cross-section 638 on Enclosure 4, and Fig. 4.4.2). It moderately dips to the W (around 30°) and is up to approximately 500 m thick. The Saas shear zone overprints the interface of Permo-Mesozoic sediments and basement of the Portjengrat unit from Schwarzberg-Weisstor to Schwarzbergchopf, and from the Mittaghorn to the Hannigalp N of Saas Fee.



Between Schwarzbergchopf and Mittaghorn, the Saas shear zone passes into and overprints the augengneisses of the Portjengrat unit.

The Saas shear zone accommodates straining along numerous smaller shear zones of up to 5 m in thickness (Fig. 4.3.7). It was active under semi-ductile conditions, which is indicated e.g. by the kakiritic overprint of the Permo-Mesozoic quartzites of the Portjengrat unit (Fig. 4.3.7). As such, the Saas shear zone - along with the Mischabel thrust described below - is the youngest major D3 shear zone of the region investigated.

In the hanging wall of the Saas shear zone, the Stockhorn and Zermatt-Saas units are thrust further to the SE over the Monte Rosa nappe and the Portjengrat unit, respectively (see Fig. 4.4.2). Large-scale evidence for this is found below the Allalin glacier (Fig. 4.3.3), where an apparent flattening of the foliations is seen. This reflects a change from a NW-dip at Lake Mattmark towards a W-dip at the Schwarzbergchopf. The resulting bending of the D2 folds is highly suggestive for large-scale SE-directed thrusting of the Zermatt-Saas unit exposed at the crest.

4.3.4 D3 Trifhorn thrust

The D3 Trifhorn thrust (cross-sections 638 and 642; Figs. 4.2.28 & 4.2.29) is best exposed at the crest between the Steintälli and the Rottälli and in the E face of the Trifhorn (Bearth, 1957; Klein, 1978; Dubach, 1998). From there, it probably follows the southern edge of the calcareous micaschists of the Farwald and Saas Fee (Fig. 4.2.26) just south of the fold axial plane trace of the D3 Trifhorn antiform (see ch. 4.2.4). However, its exact location cannot be mapped. Farther to the S (S of Saas Fee, at the western side of Saastal), the D3 Trifhorn thrust probably runs along the interface of the ortho- and paragneisses of the Portjengrat unit, where it is strongly overprinted by the late-D3 Saas shear zone (see ch. 4.3.3). In Rottälli, the Trifhorn thrust is defined by an up to 20 cm

thick band of quartz mylonites, which developed along the contact of Portjengrat orthogneisses with paragneisses (Dubach, 1998; see also Fig. 4.5.2 E-G). The Trifflhorn thrust is a dextral transpressive forelimb thrust, along which the northern part of the Portjengrat unit overthrust the southern part (cf. cross-section 646 and Fig. 4.4.2). The Trifflhorn thrust steepens from a northward dip of 50-60° as found at the Tällhorn S-crest to a dip of 70-80° as observed at the Zwischbergen pass. Kinematically, this steepening probably initiates a transition from a predominant thrusting to a dextral strike-slip movement. Using the eastern- and structurally lowermost outcrop of metasediments in the Trifflhorn E face as a hangingwall cut-off point, and the western- and structural uppermost outcrop of metasediments below the Weissmies as a footwall cut-off point, a vertical displacement of at least 2 km may be inferred as a minimum displacement value from the composite cross-section (Fig. 4.4.2). As the amount of dextral displacement cannot be inferred, however, the total amount of displacement remains unknown.

Note that the Trifflhorn thrust flattens out on the W-side of Saastal, where it is overprinted by the SE-directed Saas shear zone (ch. 4.3.3) Hence, the total amount of SE-directed thrusting drastically increases across the Saastal, i.e. structurally upwards.

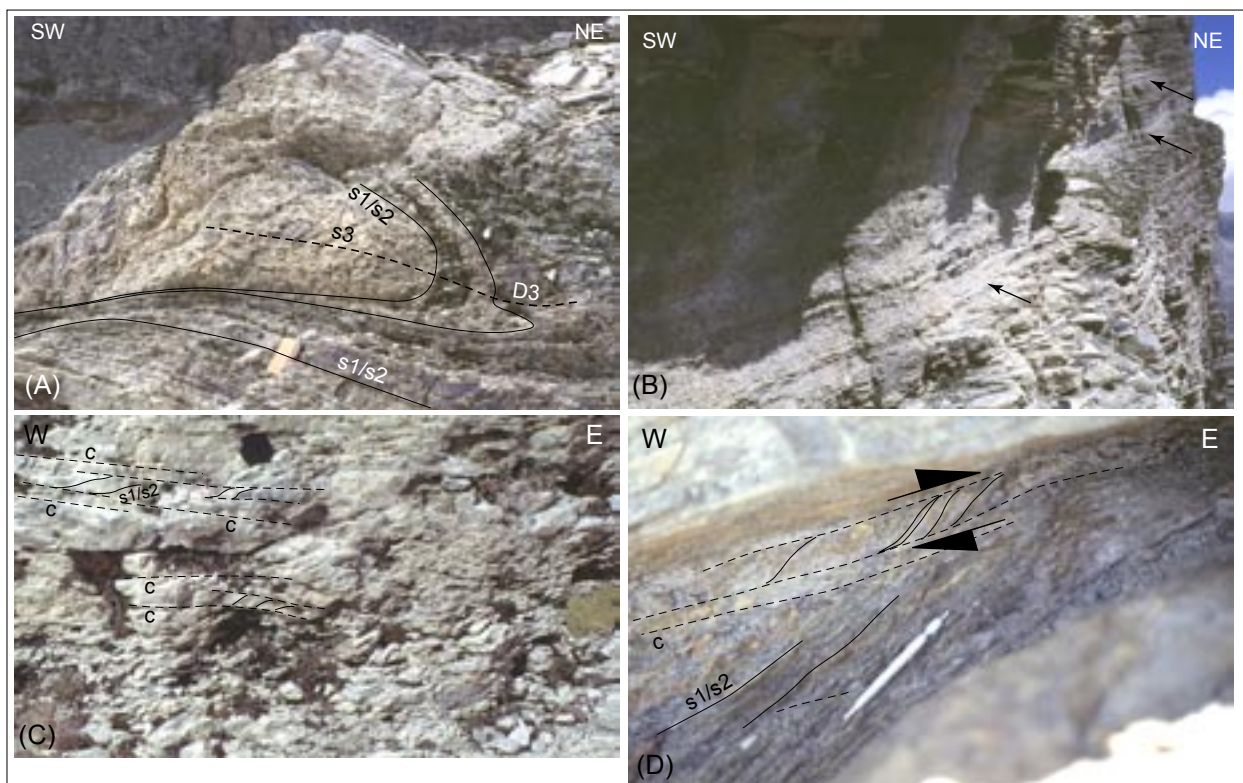


Fig. 4.3.7: D3 Saas shear zone overprinting Mesozoic quartzites and marbles of the Portjengrat unit.

(A) The penetrative cleavage s_3 (s_3 : 319/21) forming the axial plane cleavage of the recumbent D3 fold (fold axis: 322/9) is the result of contemporaneous folding and shearing along the D3 Saas shear zone under semi-ductile conditions. Therefore s_3 corresponds to the shear planes c in (C) and (D). Below the Fluchthorn in Saastal, close to P. 2926 (crds. 637 875/ 096 600).

(B) Strain partitioning led to the development of kakiritic bands of cm- to m-thickness in the quartzites (arrows; height on the left-hand side of (B) approximately 3 m). South of P. 3032, at 2960 m, at the Hangende Gletscher glacier in Saastal (crds. 638 075/ 097 375).

(C) In detail (picture shows original size), the kakiritic bands are characterized by sc -structures which indicate a top to the SE sense of shear (foliation s_1/s_2 : 296/22, shear band c : 000/35, stretching lineation SL: 306/22).

(D) The sc -structures in a white mica-rich layer in marbles, structurally situated right below the quartzites of (B), also indicate a top to the SE sense of shear (foliation s_1/s_2 : 256/10, stretching lineation: 315/05).

4.3.5 D3 Portjengrat shear zone

The E-directed, dextral transpressive D3 Portjengrat shear zone is exposed between Saas Fee in Saastal and the Zwischbergen pass/ Almagellertal - Zwischbergental. It represents a diffuse E-W striking shear zone, that accommodates straining along s_3 -foliation planes. The Portjengrat shear zone typically accounts for the augenmylonitic deformation of the granitoids of the Portjengrat unit (see Fig. 4.5.1 D). Whereas the feldspars of these augengneisses are internally deformed by cataclasis, their rims are partly dynamically recrystallized. This indicates deformation conditions at the ductile- brittle transition of feldspar, at around 500°C (Tullis & Yund, 1977). These findings suggest that the Portjengrat shear zone was active during early D3 times. The Portjengrat shear zone is overprinted by the younger Saas shear zone.

4.3.6 D3 Mischabel thrust

The probably SE-directed, and dextral transpressive D3 Mischabel thrust supposedly runs from Spielboden W of Saas Fee to "Unter dem Berg" N of Saas Grund in Saastal (see Enclosure 2 and Fig. 4.4.2). Along this whole length, however, it is never exposed. W of Saas Grund, the Mischabel thrust is considered to run along the top of the northern belt of calcareous micaschists to the Schwarzries (see Fig. 4.2.26). Its further continuation to the NE lies outside the working area and was not investigated.

The existence of the Mischabel thrust was postulated considering the geometry of the nappe stack as it is illustrated in the cross-sections 636 (in Enclosure 4) and in Fig. 4.4.2. Along the Mischabel thrust, the D3 Mischabel backfold (cf. ch. 4.2.3) must have been thrust towards the SE over the Portjengrat and Zermatt-Saas units. The kinematics will be discussed in detail in chapter 5.

4.4 Composite cross-section

In order to illustrate the connection between the individual cross-sections discussed in chapter 4.2 and 4.3 (see Enclosures 3 and 4), a composite cross-section was constructed along coordinate 638 (Saastal). For this purpose, all other cross-sections were projected into the plane of cross-section 638. The projection values used for this purpose as well as the projection procedure are shown in Fig. 4.4.1 and are listed in Table 4.2.1. This procedure achieves a best fit between the individual profiles. The values used closely correspond to the orientations of the major D3/ D4 fold axes. Due to the non-cylindricity of the structures, projections over larger distances are of course problematic. This is particularly true for all pre-D3 structures, as they die out quickly and laterally transmit their accommodated amount of deformation to adjacent structures. The insert depicted in Fig. 4.2.38 illustrates the complexity of fold superposition. It also demonstrates that a projection of pre-D3 structures over large distances is not likely to reflect the true situation expected at the location of the chosen section plane. Hence, the composite cross-section is only valid and reliable in respect to the major D3 and D4 structures, but not for older structures. Maximum projection distances are 15 km E of, and 11 km W of the section plane 638, respectively. The composite cross-section is presented in Fig. 4.4.2.

In order to illustrate the amount of interpretation, Fig. 4.4.3 depicts the location of the individual cross-sections used on the composite projection plane, as well as the gaps between these sections.

Projection procedure

- 1)** In a first step, the entire cross-section 636 was directly projected into cross-section 638, which coincides with the plane chosen for the composite cross-section.
- 2)** Because the cross-sections at the southern side of the Monte Rosa massif (625, 627, 630, 633) are located in a complicated and non-cylindrical dome-like hinge region of the D4 Vanzone antiform, only one of these cross-sections could be used for projection. For this purpose cross-section 627 was chosen, because it represents the southern continuation of cross-section 628 and is located only 1 km W of cross-section 628. In order to keep distortions small, cross-section 627 was projected into the plane of cross-section 628 in a first step.
- 3)** In this step, the composite 627 & 628 cross-section was projected into the plane of the composite 636 & 638 cross-section. The result of steps 1-3 forms the upper part of the composite cross-section along coordinate 638.
- 4)** Then the cross-sections situated E of the composite section plane were projected. The plunge values (see Fig. 4.4.1) were chosen such as to best fit each individual cross-section to the cross-section situated directly above. The chosen azimuths avoid offsets in the composite cross-section. First, cross-sections 642 and 643 were projected individually. As cross-sections 646 A & B define the total width of the Portjengrat unit, they also determined the distance between cross-section 642 and 643.
- 5)** Then the joint cross-section 646 A & B was projected into the composite section plane, optimizing its fit to the previously projected cross-sections 642 and 643.
- 6)** In a last step, the cross-sections 650 and 653 were projected individually, again optimizing their fit to the composite cross-section. This completes the lower part of the composite cross-section (Fig. 4.4.2).

Discussion

The most striking difference between the resulting composite cross-section (Fig. 4.4.2) and previously constructed cross-sections (Klein, 1978; Milnes et al., 1981; Escher et al., 1988) is the significantly greater distance between the steeply dipping Furgg zone in front of the Monte Rosa nappe in section 643 and the more flat-lying Furgg zone as seen at Gornergrat and represented in section 628. As a result, the offset between the corresponding Stockhorn and Trifflhorn antiform (see ch. 5) along the Saas shear zone is much larger than previously thought. It follows that the importance of the Saas shear zone has been largely underestimated so far. The projection azimuth chosen for the projection of the cross-sections 627 & 628 as defined in step 3) which deviates from the azimuths chosen for all other projections (see Fig. 4.4.1) is largely responsible for this situation. However, it was impossible to use any different azimuth. Any smaller value for the azimuth (e.g. 270° instead of 285°), would result in a dramatic overlap of cross-sections 628 and 638. Using a larger value than 285° for the azimuth (e.g. the azimuth of 312° corresponding to the calculated fold axis of the Stockhorn antiform, instead of the chosen 285°), would result in a large gap between the

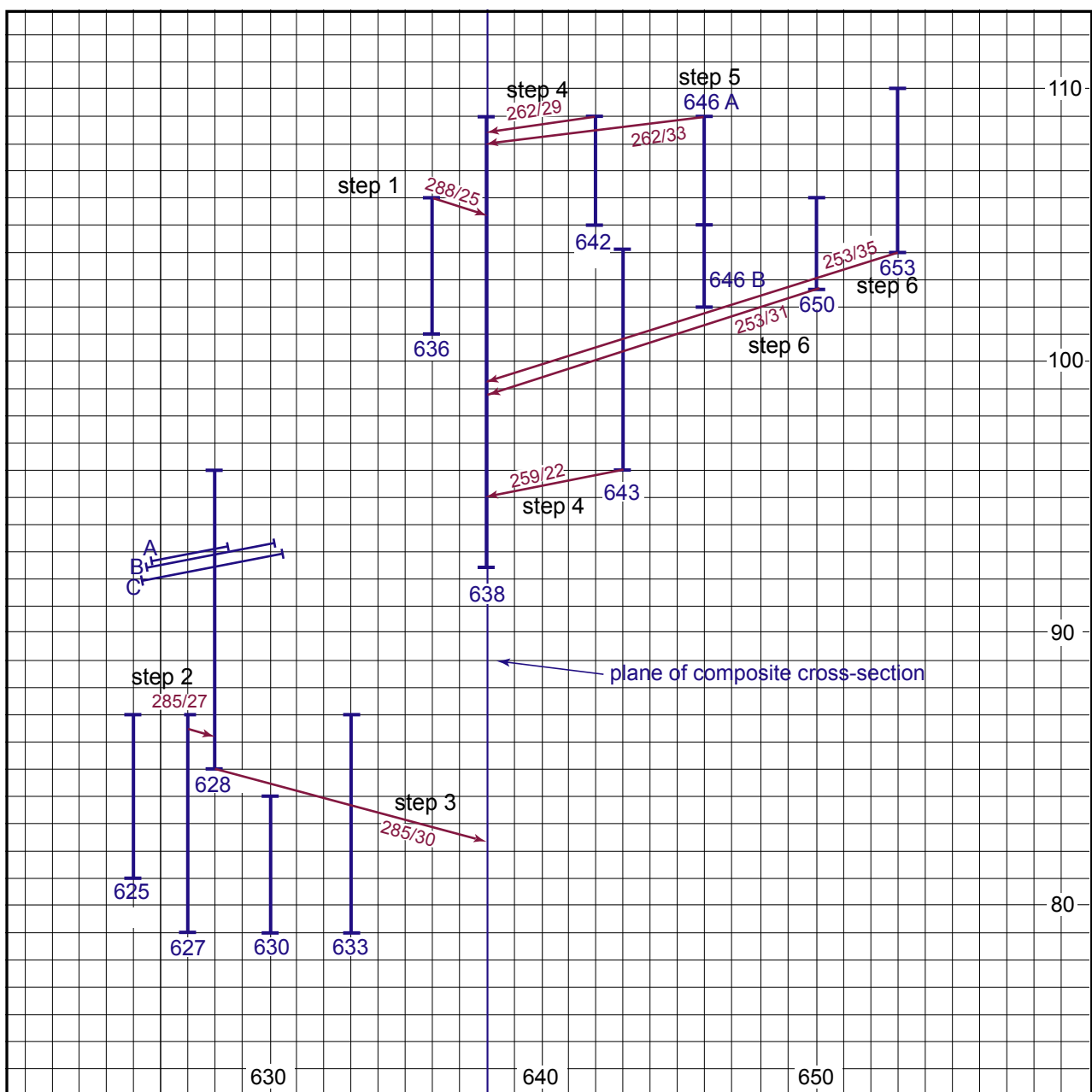


Fig. 4.4.1: Projection values and projection order of individual cross-sections into the composite cross-section plane. The steps indicated correspond to the procedure numbering described in the text.

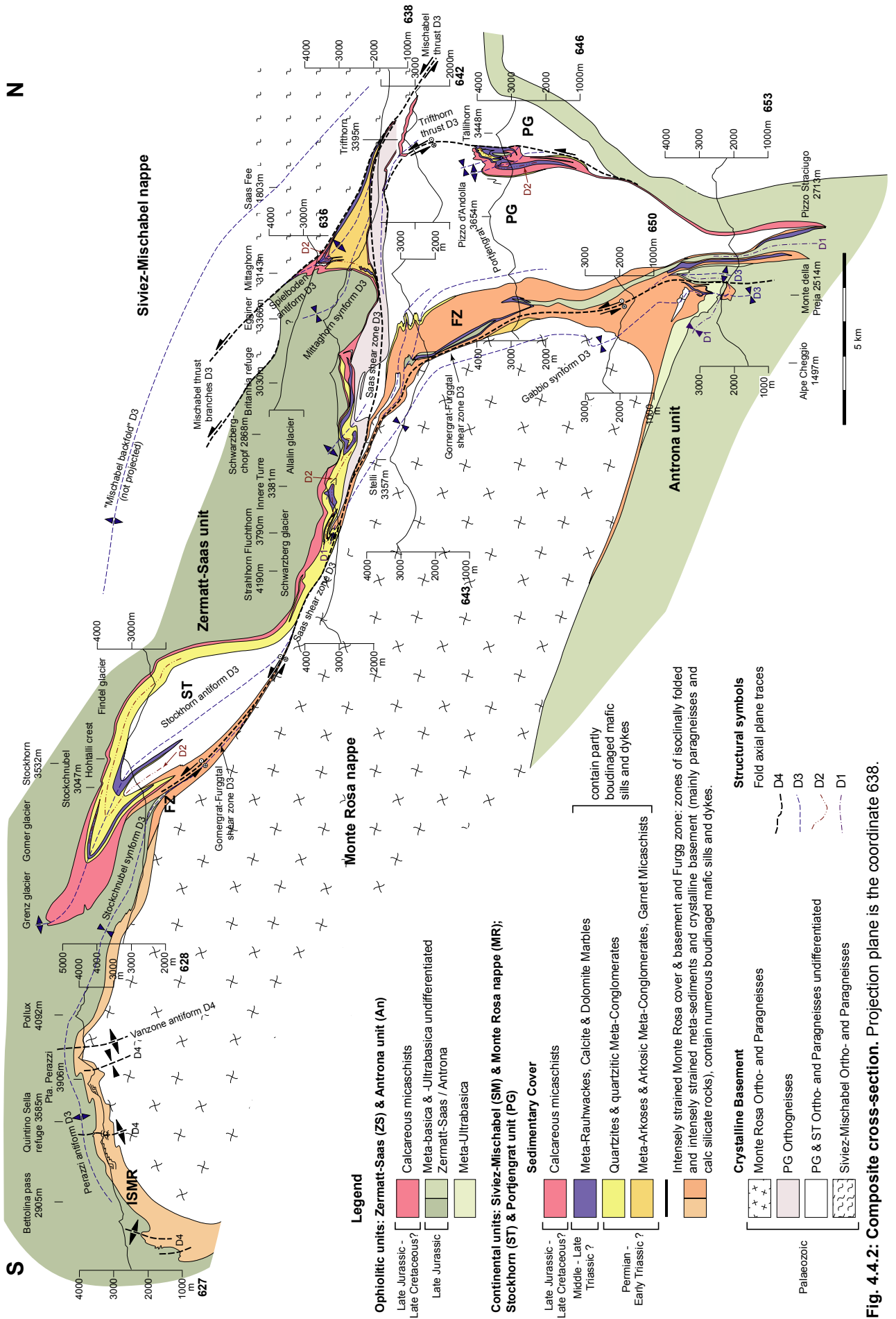


Fig. 4.4.2: Composite cross-section. Projection plane is the coordinate 638.

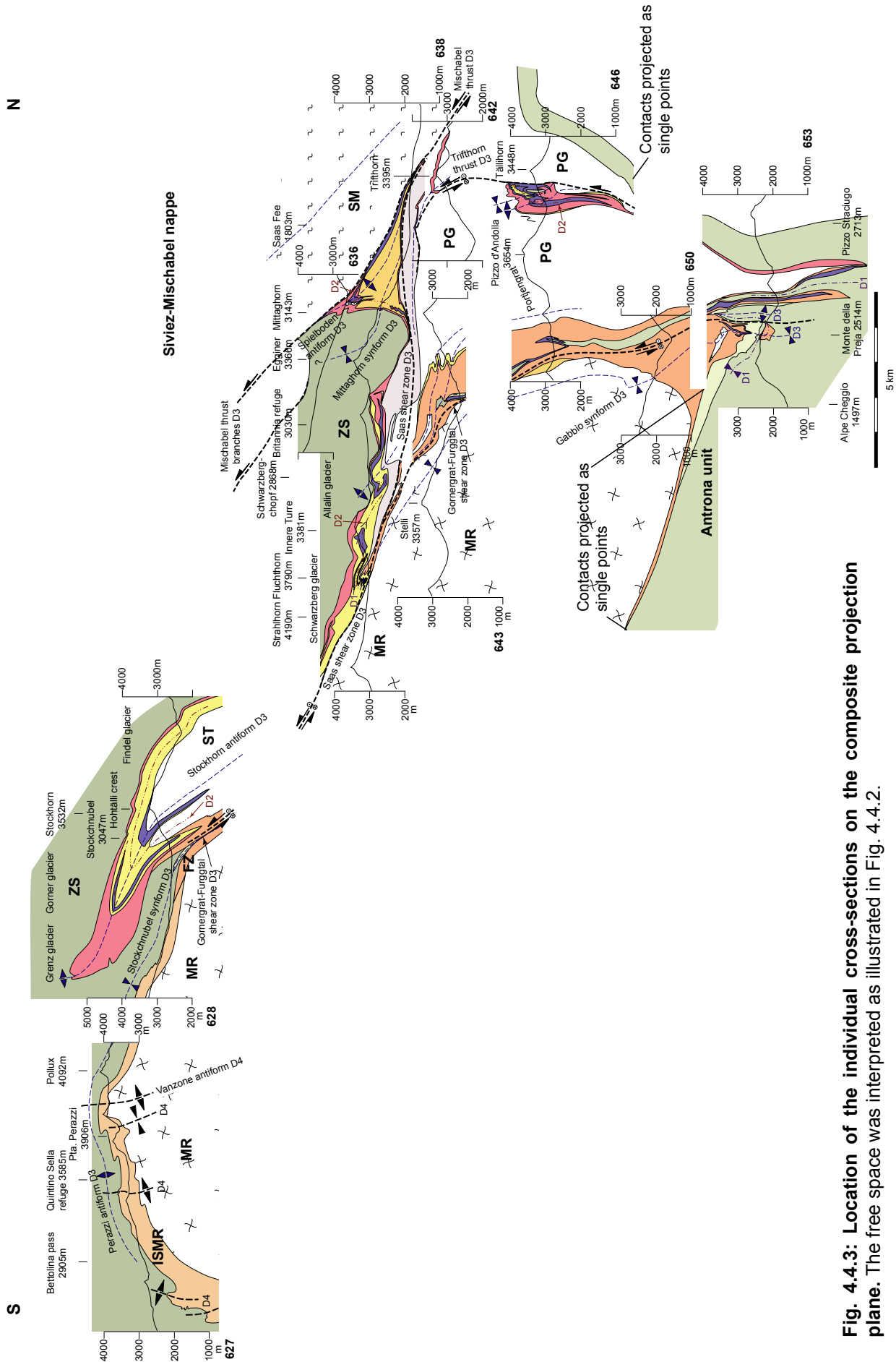


Fig. 4.4.3: Location of the individual cross-sections on the composite projection plane. The free space was interpreted as illustrated in Fig. 4.4.2.

4.5 Kinematic indicators in micro- and outcrop-scale

In order to reconstruct the kinematics of movements, shear senses associated with stretching lineations were determined macro- and microscopically. The kinematic indicators used for the determination of the sense of shear were deflections of markers and foliation, σ - and δ -clasts, mica fish, the shape preferred orientation of stretched or acicular minerals, sc-structures, and shear bands (Figs. 4.5.1 - 4.5.4; see e.g. White et al., 1980; Lister & Williams, 1979; Means, 1995; Passchier & Simpson, 1986). Additionally, the shape and lattice preferred orientation (SPO and LPO) of quartz was investigated (Fig. 4.5.5 and 4.5.6; see e.g. Simpson & Schmid, 1983; Schmid & Casey, 1986; Stipp et al., 2002). The stretching lineations are developed on the composite s0/s1/s2 foliation planes (SL1/2) as well as on newly built s3 foliation planes (SL3). The orientation of the foliation planes and associated stretching lineations is illustrated in two maps and in several lower hemisphere stereographic projections (Figs. 4.5.7 and 4.5.8).

Discussion of data

In general, two major movement directions can be distinguished: top to the NW to SW (blue arrows in Figs. 4.5.7 and 4.5.8), and top to the SE to ENE (orange arrows in Figs. 4.5.7 and 4.5.8). These two movement directions were ascribed to the two major Alpine-age kinematic contractional phases: top to the N- or NW-ward (or similar, see discussion below) nappe stacking (D1 & D2), and top to the SE-ward backthrusting and -folding (D3 & D4). As is illustrated in Figs. 4.5.7 and 4.5.8, D3 shearing affects the entire area investigated, although a strain concentration in several broad D3 shear zones (see chapter 4.3) can be observed. The overprint of D3 straining on older D1/D2 stretching lineations was substantial (see discussion below), but not necessarily destructive for D1/D2 shear sense indicators. Although an incomplete overprint of D3 onto D1/D2 shear senses often resulted in conflicting shear sense indicators (see e.g. Fig. 4.5.4 C), D1/D2 shear senses are still well preserved in many places. They are especially well preserved in the granitic gneisses of the Monte Rosa nappe (Fig. 4.5.1 A), where strain often concentrated in narrow shear zones, that leave the host rock less deformed (see Fig. 4.5.1 B for a D1/2 shear zone and Fig. 4.5.3 B-D for D3 shear zones). Fig. 4.5.1 A shows a feldspar sigma clast within such a D1/2 shear zone, indicating a top to the NW sense of shear. Fig. 4.5.1 B shows a D1/D2 shear zone of tens of centimeters in thickness. From a practically undeformed granite (not shown in the figure) forming the wall-rocks of the shear zone, a gradual fabric transition towards the center of the shear zone can be observed. SC-structures in the coarse grained gneiss are transposed to a mylonitic foliation with some remnant sigmoidally shaped feldspar grains, associated with a drastic grain size reduction.

Fig. 4.5.1 C shows slightly asymmetric garnet-pophyrocysts in paragneisses of the Stockhorn unit, indicating a dextral, top to the NW sense of shear. The retrogression to chlorite along the rims and in the asymmetric pressure shadows of the garnet grains indicates retrograde metamorphic conditions.

Shear bands are the most frequently observed shear sense indicators of both D1/2 (Fig. 4.5.2) and D3 deformation (Fig. 4.5.4). They are well developed in outcrop (Fig. 4.5.2 A-D, Fig. 4.5.4 A & B) and thin section (Fig. 4.5.2 E, Fig. 4.5.4 C-G) alike.

Figs. 4.5.2 A and B exhibit typical granitic augengneisses of the Monte Rosa nappe, where white feldspar sigma clasts and shear bands indicate a dextral, top to the NW sense of shear. However, shear bands are even better developed in the well foliated paragneisses (Stockhorn unit, Fig. 4.5.2 C and Monte Rosa nappe, Fig. 4.5.2 D).

Fig. 4.5.2 E exhibits a photomicrograph of such a D1/2 shear band. It shows the retrogression and recrystallisation of white mica to chlorite along the D1/2 shear band, as well as the grain size reduction of the recrystallized quartz grains in the shear zone.

Figs. 4.5.3 and 4.5.4 exhibit kinematic indicators ascribed to D3. In Fig. 4.5.3 A, single crystals of albite of up to 15 cm in length grew in the neck of a boudinaged basaltic dyke in the Furgg zone. Their deformation indicates synkinematic growth during dextral shearing, which is ascribed

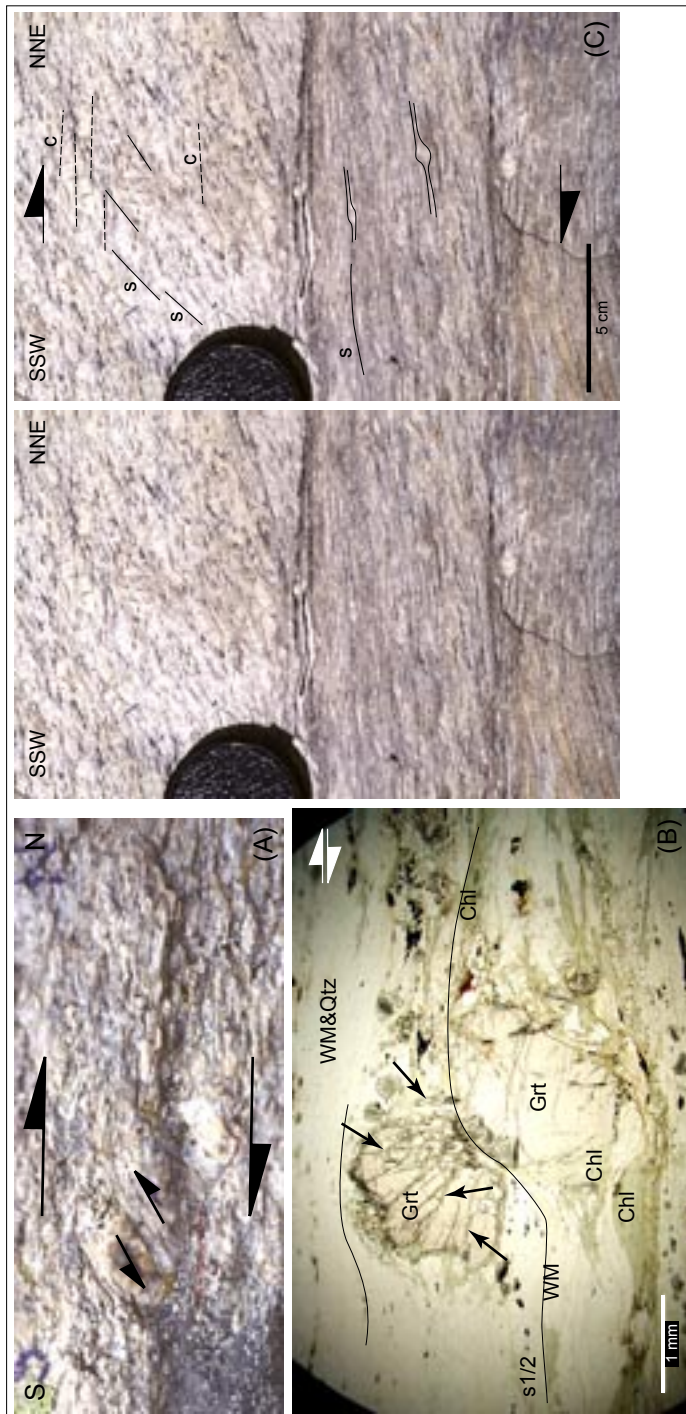


Fig. 4.5: Deformed minerals and deflected foliations as kinematic indicators during D1/D2.

(A) Feldspar sigma clast with internally developed anithetic Riedel shears, indicating a top to the NW sense of shear (Fol 237/50, SL 321/06). Granitic gneisses of the Monte Rosa nappe near the Monte Rosa refuge in Matteredal, crds. 628 700/ 089 950. Original size.

(B) Photomicrograph of paragneisses of the Stockhorn-Portjengrat unit, cut parallel to the stretching lineation. The brittlely deformed garnet sigma-clasts (arrows) are retrogressed to chlorite along their rims and in the pressure shadows. They indicate a dextral, top to the WNW, sense of shear (s1/2: 349/19, SL: 278/05) under retrograde conditions. Crossed polarized lights. At Gornergrat in Matteredal (sample 99-75, crds. 631 250/ 092 575).

(C) Shear zone with sc-structures and feldspar sigma-clasts (arrows) indicating a dextral, top to the NW, sense of shear. Towards the center of the shear zone (lower part of the figure), the s planes/ foliation are rotated into the main stretching direction (orientation of planes in the upper part of the figure: s: 234/35, c: 270/27; lower part: s: 277/36, SL: 330/29). Granitic gneisses of the Monte Rosa nappe at the western side of Lake Mattmark in Saastal (crds. 639 825/ 098 300).

to the evolution of the dextral D3 Gornergrat-Furggtal shear zone. This shear zone also overprints the amphibolitic slice of the Antrona unit in Fig. 4.5.3 B, which shows well developed sc-structures indicating a dextral, top to the E, sense of shear.

Different evolutionary stages of D3 shear zones in orthogneisses of the Monte Rosa nappe are shown in Figs. 4.5.3 B-D. Whereas in Fig. 4.5.3 B the pre-existing foliation (s planes) is still recognizable within the evolving shear zone (c planes), the pre-existing foliation in Figs. 4.5.3 C & D is already completely transposed, and is only preserved outside the walls of the shear zone.

Shear bands (extensional crenulation cleavage ECC) indicating a top to the E sense of shear are exhibited in Fig. 4.5.4. Figs. 4.5.4 A and B show outcrop views of such shear bands, that are again better developed in paragneisses (Fig. 4.5.4 A) than in orthogneisses (Fig. 4.5.4 B, both Figs. Portjengrat unit).

In Fig. 4.5.4 C and D, the photomicrographs from calcareous micaschists exhibit a complex deformation history. In both figures, the sense of shear derived from the shear bands indicates a

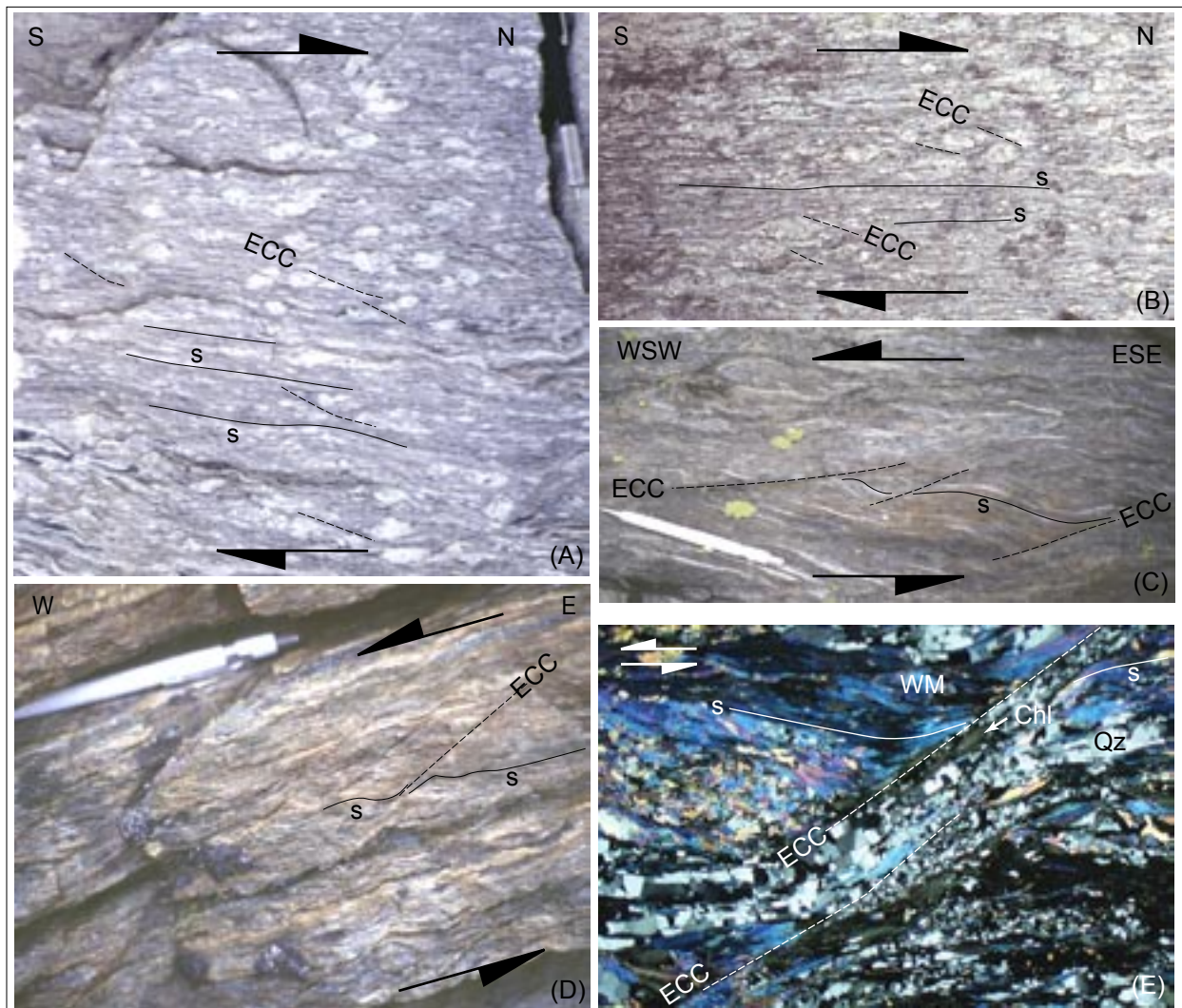


Fig. 4.5.2: Shear bands as kinematic indicators during D1/D2.

(A) & (B) Feldspar sigma clasts and shear bands (extensional crenulation cleavage ECC, dashed lines) indicating a dextral, top to the NW sense of shear. Granitic gneisses of the Monte Rosa nappe at the western side of Lake Mattmark in Saastal. **(A)** s planes/ Fol 298/30, SL 346/21. Width of view approx. 30 cm. Crds. 639 930/ 098 975. **(B)** Fol 276/40, SL 308/38. Width of view approx. 15 cm. Crds. 639 450/ 097 875.

(C) Shear bands (ECC) indicating a sinistral, top to the W sense of shear (foliation/ s planes 326/25, SL 278/16, ECC 299/51). Paragneisses of the Stockhorn unit, close to the Stockhorn at Gornergrat in Matternal; crds. 630 525/ 092 900.

(D) Shear bands indicating a sinistral, top to the WSW sense of shear (foliation/ s planes 350/85, SL 260/25). Paragneisses of the Monte Rosa nappe, close to the Coronette di Camposecco crest in Valle di Loranco; crds. 646 875/ 102 450.

(E) Photomicrograph of a shear band in a paragneiss, indicating a sinistral, top to the SW sense of shear (foliation/ s planes 310/40, SL 212/10, ECC 270/40). The foliation - in the figure defined by aligned white mica (WM) - is deflected by the shear band, and white mica is retrogressed to chlorite (Chl). Grain size reduction during recrystallisation resulted in small quartz grains (Qz) along the shear band. Crossed polarized lights; cut parallel to the stretching lineation. Garnet-bearing paragneiss of the Stockhorn unit at Tufgrat/ Gornergrat in Matternal; crds. 628 700/ 092 725.

dextral movement direction. However, the plagioclase sigma clast in Fig. 4.5.4 C as well as the rotation direction derived from the snowball garnet in the upper part of Fig. 4.5.4 D indicates the opposite movement direction. However, whether the latter is due to two generations of garnet that have grown during D1/2 and during D3 (Fig. 4.5.4 D) or due to inhomogeneous flow during D3 within the rock volume cut, was not subject of further investigation.

In Figs. 4.5.4 E and F, poikiloblastic albite and/ or zoisite grew as the latest phases of the

greenschist facies mineral paragenesis, and were deformed along shear bands. This indicates that D3 deformation proceeded down to retrograde greenschist facies conditions, as has already been described for Fig. 4.5.3 A.

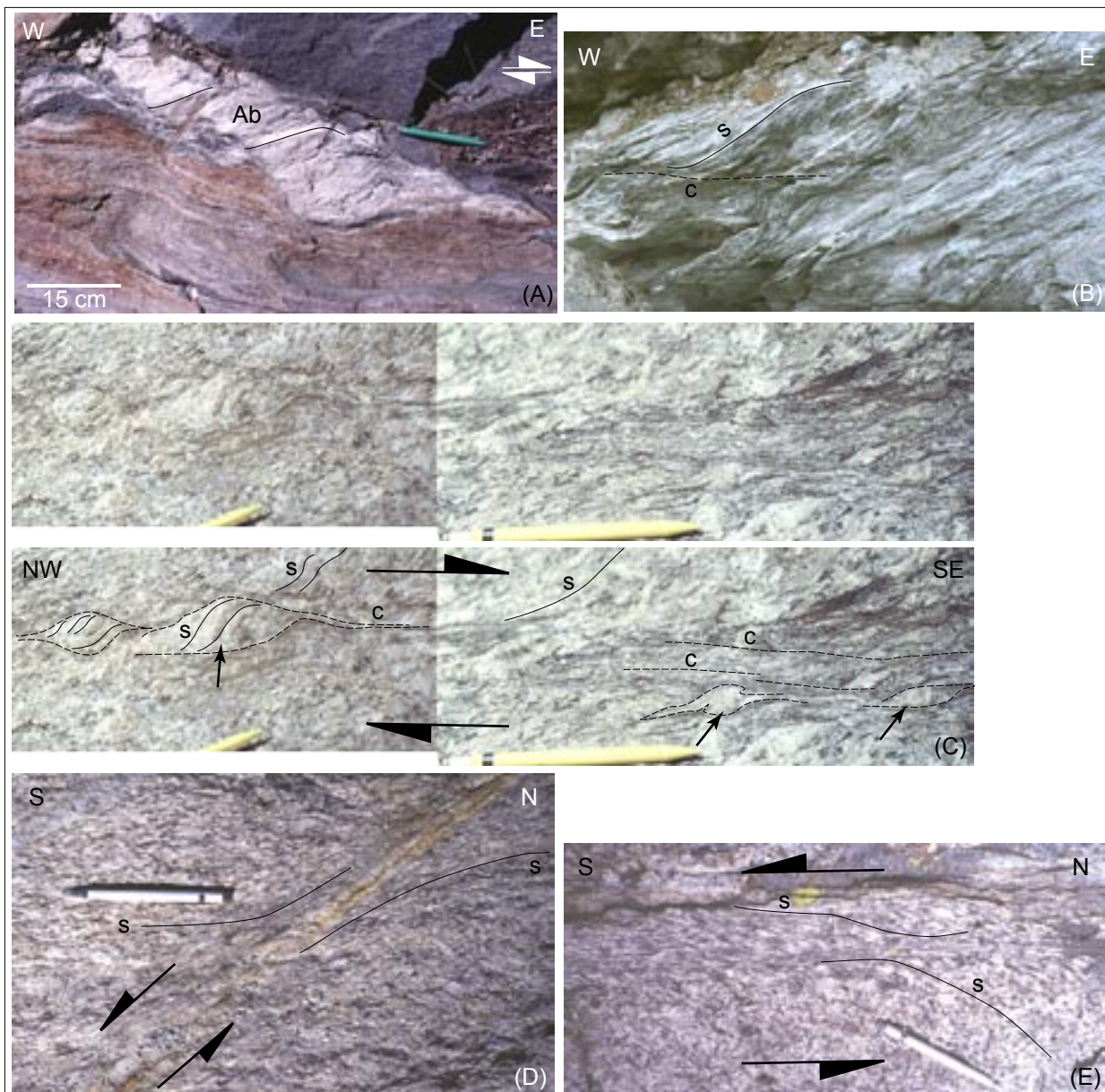


Fig. 4.5.3: Deformed minerals and deflected foliations as kinematic indicators during D3.

(A) Syndeformational growth of single crystals of albite (Ab) in a boudin neck, indicating low metamorphic conditions during dextral, top to the ESE, shearing (D3 Gornergrat-Furggtal shear zone). Furggtal zone in Furggtal (crds. 642 825/ 102 100).

(B) SC-structures indicating a dextral, top to the E sense of shear (s planes/ Fol 338/60, SL 262/22, c planes 022/51). Amphibolites of the Antrona unit, intensely strained by the D3 Gornergrat-Furggtal shear zone. At 2525 m in the small valley N of Börterrück in Furggtal; crds. 643 375/ 101 850.

(C) Sigmoidal deformation of a pre-existing foliation (s, solid lines) and feldspar clasts (arrows) in an evolving shear zone (c planes, dashed lines). The feldspar clasts indicate a dextral, top to the SE sense of movement. Shear planes: 221/15; SL: 310/01. Granitic gneisses of the Monte Rosa nappe, near Pecetto in Valle d' Anzasca (not indicated in the map of stretching lineations), crds. 639 150/ 091 460.

(D) & (E) Shear zones (c planes) in granitic gneisses of the Monte Rosa nappe with a sinistral, top to the S sense of movement. (D) Fol (s, solid lines) 295/50, c plane (dashed line): 253/57, SL on c plane: 177/20. (E) c plane 261/44, SL on c plane 340/08. Close to the Monte Rosa refuge in Matteredal, crds. 628 950 089 650.

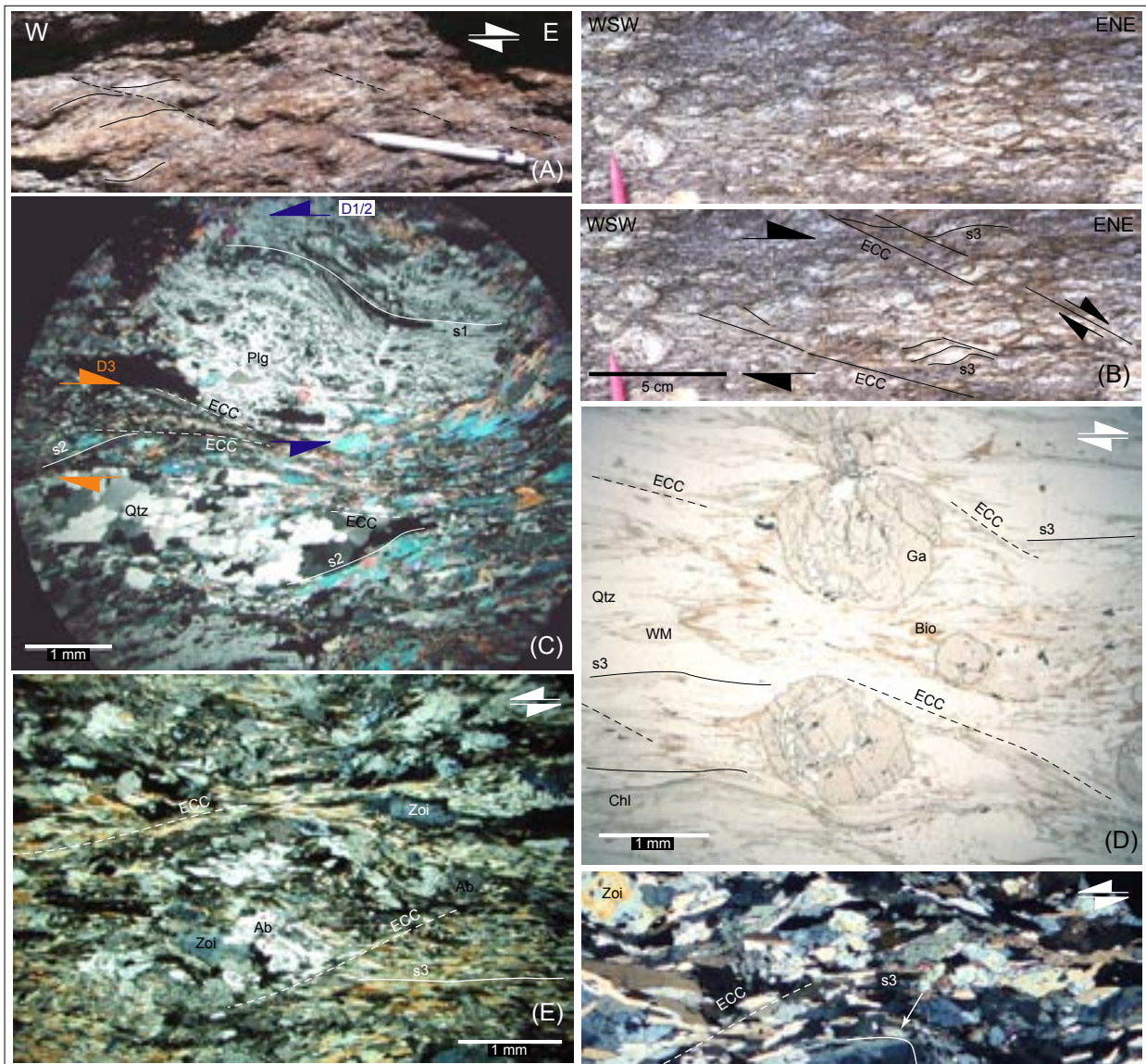


Fig. 4.5.4 : Shear bands as kinematic indicators during D3.

(A) Shear bands (ECC) indicating a dextral, top to the E sense of shear (average Fol 309/32, average c plane 348/24, average SL 258/22). Garnet micaschists of the Portjengrat unit, intensely strained by the D3 Gornergrat-Furggtal shear zone. At 2820 m, close to the Augstkummen river in Furggtal; crds. 643 900/ 102 450.

(B) Shear bands (ECC, dashed lines) in augenmylonitically deformed orthogneisses indicating a dextral, top the ESE sense of shear (s3: 328/46, SL: 291/34). Portjengrat unit, north of Passo della Preja in Valle di Loranco, at the nappe contact of Stockhorn-Portjengrat unit and Antrona unit (crds. 651 925/ 106 680).

(C) Photomicrograph of shear bands (ECC) in a metapelitic layer in calcareous micaschists. Whereas the shear bands indicate a dextral sense of shear (orange arrows), the asymmetry of the plagioclase sigma clast on top of the shear bands implies the opposite sense of shear (blue arrows). This is interpreted as incomplete overprint of D3 onto D1/D2 shearing. Crossed polarized lights; cut parallel to the stretching lineation. Zermatt-Saas unit, at Längflue in Saastal (sample 97-38, crds. 635 125/ 103 375; s1/2: 285/40; SL: 323/15).

(D) Photomicrograph of a metapelitic layer in calcareous micaschists. The quartz inclusions in the garnets define a snowball-like growth, although the rotation direction is not unequivocal. The shear bands (ECC) indicate a dextral, top to the E sense of shear. Zermatt-Saas unit, at Plattjen in Saastal (sample 97-73, crds. 639 175/ 103 675).

(E) Photomicrograph of a metabasalt. Poikiloblastic albite and zoisite grew as the last phases of the greenschist facies mineral assemblage. Their ductile deformation indicates a synkinematic growth during the formation of the shear bands (ECC). Sinistral, top to the E sense of shear (s3: 188/55, SL: 286/08). Zermatt-Saas unit at the highly strained nappe contact to the Permo-Mesozoic metasediments of the Stockhorn-Portjengrat unit (overprinted by the Saas shear zone). At Plattjen in Saastal (sample 97-74, located adjacent south of 97-73).

(F) Photomicrograph of a metabasaltic boudin in the Furgg zone. Poikiloblastic zoisite grew as the last phase in a greenschist facies mineral assemblage (zoisite, actinolite, titanite, chlorite, albite). The ductile deformation of the zoisite indicates its synkinematic growth during the formation of the shear bands (ECC). The sinistral, top to the E, sense of shear is therefore ascribed to D3 (s3: 338/34, SL: 298/27). At Gornergrat in Mattertal (sample 98-111, crds. 631 025/ 092 325).

Ab: albitic plagioclase, Akt: actinolitic hornblende, Chl: chlorite, ECC: shear bands (extensional crenulation cleavage), Ga: garnet, Plg: plagioclase, Qtz: quartz, WM: white mica, Zoi: zoisite.

In several thin sections, the shape and lattice preferred orientation of quartz was observed to define the axial plane cleavage of D1/D2 microfolds (Fig. 4.5.5 A). The respective fold axes correlate to the stretching lineation, which exhibits an associated top to the N- to W sense of shear (Fig. 4.5.5 B). Hence, the folds are considered to have evolved synkinematically with D1/D2 straining or to have been rotated into the principle stretching direction in the course of progressive deformation.

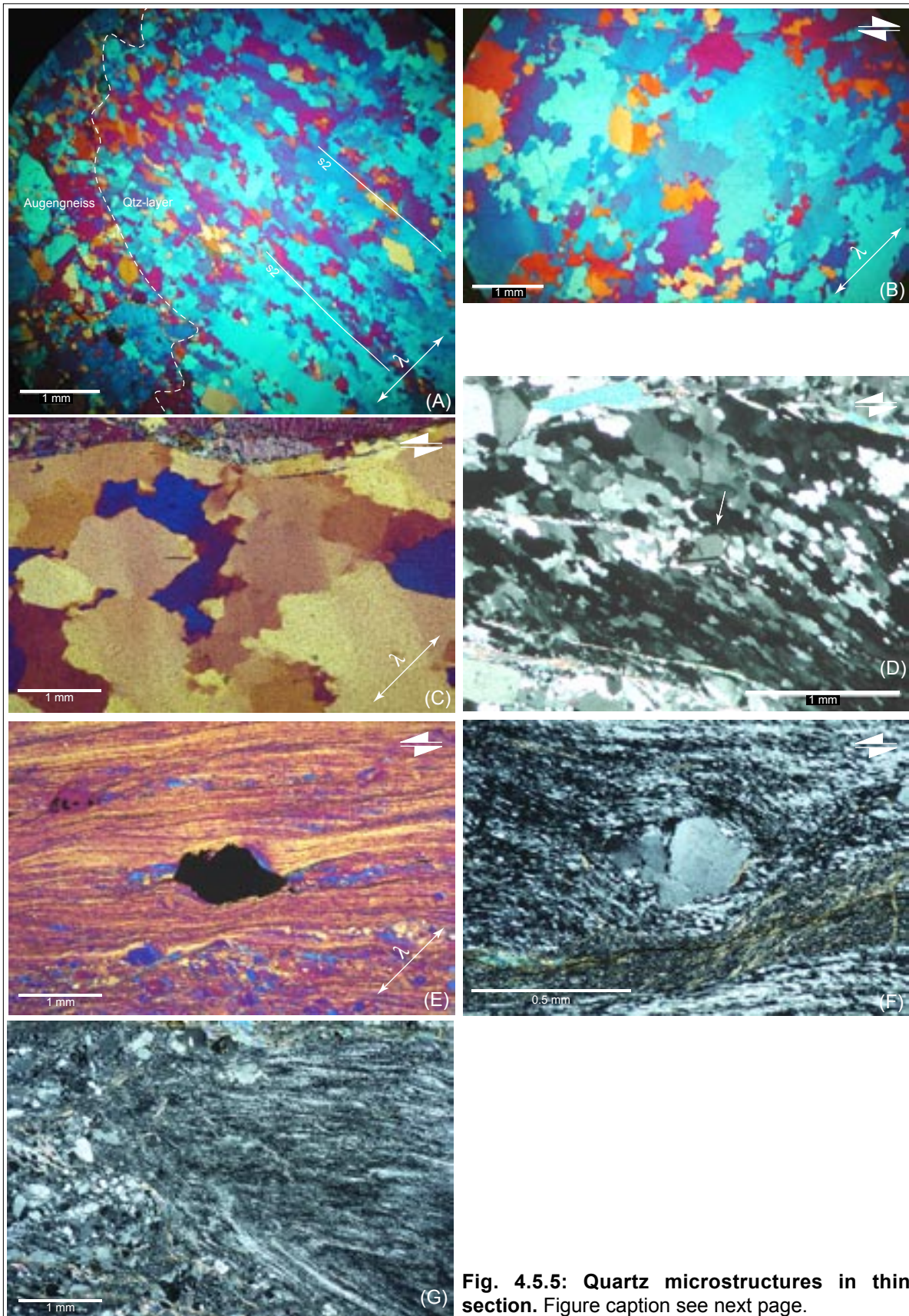


Fig. 4.5.5: Quartz microstructures in thin section. Figure caption see next page.

The quartz recrystallisation mechanism is grain boundary migration, indicating temperatures of 550 - 450°C (Stipp et al., 2002) during D1/D2 deformation (see also Fig. 4.5.5 C). However, even lower temperatures than 450°C during D1/D2 deformation are frequently indicated by a recrystallisation mechanism of subgrain rotation (e.g. Fig. 4.5.5 D), which is also associated to a top to a N- to W sense of shear.

Quartz textures of the SE-directed D3 Trifhorn thrust (see chapter 4.3.4) also exhibit subgrain rotation as recrystallisation mechanism (Fig. 4.5.5 E-G). This is interpreted as an overlap of the two movement directions in terms of temperature. Fig. 4.5.5 G shows that the fine-grained quartz recrystallises replace older folded quartz grains, supposedly of the previous D2 deformation phase (see also Fig. 4.5.5 A & B).

The quantitative determination of the LPO by texture goniometer and by U-stage was not very successful (cf. Carreras et al., 1977; Passchier, 1983), as out of a total of 24 samples 22 of the resulting pole figures of the textures were not unequivocal. In thin section, such samples may show conflicting shear sense indicators as illustrated in Fig. 4.5.4 C, which were interpreted as a superposition and incomplete overprint of D3 onto D1/2 structures. Additionally, the random textures of the 18 quartz vein- and quartzite samples resulting from texture goniometer measurements (not shown) were interpreted as single grain textures (too large grain sizes) or as impurity deflections (too high mica contents). The pole figures of the two remaining samples are exhibited in Fig. 4.5.6.

Reorientation of D1/2 stretching lineations by D3 straining

Stretching lineations range in orientation from NW- to SW-ward plunging, with rare exceptions plunging towards the S (at the southern side of the Monte Rosa massif, Fig. 4.5.7) or towards the NE (in Valle di Loranco and Valle d' Antrona, Fig. 4.5.8). Subdivided in several subareas, the stretching lineations were projected in several pole figures (Figs. 4.5.7 and 4.5.8). Depending on the subarea, the stretching lineations plotted are either SL1/2 (blue arrows in Figs. 4.5.7 and 4.5.8) or SL3 stretching lineations (orange arrows in Figs. 4.5.7 and 4.5.8). However, at Gornergrat (Fig. 4.5.7) or

Fig. 4.5.5: Quartz microstructures in thin section.

(A) & (B) Folded quartz layer in orthogneisses of the Stockhorn-Portjengrat unit.

(A) Cut perpendicular and **(B)** parallel to the D1/D2 fold axis, which coincides with the D1/D2 stretching lineation. In **(A)** quartz grains exhibit a shape preferred orientation (SPO) that defines the fold axial plane cleavage of the isoclinal D1/D2 fold. In **(B)** the crystallographic preferred orientation (CPO) of quartz in the limb of the D1/D2 fold indicates a dextral, top to the W, sense of shear. This indicates the synmylonitic folding during D2. The recrystallisation mechanism is grain boundary migration recrystallisation (GBMR), indicating intermediate temperatures (between 550° and 450°C; Stipp, 2002). At Mälliege in Saastal (sample 97-103, crds. 638 950/ 102 250, s1/2 303/29, SL: 284/20).

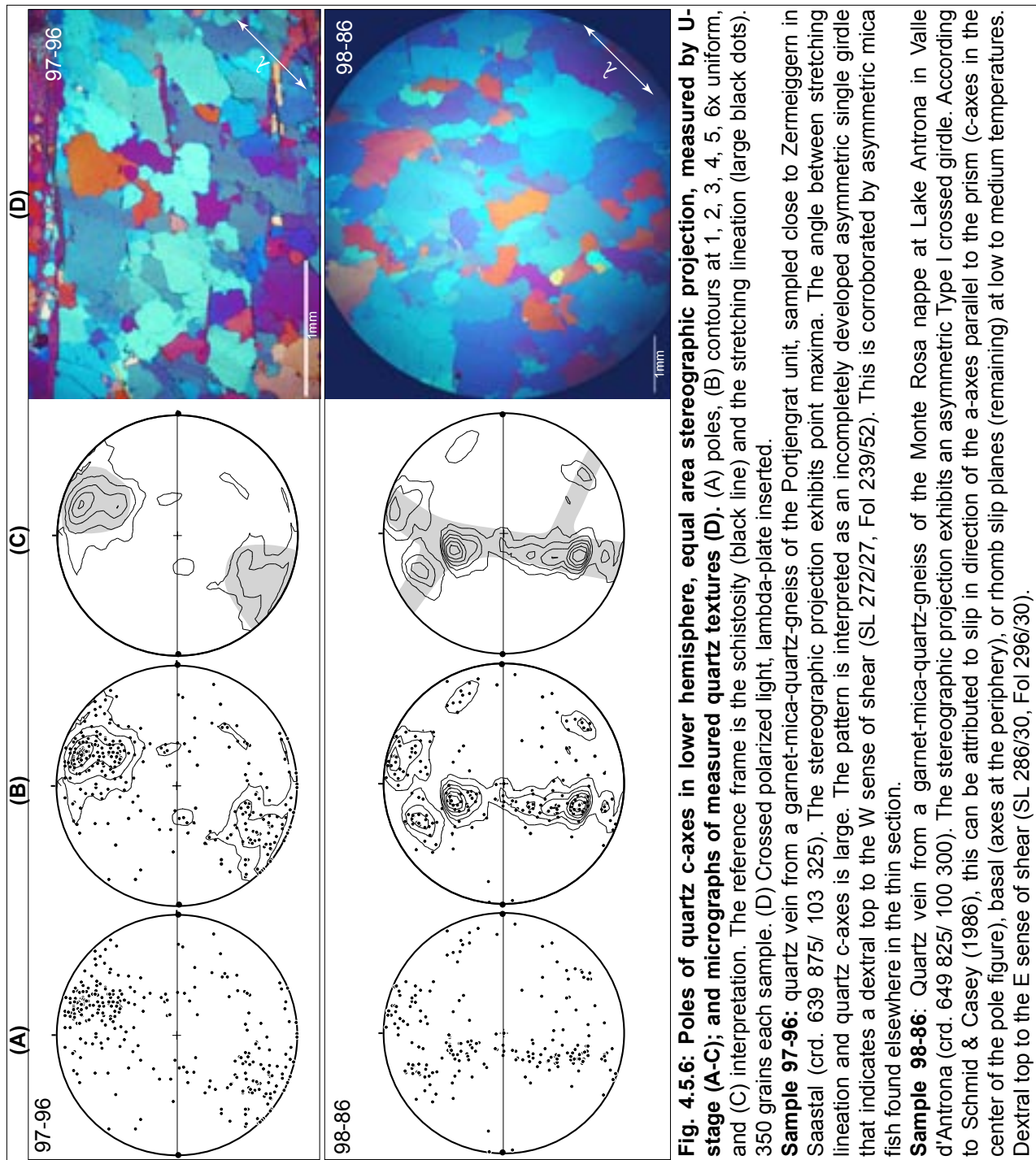
(C) Quartz c-axes which are oriented perpendicular to the lambda plate (i.e. trending from upper left to lower right) indicate a sinistral, top to the WNW, sense of shear (D1/D2). The recrystallization mechanism is GBMR. Cut parallel to the stretching lineation. Quartz layer in paragneisses of the Stockhorn-Portjengrat unit, at the contact with the Furgg zone. At Gornergrat in Matteredal (sample 99-75, crds. 631 250/ 092 575; s1/2: 349/19, SL: 278/05).

(D) Twinned plagioclase sigma-clast in the center of the figure (arrow) and SPO of quartz grains oriented at an angle of about 30° to the foliation (marked by mica) indicate a sinistral, top to the W, sense of shear. The recrystallization mechanism is subgrain rotation (SRR). This indicates lower temperatures (<450°) and illustrates the large range of temperatures over which top to the W nappe movements took place. Quartz layer in orthogneisses of the Moncucco-Camughera unit, at the base of the Antrona unit in Zwischbergental (sample 98-138, crds. 650 825/ 108 925; s1/2: 176/86, SL: 261/11). Cut parallel to the stretching lineation.

(E), (F), (G) Quartz mylonite from the D3 Trifhorn thrust (see chapter 4.3.4).

(E) Hematite sigma-clast (center of the figure), quartz sigma-clasts (bottom) and shear bands (ECC) which developed in the matrix of very fine-grained quartz, indicate a sinistral, top to the E, sense of shear. The recrystallization mechanism of SRR (see enlargement **(F)**) indicates lower temperatures (< 450°; Stipp et al., 2002). This illustrates that top to the E movements along the Trifhorn thrust started at lower temperatures.

(G) The fine-grained quartz grains recrystallized during D3 replace older folded quartz grains of the previous deformation phase D2. Occasionally cut slightly oblique to stretching lineation (sample KD 42, see Dubach, 1998; crds. 643 200/ 107 430).



at Lake Mattmark (Fig. 4.5.8), both SL1/2 and SL3 exhibit the same large range of orientations, and were therefore plotted in a single pole figure.

In the pole figures from Gornergrat (Fig. 4.5.7), Mattmark and Mittaghorn (Fig. 4.5.8), as well as from Valle d'Ayas and Valle di Gressoney, the poles of the SL1/2 stretching lineations show a great circle distribution. The associated π -poles approximate the orientation of the respective large-scale D3 or D4 fold axes of the respective subareas (see pole figures in Figs. 4.2.2, 4.2.9, 4.2.18 and 4.2.25). Hence, SL1/2 were supposedly reoriented after their formation. In the pole figures from Saas Fee and Furggtal (Fig. 4.5.8), D3 stretching lineations are exhibited. Their range in orientation is still large, so that a reorientation after their formation is also considered. In contrary, the SL3 poles in the pole figures from Almagellertal and Zwischbergen pass (Fig. 4.5.8) do not show a great circle distribution, but define a single maximum at about 267/28 (also see Fig. 4.2.25 A & B).

Three of the major D3 shear zones discussed in chapter 4.3 are considered to account for such overprint - the Gornergrat-Furggtal shear zone, the Trifhorn thrust, and the Saas shear zone

(for their location see Fig. 5.1). In their present-day orientation, the dip of both Gornergrat-Furggtal shear zone and Trifflhorn thrust is too steep to kinematically allow for thrusting (see Fig. 5.2 or 4.4.2). Such a thrusting component, however, is generally indicated by the moderate plunge of stretching lineations (in average around 30°). Since the onset of early D3 deformation, the Gornergrat-Furggtal shear zone and Trifflhorn thrust have therefore supposedly steepened in the course of progressive contraction (see reconstruction in chapter 5). As a consequence, the accommodation of contraction must have been successively passed from early thrusting into late strike-slip movements. This transition is supposed to account for a progressive rotation of the D1/D2 (see also Keller & Schmid, 2001) and early-formed D3 stretching lineations into the orientation presently observed. The Saas shear zone (see chapter 4.3.3), which is the youngest of the major shear zones in the investigated area, is considered to account for the reorientation of D1/D2 and early-formed D3 shear senses at the Gornergrat (Fig. 4.5.7) and at Saas Fee (Fig. 4.5.8).

However, the subareas Almagellertal and Zwischbergen pass are situated in the footwall of the Trifflhorn thrust, and must therefore have been equally reoriented by late-D3 straining. As all the stretching lineations in these two subareas are uniformly associated to D3 and as no D1/2 stretching lineations are preserved, the D3 overprint obviously was pervasive in the two areas. However, the early-D3 onset of straining is evidenced by the pervasive mylonitic overprint of the augengneisses in the Portjengrat shear zone (see chapter 4.3.5). The lack of a great circle distribution of their poles in the pole figure is therefore rather considered as a geometric effect. In the discussed subareas, the dip of the foliation planes is generally very steep (ranging from 50 to 90°, cf. Fig. 4.2.25 A & B). Even larger differences in the plunge of the stretching lineations would therefore result in small differences in azimuth only. On moderately dipping planes only would even small differences in plunge result in a relatively large scatter of azimuth. The consequences of the discussed findings led to the kinematic model and the reconstruction in chapter 5.

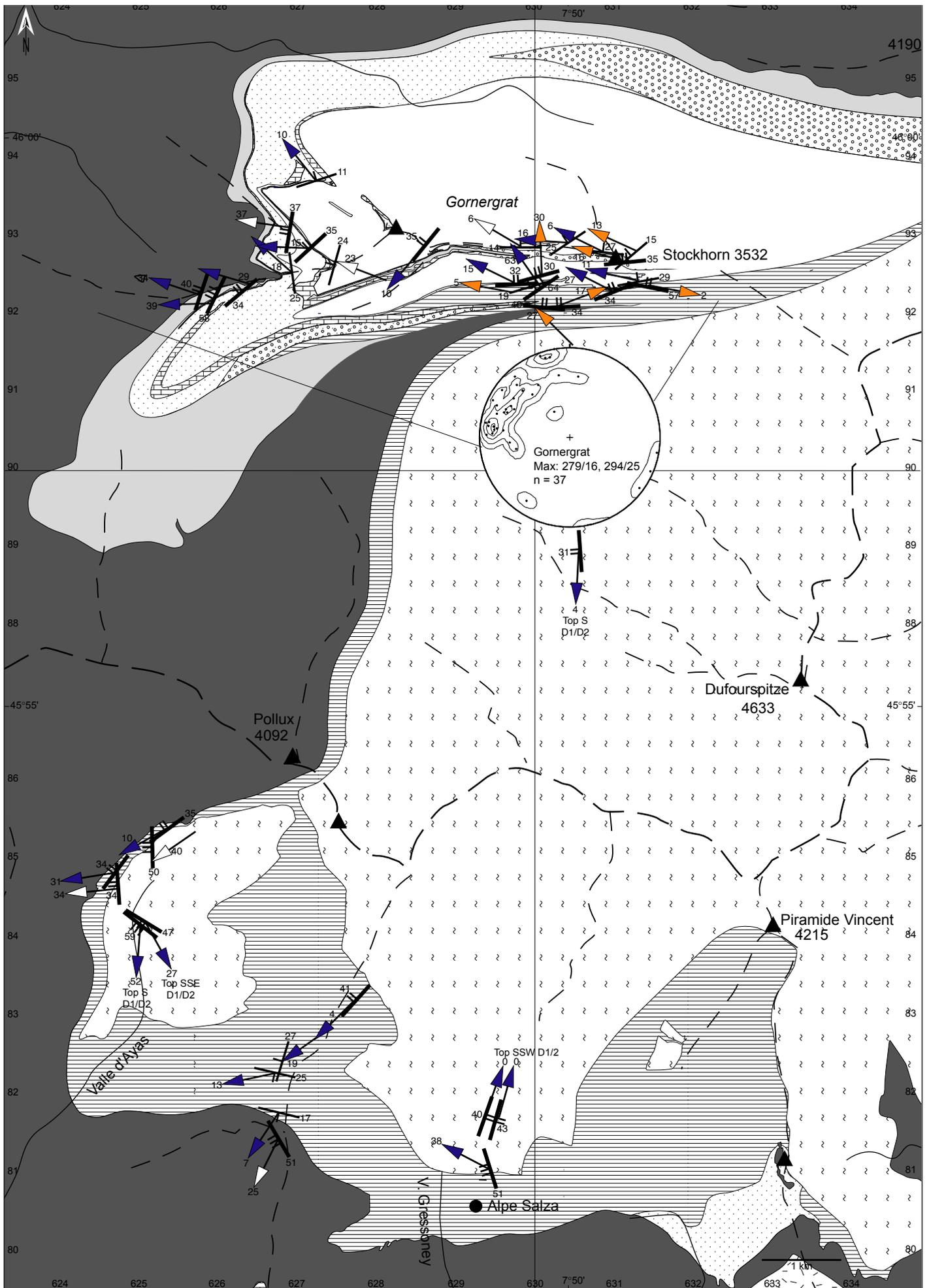


Fig. 4.5.7: Stretching lineations and associated shear senses, Monte Rosa south side. Legend see Fig. 4.5.8.

5 Kinematic model and reconstruction

This chapter aims to integrate the petrographical and structural results described in the previous sections within a kinematic model which serves as a base for a qualitative reconstruction of the nappe pile in the Monte Rosa region. Additional information of the detailed investigations of Klein (1978), Dubach (1998), Keller (2000), Rössler (2000), Weber (2001) and Bacher (2002) were considered. Additional large-scale structural information from adjacent areas (Milnes et al., 1981; Müller, 1983; Escher et al.; 1999) served to cover the entire area of interest. The information was compiled in a simplified map (Fig. 5.1) and a cross-section (Fig. 5.2) which represent the base of the reconstruction proposed in Fig. 5.3. Although contraction was accompanied by significant dextral strike-slip movements during D3 and D4 (see below), the reconstruction was performed in the plane of the cross-section, and out-of-section movements were not considered. As, additionally, the cross-section is oblique to the major D3 and D4 fold axes to various degrees, it does not exhibit true but only apparent displacements. The resulting amount of displacement is therefore a minimum value, and the reconstruction has a qualitative character only.

Kinematic overview

The large-scale framework for the kinematic evolution of the investigated area is related to the indentation of the Adriatic microplate into the European lithosphere (e.g. Stampfli & Marchant, 1997), that accounted for an approximately N-S directed stress field (Ceriani et al., 2001; Schmid & Kissling, 2000). Within this stress field, the Penninic nappe pile formed by thrusting of the individual tectonic units towards the N during mid- to late Eocene times (see e.g. Escher et al., 1997). In the investigated area, nappe stacking was accompanied by two phases of isoclinal folding (D1 and D2; see ch. 4.2) and the formation of a D1/D2 stretching lineation on the newly built axial plane cleavages (ch. 4.1 and 4.4). The succeeding D3 deformation phase supposedly reoriented the D1/ D2 stretching lineations (see chapter 4.5; also see Keller & Schmid, 2001) which presently range from an NW- to SW-ward plunge and exhibit an associated top NW to SW sense of shear, respectively (see Fig. 4.5.4 and 4.5.5).

From the late Oligocene onwards (Escher et al., 1997), the ongoing contraction led to a blocking of the further growth of the accretionary wedge and initiated a reversal of movement directions (D3 and D4). In the investigated area, strain partitioned into SE- to S-directed large-scale folds and dextral oblique thrusts during D3 (see chapter 4.2 and 4.3; also see e.g. Milnes et al., 1981; Klein, 1978). As the orientation of D3 stretching lineations ranges from a NW-to WSW-ward plunge and exhibits an associated top to the SE or ESE sense of shear (see Figs. 4.5.4 and 4.5.5), the orientation of the stress field supposedly changed from a N-S to a NW-SE or WNW-ESE orientation during later stages of D3.

5.1 Reconstruction of Vanzone phase structures (D4)

The Vanzone phase caused a significant amount of shortening of the Penninic nappe stack (Fig. 5.2 and 5.3 A). In the investigated area, the SE-directed kilometer-scale Vanzone antiform evolved as a major structure associated with this phase. Simultaneously with its emergence, the southern overturned limb of the Vanzone antiform was dextrally thrust over the Eastern and Southern Alpine units along the Canavese line (e.g. Schmid et al., 1989). As a result of ongoing contraction, the thrust plane steepened and thrusting was progressively replaced by dextral strike-slip movements (Schmid et al., 1989). D4 folding by the Vanzone antiform caused severe rotations of parts of the Penninic units around the Vanzone fold axis. Previous structures were rotated from a shallow or moderately NW-dipping position north of the Vanzone fold axial plane, into a shallow or moderately SW-dipping position close to the fold hinge of the Vanzone antiform, and, farther in the S, into an overturned and steeply NNW-dipping position. As a result, D3 folds were refolded and became synformal antiforms and antiformal synforms south of the fold axial plane of the Vanzone antiform. For example, the D3 Perazzi antiform represents the refolded D3 Stockchnubel synform. The up-doming of the Vanzone antiform and the associated dextral shearing along its southern

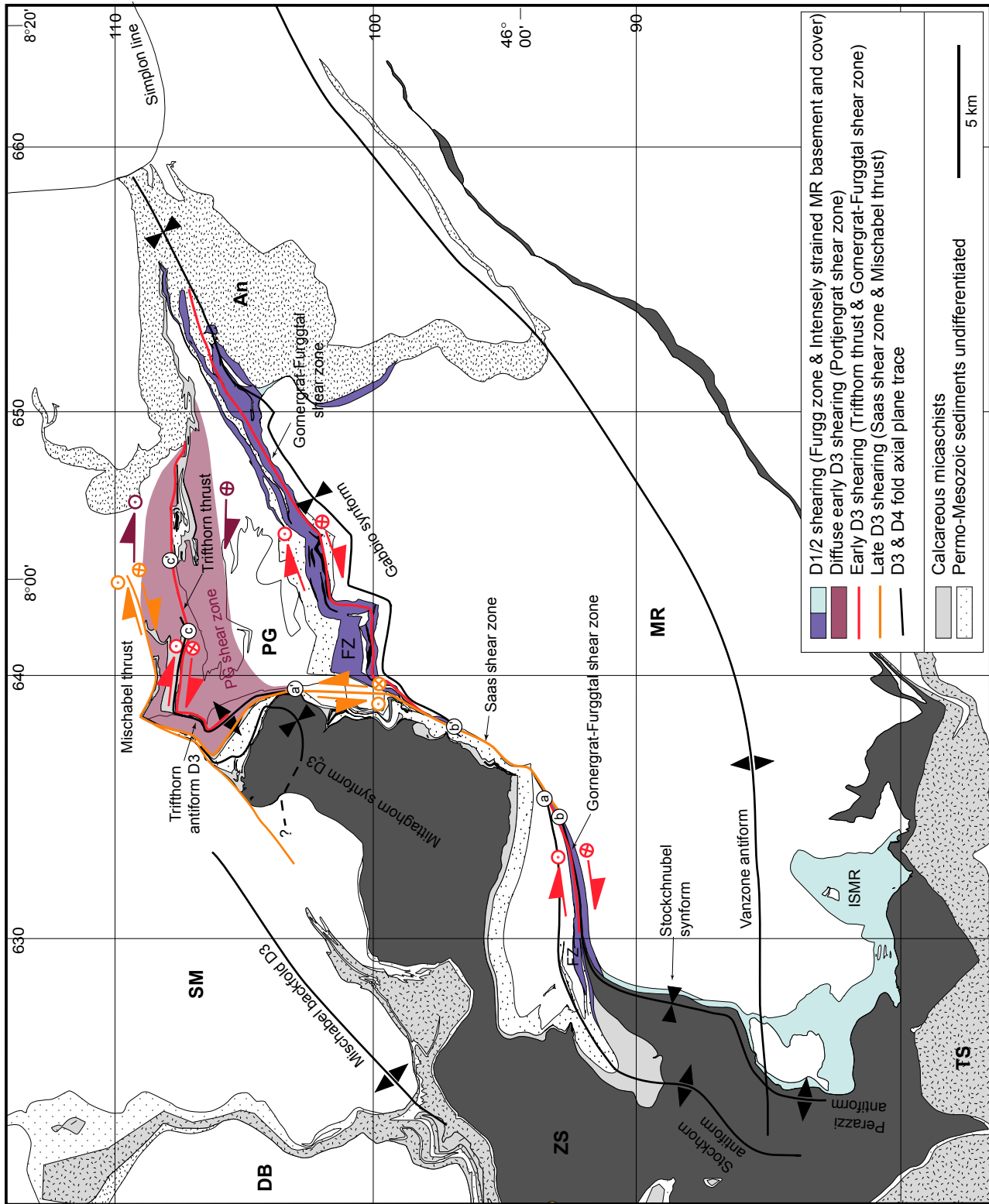


Fig. 5.1: Map view of major thrusts and shear zones and D3 and D4 fold axial planes in the Monte Rosa region.

The colors indicate the relative age of thrusts and shear zones. All D3 thrusts and shear zones are dextral and transpressive. White dots with corresponding letters (a - a') indicate the approximate location of cut-off points in the hanging wall (a, b, c) and footwall (a', b', c') of the respective shear zone. As "marker horizons" fold axial plane traces and lithostratigraphic units were chosen: **a, a'**: cut-off points of the fold axial plane trace of the Stockhorn antiform in the hanging (a) and the Trifhorn antiform in the footwall (a') of the Saas shear zone. **b, b'**: cut-off points of the Furgg zone in the hanging (b) and footwall (b') of the Saas shear zone. (b) additionally corresponds to the cut-off point of the fold axial plane trace of the Stockchnubel synform. **c, c'**: cut-off points of the Permo-Mesozoic metasediments in the hanging (c) and footwall (c') of the Trifhorn thrust. For discussion see text.

GG-FT shear zone: Gornegrat-Furggtal shear zone; PG shear zone: Portjengrat shear zone. An: Antrona unit; DB: Dent Blanche nappe; MR: Monte Rosa nappe; PG: Portjengrat unit; SE: Sesia unit; SM: Siviez-Mischabel nappe; ST: Stockhorn unit; TS: Tsate nappe; ZS: Zermatt-Saas unit.

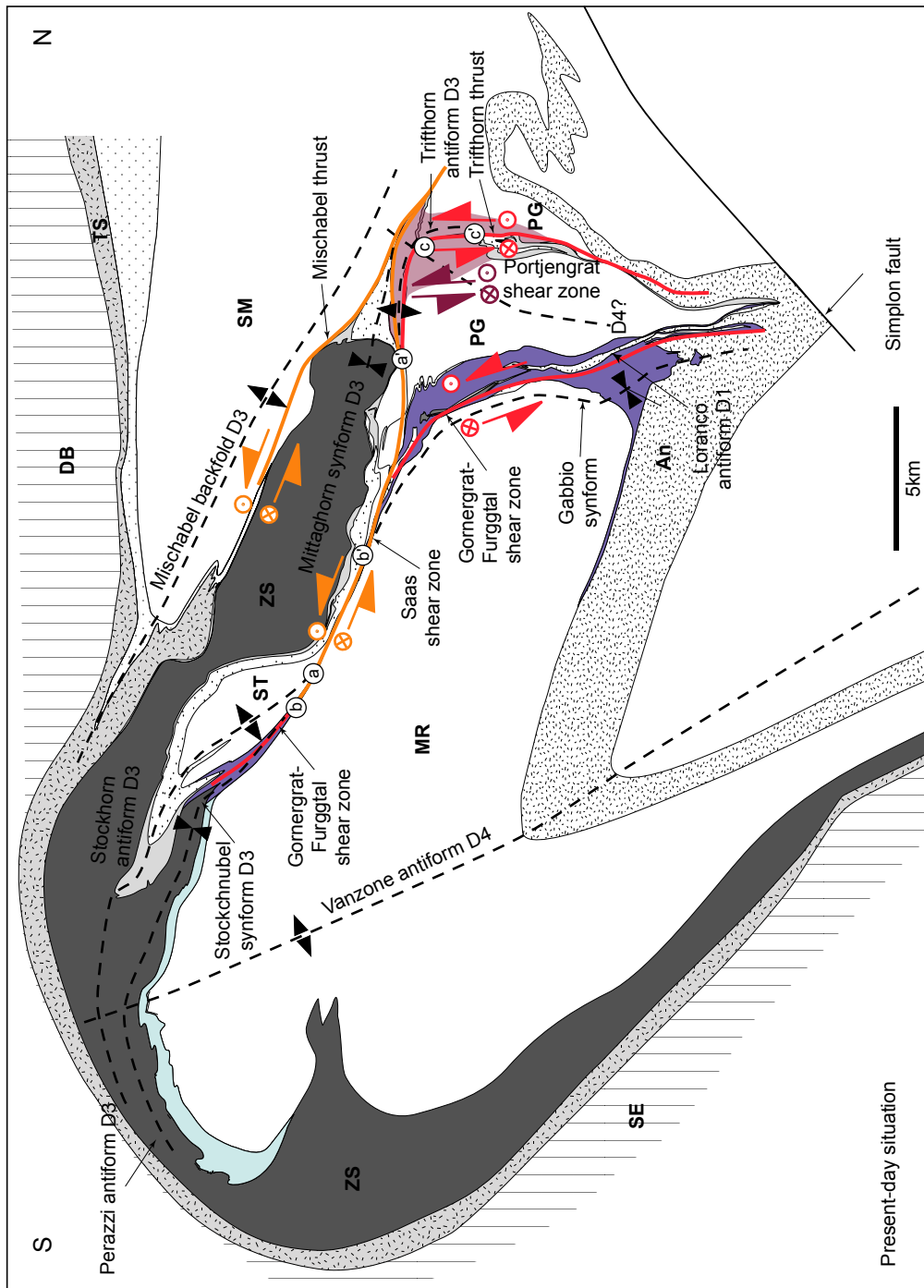


Fig. 5.2: Simplified composite cross-section illustrating the location of the major D4 and D3 fold axial planes, thrusts and shear zones.

This section forms the base of the reconstruction in Fig. 5.3. Cross-section compiled with data from Milnes et al. (1981), Escher et al. (1999), Keller & Schmid (2001) and own data. Colors and abbreviations as in Fig. 5.1. For discussion see text.

overturned limb caused a tightening of the interlimb angles of the D3 folds and an overall thinning of the tectonic units.

A second major effect of the Vanzone phase shortening can be suspected north of the Vanzone antiform. There, contraction and transpression during D4 probably accounted for the steepening of the D3 Trifhorn thrust and its rotation into a subvertical position. The approximate location of the rotation axis is indicated in Figs. 5.1 and 5.2.

The backrotation of the southern overturned limb of the D4 Vanzone antiform into a flat-lying position (Fig. 5.3 A) leads to a moderate dip of all involved structures. The D3 Perazzi antiform "disappears" in order to become the D3 Stockchnubel synform. The Penninic units south of the Vanzone fold axial plane are considered to increase in thickness, which is qualitatively illustrated in Fig. 5.3 A.

The rotation of the Trifhorn thrust plane north of the indicated rotation axis leads to a moderate NNW-ward dip of the Trifhorn thrust plane and all the structures N of it. The resulting dip

now kinematically allows not only for a strike-slip component, but also for a thrust component of the Trifhorn thrust during D3. In the moderate NNW-ward dipping position, the fold axial plane of the Trifhorn antiform can be easily extrapolated into the Antrona unit. However, the suggested location of the fold axial plane remains a matter of interpretation, as the area has not been investigated.

5.2 Reconstruction of Mischabel phase structures (D3)

During the D3 Mischabel phase, a late and an early phase of deformation can be distinguished. These will be reconstructed separately (Fig. 5.3 B and C, respectively).

5.2.1 Late-D3 structures

The two major structures associated with the late D3 Mischabel phase are the dextral oblique Saas shear zone and the dextral oblique Mischabel thrust (Figs. 5.1 and 5.2; see ch. 4.3). As the two thrusts unify in the same structural horizon (north of Saas Fee), the Saas shear zone may be regarded as the major detachment while the Mischabel thrust represents a branch thrust of the Saas shear zone.

The Siviez-Mischabel nappe, which forms the core of the D3 Mischabel backfold (Müller, 1983), was thrust towards the SE over the Zermatt-Saas unit along the late-D3 Mischabel thrust. The evolution of the D3 Mischabel backfold started in early D3 times, and it is supposed to be linked to dextral oblique shearing along the early-D3 Portjengrat shear zone. The D3 Mischabel backfold may therefore be regarded as a fault propagation fold that evolved due to shearing along the Portjengrat shear zone. As the Portjengrat shear zone was deflected and flattened by the onset of shearing along the late-D3 Saas shear zone, it was the late-D3 Mischabel thrust that kinematically enabled further growth of the Mischabel backfold. Note, however, that the Mischabel thrust was not investigated in this study (see ch. 4.3).

While the Mischabel backfold formed in the hanging wall of the Portjengrat shear zone, the D3 Mittaghorn synform is considered to have evolved by shearing in the footwall of the Portjengrat shear zone (Fig. 5.3 B). For this reason, the Mittaghorn synform supposedly does not possess a real overturned limb with a reverse facing direction of the stratigraphy. Consequently, a retro-deformation of the Mittaghorn synform does not place the Zermatt-Saas unit, forming the core of the Mittaghorn synform, on top of the Siviez-Mischabel nappe nor on top of the Tsaté nappe (see Fig. 5.3 C). Instead, the reconstruction proposed in Fig. 5.3 D places the Tsaté unit directly on top of the Zermatt-Saas unit (see also Figs. 5.3. B and C).

The Stockhorn unit, which forms the core of the Stockhorn antiform, and the Zermatt-Saas unit on top of the Stockhorn unit were thrust towards the ESE over the Monte Rosa nappe along the early-D3 Saas shear zone. For a reconstruction of the displacement, cut-off points of marker horizons had to be identified in the hanging and footwall of the Saas shear zone. Due to the intense deformation and glaciation of the considered area, however, this meets certain difficulties. In the hangingwall of the Saas shear zone, the following "marker horizons" were chosen (see Fig. 5.2): the fold axial plane trace of the D3 Stockhorn antiform, marked with (a); the fold axial plane trace of the D3 Stockchnubel synform, marked with (b); the Furgg zone, also marked with (b), as its cut-off point is located too close to the cut-off point of the Stockchnubel synform to be distinguished in Fig. 5.2. The correlating structures in the footwall of the Saas shear zone are supposedly as follows: the Trifhorn antiform, marked with (a'), as no other major antiform was identified (see Klein, 1978); the Gabbio synform, marked with (b'), as no other major synform was identified; and the Furgg zone, also marked with (b') for the reasons mentioned above.

The restoration of the displacement along the Saas shear zone unifies the Stockhorn and Trifhorn antiforms to become a single antiform (marked with (a) in Fig. 5.3 B). For a better fit, the interlimb angle of the Stockhorn antiform was opened. Also, the Stockchnubel and Gabbio synforms unify to become a single synform (marked with (b) in Fig. 5.3 B). Assuming the reconstruction in Fig. 5.3 B to be correct, the Stockchnubel-Gabbio synform probably developed as a shear fold in the footwall of the early-D3 Gornergrat-Furggtal shear zone, very similar to the evolution of the Mittaghorn synform (see above). This was already proposed for the Gabbio synform by Müller (1983)

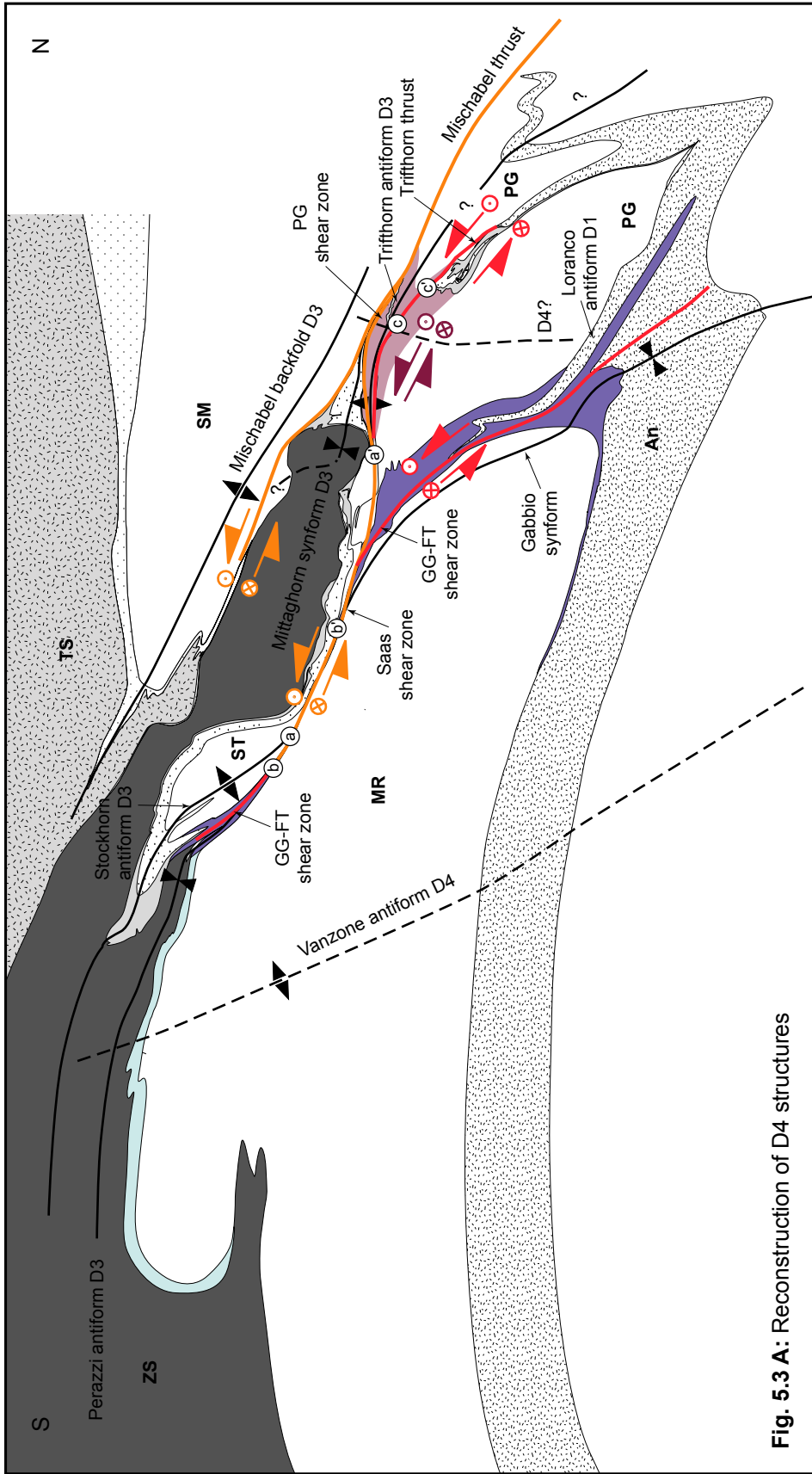


Fig. 5.3 A: Reconstruction of D4 structures

Fig. 5.3: Qualitative reconstruction of major folds and thrusts/shear zones. Not to scale.

(A) Reconstruction of major D4 folds.

(B) Reconstruction of displacement along the late-D3 Mischabel thrust and Saas shear zone.

(C) Reconstruction of displacement along the early-D3 Gornergrat-Furggal shear zone (GG-FT shear zone), Triffhorn thrust and Portjengrat shear zone (PG shear zone).

Full lines and arrows: present folds and active thrusts/shear zones; dashed lines and open arrows: location of folds and thrusts prior to reconstruction. For discussion see text.

Colour index and abbreviations as in Fig. 5.1.

and Froitzheim (2001). In the reconstruction proposed in Fig. 5.3 B, the Furgg zone was considered as a continuous horizon (see detailed discussion of the problem in chapter 4.3.1). The location of the cut-off point (b') illustrates, where the Furgg zone has been cross-cut by the Saas shear zone.

5.2.2 Early-D3 structures

After the restoration of displacement along the Saas shear zone and the Mischabel thrust (Fig. 5.3 B), four major D3 folds and three major D3 shear zones remain. The folds are (1) the Stockchnubel-Gabbio synform, (2) the Stockhorn-Trifflhorn antiform, (3) the Mittaghorn synform and (4) the Mischabel backfold. The shear zones are (1) the Gornergrat-Furggtal shear zone, (2) the Trifflhorn thrust and (3) the Portjengrat shear zone.

Fig. 5.3 B illustrates, that the Trifflhorn thrust is assumed to have developed as a blind thrust in the core of the Stockhorn-Trifflhorn antiform, along which part of the upright limb overthrusts the overturned limb of the antiform. As a marker horizon used for the restoration of the displacement along the Trifflhorn thrust, the Permo-Mesozoic meta-sediments (at the Zwischbergen pass/Almagellertal and at the Grundberg/ Saastal) were chosen. The respective hangingwall cut-off point is marked with (c) in Fig. 5.3 B, the footwall cut-off point is marked with (c').

As described in chapter 5.2.1, the Stockchnubel-Gabbio synform is assumed to have evolved as a shear fold in the footwall of the Gornergrat-Furggtal shear zone. For this reason, the Stockchnubel-Gabbio synform supposedly does not possess a real overturned limb. Consequently, the reconstruction of the Stockchnubel-Gabbio synform has only a minor effect on the large-scale geometry of the nappe stack (see Fig. 5.3 C): the reconstruction leaves the Zermatt-Saas unit resting on top of the Monte Rosa nappe.

In the hangingwall of the Gornergrat-Furggtal shear zone, however, the Stockhorn-Trifflhorn antiform has developed a real overturned limb that has to be rotated back into an upright position. This accounts for the Stockhorn-Portjengrat unit to be situated structurally below the Monte Rosa nappe after the reconstruction (see Fig. 5.3 C). Another sliver of Portjengrat unit (named "Portjengrat-North" in Figs. 5.3 C & D, see ch. 5.3) is situated below the Stockhorn-Portjengrat unit, separated by Permo-Mesozoic meta-sediments of the Portjengrat unit and by Mesozoic calcareous micaschists of uncertain affiliation. These calcareous micaschists contain a large slice of ophiolite (located at the Tällihorn south crest in Zwischbergental, see ch. 4.2.4), which is considered to be derived from the Antrona ophiolitic unit. For this reason, the Antrona unit has been extrapolated as far as to this location in the reconstruction in Fig. 5.3 C & D, regardless of the affiliation of the calcareous micaschists.

The reconstruction of the Mittaghorn synform, the Mischabel backfold and the displacement along the Portjengrat shear zone account for the Siviez-Mischabel nappe to be originally situated below the Portjengrat-Stockhorn unit (Fig. 5.3 C).

5.3 Reconstruction of D1/D2 structures

The restoration of the major D4 and D3 thrusts and folds (Fig. 5.3 C & D) results in a triangle structure, in which the pile of continental nappes is wedged between the ophiolitic units, with the Zermatt-Saas unit on top and the Antrona unit below. The major lower detachment horizon is located at the boundary of the continental units and the Antrona unit. Accordingly, the continental units are separated by the adjacent weak sedimentary series of the continental nappes (Furgg zone and Permo-Mesozoic sediments including the calcareous micaschists) and the ophiolitic Antrona unit (calcareous micaschists and serpentinites).

The mafic slice of Antrona unit that is situated in the Furgg zone between the Monte Rosa nappe and the Portjengrat-Stockhorn unit correlates to the core of the D1 Loranco antiform (see ch. 4.2.6). As described in ch. 4.1 and 4.2, such isoclinal folds formed contemporaneously with N-directed nappe stacking (D1/D2).

To distinguish between the continental sliver between the Portjengrat-Stockhorn unit and the Siviez-Mischabel nappe without having to introduce yet another new tectonic unit, this sliver was named "Portjengrat-North" unit. The situation in this structural level between the Portjengrat-Stockhorn unit and the "Portjengrat-North" unit is similar. Although the separating slice of Antrona mafics does not reach very far between the two continental units, the two continental units are still separated by thin slices of Permo-Mesozoic sedimentary cover.

The situation in the structurally deeper level between the sliver of "Portjengrat-North" unit

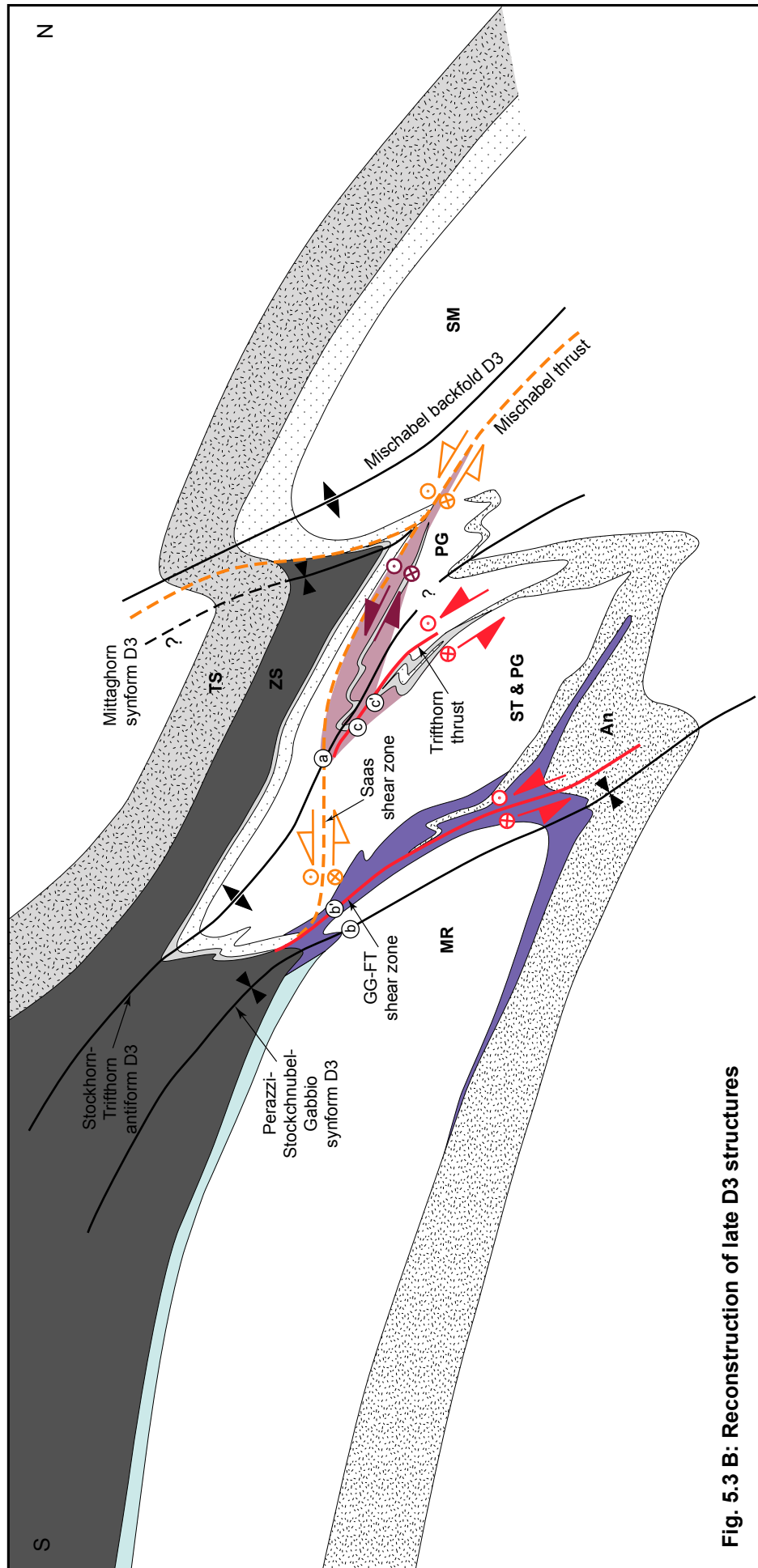


Fig. 5.3 B: Reconstruction of late D3 structures

and the structurally lower Siviez-Mischabel nappe looks similar. Again the two continental units are separated by a mafic slice of Antrona unit and by thin slices of Permo-Mesozoic sedimentary cover (see geological map, sheet Simplon, Bearth, 1972, 1973). However, this area has not been investigated in the present study.

A qualitative palinspastic reconstruction of the described D1/D2 folds and associated thrusts (schematically illustrated in Fig. 5.3 D) places all continental units into the same structural level. As described in ch. 3.2, the trace element distribution of metabasaltic intrusions from the continental tectonic units and of metabasalts from the ophiolitic tectonic units supports this tectonic palaeogeographic reconstruction. As a result, metabasalts from the Furgg zone and from the Permo-Mesozoic sedimentary cover of the Stockhorn-Portjengrat unit & northern Monte Rosa nappe were found to have a very similar trace element distribution (transitional-type MOR basalts). Therefore, the Furgg zone was considered as the high-strain equivalent of the Permo-Mesozoic cover of the Stockhorn-Portjengrat unit and Monte Rosa nappe, that was folded with the adjacent continental basement during nappe stacking (D1/ D2). As metabasalts from the Zermatt-Saas and the Antrona unit exhibit a similar transitional-type MORB chemistry, the intrusion of basaltic dykes and sills into continental crust can be considered to be associated to spreading and the formation of new oceanic crust. The close chemical relation of metabasaltic intrusions from the northern Monte Rosa nappe and the Stockhorn-Portjengrat unit therefore serve as an argument for a neighboring position of the two continental tectonic units. As metabasalts from the southern Monte Rosa nappe exhibit a different chemical composition (plume-type MOR basalts), it is assumed that the Stockhorn-Portjengrat unit was located adjacent north of the Monte Rosa nappe.

Metabasalts from the Siviez-Mischabel nappe also exhibit a plume-type MOR basaltic composition. It is therefore assumed that the Siviez-Mischabel nappe was located farther from the source that produced the transitional-type MOR basalts. Whether the Siviez-Mischabel nappe was located north of the Stockhorn-Portjengrat unit (as suggested e.g. by Keller & Schmid, 2001) or south of the Monte Rosa nappe (as suggested by Froitzheim, 2001), cannot be decided on the base of the existing geochemical data alone.

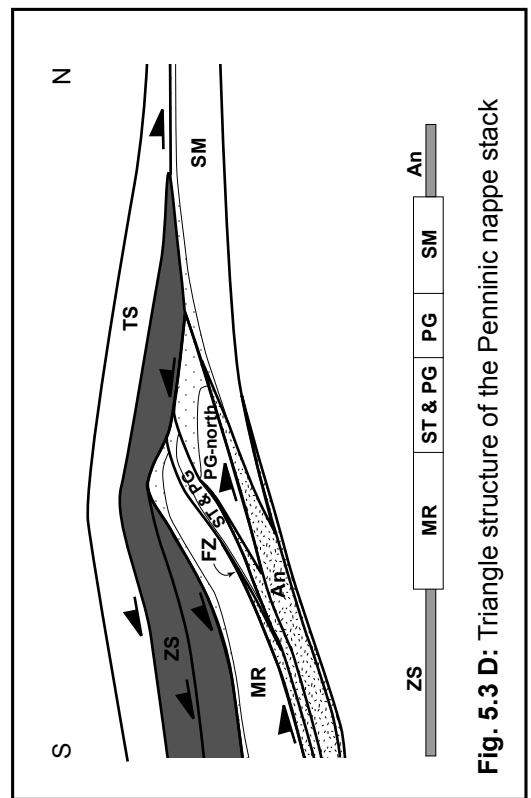
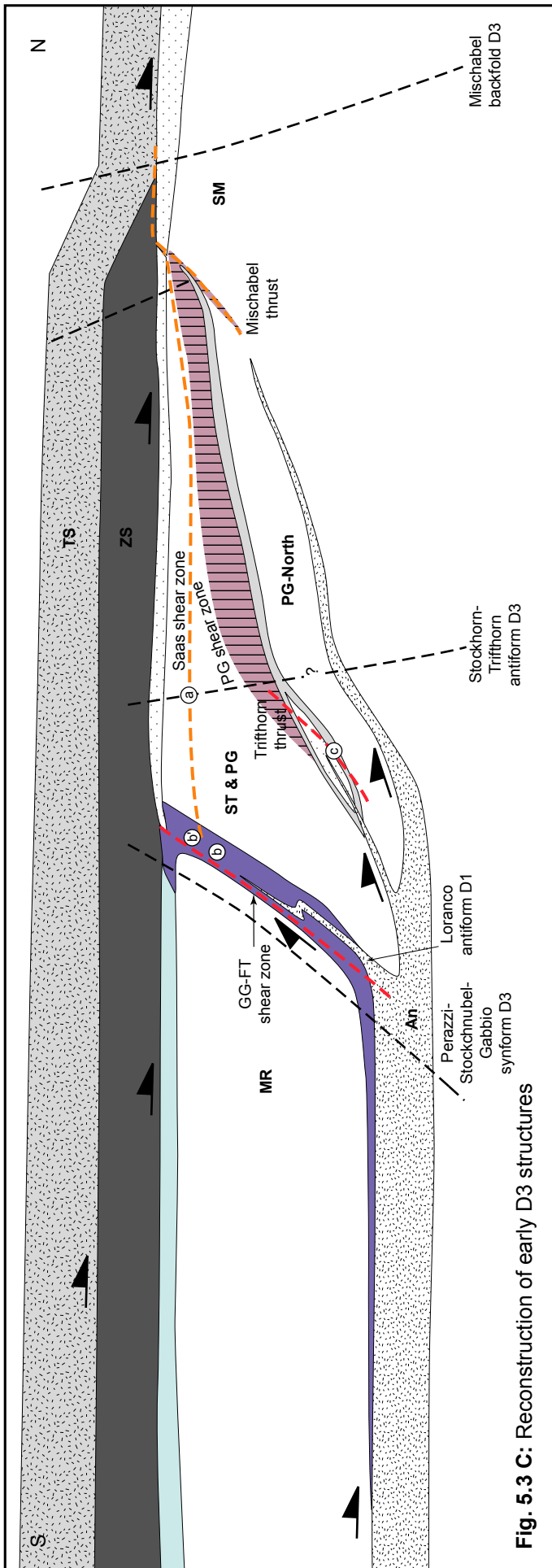
Zermatt-Saas and Antrona units - two individual or one continuous tectonic unit?

The question remaining is whether or not the Antrona and Zermatt-Saas ophiolitic units formed two individual or one continuous tectonic unit prior to nappe stacking. In the schematic drawing in Fig. 5.3 D, the Antrona and Zermatt-Saas ophiolitic units represent two individual units that are not linked near their northernmost terminations. The key area to search for such a connection is located north of the Weissmies in Saastal and Laggintal, and therefore outside the investigated area. However, in the geological map (sheet Simplon, Bearth, 1972, 1973), no such connection between Zermatt-Saas and Antrona unit is shown. The slivers of Antrona mafics situated between "Portjengrat-North" and Stockhorn-Portjengrat unit (i.e. at Zwischbergen pass), as well as between Stockhorn-Portjengrat unit and Monte Rosa nappe (i.e. the D1 Loranco antiform in the Furgg zone), cannot be connected with the Zermatt-Saas ophiolitic unit either. A connection between Antrona and Zermatt-Saas ophiolitic unit can therefore be excluded in the investigated area.

Pfeifer et al. (1989), who compared the geochemical composition of mafic rocks of the Zermatt-Saas and Antrona ophiolitic units, were not able to solve the problem unambiguously either. Although they found systematic differences between the two ophiolitic units, such differences may have been caused within two sectors of the same (Piemont-Ligurian) ocean basin as well as within two separate oceanic basins (Piemont-Ligurian and Valaisian).

Should the situation illustrated in Fig. 5.3 D be correct, then the Zermatt-Saas ophiolitic unit would be part of the Piemont-Ligurian ocean. The Monte Rosa nappe, Portjengrat-Stockhorn unit and Siviez-Mischabel nappe would be part of the Briançonnais microcontinent, and the Antrona ophiolitic unit would be part of the Valais ocean. This is the situation that was proposed in the model of Keller & Schmid (2001) and by many previous authors (Bearth, 1945a, 1954b; Escher et al., 1997; Laubscher, 1991; Dal Piaz, 1999; Schmid & Kissling, 2000).

The arrows indicating a southward shearing of the Zermatt-Saas ophiolitic unit during nappe



stacking in Fig. 5.3 D, refer to top to the S shear senses that have been found in numerous smaller shear zones in the Monte Rosa nappe close to the contact of the Zermatt-Saas unit - e.g. at the Monte Rosa refuge in Matternal and in the upper Valle d'Ayas. The metamorphic evolution of such a shear zone in white schists of the Monte Rosa nappe was described in detail from the upper Valle d'Ayas by Pawlig & Baumgartner (2001). The authors found that the top to the S-directed shear senses are associated to high pressure metamorphic conditions and therefore to early nappe stacking.

Consequently, Fig. 5.3 D illustrates a wedge structure formed by the Zermatt-Saas and the Antrona ophiolitic units, into which the continental units were thrust and stacked. Note, that the required opposite sense of shear may be found in any structural level close to the upper ophiolitic unit, which is represented by the Zermatt-Saas unit in the investigated area. However, the data published on such top to the S-directed movements associated with nappe stacking are not yet sufficient to prove the proposed wedge structure, and further investigation is needed.

The former position of the Antrona unit relative to the Zermatt-Saas unit could not be unraveled in this study. As there is no connection between the two ophiolitic tectonic units in the investigated area, the Antrona unit was considered as an individual tectonic unit positioned north of the continental tectonic units to represent former Valais oceanic crust. However, it is also conceivable that the Antrona unit formerly was the northernmost part of the Piemont-Ligurian ocean and evolved from the imbrication of this single oceanic nappe by N-directed ramp thrusting. The overthrusting of the newly formed Antrona slice by the Zermatt-Saas unit would then have been the first stage in the evolution of the Penninic nappe pile and have been succeeded by the formation of the triangle structure as described above.

6 Summary

Structural and kinematic evolution

The Monte Rosa region consists of Penninic nappes that represent the fossil high-grade accretionary wedge of the Western Alpine arc. It originated during mid- to late Eocene N- to NW-directed detachment and stacking of both pre-Permian continental crystalline upper crust and Permo-Mesozoic strata as well as late Jurassic oceanic crust along the central and western part of the convergent Adriatic plate margin (Laubscher 1991; Stampfli & Marchant, 1997; Escher et al., 1997; Dal Piaz, 1999; Schmid & Kissling, 2000). The Penninic nappe stack comprises the ophiolitic Zermatt-Saas and Antrona units, the continental Siviez-Mischabel and Monte Rosa nappe and the continental Portjengrat and Stockhorn unit.

Nappe stacking occurred contemporaneously with early exhumation from eclogite facies conditions ($T \sim 600^\circ \text{C}$, $p \sim 2.7 \text{ GPa}$, Barnicoat & Fry, 1986). In the absence of a marked competence contrast considering large-scale deformation, shortening was accommodated along broad ductile shear zones and by pervasive synmylonitic isoclinal and sheath folding (D1 and D2; D2 = Ragnoranda phase; e.g. Klein, 1978; Milnes et al., 1981; Lacassin & Mattauer, 1985). This involved all the units, regardless of lithology. The Furgg zone (FZ) and the intensely strained Monte Rosa cover and basement (ISMR) represent two of these ductile shear zones (see Figs. 5.1 & 5.2), that united slivers of all involved units to a complex and highly strained lithological association.

From the late Oligocene onwards, ongoing contraction led to a blocking of the further growth of the accretionary wedge and a reversal of nappe movement directions in the investigated area (D3 = Mischabel phase; e.g. Milnes et al., 1981; Escher et al., 1997). SE- to S-verging large-scale folds evolved along with dextral transpressive thrusts and shear zones (see Fig. 5.3). Early D3 contraction was accommodated by the broad and diffuse dextral transpressive Portjengrat shear zone, along which the Mischabel antiform supposedly nucleated as a fault propagation fold. Progressive shortening led to the formation of the SE-directed dextral transpressive Gornergrat-Furggtal shear zone further in the S, that supposedly evolved as an emergent forelimb thrust of the S- to SE-vergent Stockhorn-Trifhorn antiform. In the core of this antiform the Trifhorn thrust evolved as a blind thrust. In the footwall of the Gornergrat-Furggtal shear zone, the Gabbio synform supposedly also nucleated as a fault-bent fold.

Late D3 shortening was accommodated by the moderately W-dipping dextral transpressive Saas shear zone that crosscut all the older shear zones and served a major detachment in the investigated area. Along its branch thrust - the Mischabel thrust - the Mischabel antiform was thrust towards the ESE. Thereby the Mittaghorn synform supposedly nucleated as a thrust-bent fold in the footwall of the Mischabel thrust.

Further contraction finally led to an up-doming of the Penninic nappe pile by SE-directed large-scale folding (Vanzone antiform) and dextral transpressive thrusting related to the movements along the Periadriatic line system (D4 = Vanzone phase; e.g. Schmid et al., 1989; Dal Piaz, 2001). As a result, D3 structures were refolded or rotated. For example, the D3 Stockhorn synform was refolded to form the D3 Perazzi antiform south of the D4 Vanzone fold axial plane. Additionally, both the D3 Trifhorn thrust and the D3 Gornergrat-Furggtal shear zone were rotated into a steep-dipping position, enforcing a shift from thrusting to dextral strike-slip movements along those faults. The latest tonalite intrusions into the southern overturned limb of the Vanzone antiform ("Southern Steep Belt") at 25 Ma post-date the Vanzone phase and place a lower time marker to the SE-directed folding and up-doming of the Penninic nappe stack (Laubscher, 1983; Dal Piaz, 2001).

Geochemistry of meta-basalts

The continental tectonic units in the Monte Rosa region are characterized by the abundant occurrence of fragmented amphibolites. In order to determine their original magmatic signatures and therefore their mantle source and geotectonic origin, whole rock geochemical analyses of amphibolites from the continental and adjacent ophiolitic tectonic units were performed.

Mg numbers and Ni contents indicate that the amphibolites were derived from fractionated

magmas with compositions ranging from E- to N-MORB. Based on their Ni, Ti, REE and Nb systematics, the metabasalts from the ophiolitic Zermatt-Saas and Antrona units and from the Furgg zone and the continental Portjengrat unit are ascribed to a common origin. They represent a coherent suite ranging from T- to N-MORB. In contrast, amphibolites from the continental Siviez-Mischabel and Monte Rosa nappes were derived from enriched MORB and/or gabbroic precursors, which are not related to the metabasalts from the ophiolites, the Furgg zone or the Portjengrat unit.

The geochemical differences between the basalts of the ophiolitic Zermatt-Saas and Antrona units and the adjacent continental Furgg zone and the Portjengrat unit are very subtle. Most mafic rocks were derived from low to moderate degrees of melting of an N-MORB type mantle source. Some compositional parameters such as $(\text{Ce}/\text{Sm})_n$, Zr^* and $(\text{Nb}/\text{Zr})_n$ indicate a transition from T-MORB compositions in the continental units towards less enriched compositions in the ophiolitic units. The Y, Ti, V, and Zr concentrations are highly correlated in the metabasalts from the Furgg zone, whereas such inter-element correlations are less well defined in the metabasalts from the ophiolitic units. This renders an interpretation of most of the Furgg zone amphibolites as tectonically incorporated ophiolitic fragments unlikely. The data rather suggest that the distal continental units (Portjengrat unit and Furgg zone) and the nearby ophiolitic units were intruded by similar magmas. Since the Portjengrat unit gradually passes into the Furgg zone by an increase in displacement and the abundance of amphibolites, the Portjengrat and Furgg zone are interpreted as a formerly continuous tectonic unit. This unit is interpreted as the ocean-continent transition zone of the Briançonnais into the immediately adjacent oceanic Antrona unit. The paleogeographic position of the Antrona unit (Valais vs. Piemont-Liguria ocean), however, cannot be resolved from the geochemical data.

Palinspastic reconstruction

In a qualitative palinspastic reconstruction, the restoration of the D4 and late-D3 structures (D4 Vanzone antiform, late-D3 Saas shear zone and Mischabel thrust) leads to the combination of the Stockhorn and Portjengrat unit to form a continuous unit (Fig. 5.3 A & B). The restoration of the remaining D3 thrusts and folds (Fig. 5.3 C & D) results in a triangle structure, in which the pile of continental nappes is wedged between the ophiolitic units. The ophiolitic Zermatt-Saas unit represents the top and the ophiolitic Antrona unit the base of this triangle structure. Within this structure, the Monte Rosa nappe forms the southern- and structurally uppermost, and the Siviez-Mischabel nappe the northern- and structurally lowermost continental unit. The ductile and major lower detachment horizon is located at the boundary of the continental nappes and the ophiolitic Antrona unit, where the rheologically weak sedimentary cover of the continental nappes (Permo-Mesozoic sediments including calcareous micaschists) and the calcareous micaschists and serpentinites of the ophiolitic Antrona unit meet. Accordingly, tectonic slivers of all the involved lithologies can be found along the detachment.

Branch thrusts of this lower detachment, comprising a similar rock association, separate the continental units, e.g. the Furgg zone, that separates the Monte Rosa nappe from the Stockhorn-Portjengrat unit. A reconstruction of the displacement of the Furgg zone places the Monte Rosa nappe adjacent to the Stockhorn-Portjengrat unit. Since the Stockhorn-Portjengrat unit and the Monte Rosa nappe share a similar high-grade metamorphic evolution (see e.g. Le Bayon et al., 2001; Pawlig & Baumgartner, 2001), and since the Portjengrat unit and the Furgg zone share amphibolites that are derived from the same magmatic mantle source, the Monte Rosa nappe and the Stockhorn-Portjengrat unit were considered as a previously continuous tectonic unit.

In accordance to the structural significance of the Furgg zone, the highly strained Permo-Mesozoic sediments in Zwischbergental (e.g. D2 Weissmies folds, ch. 4.2.4) and also in Laggintal (see geological map, sheet Simplon; Bearth, 1972, 1973) may be regarded as such D1/D2 branch thrusts of the major lower detachment of the triangle structure. The reconstruction of these branch thrusts and the lower detachment places all continental units into the same structural level north of the ophiolitic Zermatt-Saas unit (Fig. 5.3 D). As the Zermatt-Saas unit represents Piemont-Ligurian oceanic crust, the continental units are supposed to have formed part of the Briançonnais microcontinent. The former position of the low-grade metamorphic Siviez-Mischabel nappe, however, was not investigated further in this study and remains unclear - either it was situated directly adjacent

to the Monte Rosa-Stockhorn-Portjengrat unit or in a distance farther north.

The former position of the Antrona unit relative to the Zermatt-Saas unit is not secured either. As there is no connection between the two ophiolitic tectonic units in the investigated area, the Antrona unit was considered as an individual tectonic unit positioned north of the continental tectonic units to represent former Valais oceanic crust. However, it is also conceivable that the Antrona unit formerly was the northernmost part of the Piemont-Ligurian ocean and evolved from the imbrication of this single oceanic nappe by N-directed ramp thrusting. The overthrusting of the newly formed Antrona slice by the Zermatt-Saas unit would then have been the first stage in the evolution of the Penninic nappe pile and have been succeeded by the formation of the triangle structure as described above.

7 References

- Amato J., Baumgartner L., Johnson C., and Beard B. (1997):** Tertiary high-pressure metamorphism at Lago di Cignaga, Italy, as determined by Sm-Nd dating of eclogite. *Terra nova* **9**, 30-31.
- Amato J.M., Johnson C.M., Baumgartner L.P., and Beard B.L. (1999):** Rapid exhumation of the Zermatt-Saas ophiolite deduced from high-precision Sm-Nd and Rb-Sr geochronology. *Earth Planet. Sci. Lett.* **171** (3), 425-438.
- Argand E. (1911):** Les nappes de recouvrement des Alpes Pennines et leurs prolongements structuraux. *Beitr. geol. Karte Schweiz* **31**, 1-26.
- Bacher C. (2002):** Strukturen und Metamorphose in der Furggzone (Furggtal bei Saas Almagell, Wallis). Unpubl. diploma thesis, University of Basel, 83 pp.
- Bagnoud A., Wernli R., and Sartori M. (1998):** Discovery of Paleogene planctonic foraminifers in the Sion-Courmayeur zone at Sion (Valais, Switzerland). *Eclogae geol. Helv.* **91** (3), 421-429.
- Barnicoat A.C. and Fry N. (1986):** High-pressure metamorphism of the Zermatt-Saas ophiolite zone, Switzerland. *J. Geol. Soc. London* **143** (4), 607-618.
- Barnicoat A.C., Rex D.C., Guise P.G., and Cliff R.A. (1995):** The timing and nature of greenschist facies deformation and metamorphism in the upper Pennine Alps. *Tectonics* **14** (2), 279-293.
- Baud A. (1972):** Observations et hypothèses sur la géologie de la partie radicale des Préalpes médianes. *Eclogae geol. Helv.* **65**, 43-55.
- Baud A. and Septefontaine M. (1980):** Présentation d'un profile palinspastique de la nappe des Préalpes médianes en Suisse occidentale. *Eclogae geol. Helv.* **73** (2), 651-660.
- Bearth P. (1942):** Über die Granitgneise der Monte-Rosa (Mischabel)- Decke. *Schweiz. Mineral. Petrogr. Mitt.* **22** (2), 378-379.
- Bearth P. (1945a):** Über das Verhältnis von Kristallisation und Bewegung in der Monte Rosa-Bernhard-(Mischabel)-Decke. *Schweizer. Mineral. Petrogr. Mitt.* **25** (2), 537-538.
- Bearth P. (1945b):** Über spätalpine granitische Intrusionen in der Monte Rosa-Bernhard- Decke. *Schweizer. Mineral. Petrogr. Mitt.* **25** (1), 1-22.
- Bearth P. (1948):** Über Albitisierung im Altkristallin des Monte Rosa. *Schweiz. Mineral. Petrogr. Mitt.* **28** (1), 140-145.
- Bearth P. (1949):** Bemerkungen zur Metamorphose und Granitbildung im Monte Rosa- Gebiet. *Schweiz. Mineral. Petrogr. Mitt.* **29** (1), 193-197.
- Bearth P. (1952):** Geologie und Petrographie des Monte Rosa. *Beitr. Geol. Karte Schweiz (Neue Folge)* **96**, 1-94.
- Bearth P. (1953a):** Blatt Zermatt, Geologischer Atlas der Schweiz. Nr. 29. 1:25'000. Schweiz. Geol. Kommission, Basel.
- Bearth P. (1953b):** Erläuterungen Blatt Zermatt, Geologischer Atlas der Schweiz. Nr. 29. 1:25'000. Schweiz. Geol. Kommission, Basel.
- Bearth P. (1954a):** Blatt Monte Moro, Geologischer Atlas der Schweiz. Nr. 30. 1:25'000. Schweiz. Geol. Kommission, Basel.
- Bearth P. (1954b):** Blatt Saas, Geologischer Atlas der Schweiz. Nr. 31. 1:25'000. Schweiz. Geol. Kommission, Basel.
- Bearth P. (1956):** Geologische Beobachtungen im Grenzgebiet der lepontinischen und penninischen Alpen. *Eclogae geol. Helv.* **49** (2), 279-290.
- Bearth P. (1957):** Erläuterungen Blatt Saas und Monte Moro, Geologischer Atlas der Schweiz. Nr. 30, 31. 1:25'000. Schweiz. Geol. Kommission, Basel.
- Bearth P. (1964a):** Blatt Randa, Geologischer Atlas der Schweiz. Nr. 43. 1:25'000. Schweiz. Geol. Kommission, Basel.
- Bearth P. (1964b):** Erläuterungen Blatt Randa, Geologischer Atlas der Schweiz. Nr. 43. 1:25'000. Schweiz. Geol. Kommission, Basel.
- Bearth P. (1967):** Bericht über die Exkursion der Schweizerischen Mineralogischen und Petrographischen Gesellschaft nach Zermatt. *Beitr. Geol. Karte Schweiz (Neue Folge)* **132** (1), 15-26.
- Bearth P. (1972):** Blatt Simplon, Geologischer Atlas der Schweiz. Nr. 61. 1:25'000. Schweiz. Geol. Kommission, Basel.
- Bearth P. (1973):** Erläuterungen Blatt Simplon, Geologischer Atlas der Schweiz. Nr. 61. 1:25'000. Schweiz. Geol. Kommission, Basel.
- Bearth P. (1976):** Zur Gliederung der Bündnerschiefer in der Region von Zermatt. *Eclogae geol. Helv.* **69** (1), 149-161.
- Bearth P. (1978a):** Blatt St. Niklaus, Geologischer Atlas der Schweiz. Nr. 71. 1:25'000. Schweiz. Geol. Kommission, Basel.
- Bearth P. (1978b):** Erläuterungen Blatt St. Niklaus, Geologischer Atlas der Schweiz. Nr. 71. 1:25'000. Schweiz. Geol. Kommission, Basel.
- Bearth P. and Schwander H. (1981):** The post-Triassic sediments of the ophiolite zone Zermatt-Saas Fee and the associated manganese mineralizations. *Eclogae geol. Helv.* **74** (1), 189-205.
- Bearth P. and Stern W. (1971):** Zum Chemismus der Eklogite und Glaukophanite von Zermatt. *Schweiz. Mineral. Petrogr. Mitt.* **51**, 349 - 359.
- Bearth P. and Stern W. (1979):** Zur Geochemie von Metapillows der Region Zermatt-Saas. *Schweiz. Mineral. Petrogr. Mitt.* **59** (3), 349-373.
- Beccaluva L., Dal Piaz G.V., and Macciotta G. (1984):** Transitional to normal MORB affinities in ophiolitic metabasites from Zermatt-Saas, Combin and Antrona units, Western Alps. *Geol. en Mijnbouw* **63**, 165-177.
- Bill, M., Nägler, T.F. and Masson, H. (2000):** Geochemistry, Sm-Nd and Sr isotopes of mafic rocks from the earliest oceanic crust of Alpine Tethys. *Schweiz. Mineral. Petrogr. Mitt.* **80**, 131-145.
- Blumenthal M.M. (1952):** Beobachtungen über den Bau und Verlauf der Muldenzone von Antrona zwischen der Walliser Grenze und dem Locarnese. *Eclogae geol. Helv.* **45**, 220-251.

- Bucher, K. and Frey, M. (1994):** Petrogenesis of metamorphic rocks. Springer, Berlin. 318 pp.
- Boynton W.V. (1984):** Cosmochemistry of the rare earth elements: meteorite studies. In: Henderson P. (ed.): Developments in Geochemistry 2 - Rare Earth Element Geochemistry. Elsevier, Amsterdam, 63-114.
- Carreras J., Estrada A., and White S. (1977):** The effects of folding on the c-axis fabrics of a quartz mylonite. *Tectonophysics* **39** (1-3), 3-24.
- Carrupt E. and Schlup M. (1998):** Métamorphisme et tectonique du versant sud du Val Bognanco (Pennique, Alpes italiennes). *Bull. Soc. Vaud. Sci. Nat.* **86** (1), 29-59.
- Casey J.F. (1997):** Comparison of major- and trace element geochemistry of abyssal peridotites and mafic plutonic rocks with basalts from the MARK region of the Mid-Atlantic Ridge. *Proc. Ocean. Drill. Prog. Sci. Res.* **153**, 181-241.
- Chadwick B. (1974):** Glaucofane Fabric in the Cover of the Monte Rosa Nappe, Zermatt-Saas Fee, Southwest Switzerland. *Geol. Soc. Am. Bull.* **85** (6), 907-909.
- Chopin C. (1981):** Talc-phengite; a widespread assemblage in high-grade pelitic blueschists of the Western Alps. *J. Petrol.* **22** (4), 628-650.
- Chopin C. and Monie P. (1984):** A unique magnesiochloritoid-bearing, high-pressure assemblage from the Monte Rosa, Western Alps; petrologic and ⁴⁰Ar- ³⁹Ar radiometric study. *Contr. Min. Petrol.* **87** (4), 388-398.
- Colombi A. (1989):** Métamorphisme et géochimie des roches mafiques des Alpes ouest-centrales (géoprofil Viège-Domodossola-Locarno). *Mémoires de Géologie* 4. Imprive S.A., Lausanne, 216 pp.
- Coward M.P. and Dietrich D. (1989):** Alpine tectonics - an overview. In: Coward M.P. and Dietrich D. (eds): *Alpine tectonics*. 45. Spec. Pub. Geol. Soc. London, 1-29.
- Cullers R.L. and Graf J.L. (1984):** Rare earth elements in igneous rocks of the continental crust: predominantly basic and ultrabasic rocks. In: Henderson P. (ed.): *Developments in Geochemistry 2 - Rare Earth Element Geochemistry*. Elsevier, Amsterdam, 237 - 274.
- Dal Piaz G.V. (1964):** Il cristallino antico del versante meridionale del Monte Rosa paraderivati a prevalente metamorfismo alpino. *Rendiconti Soc. Min. Italiana Anno XX*, 101-135; 4 Tav.
- Dal Piaz G.V. (1965):** La formazione mesozoica dei calcescisti con pietre verdi fra la Valsesia e la Valtournanche ed i suoi rapporti strutturali con il ricoprimento Monte Rosa e con la zona Sesia-Lanzo. *Boll. Soc. Geol. Italiana* **84** (1), 67-104.
- Dal Piaz G.V. (1966):** Gneiss ghiandoni, marmi ed anfiboliti antiche del ricoprimento Monte Rosa nell' alta Valle d'Ayas. *Beitr. Geol. Karte Schweiz (Neue Folge)* **132** (1), 103-132.
- Dal Piaz G.V. (1971):** Nuovi ritrovamenti di cianite alpina nel cristallino antico del Monte Rosa. *Rend. Soc. Italiana Min. Petrol.* **27** (2), 437-477.
- Dal Piaz G.V. (1999):** The Austroalpine-Piemont nappe stack and the puzzle of Alpine Tethys. *Mem. Sci. Geol.* **51** (1), 155-176.
- Dal Piaz G.V. (2001):** Geology of the Monte Rosa massif: historical review and personal comments. *Schweiz. Mineral. Petrogr. Mitt.* **81**, 275-303.
- Dal Piaz G.V. and Lombardo B. (1986):** Early Alpine eclogite metamorphism in the Penninic Monte Rosa-Gran Paradiso basement nappes of the northwestern Alps. *Blueschists and Eclogites. Geol. Soc. Am. Mem.* **164**, 249-265.
- Desmurs, L., Müntener, O. and Manatschal, G. (2002):** Onset of magmatic accretion within a magma-poor rifted margin: A case study from the Platta ocean-continent transition, Eastern Switzerland. *Contrib. Mineral. Petrol.* **144**, 365-382.
- Deville E., Fudral S., Lagabrielle Y., Marthaler M., and Sartori M. (1992):** From oceanic closure to continental collision: a synthesis of the 'Schistes lustrés' metamorphic complex of the Western Alps. *Geol. Soc. Am. Bull.* **104** (2), 127-139.
- Dostal J. and Capedri S. (1979):** Rare earth elements in high-grade metamorphic rocks from the Western Alps. *Lithos* **12**, 41 - 49.
- Drake M.J. and Weill D.F. (1975):** Partition of Sr, Ba, Ca, Y, Eu²⁺, Eu³⁺, and other REE between plagioclase feldspar and magmatic liquid: an experimental study. *Geochim. Cosmochim. Acta* **39**, 689-712.
- Dubach K. (1998):** Die Grenzzone von Portjengrat- Einheit und Siviez-Mischabel- Decke im Almagellertal, Wallis. Unpubl. Diploma thesis, University of Basel, 61 pp.
- Eisele J., Geiger S., and Rahn M. (1997):** Chemical characterization of metabasites from the Turtmann valley (Valais, Switzerland): implications for their protoliths and geotectonic origin. *Schweiz. Mineral. Petrogr. Mitt.* **77** (3), 403-417.
- Engi M., Scherrer N.C., and Burri T. (2001):** Metamorphic evolution of pelitic rocks of the Monte Rosa nappe: Constraints from petrology and single grain monazite age data. *Schweiz. Mineral. Petrogr. Mitt.* **81**, 305-328.
- Escher A. (1988):** Structure de la nappe du Grand Saint-Bernard entre le Val de Bagnes et les Mischabel. *Geol. Berichte Landeshydrol. geol.* **7**, 3-26.
- Escher A., Hunziker J.-C., Marthaler M., Masson H., Sartori M., and Steck A. (1997):** Geologic framework and structural evolution of the western Swiss-Italian Alps. In: Pfiffner O.A., Lehner P., Heitzmann P., Müller S., and Steck A. (eds): *Deep structure of the Swiss Alps: Results from NRP 20*. Birkhäuser, Basel, 205-221.
- Escher A., Masson H., and Steck A. (1988):** Coupes géologiques des Alpes occidentales suisses. *Mém. Géol. Lausanne, Rapp. géol. serv. hydrol. géol. nat.* **2**, 1-11, incl. 1 map, 2 tables, 1 plate.
- Escher A., Masson H., and Steck A. (1993):** Nappe geometry in the western Swiss Alps. *J. Struc. Geol.* **15** (3-5), 501-509.
- Escher A. and Sartori M. (1991):** The geology of the Zermatt - Gornergrat area. *NFP 20 Bull.* **9**, 5-11.
- Evans B.W., Trommsdorff V., and Goles G.G. (1981):** Geochemistry of high-grade eclogites and metarodngites from the Central Alps. *Contr. Min. Petrol.* **76**, 301-311.

- Frey M., Hunziker J.C., O'Neil J.R., and Schwander H.W. (1976):** Equilibrium-disequilibrium relations in the Monte Rosa granite, Western Alps; petrological, Rb-Sr and stable isotope data. *Contrib. Mineral. Petrol.* **55** (2), 147-179.
- Froitzheim N. (2001):** Origin of the Monte Rosa nappe in the Pennine Alps - A new working hypothesis. *Geol. Soc. Am. Bull.* **113** (5), 604-614.
- Fügenschuh B., Loprieno A., Ceriani S., Schmid S.M. (1999):** Structural analysis of the Subbrianconnais and Valais units in the area of Moutiers (Savoy, Western Alps); paleogeographic and tectonic consequences. In: Engi M., Matter A., Pfiffner A., Trümpy R., Berger W.H. (eds.): *Geological dynamics of alpine-type mountain belts; ancient and modern.* *International Journal of Earth Sciences* **88** (2), 201-218.
- Gebauer D. (1999):** Alpine geochronology of the Central and Western Alps: new constraints for a complex geodynamic evolution. *Schweiz. Mineral. Petrogr. Mitt.* **79** (1), 191-208.
- Gelinas L., Mellinger M., and Trudel P. (1982):** Archaean mafic metavolcanics from the Rouyn-Noranda district, Abitibi greenstone belt, Quebec. 1. Mobility of the major elements. *Canad. J. Earth Sci.* **19**, 2258-2275.
- Grauch R.I. (1989):** Rare earth elements in metamorphic rocks. In: Lipin B.R. and McKay G.A. (eds): *Geochemistry and mineralogy of rare earth elements.* 21. *Mineral. Soc. America, Washington D.C.*, 147-167.
- Güller A. (1947):** Zur Geologie der südlichen Mischabel- und der Monte Rosa- Gruppe. *Eclogae geol. Helv.* **40**, 39-161.
- Hellwig D. and Vogler W.S. (2001)** Fluids do it! Shear zone phyllonitisation as a key process for the emplacement of the Dent Blanche nappe, Western Alps. *Deformation Mechanisms, Rheology & Tectonics 2001*, Noordwijkerhout, The Netherlands, **71**.
- Henderson P. (1984):** General geochemical properties and abundances of the rare earth elements. In: Henderson P. (ed.): *Developments in Geochemistry 2 - Rare Earth Element Geochemistry.* Elsevier, Amsterdam, 1-32.
- Huang T.-K. (1935a):** Carte géologique de la région Weissmies-Portjengrat (Valais). 1:25'000. *Schweiz. Geol. Kommission, Basel.*
- Huang T.-K. (1935b):** Etude géologique de la région Weissmies-Portjengrat (Valais). *Bull. Soc. Neuchatel Sci. Nat.* **60**, 3-76.
- Humphris S.E. (1984):** The mobility of the rare earth elements in the crust. In: Henderson P. (ed.): *Developments in Geochemistry 2 - Rare Earth Element Geochemistry.* Elsevier, Amsterdam, 317-342.
- Hunziker J.-C. (1969):** Rb-Sr Altersbestimmung aus den Walliser Alpen. *Hellglimmer und Gesamtgesteinsalters-Bestimmung.* *Eclogae geol. Helv.* **62**, 527-542.
- Hunziker J.C. (1970):** Polymetamorphism in the Monte Rosa, Western Alps. *Eclogae geol. Helv.* **63** (1), 151-161.
- Irvine T.N. and Baragar W.R.A. (1971):** A guide to the chemical classification of the common volcanic rocks. *Canad. J. Earth Sci.* **8**, 523-548.
- Jaboyedoff M., Béglé P., and Lobrinus S. (1996):** Stratigraphie et évolution structurale de la zone de Furgg, au front de la nappe du Mont-Rose. *Bull. Soc. Vaudoise Sci. Nat.* **84** (2), 191-210.
- Jeanbourquin P. and Burri M. (1991):** Les métasédiments du Penninique inférieur dans la région de Brigue-Simplon. *Lithostratigraphie, structure et contexte géodynamique dans le bassin Valaisan.* *Eclogae geol. Helv.* **84** (2), 463-481.
- Keller L. (2000):** Kinematik der duktilen Scherung an der Front der Monte Rosa Decke (Val Loranco, Italien). Unpubl. diploma thesis, University of Basel, 90 pp.
- Keller L. and Schmid S.M. (2001):** On the kinematics of shearing near the top of the Monte Rosa nappe and the nature of the Furgg zone in the Val Loranco (Antrona valley, N. Italy): tectono-metamorphic and palaeogeographical consequences. *Schweiz. Mineral. Petrogr. Mitt.* **81**, 347-367.
- Klein J.A. (1978):** Post-nappe folding southeast of the Mischabelrückfalte (Pennine Alps) and some aspects of the associated metamorphism. *Leidse geol. Medel.* **51** (2), 233-312.
- Kramer J., Abart R., Müntener O., Schmid S.M., Stern W.-B. (2003):** Geochemistry of metabasalts from ophiolitic and adjacent distal continental margin units: Evidence from the Monte Rosa region (Swiss and Italian Alps). *Swiss Bull. Mineral. Petrol.* **83** (2), 217-240.
- Lacassin R. (1984):** Etude des mécanismes de déformation dans le versant nord de la nappe du Mont Rose (Alpes Suisses) et relation avec les grands chevauchements. Unpubl. PhD thesis, Université des Sciences et Technique du Languedoc, 230 pp.
- Lacassin R. (1987):** Kinematics of ductile shearing from outcrop to crustal scale in the Monte Rosa Nappe, Western Alps. *Tectonics* **6** (1), 69-88.
- Lacassin R. and Mattauer M. (1985):** Kilometre-scale sheath fold at Mattmark and implications for transport directions in the Alps. *Nature* **315** (6022), 739-742.
- Laduron D. and Merlyn M. (1974):** Evolution structurale et métamorphique de l'antiforme de Vanzone (Valle Anzasca et Valle Antrona; province de Novara, Italie). *Bull. Soc. Geol. France* **16** (3), 264-265.
- Laubscher H. (1983):** The late alpine (periadriatic) intrusions and the Insubric line. *Mem. Soc. Geol. It.* **26**, 21-30.
- Laubscher H. (1991):** The arc of the Western Alps today. *Eclogae geol. Helv.* **84** (3), 631-659.
- Le Bas M.J., Le Maître R.W., Streckeisen A., and Zanettin B. (1986):** A chemical classification of volcanic rocks based on the total alkali-silica diagram. *J. Petrol.* **27**, 745-750.
- Le Bayon R., Schmid S.M., and De Capitani C. (2001):** The metamorphic evolution of the Monte Rosa nappe and its relation to exhumation by fore- and back-thrusting in the Western Alps. *Geol. Paläont. Mitt. Innsbruck* **25**, 132-133.
- Lemoine M. and Trümpy R. (1987):** Pre-oceanic rifting in the Alps. *Tectonophysics* **133**, 305-320.
- Liati A., Gebauer D., Froitzheim N., and Fanning M. (2001):** U-Pb SHRIMP geochronology of an amphibolitized eclogite and an orthogneiss from the Furgg zone (Western Alps) and implications for its geodynamic evolution. *Schweiz. Mineral. Petrogr. Mitt.* **81**, 379-393.

- Lister, G.S. and Williams, P.F. (1979):** Fabric development in shear zones: theoretical controls and observed phenomena. *J. Struc. Geol.* **1**, 283-297.
- Mac Geehan P.J. and Mac Lean W.H. (1980):** An Archaean sub-seafloor geothermal system, 'calc-alkali' trends, and massive sulphide genesis. *Nature* **286**, 767-771.
- Mancktelow N. (1990):** The Simplon fault zone. *Beitr. geol. Karte Schweiz (Neue Folge)* 163. *Landeshydrol. -geol. und Schweiz. geol. Kommission*, 1-74 pp.
- Mancktelow N.S. (1992):** Neogene lateral extension during convergence in the Central Alps; evidence from interrelated faulting and backfolding around the Simplonpass; Switzerland. *Tectonophysics* **215**, 295-317.
- Mancktelow N.S. and Pavlis T.L. (1994):** Fold-fault relationships in low-angle detachment systems. *Tectonics* **13** (2), 668-685.
- Markley M.J., Teyssier C., and Caby R. (1994):** Imbricate thrusting within the Siviez-Mischabel Nappe, Switzerland. *Abs. Geol. Soc. Am.* **26** (7), 316.
- Markley M.J., Teyssier C., Cosca M.A., Caby R., Hunziker J.C., and Sartori M. (1998):** Alpine deformation and ⁴⁰Ar/³⁹Ar geochronology of synkinematic white mica in the Siviez-Mischabel nappe, western Pennine Alps, Switzerland. *Tectonics* **17** (3), 407-425.
- Marthaler M. (1981):** Découverte de foraminifères planctoniques dans les "schistes lustrés" de la pointe de Tourtemagne (Valais). *Bull. Soc. Vaud. Sci. Nat.* **75**, 171-178.
- Marthaler M. (1984):** Géologie des unités penniniques entre le Val d'Anniviers et le Val de Tourtemagne (Valais, Suisse). *Eclogae geol. Helv.* **77** (2), 395-448.
- Marthaler M. and Stampfli G.M. (1989):** Les Schistes lustrés à ophiolites de la nappe du Tsaté: un ancien prisme d'accrétion issu de la marge active apulienne? *Schweiz. Mineral. Petrogr. Mitt.* **69**, 211-216.
- Mattirolo E., Novarese V., Franchi S., and Stella A. (1912):** Foglio Monte Rosa, Carta Geologica d' Italia. No. 29. 1: 100'000. *Serv. Geol. Italiano, Novara.*
- Mattirolo E., Novarese V., Franchi S., and Stella A. (1927):** Foglio Varallo, Carta geologica d' Italia. No. 30. 1:100'000. *Serv. Geol. Italiano, Roma.*
- Means, W.D. (1995):** Shear zones and rock history. *Tectonophysics* **238**, 229-254.
- Menzies, M. and Hawkesworth, C.J. (1987):** Upper mantle processes and composition. In: Nixon, P. (ed.): *Mantle xenoliths*. 725-738. *Wiley, New York.*
- Meyer J. (1983):** Mineralogie und Petrologie des Allalingsabbros. Unpubl. PhD thesis, University of Basel, 331 pp.
- Middlemost E.A.K. (1975):** The basalt clan. *Earth Sci. Rev.* **11**, 337-364.
- Milnes A.G., Greller M., and Müller R. (1981):** Sequence and style of major post-nappe structures, Simplon-Pennine Alps. *J. Struc. Geol.* **3** (4), 411-420.
- Mosar J., Stampfli G.M., and Girod F. (1996):** Western Préalpes Médiannes Romandes: Timing and structure. A review. *Eclogae geol. Helv.* **89** (1), 389-425.
- Mottl M.J. (1983):** Metabasalts, axial hot springs, and the structure of hydrothermal systems at mid-ocean ridges. *Geol. Soc. Am. Bull.* **94**, 161-180.
- Müller C. (1989):** Albitisation of the Zermatt area, Western Alps. Unpubl. PhD thesis, University of Basel, 285 pp.
- Müller R. (1983):** Die Struktur der Mischabelfalte (Penninische Alpen). *Eclogae geol. Helv.* **76** (2), 391-416.
- Novarese V. and Stella A. (1913):** Foglio Domodossola, Carta geologica d'Italia. No. 15. 1:100'000. *Serv. Geol. Italiano, Novara.*
- Oskarsson M., Sigvaldason G.E., and Steinthorsson S. (1982):** A dynamic model of rift zone petrogenesis and the regional petrology of Iceland. *J. Petrol.* **23**, 28-74.
- Passchier C.W. (1983):** The reliability of asymmetric c-axis fabrics of quartz to determine sense of vorticity. *Tectonophysics* **99**, T9-T18.
- Passchier C.W. and Simpson C. (1986):** Porphyroclast systems as kinematic indicators. *J. Struc. Geol.* **8** (8), 831-843.
- Passchier C.W. and Trouw R.A.J. (1996):** *Microtectonics*. Springer, Heidelberg, 289 pp.
- Pawlig S. and Baumgartner L.P. (2001):** Geochemistry of a talc-kyanite-chloritoid shear zone within the Monte Rosa granite, Val d'Ayas, Italy. *Swiss Bull. Min. Petrol.* **81** (3), 329-346.
- Pearce J.A. (1976):** Statistical analysis of major element patterns in basalts. *J. Petrol.* **17**, 15 - 43.
- Pearce J.A. (1982):** Trace element characteristics of lavas from destructive plate boundaries. In: Thorpe R.S. (ed.): *Andesites - Orogenic andesites and related rocks*. John Wiley & Sons, Chichester, 525-548.
- Pearce J.A. (1983):** Role of the sub- continental lithosphere in magma genesis at active continental margins. In: Hawkesworth C.J. and Norry M.J. (eds.): *Continental basalts and mantle xenoliths*. Shiva Publishing Ltd., Cheshire, 230-250.
- Pennacchioni G. and Guermani A. (1993):** The Mylonites of the Austroalpine Dent Blanche nappe along the northwestern side of the Valpelline valley (Italian Western Alps). *Mem. Sci. Geol.* **45**, 37-55.
- Pfeifer H.R., Colombi A., and Ganguin J. (1989):** Zermatt-Saas and Antrona Zone: A petrographic and geochemical comparison of polyphase metamorphic ophiolites of the West-Central Alps. *Schweiz. Mineral. Petrogr. Mitt.* **69** (2), 217-236.
- Philpotts A.R. (1990):** *Principles of igneous and metamorphic petrology*. Prentice-Hall Int. (UK) Ltd., London, 498 pp.
- Presnall D.C., Dixon J.R., O'Donnell T.H., and Dixon S.A. (1979):** Generation of mid-ocean ridge tholeiites. *J. Petrol.* **20** (1), 3-35.
- Puschnig, A.R. (2000):** The oceanic Forno Unit (Rhetic Alps). *Eclogae Geol. Helv.* **93**: 103-124.
- Rampone, E., Hofmann, A.W. and Raczek, I. (1998):** Isotopic contrasts within the Internal Liguride Ophiolite (N. Italy): the lack of a genetic mantle-crust link. *Earth Planet. Sci. Lett.* **163**, 175-189.
- Ramsay J.G. and Huber M.I. (1987):** *The Techniques of Modern Structural Geology*. 1: Stress and strain, 2: Folds and

- fractures. Academic Press, 700 pp.
- Reddy S.M., Wheeler J., and Cliff R.A. (1999):** The geometry and timing of orogenic extension: An example from the Western Italian Alps. *J. Metamorphic Geol.* **17** (5), 573-589.
- Reinecke T. (1991):** Very-high-pressure metamorphism and uplift of coesite-bearing metasediments from the Zermatt-Saas zone, Western Alps. *Europ. J. Mineral.* **3** (1), 7-17.
- Reinecke T. (1995):** Ultrahigh- and high-pressure metamorphic rocks of the Zermatt-Saas zone, Western Alps - record of burial and exhumation paths. *Bochumer geol. geotech. Arb.* **44**, 152-157.
- Reinecke T. (1998):** Prograde high-to ultrahigh-pressure metamorphism and exhumation of oceanic sediments at Lago di Cignana, Zermatt-Saas Zone, Western Alps. *Lithos* **42** (3-4), 147-189.
- Ring U. and Merle O. (1992):** Forethrusting, backfolding, and lateral gravitational escape in the northern part of the Western Alps (Monte Rosa region). *Geol. Soc. Am. Bull.* **104** (7), 901-914.
- Rollinson H.R. (1993):** Using geochemical data: evaluation, presentation, interpretation. Longman, Singapore, 352 pp.
- Rössler C. (2000):** Transport und Faltung in der Furggzone und in den angrenzenden Einheiten (südliches Saastal, Wallis, Schweiz). Unpubl. diploma thesis, University of Basel, 74 pp.
- Rubatto D. and Gebauer D. (1999):** Eo/Oligocene (35 Ma) high-pressure metamorphism in the Gornergrat Zone (Monte Rosa, Western Alps): implications for paleogeography. *Schweiz. Mineral. Petrogr. Mitt.* **79** (3), 353-362.
- Rubatto D., Gebauer D., and Compagnoni R. (1997):** Dating the UHP/ HP metamorphism in the Western Alps (Sesia-Lanzo and Zermatt-Saas-Fee): Evidences for subduction events at the Cretaceous-Tertiary boundary and in the Middle Eocene. *Terra Abstracts* **9** (1), 30-31.
- Saccani, E., Padoa, E. and Tassinari, R. (2000):** Preliminary data on the Pineto gabbroic massif and Nebbio basalts: Progress toward the geochemical characterization of Alpine Corsica ophiolites. *Ofioliti* **25**, 75-85.
- Sartori M. (1987):** Structure de la zone du Combin entre les Diablons et Zermatt (Valais). *Eclogae geol. Helv.* **80**, 789-814.
- Sartori M. (1990):** L'Unité du Barrhorn (Zone pennique, Valais, Suisse). Unpubl. PhD thesis, Université de Lausanne, 156 pp.
- Saunders A.D. (1984):** The rare earth element characteristics of igneous rocks from the ocean basins. In: Henderson P. (ed.): *Developments in Geochemistry 2 - Rare Earth Element Geochemistry*. Elsevier, Amsterdam, 205-236.
- Saunders A.D. and Tearney J. (1984):** Geochemical characteristics of basaltic volcanism within back-arc basins. In: Kohelaar B.P. and Howells M.F. (eds.): *Marginal basin geology*. 16. Spec. Publ. Geol. Soc. London, 59-76.
- Schilling J.-G., Zajac M., Evans R., Johnston T., White W., Devine J.D., and Kingsley R. (1983):** Petrologic and geochemical variations along the Mid-Atlantic Ridge from 27°N to 73°N. *Am. J. Sci.* **283**, 510-586.
- Schmid S.M., Aebli H.R., Heller F., and Zingg A. (1989):** The role of the Periadriatic Line in the tectonic evolution of the Alps. In: Coward M.P. and Dietrich D. (eds.): *Alpine tectonics*. 45. Geol. Soc. London Spec. Pub., 153-171.
- Schmid S.M. and Casey M. (1986):** Complete fabric analysis of some commonly observed quartz c-axis patterns. *Geophysical Monograph* **36**, 263-286.
- Schmid S.M. and Kissling E. (2000):** The arc of the Western Alps in the light of geophysical data on deep crustal structure. *Tectonics* **19** (1), 62-85.
- Schmid S.M., Zingg A., and Handy M. (1987):** The kinematics of movements along the Insubric Line and the emplacement of the Ivrea Zone (Italy, Switzerland). *Tectonophysics* **135** (1-3), 47-66.
- Simpson C. and Schmid S.M. (1983):** An evaluation of criteria to deduce the sense of movement in sheared rocks. *Geol. Soc. Am. Bull.* **94** (11), 1281-1288.
- Spear F.S. (1993):** Metamorphic phase equilibria and pressure- temperature- time paths. Mineral. Soc. Am. Bull. Mineral. Soc. America, Washington D.C., 799 pp.
- Stampfli G.M. and Marchant R.H. (1997):** Geodynamic evolution of the Tethyan margins of the Western Alps. In: Pfiffner O.A., Lehner P., Heitzmann P., Müller S., and Steck A. (eds.): *Deep structure of the Swiss Alps: results of NRP 20*. Birkhäuser, Basel, 223-239.
- Steck A. (1990):** Une carte des zones de cisaillement ductile des Alpes Centrales. *Eclogae geol. Helv.* **83** (3), 603-627.
- Steck A., Epard J.-L., Escher A., Gouffon Y., and Masson H. (1999):** Feuille Monte Rosa, Carte tectonique des Alpes de Suisse occidentale et des régions avoisinantes. No. 47. 1:100'000. Serv. hydrol. géol. nat., Bern.
- Steck A., Epard J.-L., Escher A., Marchant R., Masson H., and Spring L. (1989):** Coupe tectonique horizontale des Alpes centrales. *Mém. Géol. Lausanne, rapp. géol. Serv. hydrol. et géol. nat.* **5**, 1-8.
- Steck A. and Hunziker J.-C. (1994):** The Tertiary structural and thermal evolution of the Central Alps - Compressional and extensional structures in an orogenic belt. *Tectonophysics* **238** (1-4), 229-254.
- Stille P. and Tatsumoto M. (1985):** Precambrian tholeiitic-dacitic rock-suites and Cambrian ultramafic rocks in the Pennine nappe system of the Alps: Evidence from Sm-Nd isotopes and rare earth elements. *Contr. Min. Petrol.* **89**, 184-192.
- Stipp M.K.D., Stünitz H., Heilbronner R., and Schmid S.M. (2002):** The eastern Tonale fault zone: a 'natural laboratory' for crystal plastic deformation of quartz over a temperature range from 250 to 700°C. *J. Struct. Geol.* **24**, 1861-1884.
- Sun S.S. and McDonough W.F. (1989):** Chemical and isotopic systematics of oceanic basalts: implications for mantle composition and processes. In: Saunders A.D. and Norry M.J. (eds.): *Magmatism in ocean basins*. Spec. Pub. 42. Geol. Soc. London, 313-345.
- Thélin P., Sartori M., Burri M., Gouffon Y., and Chessex R. (1993):** The Pre-Alpine Basement of the Briançonnais (Wallis, Switzerland). In: von Raumer J.F. and Neubauer F. (eds.): *Pre-Mesozoic Geology in the Alps*. Springer, Berlin, 297-315.
- Thélin P., Sartori M., Lengeler R., and Schaerer J.P. (1990):** Eclogites of Paleozoic or early Alpine age in the basement

- of the Penninic Siviez-Mischabel nappe, Wallis, Switzerland. *Lithos* **25** (1-3), 71-88.
- Tullis J. and Yund R.A. (1977):** Experimental Deformation of dry Westerly Granite. *J. Geophys. Res.* **82**, 5705-5718.
- Tullis J. and Yund R.A. (1980):** Hydrolytic weakening of experimentally deformed Westerly granite and Hale albite rock. *J. Struc. Geol.* **2** (4), 439-451.
- van der Klauw S.N.G.C., Reinecke T., and Stöckert B. (1997):** Exhumation of ultrahigh-pressure metamorphic oceanic crust from Lago di Cignaga, Piemontese zone, Western Alps: the structural record in metabasites. *Lithos* **41**, 79-102.
- Venturelli G., Thorpe R.S. and Potts P.J. (1981):** Rare earth and trace element characteristics of ophiolitic metabasalts from the Alpine-Apennine belt. *Earth Planet. Sci. Lett.* **53**, 109-123.
- von Raumer J.F., Galetti G., Pfeifer H.R., and Oberhänsli R. (1990):** Amphibolites from Lake Emosson/ Aiguilles Rouges, Switzerland: tholeiitic basalts of a Palaeozoic continental rift zone. *Schweiz. Mineral. Petrogr. Mitt.* **70**, 419-435.
- Weber A. (2001):** Zur strukturellen und metamorphen Entwicklung der Furgg-Zone und angrenzender Einheiten im südlichen Saastal, Wallis, Schweiz. Unpubl. diploma thesis, University of Bonn, pp. 75.
- Wetzel R. (1972):** Zur Petrographie und Mineralogie der Furgg-Zone (Monte Rosa-Decke). *Schweiz. Mineral. Petrogr. Mitt.* **52** (2), 161-236.
- White, S.H., Burrows, S.E., Carreras, J., Shaw, N.D. and Humphreys, F.J. (1980):** On mylonites in ductile shear zones. *J. Struc. Geol.* **2**, 175-187.
- Wilkinson J.F.K. (1982):** The genesis of mid-ocean ridge basalt. *Earth Sci. Rev.* **18**, 1-57.
- Wilson M. (1989):** Igneous petrogenesis - a global tectonic approach. Chapman & Hall, London, 466 pp.
- Wood D.A., Joron J.-L., and Treuil M. (1979):** A re-appraisal of the use of trace elements to classify and discriminate between magma series erupted in different tectonic settings. *Earth Planet. Sci. Lett.* **45**, 326-336.
- Wüst G.H. and Baehni, L.A. (1986):** The distinctive tectonometamorphic evolution of two basement complexes belonging to the Grand-Saint-Bernard nappe (Val de Bagnes, Valais). *Swiss Bull. Min. Petrol.* **6**, 53-71.
- Zingg A. and Hunziker J.C. (1990):** The age of movements along the Insubric line west of Locarno (northern Italy and southern Switzerland). *Eclogae geol. Helv.* **83** (3), 629-644.

Index of figures

Fig. 1.1.1: Regional overview of the investigated area.....	2
Fig. 1.2.1: Simplified geological sketch map of the Monte Rosa region.....	4
Fig. 2.1: Synthetic stratigraphic profiles of the Stockhorn & Portjengrat unit, Monte Rosa nappe, Siviez-Mischabel nappe, and Zermatt (ZS) & Antrona unit in the investigated area.....	8
Fig. 3.1.1: AFM-diagram for the classification of meta-basalts.....	16
Fig. 3.1.2: Harker diagrams using major elements for the classification of meta-basalts.....	18
Fig. 3.1.3: Chondrite-normalized abundances of the rare earth elements partitioned between common mineral and basaltic melt following 75% equilibrium crystallisation.....	19
Fig. 3.1.4: Chondrite-normalized plot of REE abundances in typical island arc basalts, alkali olivine basalts, tholeiitic continental flood basalts, MORB and Archean komatiites.....	20
Fig. 3.2.1 (1): Sample locations in a simplified geological sketch map of the Monte Rosa region.....	24
Fig. 3.2.2 (2): Schematic S-N cross-section of the Monte Rosa region (Kramer 2002), modified after Milnes et al. (1981).....	25
Fig. 3.2.3 (3): Total alkali versus silica diagram after Le Bas et al. (1986).....	31
Fig. 3.2.4 (4): Concentrations of selected major and trace elements versus Mg#.....	32
Fig. 3.2.5 (5): Concentrations of selected major and trace elements versus Zr concentrations.....	33
Fig. 3.2.6 (6): Chondrite-normalized rare earth element concentrations, normalisation values from Boynton (1984).....	34
Fig. 3.2.7 (7): Primitive mantle-normalized diagrams of selected trace elements of amphibolites from the Monte Rosa region and surrounding areas.....	35
Fig. 3.2.8 (8): Compatible (Ni) versus incompatible (Nb, Ce) plots.....	36
Fig. 3.2.9 (9): Incompatible element ratio plots for metabasalts from the Furgg zone and adjacent areas, and comparison with basalts from other Piemont-Ligurian ophiolites.....	37
Fig. 4.1.1: Development of foliation in thin section or outcrop.....	52
Fig. 4.1.2: Photomicrograph of tremolite (Trem) that is retrogressed to talc (Tlc) in Mesozoic marbles.....	54
Fig. 4.1.3: Photomicrograph of the symplectitic intergrowth of actinolite and albite.....	54
Fig. 4.2.1: Geographic overview of the field area and location of the cross-sections.....	58
Fig. 4.2.2: Lower hemisphere stereographic projections of foliation poles, calculated Π -poles, and fold axes (FA), cross-sections 625, 627, 630, and 633.....	60
Fig. 4.2.3: Hinge region of the D4 Vanzone antiform as seen from near the Mezzalama refuge, Valle d'Ayas.....	63
Fig. 4.2.4: D4 crenulation cleavage in orthogneisses of the Monte Rosa nappe.....	64
Fig. 4.2.5: View of the crest between Valle d'Ayas and Valle di Gressoney below the Quintino Sella refuge, as seen from the Felik glacier towards the west.....	65
Fig. 4.2.6: 270°- panoramic view of the border crest between Italy and Switzerland in the upper Valle d'Ayas.....	66
Fig. 4.2.7: View of the SW crest of the Vincentpiramide, i.e. the crest between Valle di Gressoney and Valle di Sesia, from approximately 3800 to 4000 m elevation.....	67
Fig. 4.2.8: D3 Camoscio synform at the Corno del Camoscio, crest between Valle di Gressoney and Valle di Sesia.....	68
Fig. 4.2.9: Lower hemisphere stereographic projection of foliations, fold axes, and stretching lineations. Cross-section 628.....	69
Fig. 4.2.10: View of Gornergrat from Pollux towards the N.....	71
Fig. 4.2.11: Parasitic fold hinges of the D3 Stockhorn antiform.....	72
Fig. 4.2.12: M-shaped flexural-slip folds in the hinge of the D3 Stockhorn antiform.....	72
Fig. 4.2.13: Top view of an asymmetrically refolded basaltic layer in garnet micaschists in the Furgg zone.....	72
Fig. 4.2.14: View of Schalbeterflue/ Pollux north crest, from Liskamm towards the W.....	73
Fig. 4.2.15: D2 Chini synform refolding the Permo-Mesozoic cover of the Stockhorn unit.....	74
Fig. 4.2.16: Mesozoic calcite and dolomite marbles of the Stockhorn unit.....	75
Fig. 4.2.17: Tight to isoclinal D2 folds in paragneisses of the Stockhorn unit (Gadmen folds).....	75
Fig. 4.2.18: Lower hemisphere stereographic projections of foliations, fold axes, and stretching lineations, cross-sections 638 and 636.....	77
Fig. 4.2.19: D1/D3 fold superposition in metasediments of the Portjengrat unit (D1/D3 Fluchthorn fold).....	78
Fig. 4.2.20: View of Schwarzbergchopf, west of the Schwarzberg glacier in Saastal, from the Nollenhorn.....	78
Fig. 4.2.21: View of the Mittaghorn, Saastal, from Furggtal.....	79
Fig. 4.2.22: Superposition of three folding phases in the Permo-Mesozoic metasedimentary cover of the Portjengrat unit.....	80
Fig. 4.2.23: Superposed folding in quartzites and quartzitic conglomerates of the Portjengrat unit.....	81
Fig. 4.2.24: Asymmetric parasitic folds in the overturned northern limb of the D3 Gabbio synform.....	81
Fig. 4.2.25: Lower hemisphere stereographic projections of foliations, fold axes and stretching lineations. Cross-sections 642, 646, 643, and 653.....	83
Fig. 4.2.26: Metasedimentary belts between ortho- and paragneisses of the Portjengrat unit at Saas Fee and Saas Grund in Saastal.....	85
Fig. 4.2.27: Contact of augengneisses (Portjengrat unit; on top), marbles (light) and calcareous micaschists (grey).....	86
Fig. 4.2.28: View of Almagellertal, Zwischbergen pass and Portjengrat from the Mittaghorn towards the east.....	86
Fig. 4.2.29: View of the Permo-Mesozoic metasediments of the Zwischbergental from Pizzo del Büsin towards the WNW.....	87
Fig. 4.2.30: (A) View of the Tällihorn S-crest from the Zwischbergen pass. (B) D3 Zwischbergen antiform.....	88
Fig. 4.2.31: View towards the W onto the metasediments at the Zwischbergen pass, Almagellertal - Zwischbergental.....	89
Fig. 4.2.32: View of the NE side of Furggtal from the Nollenhorn.....	91
Fig. 4.2.33: View of the NW side of Furggtal onto the Nollenhorn N-crest, the crest between Furggtal and Saastal, from the Börterrück, Furggtal.....	93
Fig. 4.2.34: 270°-view from north to west of the NE side of Furggtal - from the Sonnighorn to the Börterrück.....	94
Fig. 4.2.35: View of Monte della Preja NE face and the small unnamed pass (2440 m) between its main and north summit.....	96
Fig. 4.2.36: Core of the D3 Passo della Preja synform at the Passo della Preja, Valle di Loranco - Valle di Bognanco.....	97
Fig. 4.2.37: View of Monte della Preja E crest, Pass P. 2325 (above Alpe Pasquale), and „Monte Pasquale“, Valle di Loranco - Valle di Bognanco - view towards the N.....	98
Fig. 4.2.38: Third dimension of the „Monte Pasquale“ - view towards the E from Monte della Preja.....	99

Fig. 4.3.1: Basaltic dykes and sills.....	101
Fig. 4.3.2: Meso-scale structures in the Furgg zone and the intensely strained Monte Rosa cover and basement.....	102
Fig. 4.3.3: Late-D3 Saas shear zone overprinting older structures.....	103
Fig. 4.3.4: D3 Gornergrat-Furggtal shear zone overprinting older structures.....	104
Fig. 4.3.5: Gornergrat-Furggtal shear zone in (A) Saastal, (B) Furggtal, and (C) Valle Antrona.....	105
Fig. 4.3.6: Meso-scale folds and fractures associated with the D3 Gornergrat-Furggtal shear zone.....	106
Fig. 4.3.7: D3 Saas shear zone overprinting Mesozoic quartzites and marbles of the Portjengrat unit.....	107
Fig. 4.4.1: Projection values and projection order of individual cross-sections into the composite cross-section plane.....	110
Fig. 4.4.2: Composite cross-section.....	111
Fig. 4.4.3: Location of the individual cross-sections on the composite projection plane.....	112
Fig. 4.5.1: Deformed minerals and deflected foliations as kinematic indicators during D1/D2.....	114
Fig. 4.5.2: Shear bands as kinematic indicators during D1/D2.....	115
Fig. 4.5.3: Deformed minerals and deflected foliations as kinematic indicators during D3.....	116
Fig. 4.5.4: Shear bands as kinematic indicators during D3.....	117
Fig. 4.5.5: Quartz microstructures in thin section.....	118
Fig. 4.5.6: Poles of quartz c-axes in lower hemisphere, equal area stereographic projection, measured by U-stage; and micrographs of measured quartz textures (D).....	120
Fig. 4.5.7: Stretching lineations (D1/D2 and D3) and associated shear senses, Monte Rosa south side.....	122
Fig. 4.5.8: Stretching lineations and associated shear senses, Monte Rosa north side.....	123
Fig. 5.1: Map view of major thrusts and shear zones and D3 and D4 fold axial planes in the Monte Rosa region.....	126
Fig. 5.2: Simplified composite cross-section illustrating the location of the major D4 and D3 fold axial planes, thrusts and shear zones.....	127
Fig. 5.3: Qualitative reconstruction of major folds and thrusts/ shear zones:	
Fig. 5.3 A: Reconstruction of D4 structures.....	129
Fig. 5.3 B: Reconstruction of late D3 structures.....	131
Fig. 5.3 C: Reconstruction of early D3 structures.....	133
Fig. 5.3 D: Triangle structure of the Penninic nappe stack.....	133

Index of tables

Tab. 1.2.1: Timing of selected major events affecting the Monte Rosa region.....	5
Tab. 3.2.1 (1): Sample descriptions of the studied amphibolites.....	44
Tab. 3.2.2 (2): Analytical data, Mg# number, Zr/ Y ratio and Cen/Ybn ratio.....	46
Tab. 4.1: Characteristics of deformation phases.....	50
Tab. 4.2.1: Projection values of cross-sections.....	60

CURRICULUM VITAE

Ms. Julia Kramer

Date of birth August 17th, 1970 in Ulm, Germany
Citizenship German

Academic education

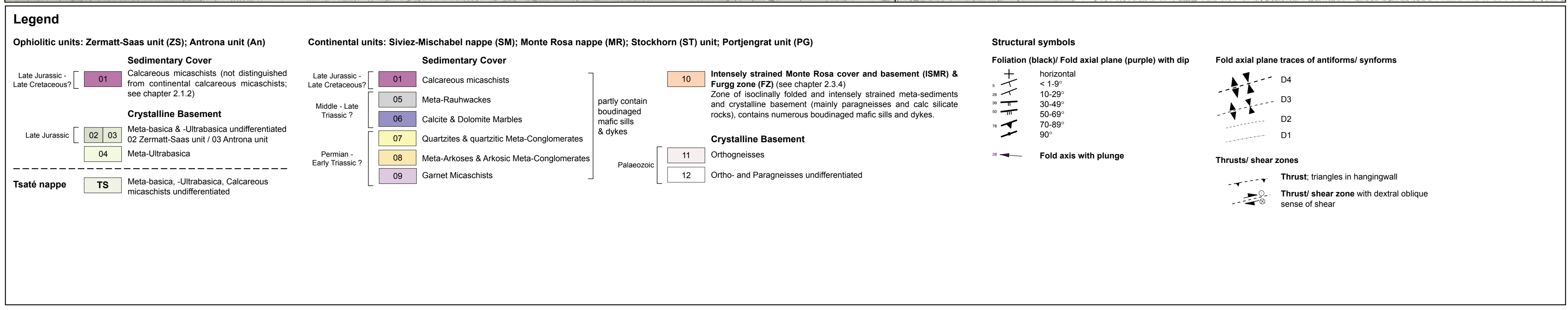
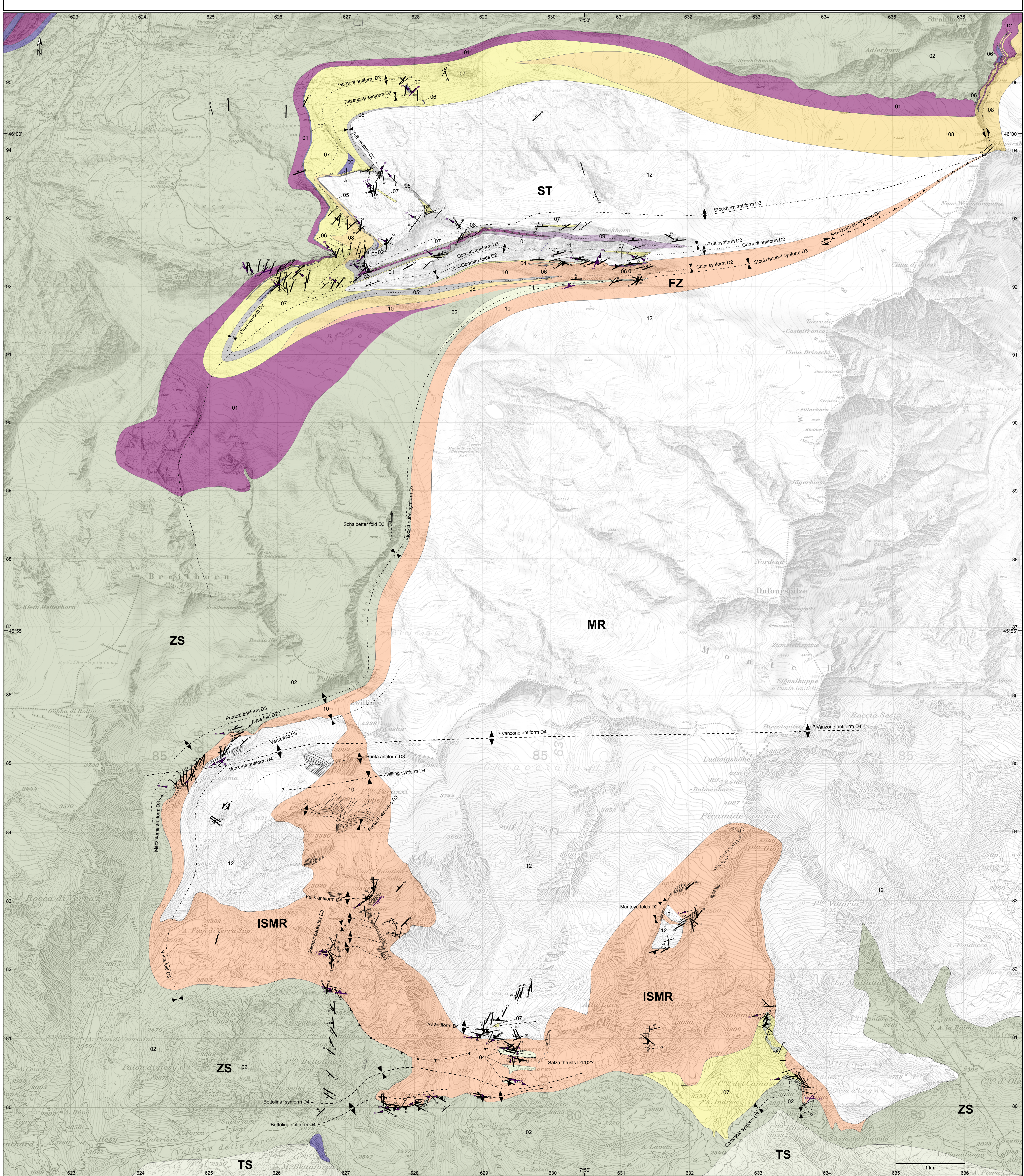
- Apr 1997 - Oct 2002** PhD in Earth Sciences, University of Basel, Switzerland.
“Structural evolution of the Penninic units in the Monte Rosa region, Swiss and Italian Alps.”
Initiators of the project, referees and co-referee: Prof. Dr. N. Froitzheim (University of Bonn, Germany), Prof. Dr. M. Frey, Prof. Dr. S.M. Schmid, Prof. Dr. R. Abart (all University of Basel), PD. Dr. N. Mancktelow (Swiss Federal Institute of Technology/ ETH Zurich, Switzerland).
- Oct 1991 - May 1996** Diploma in Geology, University of Karlsruhe (Institute of Technology), Germany.
“Tectonics of the southern margin of the Northern Calcareous Alps between St. Anton and Gand, Tyrol (Austria).”
Referee and co-referee: Prof. Dr. G.H. Eisbacher and Prof. Dr. J. Kley.
- Oct 1990 - Sep 1991** Student of Music, Robert-Schumann- Hochschule (college of music), Düsseldorf, Germany.
-

Professional experience

- Apr 1997 - Dec 2002** Research and teaching assistant at the Dept. of Earth Sciences, University of Basel, Switzerland.
Assisted in supervision of five diploma students. Assisted in teaching graduate and undergraduate level field courses in structural geologic, stratigraphic and petrologic mapping techniques; structural geology and introductory geology/ geophysics.
- May 1996 - Mar 1997** Consultant geologist for three engineering offices in Germany.
- Oct 1992 - Aug 1995** Teaching assistant at the Dept. of Geology, University / Institute of Technology of Karlsruhe, Germany.
Assisted in teaching graduate and undergraduate level courses in optical crystallography, palaeontology, introductory geology/ mineralogy.

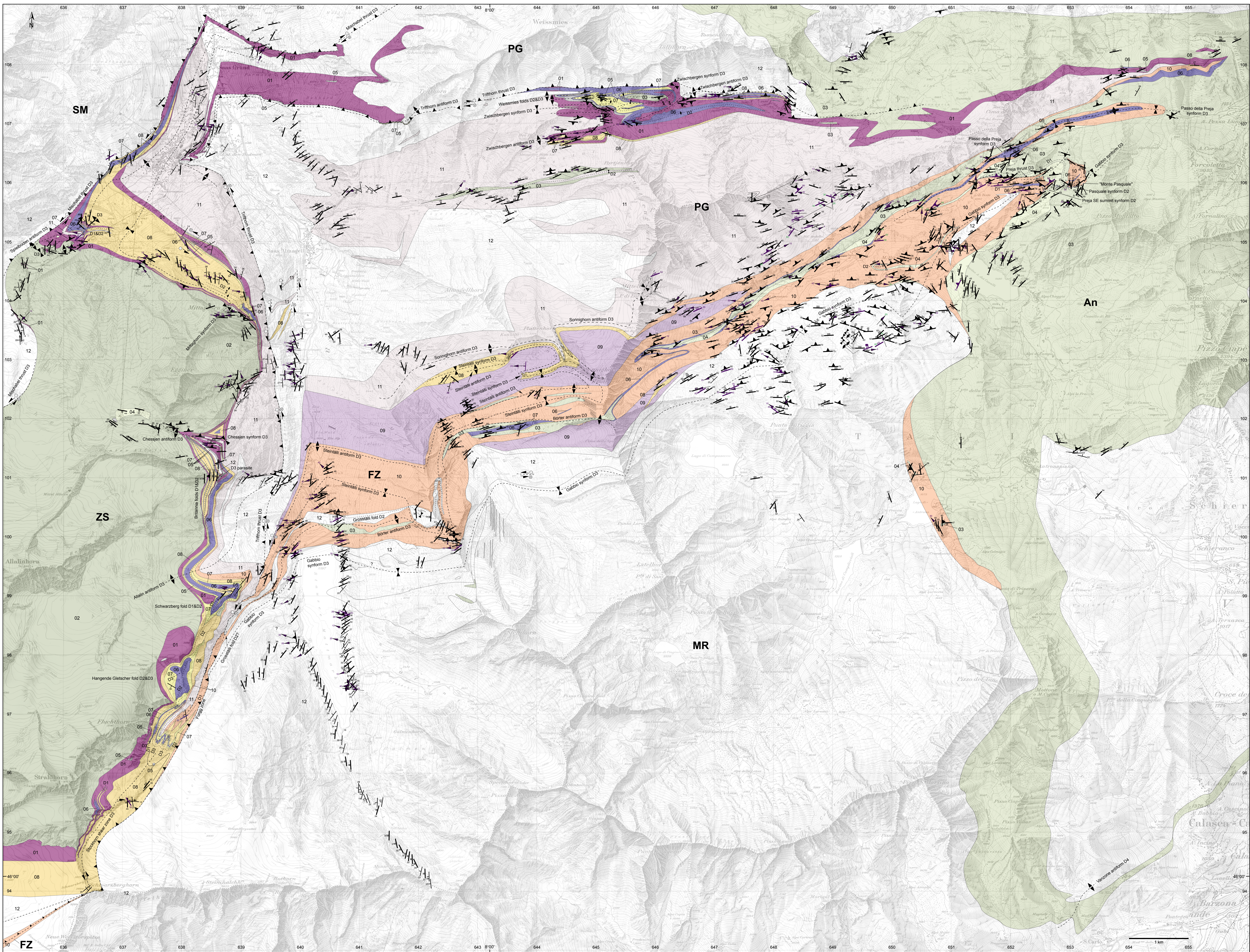
Geologic- tectonic map 1: 25'000 Monte Rosa South (Gornergrat/ Matter, upper Valle d'Ayas and Valle di Gressoney) PhD Julia Kramer (2002)

Topographic basis: Landeskarte der Schweiz, 1:25'000: sheets 1348 Zermatt & 1349 Monte Moro; and 1:50'000: sheets 285 Domodossola & 294 Gressoney



Geologic- tectonic map 1: 25'000 **Monte Rosa North (upper Saastal, Almagellertal, Furggtal, Zwischbergental, Valle di Loranco, Valle di Bognanco, Valle d'Antrona, Valle d'Anzasca)** **PhD Julia Kramer (2002)**

Topographic basis: Landeskarte der Schweiz 1:25'000: 1328 Randa, 1329 Saas, 1348 Zermatt, 1349 Monte Moro; and 1:50'000: 285 Domodossola



Legend

Ophiolite units: Zermatt-Saas unit (ZS); Antrona unit (An)

Sedimentary Cover	
Late Jurassic - Late Cretaceous?	01 Calcareous micaschists (not distinguished from continental calcareous micaschists; see chapter 2.1.2)
Crystalline Basement	
Late Jurassic	02 03 Meta-basica & Ultrabasica undifferentiated
	04 Zermatt-Saas unit / 03 Antrona unit
	04 Meta-Ultrabasica

TS	Tsaté nappe
	Meta-basica, -Ultrabasica, Calcareous micaschists undifferentiated

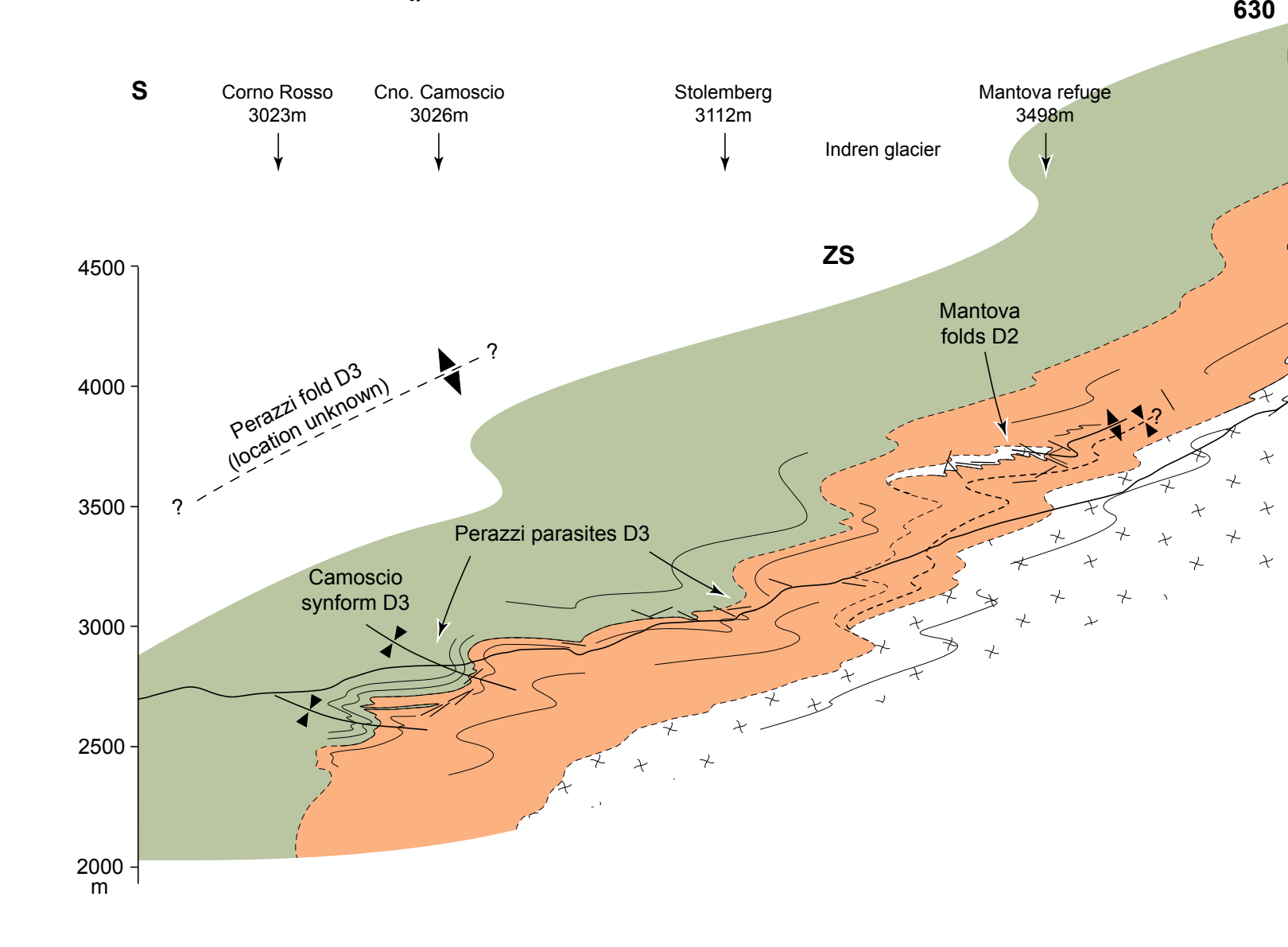
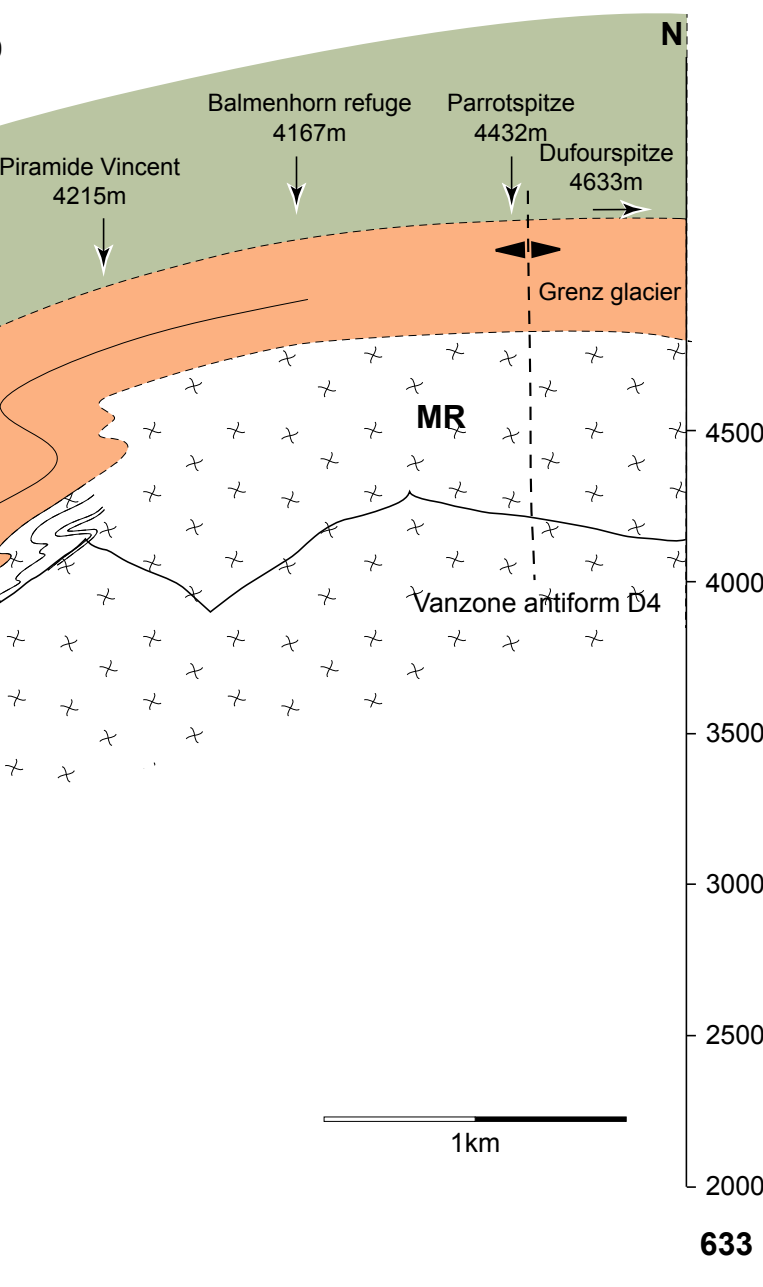
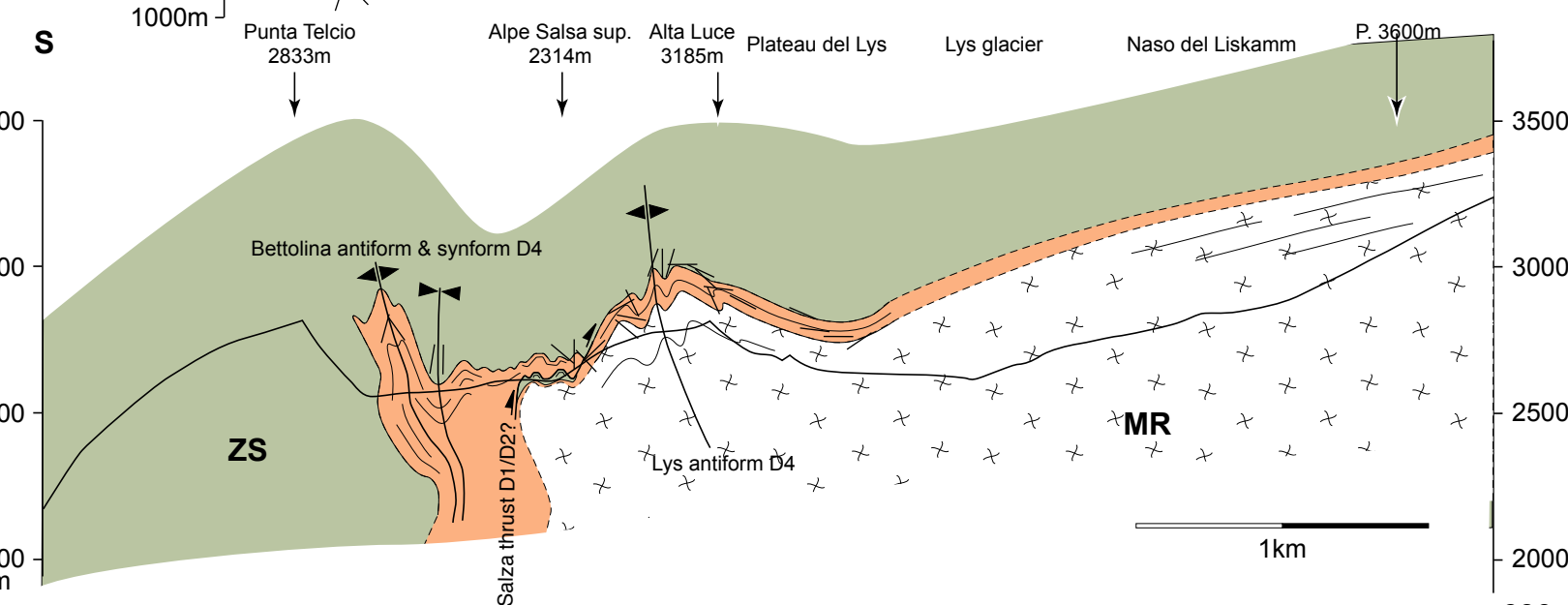
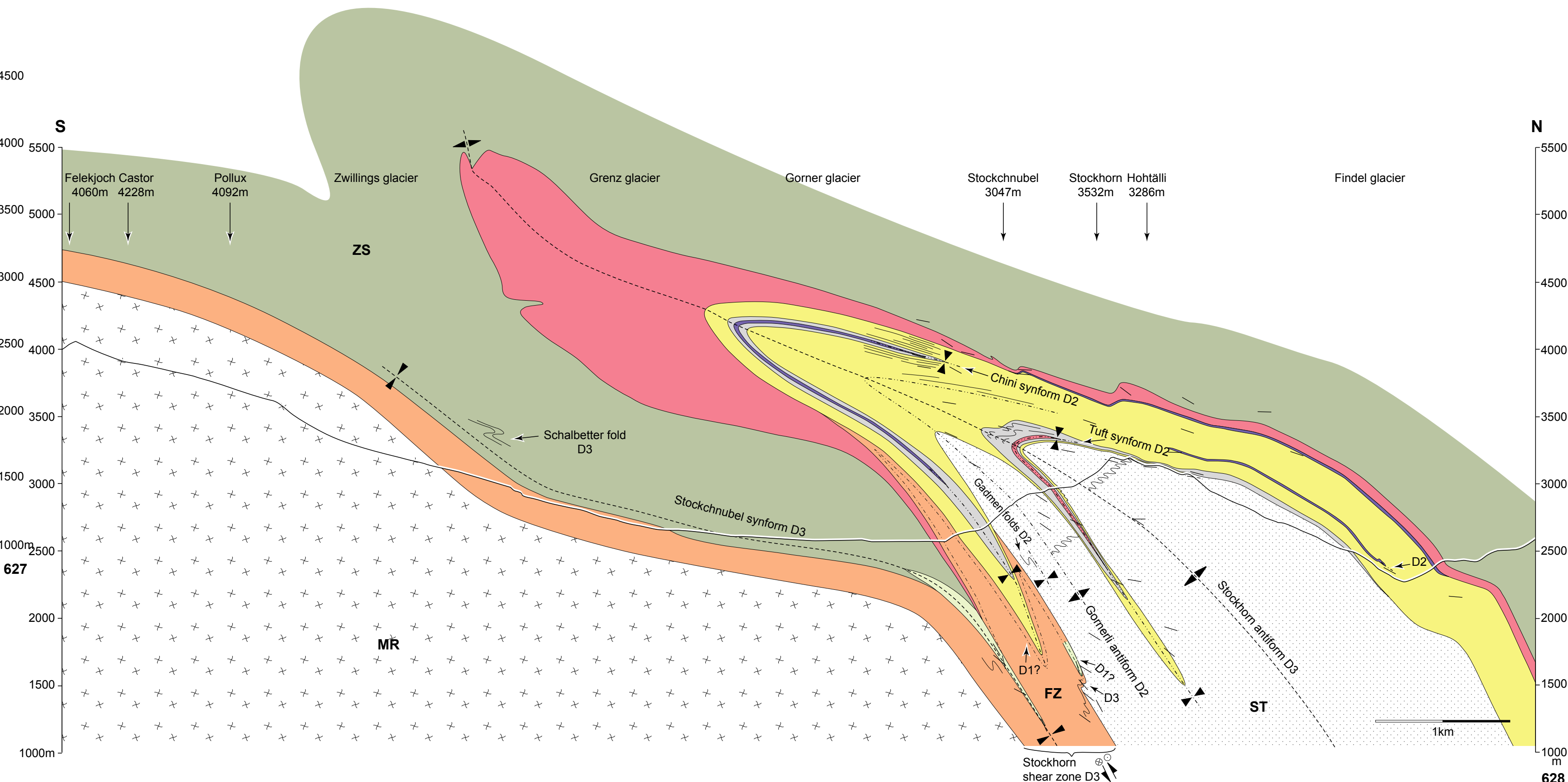
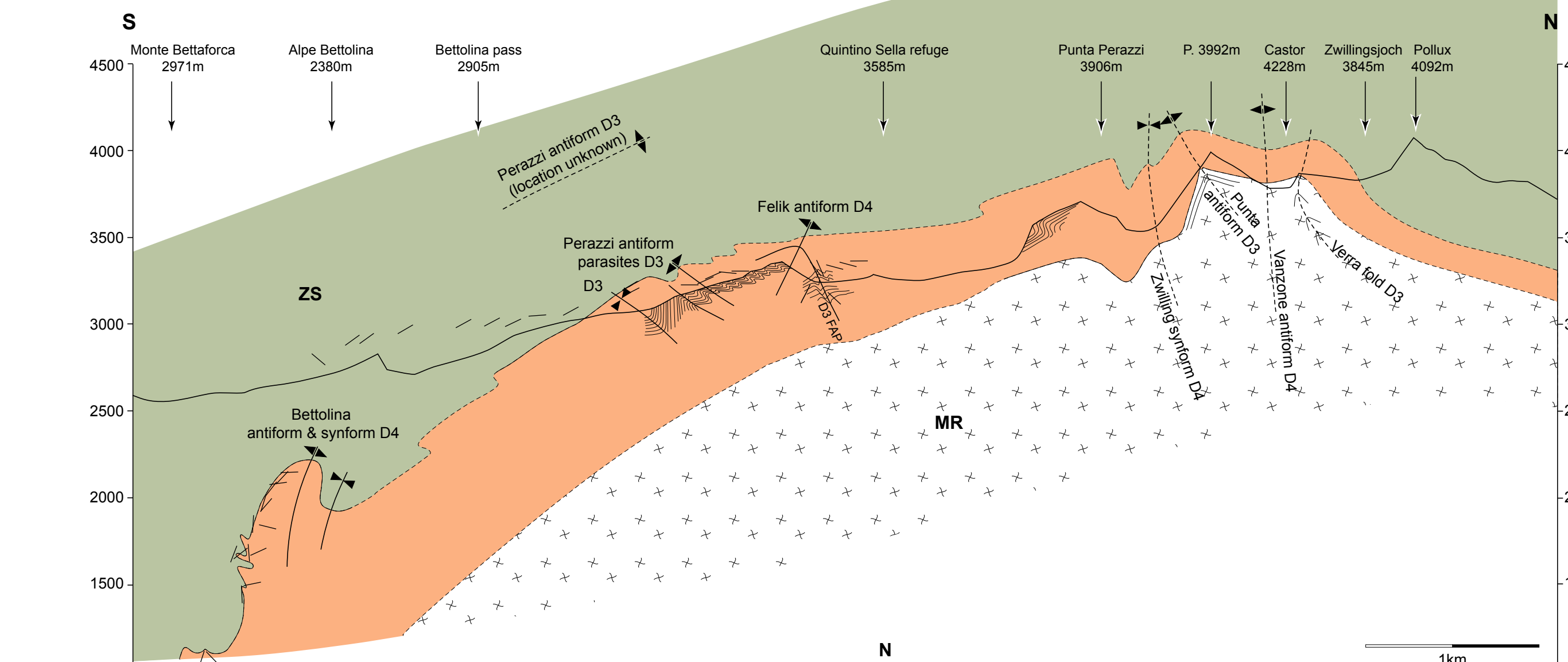
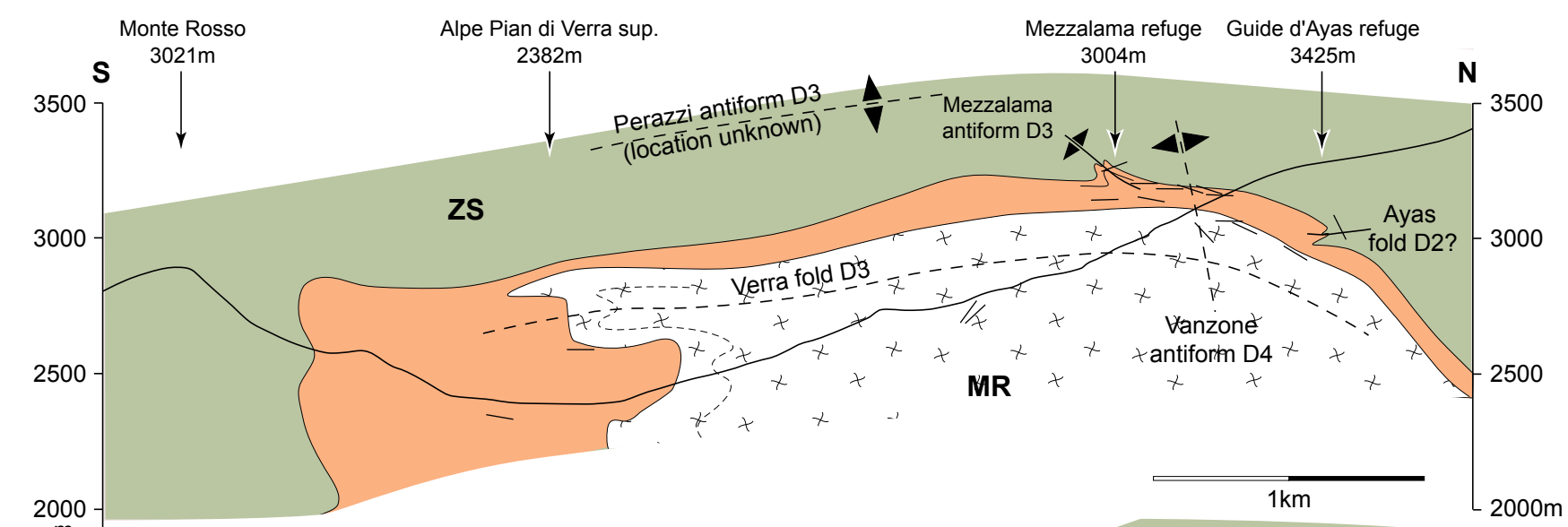
Continental units: Siviez-Mischabel nappe (SM); Monte Rosa nappe (MR); Stockhorn (ST) unit; Porfingrat unit (PG)

Sedimentary Cover	
Late Jurassic - Late Cretaceous?	01 Calcareous micaschists
	05 Meta-Rauhewackes
Middle - Late Triassic ?	06 Calcite & Dolomite Marbles
	07 Quartzites & quartzitic Meta-Conglomerates
	08 Meta-Arkoses & Arkosic Meta-Conglomerates
Paleozoic	09 Garnet Micaschists
	10 Intensely strained Monte Rosa cover and basement (ISMR) & Furgg zone (FZ) (see chapter 2.3.4)
	Zone of socially folded and intensely strained meta-sediments and crystalline basement (mainly paragneisses and calc silicate rocks), contains numerous boudinaged mafic sills & dykes
Crystalline Basement	
	11 Orthogneisses
	12 Ortho- and Paragneisses undifferentiated

Structural symbols

	Foliation (black/ Fold axial plane (purple) with dip
	horizontal < 1-9°
	10-29°
	30-49°
	50-69°
	70-89°
	90°
	Fold axis with plunge
	Fold axial plane traces of antiforms/ synforms
	D4
	D3
	D2
	D1
	Thrusts/ shear zones
	Thrust: triangles in hanging wall
	Thrust/ shear zone with dextral oblique sense of shear

Enclosure 3
Cross-sections 1:25'000 Monte Rosa South and Gornergrat (625, 627, 630, 633, 628, 628 E-W section)
 PhD Julia Kramer (2002)



Legend for cross-sections

Ophiolitic units: Zermatt-Saas (ZS) & Antrona unit (An)

- Late Jurassic - Late Cretaceous? Calc micaschists
- Meta-basica & -Ultrabasica undifferentiated
- Late Jurassic Zermatt-Saas / Antrona
- Meta-Ultrabasica

Continental units: Siviez-Mischabel (SM) & Monte Rosa nappe (MR); Stockhorn (ST) & Portjengrat unit (PG)

Sedimentary Cover

- Meta-Rauhawackes
- Meta-Rauhawackes, Calcite & Dolomite Marbles undifferentiated
- Quartzites & quartzitic Meta-Conglomerates
- Meta-Arkoses & Garnet Micaschists undifferentiated (section 643 Furgg)
- Meta-Arkoses & arkosic Meta-Conglomerates, minor Quartzites undifferentiated (all other sections)

contain partly boudinereered mafic sills & dykes

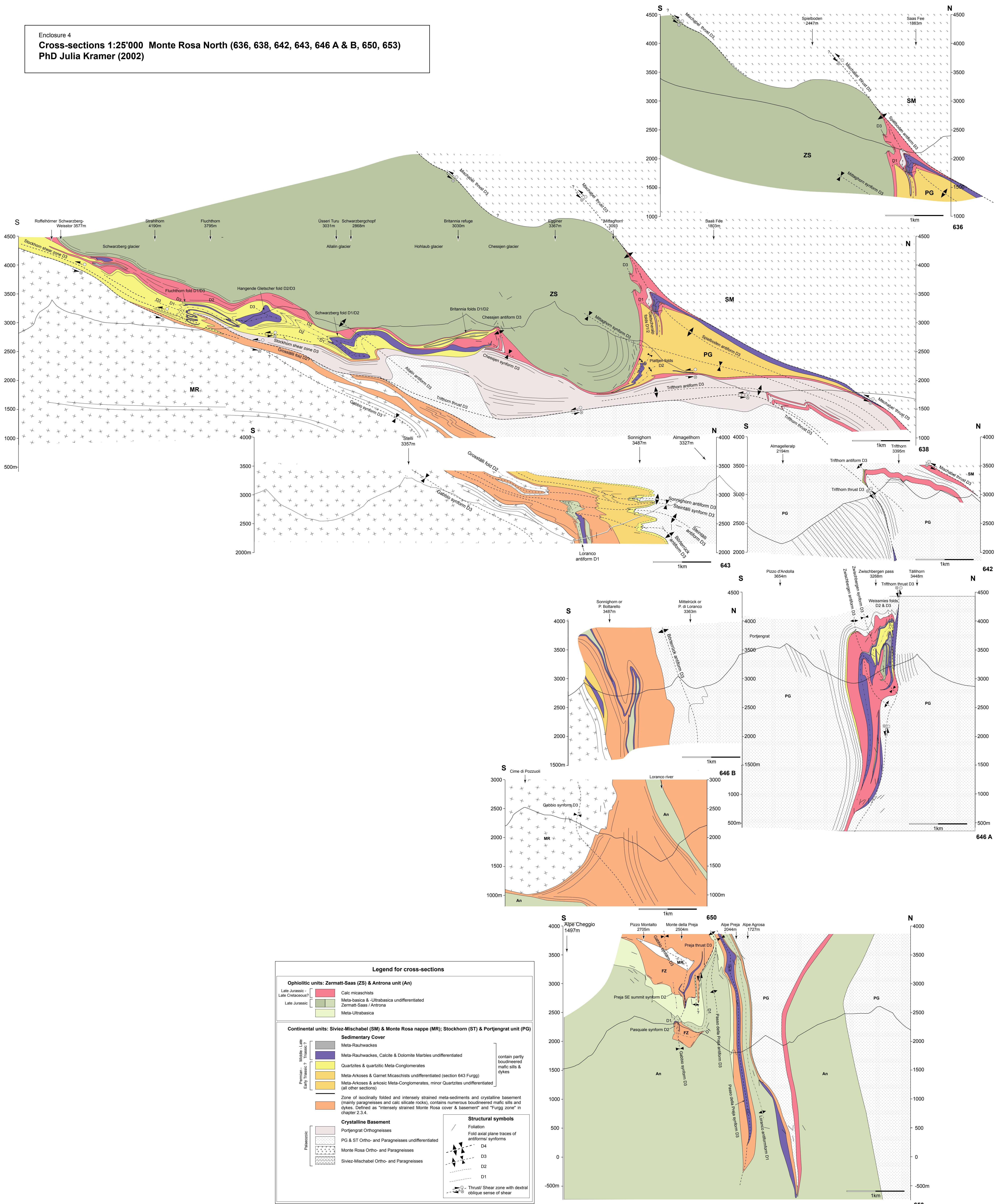
Crystalline Basement

- Portjengrat Orthogneisses
- PG & ST Ortho- and Paragneisses undifferentiated
- Monte Rosa Ortho- and Paragneisses
- Siviez-Mischabel Ortho- and Paragneisses

Structural symbols

- Foliation
- Fold axial plane traces of antiforms/ synforms
- D4
- D3
- D2
- D1
- Thrust/ Shear zone with dextral oblique sense of shear

Enclosure 4
Cross-sections 1:25'000 Monte Rosa North (636, 638, 642, 643, 646 A & B, 650, 653)
 PhD Julia Kramer (2002)



Legend for cross-sections

Ophiolitic units: Zermatt-Saas (ZS) & Antrona unit (An)	
Late Jurassic - Late Cretaceous	Calc micaschists
Late Jurassic	Meta-basica & -Ultrabasica undifferentiated Zermatt-Saas / Antrona
	Meta-Ultrabasica

Continental units: Siviez-Mischabel (SM) & Monte Rosa nappe (MR); Stockhorn (ST) & Portjengrat unit (PG)	
Sedimentary Cover	
Middle - Late Triassic - 7	Meta-Rauhawackes
Premian - Middle - Late Triassic - 7	Meta-Rauhawackes, Calcite & Dolomite Marbles undifferentiated
Early Triassic - 7	Quartzites & quartzitic Meta-Conglomerates
	Meta-Arkoses & Garnet Micaschists undifferentiated (section 643 Furgg)
	Meta-Arkoses & arkosic Meta-Conglomerates, minor Quartzites undifferentiated (all other sections)
Zone of isoclinally folded and intensely strained meta-sediments and crystalline basement (mainly paragneisses and calc silicate rocks), contains numerous boudiniferous mafic sills and dykes. Defined as "intensely strained Monte Rosa cover & basement" and "Furgg zone" in chapter 2.3.4.	
Crystalline Basement	
Palaeozoic	Portjengrat Orthogneisses
	PG & ST Ortho- and Paragneisses undifferentiated
	Monte Rosa Ortho- and Paragneisses
	Siviez-Mischabel Ortho- and Paragneisses

Structural symbols	
	Foliation
	Fold axial plane traces of antiforms/ synforms
	D4
	D3
	D2
	D1
	Thrust/ Shear zone with dextral/oblique sense of shear